DIPARTIMENTO
DI GEOSCIENZE

UNIVERSITÀ
DEGLI STUDI
DI PADOVA

via Gradenigo,6
35131 Padova
tel +39 049 8279110
fax +39 049 8279134
CF 80006480281
P.IVA 00742430283

PhD candidate
Chiara Balestrieri

Title of the thesis: LE DINAMICHE DELLA CALCIFICAZIONE E DELLA PRODUZIONE DI CARBONATO DEI COCCOLITOFORIDI NELL'OCEANO MERIDIONALE E NELL' OCEANO PACIFICO EQUATORIALE ORIENTALE, DURANTE L'ULTIMA DEGLACIAZIONE.

Supervisor
Prof. Claudia Agnini

Evaluator: Silvia Gardin

We would thank the reviewer for her careful al comprehensive comments on the thesis. We have appreciated most of them and changed test and figures consequently.
In the following, you can find the replay to all of them.

Chapter 1:
-The reviewer suggested to add the location of the studied cores in the world map. We have added the site locations in the map (see Fig. 1.5, page 12).
-The reviewer suggested to clarify the reason why we have used different methodologies at the different sites. We thank for the comment and we have better defined our choice by implementing section 1.2 at page 15.

Chapter 2:
-The reviewer suggested to perform statistical analyses on the obtained results in case of a publication. We are in agreement with this comment, however, this chapter is, at least for now not more than a draft and we believe we can make important improvements with more time available, which we will find for the submission of the paper to a journal.
-The reviewer wondered if the carbonate content of the tap water employed in our samples preparation have been evaluated. We do agree with this comment, however we did not used deionized water and we did not calculate the carbonate content of the tap water as it is usually performed for standard analyses (*e.g.* D' Amario et al., 2018).

Chapter 3:
-The reviewer suggested to add a supplementary figure tracing the deep vs surface ocean dynamics. We thank for the comment and we have implemented the chapter with a figure showing surface, intermediate and deep ocean dynamics in the Southern Ocean (see Fig. S3, page 68).
-The reviewer commented on the fact that we have proposed only linear correlations among our data. Indeed, we have applied linear correlations for our datasets just because we have tried with more complicated possible relationships but the linear correlation is the one that better fits.
-The reviewer commented on the possible impact of changes in salinity as a possible factor influencing the calcification rate of coccolithophores. In the discussion of chapter 3, we have taken into account this ecological parameter, but its variation trough time is not significantly correlated with the changes observed in our data so that we have not been able to support the idea that changes in salinity are in fact responsible for modifications documented in coccolithophore assemblages.
-The reviewer commented on the preservation of our material asking for more details. In particular, she asked: "How preservation of the studied material has been assessed? Is CEX index reliable? Can the preservation impact be reliably estimated without any SEM analysis of the final filtration?"
In order to define preservation of the studied material we evaluated our samples based on SEM analyses. Specifically, for this site, we use SEM analyses in order to corroborate our dissolution-proxy based interpretations because the site is located below the Carbonate Compensation Depth (CCD). However, we do believe that preservation impact can be assessed and estimated based on common analyses and multiproxy reconstructions, if the site is positioned above or almost above the Carbonate Saturation Horizon (CSH).
CEX index has been considered a reliable tool and has been previously used for dissolution-based interpretations by many authors (*e.g.* Dittert et al., 1999; Boeckel and Baumann*,* 2004; Marino et al., 2009; Amore et al., 2012). However, our data suggest that factors other than dissolution could in fact have biased this proxy. To address this point we have now added a paragraph (3.5.2: Carbonate system and dissolution dynamics in the deep SO) to better explain the complexity in understanding the dissolution dynamics at this site if only this proxy is used.
-The reviewer made a good point when she asked several questions as for instance: "Is there any way to solve the problem of fragmented/broken coccoliths that are not quantified for the carbonate flux? Are errors really considered? What are the limitation of the analytical technique? How much (quantitatively) this bias does/doesn't impact the final results, especially when the counted coccoliths have different sizes?"
All these questions are crucial because they can substantially affect the estimates of coccolithophore carbonate production. All the authors that have worked on this topic in the last fifteen years are aware that the shape index proposed by Young and Ziveri (2000) allows to assess the coccolith mass (pg) of different taxa but still lack in estimating the contribution of the broken/fragmented coccoliths. However, this method represents the best tool to address this issue at present. We clearly need a more powerful methodology but for now, as also evidence by the authors, this still remains the only way to evaluate the coccolith carbonate production without losing the information related to the taxonomy. This point and commentary is now available in the discussion of this chapter (see section 3.3.3a, page 43).

Chapter 4:
-The reviewer suggested to add a conceptual model that explains which are the main mechanisms controlling the response of coccoliths (calcification/production) to atmCO_2 increase. We thank for this comment and we have added a conceptual model based on this suggestion in order to clarify the various environmental parameters that can influence coccolith carbonate production (specifically *Emiliania huxleyi* mass, pg); (see Fig. 4.3, page 98).

Chapter 5:
-The reviewer wondered about the reason why we did not consider the contribution of other phytoplankton to the POC in our calculations. We are in agreement with this comment, however we based our analyses on literature assumptions which already considered this issue (see McClelland et al., 2016).

Chapter 6:
-The reviewer suggested to develop a more comprehensive conclusive chapter. We thank for the comment, however the final aim of this chapter was to briefly summarize all the final conclusions that we already had exhaustively explored within each single chapter.

Final minor comments
We added a glossary of abbreviations used in the different chapters, as the reviewer suggested. The reviewer suggested to add a general bibliography list, we thank for the comment and we have eventually kept the original structure of the thesis that is based on four different papers with their own bibliography and a final bibliography list which refers to and completes the others. The reviewer suggested to add SEM images of the filter. This is a good point but we couldn't accomplish this request because we did not taken images of coccoliths on the filter.

Evaluator: Emanuela Mattioli

We would warmly thank the reviewer for her thorough and exhaustive review of the thesis. To address her comments, we have decided to replay point by point to each single comment:

Chapter 1 and 2:
-The reviewer suggested to better define the type of coccolithophore abundances' (relative, absolute or fluxes) dynamics in the surface ocean as a response to changes in nutrient concentrations and to specify coccolith- produced carbonates dynamics at the sea-floor. The reviewer is right and we have decided to implement sections 1.1.1 and 1.1.2 (see pages 6 and 9) to address this point.

Chapter 3:
-The reviewer asked on the possibility to discriminate between dissolution- and environmentally-driven changes on coccolith assemblages. We thank for this comment because it is a crucial issue in the discussion of this chapter, in fact along the text we have tried to explain the difficulty in disentangling the role played by each process at this Site. Both dissolution and environmental changes could substantially alter/ modify the coccolith species abundance as well as the

carbonate and calcification dynamics and this is what we have suggested to occur at Site 1089 (see section 3.6, page 62).
-The reviewer suggested to better emphasize the reason why we have chosen to estimate the coccolith carbonate production with two different approaches. These two methods, the shape index (Young and Ziveri, 2000) and the SYRACO methods, have limits and benefits and while the SYRACO method provides a better estimation of *Emiliania huxleyi* mass (pg) the shape index methods is able to give information on the carbonate contribution of the different taxonomic component of the assemblages. This point is now emphasized in the new version of the text.

-The reviewer suggested to organize coccolith assemblages (relative and absolute abundances) in two sets of scales (*e.g.* coccoliths lower than 10% and upper than 50%) in Fig. 3.3. We thank for the comment, however we have decided to order the different taxa based on their ecological affinity. Up to us, this makes the reading of the figure as well as the flow of the discussion easier because the paleoecological affinity rather that the relative abundance of the different taxa are used to interpreted the observed trends. Finally, the reviewer suggested to better define the grey lined areas in the caption of Figure 3.3. We have implemented the caption (see Fig. 3 3).

Chapter 4:
-The reviewer made comments on "Why using different preparation methods in different chapters? Why 500 coccoliths were counted in the Atlantic site versus 300 in the Pacific site?" These are good points. Regarding the first issue, we have decided to process samples using different preparation techniques because our data on first case study have highlighted that these different methods assure comparable results so that have used the less time consuming method in the following case studies.
Regarding the second issue, we have implemented the text in order to explain why we have decided to count a different number of coccoliths. This is essentially related to the number of coccolith that was counted in previous works from the different study areas. This allows for a more comparison between datasets. To address this point we have implemented in the text in Chapter 1, section 1.2 at page 15.
-The reviewer commented: "At page 90, in order to explain the absolute abundances of *E. huxleyi* lower than expected, you invoke the possibility that dissolution occurred. Are these interpretations coherent with the dissolution index you have calculated?" This is a good point. Our hypothesis is in fact consistent with both the CEX index and the planktic foraminifera fragmentation index trends (see paragraph 4.5.2, page 89).

Signature

Chiara Balestrieri

Chiara Balestrieri

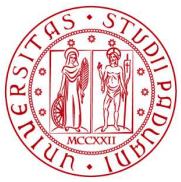

UNIVERSITÀ
DEGLI STUDI
DI PADOVA

Head Office: Università degli Studi di Padova

Department of Geosciences

Ph.D. COURSE IN: Earth Sciences
SERIES XXXI

COCCOLITHOPHORE CARBONATE AND CALCIFICATION DYNAMICS IN THE SOUTHERN AND EASTERN EQUATORIAL PACIFIC OCEANS, DURING THE LAST DEGLACIATION

Coordinator: Prof. Claudia Agnini
Supervisor: Prof. Claudia Agnini
Co-Supervisor: Prof. Patrizia Ziveri

Ph.D. student: Chiara Balestrieri

“If nothing ever changed there would be no butterflies”.

Wendy Mass

“Fate whispers to the warrior: 'You cannot withstand the storm.'
The warrior whispers back, 'I am the storm.'”

Jake Remington

CONTENTS

Summary

Over the last 800 ky the Earth's climate system has been triggered by orbitally- forced oscillations, referred to as glacial- interglacial cycles. However, the detailed dynamics of these cycles, specifically the transition between glacial into interglacial phase, are still to be completely understood. An interesting feature of these phases is that atmospheric CO_2 and CH_4 concentrations are better correlated with Antarctica and Greenland rather than with North Hemisphere temperatures, and this suggests the hypothesis that greenhouse gases are important amplifiers of the orbital forcing in the glacial-interglacial cycles. The cyclicity of biological marine productivity on glacial-interglacial scale observed both in the Pacific and further supports the idea that climate changes are cyclic and control the global carbon dynamics.

Here, we investigate the role played by coccolithophores, a group of calcifying phytoplankton tightly connected to the global climate through the carbon cycle, during the last deglaciation in the Southern Ocean and Eastern Equatorial Pacific. The present thesis focuses on Termination I (TI), the latest warming event that the Earth has experienced, with the final aim to provide new insights on climate dynamics that are not still completely understood. In this PhD thesis, the response of calcareous phytoplankton to increased temperatures (global warming), shifts in the carbonate system (ocean acidification) and enhanced water column stratification (as a response to the increase in temperatures) have been analyzed. Our results are based on sediment samples recovered from two sites located in the South Atlantic area of the Southern Ocean (ODP1089 and PS2498-1; Chapters 2,3,4) and one in the Eastern Equatorial Pacific Ocean, off the coast of Ecuador (Site ODP1238; Chapter 5). These three case studies allowed an evaluation of the repeatability of our analyses (Chapter 2) and, more importantly, a better comprehension on several aspects related to coccolithophore community evolution and coccolith carbonate production such as: 1) the coccolith absolute abundances, 2)the components of the nannoplankton assemblages, the changes in coccolith mass and calcification dynamics of *Emiliania huxleyi* and 3) the main morphological / environmental control factors at high latitudes (Chapter 3 and 4) and low latitudes (Chapter 5).

Overall, the results presented in this thesis suggest that coccolith assemblages at high latitudes are mainly composed by *Emiliania huxleyi* and *Calcidiscus leptoporus*. We propose an enhanced

carbonate counter pump as a trigger mechanism increasing the deep ocean alkalinity in the last glacial at Site ODP1089, and increased pCO_{2sw} during the interglacial at Site PS2498-1. At low latitudes (Site ODP1238), we have observed an increase in calcification is more active in compared to photosynthesis activity during the deglaciation. Finally, the mass and calcification of *E. huxleyi* seem to be controlled by the carbonate system of the entire water column.

Riassunto

L'evoluzione del clima terrestre, durante gli ultimi 800.000 anni è caratterizzata dacicli climatici glaciale - interglaciale (freddo/caldo) forzati da oscillazioni dei parametri orbitali. Tuttavia, la dinamica della transizione tra la fase glaciale e la fase interglaciale rimane non è ancora completamente chiara. Un'importante peculiarità riguardante queste specifiche fasi di transizione è che le concentrazioni atmosferiche di anidride carbonica e metano sono correlate con le temperature registrate in Antartide e Groenlandia piuttosto che con quelle dell'emisfero settentrionale. Questa osservazione supporta l' ipotesi che i gas serra possano giocare un ruolo fondamentale come amplificatori della forzante orbitale per il sistema climatico. A favore di questa ciclicità climatica esistono evidenze legate alla variazioni di produttività osservate sia in Atlantico che Pacifico. In questa tesi di dottorato abbiamo investigato il ruolo dei coccolitoforidi, un gruppo di alghe unicellulari che influenzano il clima attraverso il ciclo globale del carbonio, durante l'ultima deglaciazione nell'Oceano Meridionale e Oceano Pacifico equatoriale orientale. Questo studio si è concentrato sull'ultima Terminazione (TI), che rappresenta l'ultimo evento di riscaldamento climatico che la Terra abbia sperimentato, con lo scopo di cercare di fornire maggiori informazioni sulle possibili dinamiche che si attivano alla transizione tra glaciale e interglaciale.è. Si è quindi considerato questo intervallo per analizzare le possibili risposte del fitoplancton ai processi quali l' aumento delle temperature (riscaldamento globale), la variazione degli equilibri nel sistema carbonatico (acidificazione delle acque) e l'incremento della stratificazione delle acque (come risposta all'aumento di temperature delle acque). I nostri risultati si basano su campioni di sedimento provenienti da due siti localizzati nell'area del sud Atlantico nell'Oceano Meridionale (ODP1089 e PS2498-1; Capitoli 2,3,4) e uno nell'area dell'Oceano Pacifico equatoriale orientale, a largo dell' Ecuador (Capitolo 5). Questi tre casi studio ci hanno permesso di valutare la ripetibilità dei nostri risultati (Capitolo 2) e, sopratutto, di comprendere molteplici aspetti della comunità a coccolitoforidi e delle dinamiche di questo gruppo nella

produzione carbonatica, come ad esempio: 1) le abbondanze assolute dei coccoliti, 2) le loro abboandanze relative, 3) le dinamiche della massa e della calcificazione di *Emiliania huxleyi* e 4) i principali controlli morfologici/ ambientali alle alte latitudini (Capitoli 3 e 4) e basse latitudini (Capitolo 5). In generale, i risultati presentati in questa tesi suggeriscono che l'associazione a coccoliti alle alte latitudini risulta principalmente composta da *E. huxleyi* e *Calcidiscus leptoporus*. Inoltre, si ipotizza che la pompa carbonatica abbia funzionato come fattore d'innesco per aumento di alcalinità della parte piu profonda dell'oceano durante l' ultimo glaciale (ODP1089), e abbia prodotto un aumento della pressione dell'anidride carbonica discolta in acqua durante la fase interglaciale (PS2498-1). Alle basse latitudini (ODP1238), abbiamo osservato un aumento dell'attività di calcificazione rispetto a quella fotosintetica durante la deglaciazione. Infine, l'analisi della massa e del grado di calcificazione di *E. huxleyi* sembra indicare questi due parametri sono controllati dalla chimica delle acque superficiali e profonde.

CHAPTER 1

1.1 Introduction

The aim of this PhD thesis is to improve our understanding on the role played by primary producers in the global carbon cycle in two different but crucial areas of the ocean, the Southern Ocean and the Eastern Equatorial Pacific Ocean, during the last 30 ky with a special emphasis on the glacial-interglacial transition. In detail, this thesis is focused on an abundant and common group of calcareous phytoplankton, the coccolithophores, which lie at the base of the food web and play a fundamental role in the marine biological pumps sequestering and releasing carbon dioxide in the ocean. This complicated processes also influence the ocean alkalinity at sea surface and floor (Raven and Falkowski, 1999; Young and Ziveri 2000; Renaud et al., 2002; Rickaby et al., 2010; Findlay et al., 2011; Sett et al., 2014; Suchéras-Marx and Henderiks, 2014; Martínez-Botí et al., 2015; McClelland et al., 2016; Monteiro et al., 2016; Krumhardt et al., 2017; Balch, 2018; Balestrieri et al., in review).

1.1.1 Millennial-scale glacial-interglacial cycles of the last 800 ka

Since the last ~50 Ma, the Earth's climate has been characterized by a progressive cooling (Zachos et al., 2008). During this cooling phase, ice sheets formed on the Antarctic continent ~40 Ma ago, while the first evidence of Northern Hemisphere (NH) glaciation appeared dated around ~2.6 Ma ago, where alternations between cold-glacial periods and warmer intervals started (Shackleton et al., 1984). Later on, at ca. 1 Ma the so-called Mid-Pleistocene Transition coincides with the occurrence of cycles with a recurrent period closer to 100 ky. (Imbrie et al., 1984; Shackleton et al., 1990; Fig. 1.1). Complementary climate records (deep sea sediments, continental deposits, loess and ice cores) have documented a wide range of climate variability on Earth that have been defined as glacial-interglacial climate changes (Imbrie and Imbrie 1980; Broecker, 1984; Imbrie et al., 1993). It has been shown that much of this variability is related to orbital parameters such as precession, obliquity and eccentricity of the Earth's orbit (Milankovitch, 1941; Berger 1978; Hays et al., 1976; Imbrie et al., 1992, 1993). However, understanding the triggers/forcing active during the glacial/interglacial remains a fundamental issue if we want to comprehend the complicated dynamics of the climate system and their repercussion in the climate evolution. The

atmospheric CO_2 and CH_4 concentrations, which are important climate proxies, nicely correlate with Antarctica and Greenland temperatures respectively (Fig. 1.1; Barnola et al., 1987; Chappellaz et al., 1990) and this indicates that greenhouse gases are important as amplifiers of the initial orbital forcing by contributing to the glacial-interglacial cycle. However, we should be aware that the natural system has been profoundly modified by the human activities that have increased the concentrations of greenhouse gases in the atmosphere. If on one hand we need to understand how the Earth's system works, on the other hand we know that this system has been altered by humans and likely produce a prominent warming in the next centuries (Intergovernmental Panel on Climate Change (IPCC), 2013). In this contest, studying the last deglaciation is of particular relevance, because this climatic transition represents the entry in the latest warm phase that the Earth is still experiencing.

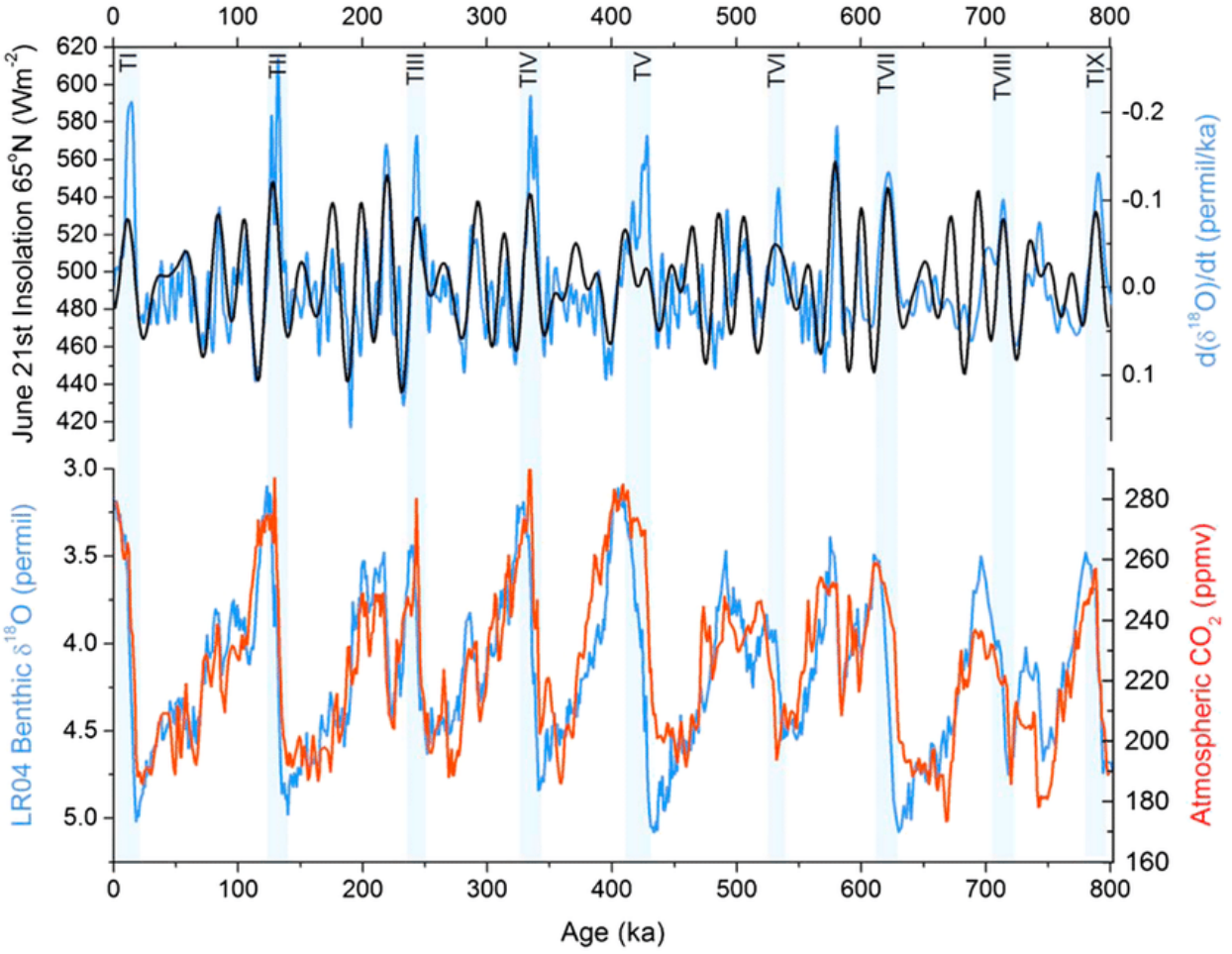

Figure 1.1: Forcing and climate proxies for the last 800 ky. (top) The rate of change of the benthic isotope ratio (light blue), overlying a plot of Northern Hemisphere insolation forcing (black). (bottom) Benthic

LR04 isotope record (blue) (Lisiecki and Raymo, 2005) and ice core CO_2 (red) (Lüthi et al., 2008; Bereiter et al., 2015).

A part from CO_2 data that represent the only direct measurement of CO_2 in the past atmosphere, all the rest of the of paleoclimate proxies, as for instance $\delta^{18}O$, are indirect indicators of paleoenviromental parameters. From their first as paleoclimatic proxy (Emiliani, 1995), oxygen isotopes have been widely used because they are able to reconstruct the complicated evolution of ice global volume through time (Fig. 1.2c; Chappell and Shackleton, 1986). An interesting observation is that climate change observed in the glacial-interglacial regime have caused productivity fluctuations in the ocean (Fig. 1.2d; Arrhenius, 1952; Moreno et al., 2002; Flores et al., 2003; Flores et al., 2012). However, the straightforward reconstruction of productivity trends on glacial-interglacial scale is a quite complicate task because different proxies provide inconsistent results (Charles et al., 1991; Mortlock et al., 1991; Kumar et al., 1995; Ikehara et al., 2000; Latimer and Filippelli, 2001). Moreover, the idea that productivity changes are related to climate evolution, the so-called, the productivity-climate hypothesis, received a considerable support but the validity of this theory for both the Pacific and Atlantic Ocean should be tested (Arrhenius 1952; Parkin and Shackleton 1973; Pedersen 1983). In fact, some sediments do appear to reflect periodic increases in calcite accumulation rate in response to an enhanced biological production of coccolithophores (Arrhenius, 1952; Pedersen 1983; Howard and Prell 1994; Flores et al., 2012; Fig. 1.2). This group displays an articulated biogeographical distribution that is mainly linked to their paleocological affinity, in particular, in mesotrophic/oligotrophic water conditions coccolithophores show their optimum growth (relative abundances; Poulton et al., 2017), being the dominant phytoplankton group, while under eutrophic water conditions, mostly at high latitudes and high nitrate low-chlorophyll zones, coccolithophore production is lower, if still relevant, because in these areas they compete with other primary producers (such as diatoms) (Margalef, 1978). It should be taken in mind that in most of these environments, the total carbonate content of sediments is highly influenced by carbonate biological production that is mainly given by coccolithophores and foraminifera with a minor component that is also related to pteropods and calcareous dinoflagellates; (Salter et al., 2014; Riebesell et al., 2016). Though the carbonate exported to the sea floor comes from different calcareous groups, coccolithophores play for sure the main role and detailed studies on how this important contribution could change is absolutely needed. Accumulation of coccolithophores on the sea floor is controlled by different factors such

as production, dissolution (along the water column and in the sediments), and dilution (from organic and/or terrigenous inputs) so that being able to disentangle the contribution of each of these processes could allow to estimate the real amount of carbonate produced. The variability in $CaCO_3$ production could be related to different processes in different environments. In the photic zone, the carbonate production is mainly controlled by ocean-atmosphere CO_2 exchanges. At deeper depths, the main process affecting carbonates is dissolution (*e.g.,* water column dissolution, interface dissolution before burial below the saturation horizon, pore-water dissolution above the calcite saturation horizon due to respiration CO_2 released to the pore waters) which is able to increase the water alkalinity altering the deep ocean carbonate balance (Broecker 2003b). As CO_2 is exchanged between the ocean and the atmosphere, a combination of physical and biological feedbacks in the Southern Ocean (SO) have been identified as being part of reducing 80-90 ppm of atmospheric CO_2, during the Last Glacial Maximum (LGM), such as: (i) change in the ocean circulation related to the equatorward shift of the Southern Hemisphere westerlies; (ii) enhanced deep ocean stratification playing the role of sequestering carbon in the ocean reservoir, (iii) an expansion of sea- ice that reduced the CO_2 outgassing over the Southern Ocean; (iv) a reduction on the mixing of Antarctic and Artic waters which lead to a major leak of the abyssal carbon; (v) and a reorganization of the biological and carbonate pumps (Stephens and Keeling, 2000; Sigman et al., 2010; Ferrari et al., 2013; Gottschalk et al., 2015; Martínez-Botí et al., 2015). If the SO was highly stratified, likely characterized by reduced water ventilation and/or a more efficient biological pump (probably boosted by iron fertilization) and able to sequester a high amount of carbon, the Eastern Equatorial Pacific Ocean was characterized by a reduced delivery of carbon, caused by a diminished transfer of intermediate water within the Oceanic tunneling leakage from the SO (Keeling and Visbeck, 2001; Liu & Yang, 2003; Martínez-Garcia et al., 2009; Martínez-Botí et al., 2015).

In this PhD thesis, we aim to reconstruct the role played by coccolithophores in the carbonate production during the last deglaciation in two areas of the ocean (Southern and Eastern Equatorial Pacific Oceans) which seemed to have played a central role in the ocean-atmosphere CO_2 exchanges. Finally, we also aim to analyze the coccolithophore mass, morphometry and calcification dynamics in order to detect the possible environmental parameters that may have controlled the carbonate production.

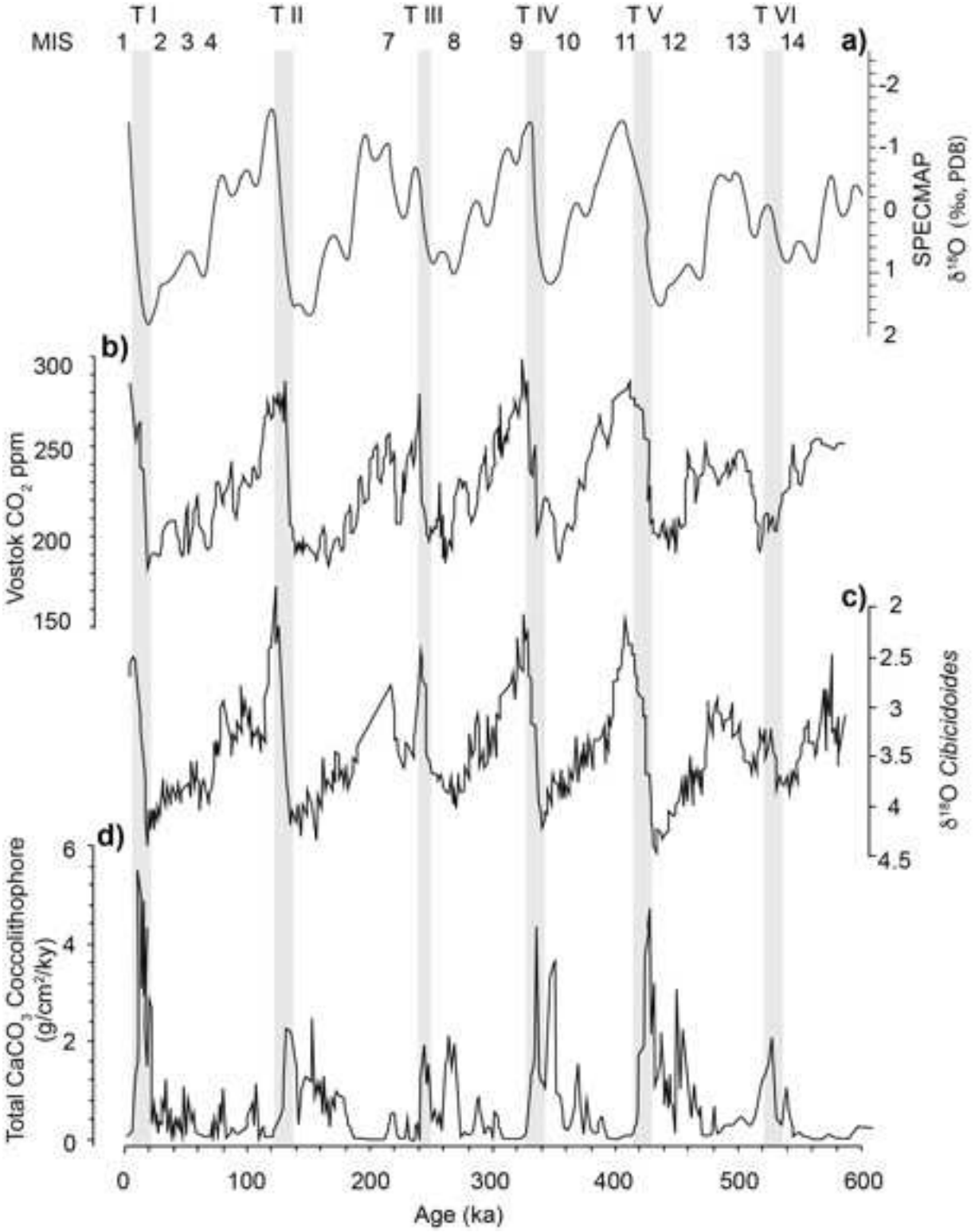

Figure 1.2: Paleoclimatic proxies for the last 600 ky. a) SPECMAP $\delta^{18}O$ (Imbrie et al., 1984); b) CO_2 content in the Vostok ice core (Siegenthaler et al., 2005); c) $\delta^{18}O$ *Cibicidoides* at Site ODP1089 (Hodell et al., 2001); d) estimation of the coccolithophore carbonate content at Site ODP1089 (Flores et al., 2012).

1.1.2 Coccolithophores

Coccolithophores, a group belonging to the class of Prymnesiophyceae (Billard and Inouye, 2004), are highly important marine calcareous phytoplankton organisms. They have played an important role in carbon cycle both in the inorganic and organic carbon pumps since their first appearance in the Triassic (~225 Ma ago; Bown et al., 2004; Fig. 1.2). In the modern ocean, ca. 280 species have been recognized based on the morphological characters of their skeletons (Young et al., 2003), which are the main constituent of the carbonate sediments deposited at the sea floor of the oceans. Coccolithophore cells secrete a coccosphere which covers the organisms and consists of microscopic platelets of calcium carbonate called coccoliths. When the organism dies, attached to marine snow or packed into the fecal pellets of copepods, it falls through the water column and eventually reaches the sea floor (De Vargas et al., 2007). The pelagic rain of these organisms is very important in the marine carbonate system because only part of the organic and inorganic carbon originally produced by these algae finally enters the geologic record as sediments (calcareous deep-sea ooze), where they represent 40-60% of the carbonate deposits in the tropical oceans but also at higher latitudes (Balch et al., 2007, Köbrich, 2008; Broecker and Clarck, 2009). The chemical interaction between coccolithophores and ocean waters altered the ocean alkalinity and the ocean /atmosphere CO_2 exchanges. The two biogeochemical pumps control the atmospheric CO_2 levels: 1) the alkalinity pump or carbonate counter pump which produces particulate inorganic carbon (PIC), is related to the secretion of coccoliths. If calcification is high, total alkalinity and the abundance of dissolved inorganic carbon (DIC) in the euphotic zone decrease while the CO_2 dissolved in the sea water increases. During calcification, for every mole of $CaCO_3$ produced, 2 mol of HCO_3^- are consumed and 1 mol of CO_2 returns to the ocean (Gattuso et al., 1995). 2) The biological pump which produces particulate organic carbon (POC) through the photosynthesis consuming CO_2. Therefore, the net effect of coccolithophores on atmospheric CO_2 depends on the balance between the increase of CO_2 caused by the alkalinity pump and the decrease of CO_2 promoted by biological pump (Fig. 1.3; Rost and Riebesell, 2004). Carbon dioxide is a greenhouse gas and its increase in abundance in the ocean-atmosphere system produces two main effects, warming and and ocean acidification (OA; The Royal Society, 2005). The increase of seawater CO_2 concentrations affects the equilibrium among the different species of the dissolved inorganic carbon (CO_2, CO_3^{2-} HCO_3^-) causing the decrease of [CO_3^{2-}] and thus the lowering of the

pH (Langdon et al., 2000). Since the calcification of coccolithophore is highly sensitive to low pH values, coccolithophores are expected to be extremely susceptible to OA (Meyer and Riebesell, 2015) especially in polar waters where low temperatures cause higher solubility of CO_2 (Yamamoto-Kawai et al., 2009). However, despite all, coccolithophores thrive in a wide variety of ecological niches, occupying eutrophic to oligotrophic marine, cold to warm, dull to lit, and mixed to stratified environments. In these different niches, the growth rate is different because it depends on multiple and synergic environmental parameters, both physical and biological, these are: temperature- dependent growth optima (Balch, 2004), micronutrients and trace elements concentrations (Nöel et al., 2004; Segovia et al., 2018), competition and grazing with other phytoplankton species (Brussard et al., 2004; Frada et al., 2008, 2012; Harvey et al., 2015). Among trace elements, the iron is the particularly important because is a limiting factor for the coccolithophore growth rate, and this becomes crucial especially with low pH values, conditions at which the accessibility of Fe to phytoplankton is reduced (Martin & Gordon, 1990; Martin et al., 1994; Marchetti & Maldonado, 2016). This is particular important in areas such as the Southern Ocean and the Eastern Equatorial Pacific Ocean, in which iron appears to be a key trace nutrient for increased growth rates in coccolithophores (Balch et al., 2011; Balch et al., 2016) and enhanced carbonate counter pump (Salter et al. 2014; Rembauville et al., 2016; Balestrieri et al., in review.). Recently, it has also been demonstrated that calcification can be favor by the availability of silicon. Some species as for instance *Coccolithus pelagicus* and *Calcidiscus leptoporus* show a silicon dependency that *Emiliania huxleyi* and *Gephyrocapsa oceanica* do not seem to have (Durak et al., 2016).

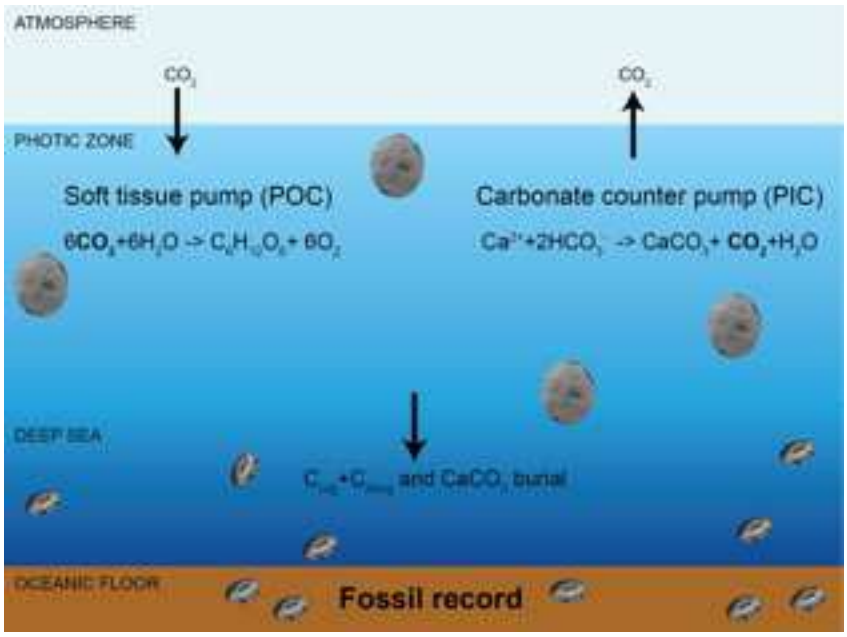

Figure 1.3 (previous page): Coccolithophore interactions with the carbon cycle (C_{org}= organic carbon, C_{inorg}= inorganic carbon) through photosynthesis (soft tissue pump) and calcification (carbonate counter pump) with the particulate organic carbon (POC) and particulate inorganic carbon (PIC) production, respectively.

Though global and regional estimates of calcification rates show contradictory results. Beaufort et al. (2011) showed decreased calcification in coccolithophores at low pH, while other authors (Grelaud et al., 2009 and Balestrieri et al., in review.) showed higher rate of calcification with increasing pCO_2. These contradictory results suggest that the response of coccolithophores is not the same for all the taxa but is rather species-specific and this will make any estimate/prediction on the responses of coccolithophore to future OA difficult. Pelagic calcifiers (coccolithophores and foraminifera) dominate the global ocean carbonate production with estimates of the total carbonate production varying from 0.6 to 1.08 Pg PIC y^{-1} (Smith & Gattuso, 2011) and 1.6 Pg PIC y^{-1} (Balch et al., 2007; Smith & Mackenzie, 2016; Fig. 1.4).An important consideration on the amount of carbonate preserved with respect to that originally produced is that if the the photosynthesis -calcification ratio is of ca 0.011-0.031 in equilibrium conditions (Sarmiento et al., 2002; Balch et al., 2018), and the calcification rate of 1.6 Pg PIC y^{-1}, only 9% of PIC should remain preserved (1.46 Pg PIC y^{-1}; Smith & Mackenzie, 2016; Fig. 1.4).

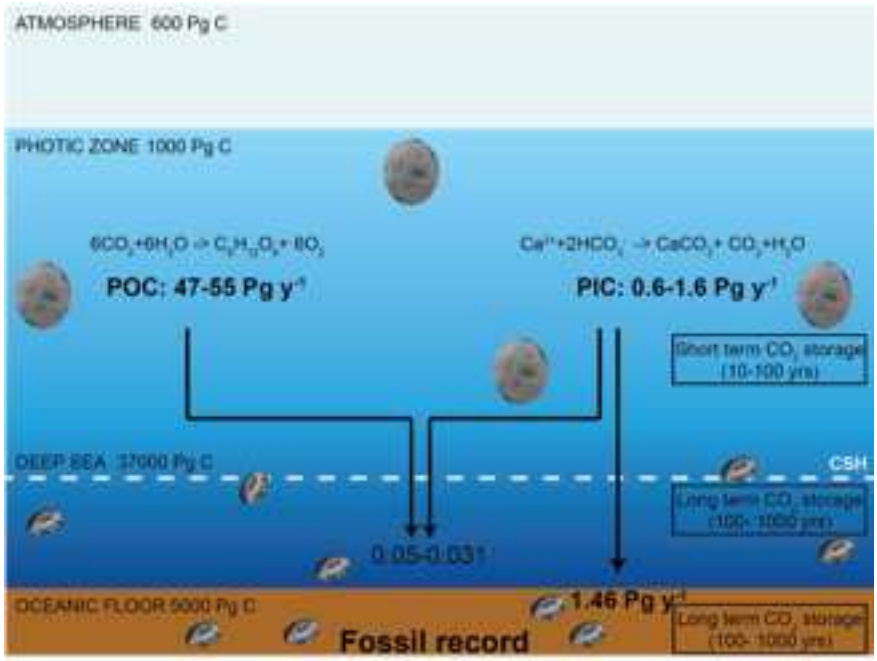

Figure 1.4 (previous page): Coccolithophore interactions with the carbon cycle through photosynthesis and calcification. Particulate organic carbon (POC; 47-55 Pg y^{-1}) and particulate inorganic carbon (PIC; 0.6-1.6 Pg y^{-1}) (Balch et al., 2018). After dissolution effects (below the Carbonate Saturation Horizon, CSH) the PIC quantity is 1.46 Pg y^{-1}. PIC:POC ratio quantity is estimated between 0.05-0.031 (Sarmiento et al., 2002). We also indicate the approximated sizes of reservoir expressed as petagrams of carbon (Pg C: 1 Pg= 10^{15} g= 1 gigaton), (Zeebe and Ridgwell,2011).

1.1.3 The Southern and Eastern Equatorial Pacific Oceans

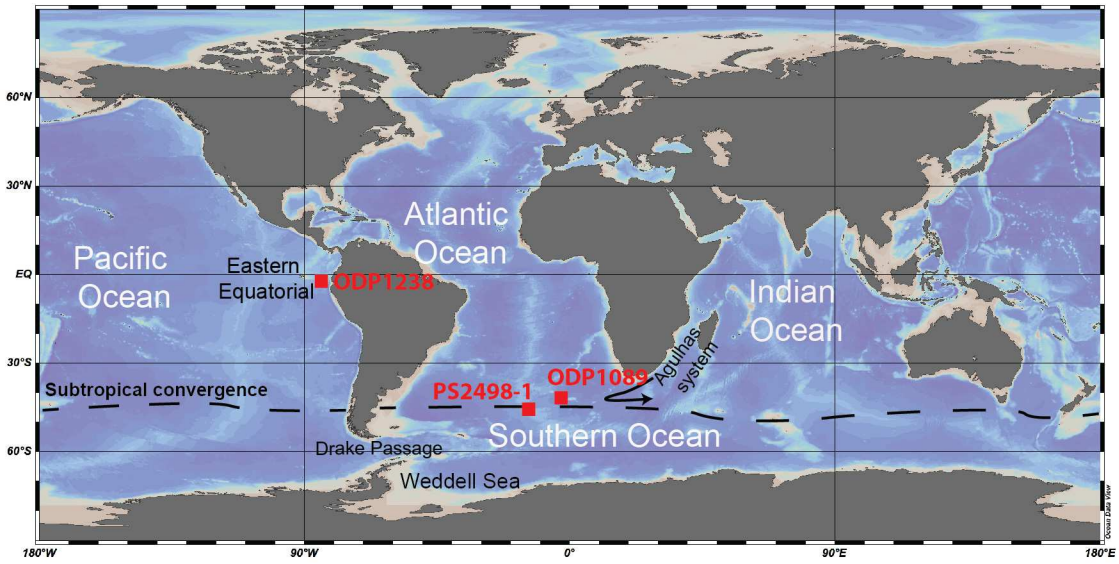

Figure 1.5 (previous page): Map of the Global Oceanic System and the sub-systems: Agulhas System, Drake Passage, Weddell Sea and Eastern Equatorial Pacific Ocean (World Ocean Atlas 2013; Ocean Data View). The Southern Ocean is bounded to the north with the Subtropical Front (~ 45° S; Mejía et al., 2014). In red the three ODP Sites considered for this thesis (ODP1238, PS2498-1, ODP1089).

The Southern Ocean (SO) and the Eastern Equatorial Pacific Ocean (EEP) are two high-nitrate, low-chlorophyll (HNLC) zones of the global ocean. This condition is mainly characterized by the persistence of high nutrient concentrations (nitrate and phosphate) in the sea surface throughout the year. The eutrophic condition of these water masses is however characterized by micronutrient (iron) limitation, which prevents the full biological utilization of the nutrients (Hart, 1934; Martin & Fitzwater, 1989) effectively present in the waters. This peculiar feature is called the iron hypothesis and has been tested in the Subarctic Pacific, Southern and Equatorial Pacific oceans through small-scale live experiments (de Baar, H.J.W. et al., 1990; Martin & Gordon, 1990; Martin et al., 1994; Watson et al., 1994), which have evidenced for Subantarctic high fluxes of both organic and inorganic carbon (Salter et al., 2014; Rembauville et al., 2017). The Southern Ocean is today an area of strong upwelling which bring to the surface high concentration of carbon and nutrient waters. From the paleoceanography point of view, the presence of the westerlies controls the eastward Antarctic Circumpolar Current (ACC) by shifting its direction to the north and to the south during glacial/interglacial cycles (Mejía et al., 2014) and allowing for the Aeolian delivery of micronutrients on the surface waters. In the Southern Ocean, south of the Polar Front, this water mass is fed by cold Circumpolar Deep Water that is enriched in silicon and, to a lesser extent, iron (Balch et al., 2018). These conditions favor the dominance of large diatoms (Brzezinski et al., 2011). Successively, the Ekman pumping shifts this water mass equatorward as Subantarctic Mode Water (SAMW). Finally, SAWW, which is the residue of the ACC, sinks at the Subtropical Front but before it creates the environmental conditions (low iron and nitrate concentration) for coccolithophore grow that this stage (Balch et al., 2018). This water mass goes further down and become an intermediate water able to affect thermocline/ nutricline of the low-latitude oceans, such as for instance the EEP Ocean (Toggweiler et al., 1991; Martínez-Botí et al., 2015). This complicated connection, referred as to the Oceanic tunneling of intermediate waters, connects high latitudes to low latitude waters, the latter thus inheriting the geochemical and thermal features of the SO (Fine et al., 1994). The EEP ocean is at present one of the main oceanic CO_2 source for the atmosphere (Takahashi et al., 2009) and the likely reduced connection with the SO during the glacials could have resulted in a lower amount of CO_2 arriving in EEP. This hypothesis is based

on the fact that during the glacial the SO has acted as a carbon reservoir through a higher efficiency of biological pump/ enhanced coccolithophore carbonate pump which was able to store carbon. During interglacials, the connection between SO and EEP is reactivated and an enormous amount of carbon was transported from the high latitudes of the Atlantic Ocean to the equatorial latitudes of the Pacific Ocean and the eventually released to the atmosphere (Keeling & Visbeck, 2001). So, investigating these two important areas is crucial because, though they are far apart, they are connected through a complicated current pathway and thus able to play an important role in the carbon cycle dynamics that may have forced the climate evolution during glacial/interglacial transitions.

1.1.3.1 Carbonate system characteristics in the Southern and Eastern Equatorial Pacific waters

The intermediate ocean waters are usually oversaturated with respect to carbonate up they reach the calcite saturation horizon (CSH with Ω=1.0; Fig. 1.4; Ridgwell and Zeebe, 2005). In principle, the saturation state of oceans is controlled by Ca^{2+} and CO_3^{2-} concentrations. but the long residence time of calcium (10^6 years) allows to assume that its concentration has remained unchanged on glacial cycle time scale (~10^5 yr). In contrast, the dissolved inorganic carbon (i.e. CO_2, HCO_3^- and CO_3^{2-}) changes on a timescale roughly equal to that this scale (10^5 yr). In particular, the carbonate ions present in the deep waters make up only the 5% of the total dissolved inorganic carbon and its residence time turns out to be ~5000 yr (Broecker et al., 2003). The decreasing in the [CO_3^{2-}] through the water column is due to the progressive increase in under saturation of waters which finally reach the CSH where no calcite is preserved. Water masses located at intermediated depths (around 1500 m) in the Pacific, Indian and Southern oceans have carbonate ion concentrations of ca. 83± 8 μmol kg^{-1}, while in the Atlantic the concentrations are higher (112± 5 μmol kg^{-1} even considering deeper water masses this is essentially related to the ageing of water masses (Broecker et al., 2003). In the study cores, we discuss the carbonate saturation state and realize that it is controlled by the water depth and local conditions. The next step is to compare carbonate saturation state with microfossils proxy (*i.e.* coccolith dissolution index and foraminifera fragmentation index; Peterson and Prell; 1985; Wu and Berger, 1989; Dittert et al., 1999; Boeckel and Baumann, 2004; Marino et al., 2009; Amore et al., 2012) in order to detect changes in the carbonate systems.

1.2 Objectives

The main objective of this PhD thesis is to understand the role played by coccollithophores in two important areas of the ocean and to assess their relationship/potential influence to the carbon cycle variability within the glacial/interglacial dynamics. In this work we evaluat the post depositional effects on coccolith preservation, in order to infer changes in the carbonate system and hence in the biogeochemical carbon cycles. Recently, these environmental parameters have been under major attention for understanding the dynamic between the connection of different part of the ocean and the atmosphere. Under the ongoing climate change (ocean warming and acidification), primary producers, such as coccolithophores, can play or have played (during the last deglaciation) an important role in the ocean cycles by sequestering or releasing carbon dioxide. The coccolith assemblages were analyzed throughout a combination of qualitative and quantitative techniques: species /morphotype identification and counting using light (LM) and scanning electron microscopes (SEM), image analyses for *E. huxleyi* and *C. leptoporus* coccolith morphometrics, and automated measurements of *E. huxleyi* coccolith mass with the Système de Reconnaissance Automatique de Coccolithes (SYRACO; Beaufort and Dollfus, 2004; Dollfus and Beaufort, 1999). We carried out two different sample preparations (filtration and decantation techniques) for the three different sites because the main aim was to evaluate the absolute numbers of coccolith individuals using high time efficiency methods (decantation rather than filtration method). These counts were useful indeed, in order to get the coccolith actual carbonate contribution to the sediment fraction and hence their accumulation rates in order to understand their dynamics with the seawater carbonate system. We performed different counting methods: we counted the index species versus the total assemblage, which is affected by terrigenous and other microfossil dilution, and the index species versus a fixed number of taxonomically related forms (Rio et al, which makes this method not affected by the sample preservation, dilution and paleoecological exclusion; Shackleton, 1984). These methods have been firstly extensively applied by many authors (Rio et al., 1990; Ziveri et al., 1995; Ziveri et al., 1999; Young and Ziveri 2000) in order to infer ecological changes in the coccolithophore assemblage, post-depositional effects analysis on coccolith preservation within different species and their accumulation rates. We counted different numbers of coccolith in the Atlantic (500 of coccoliths per smear slide) and the Pacific (300 of coccoliths per smear slide) Oceans, due to literature analyses we peformed in order to get a general idea on the amount of coccolith that usually occur in these two different areas.

This thesis includes the Introduction chapter (Chapter 1) and four main chapters. Chapter 2 is based on sediment samples from PS2498-1 (Subantarctic zone). In this first chapter we evaluate the repeatability of our samples by preparing them with the filtration method in order to get the significance level of our data. In Chapter 3, we investigate sediment samples from ODP Site 1089 (South Atlantic) trying to evaluate the coccolith carbonate production and *E. huxleyi* mass dynamics. Chapter 4 is focused on analyzing the coccolith carbonate contribution and the CO_2 produced through the carbonate counter pump. We also analyze changes in the degree of calcification and the axis length of *E. huxleyi* and *C. leptoporus* to explain the causes and the processes involved. Finally, in the last chapter (5) we reconstruct the PIC:POC ratio using data of the *E. huxleyi* mass obtained with the SYRACO. For this analysis we investigate sediment samples recovered from ODP Site 1238 (Eastern Equatorial Pacific Ocean). All of the described coccolith patterns and environmental correlations are discussed in view of the glacial/interglacial variability.

CHAPTER 2

Repeatability of Holocene coccolith absolute abundances using the filtration method (Subantarctic zone)

Abstract

The filtration technique is a common preparation method applied to samples where coccolith absolute abundances will be calculated. We prepared replicas of the same samples collected from a sedimentary succession recovered at Site PS2498-1, which is located in the Southern Ocean and covers the last 19 kyr. We observe that the distribution of the material over the filter membrane is not homogeneous and we test the repeatability of the absolute counts among replicas using the funnel filtration system. The irregular arrangement of coccoliths on the filter is likely controlled by a discontinuous pressure that may have occurred in the water vacuum pump of the filtration system. We also noticed relatively high standard deviations for replicas of the same sample that are likely related to size of coccoliths, this is especially true for *Calcidiscus leptoporus*. *Helicosphaera carteri*, *Emiliania huxleyi* and *Gephyrocapsa muellerae* show relatively similar results.

2.1 Introduction

Absolute abundance data of microfossils, such as calcareous nannoplankton, are becoming a source of valuable data to infer paleoclimatic and paleoceanographic conditions. A precise evaluation of these absolute abundances are important to investigate (i) coccolith ecology (*e.g.* Okada and Honjo, 1973); (ii) coccolith seasonal productions or fluxes (*e.g.* Ziveri et al., 2000; Mejía et al., 2014) and (iii) coccolith species- specific carbon export as part of the global carbon budget in the present and past oceans (Young and Ziveri, 2000). The methods used to obtain an accurate extraction, a good analysis and reliable absolute counts are still in progress and may be subject to improvements (Beaufort, 1991; Bown and Young, 1998; Geisen et al., 1999; Koch and Young, 2002; Herrle and Bollmann, 2004). One of the most common method that has been

proposed and used is a filtration technique that uses a funnel as a tool to convey the sample solution. This method has been first proposed by McIntyre and Bè (1967) and Okada and Honjo (1973) and subsequently modified by many authors (Backman and Shackleton, 1983; Andruleit 1996; Okada, 2000; Bollmann et al., 2002). The application of this method has evidenced for some limits such as the difficulty to adjust the amount of material to be filtered, the uneven distribution of the material over the filter membrane due to air locking in part of the system conduction, the irregular flow velocities of the filtered water (Herrle and Bollmann, 2004; Bollmann et al., 2002). Since these possible causes of bias are difficult to eliminate, it is crucial to understand the accuracy and repeatability that can be obtained among different replicas using a filter funnel system method (Andruleit et al., 1996; Herrle and Bollmann, 2004). In this study we focus on the analysis of replicas of the same samples in order to evaluate the degree of repeatability of the counts performed on different slides and verify that the sole source of error is related to the method preparation.

2.2 Material and Methods

We analyzed 61 samples recovered from Site PS2498-1. The study interval is 132 cm-thick and documents the time interval from 2 ka to 19 ka. The adopted age model is based on ^{14}C values (Martínez-Botí et al., 2015).

2.2.1 Sample preparation

We have followed the filtration technique of Andruleit (1996) based on a device called funnel system (Herrle and Bollmann, 2004); we weighted about 30 mg from dry < 63 μm sediment fraction. This material was put in small glass vials (50 ml). Successively, 40 ml of tap water were added in each vial and the solution was placed in an ultrasonic bath for 30 seconds. At the end, 5 ml of solution was filtered onto polycarbonate membranes (0.45 μm pore size, Millipore®). This procedure has been performed three time in order to have three replicas (A, B, C) for each sample. The filters are placed in Petri plate, put in the ovenand dried at 40 °C for 12 hours. For light microscope analysis a portion of each filter was cut and mounted onto a glass slide, a drop of Canada balsam (density at 20°C: 0.99; ROTH) was placed onto the slide to fixed the sample with a cover slip.

2.2.2 Counting technique

Absolute abundances of all the specimens were detected relative to the unit area of the slide examined (1 mm^2; Crow et al., 1960; Rio et al., 1990a, 1990b) using a ZEISS Axioskop40 and a ZEISS Axiophot transmitted light microscope at 1250X magnification.

2.2.3 Standard deviations

In order to evaluate the repeatability of the different replicas of the same sample, we calculate the standard deviations (σ) using the following expression (Bradley and Copeland, 1957; Altman & Bland, 2005):

$$\sigma = \sqrt{\frac{\Sigma_{i=1}^{N} (xi - xm)^2}{N-1}}$$

where xi is the number of individuals, xm is the mean value and N is the number of observations.

2.3 Results

2.3.1 Material dispersion over a filter membrane

Most filtration devices produce an uneven distribution of the filtered material (Herrle and Bollmann, 2004; Bollmann et al., 2002) but sometimes, when the problem is very relevant and/or the density of the sample is relatively high, the non-homogeneous pattern can be appreciated even at naked eye. In order to detect the distribution of the material in the filter membrane, we first determined the number of coccoliths per field of view (N/mm^2 per FOV) along radial transects, from the center to the outer part of the filter membrane. In 9 samples, the number of counted coccoliths, ranging from 20 to 40 N/mm^2, increases toward the rim of the filter, where the larger coccoliths has been preferentially found (e.g. *Calcidiscus leptoporus*), (*e.g.,* samples 17-19 cm; 71-72 cm; 74.5-76 cm; Figs. 2.1 and 2.2). In other samples the trend observed is opposite with the higher concentration of coccoliths recorded in the central part of the filter membrane but the density does not show a significant variation 35-45 N/mm^2 (sample 24-25 cm; Fig. 2.1). If we compare different replicas of the same sample, the number of coccoliths does not show any systematic trends, with some replicas displaying an increasing pattern (*e.g.,* samples 7.5-9B; 24-

25B; 42.5-44C; 55-57B; 71-72B-C; 74.5-76B) and some others showing a decreasing trend (samples 7.5-9C; 24-25C; 55-57C; 74.5-76C; 77-80B-C; Fig. 2.1 and 2.2). In the samples in which *C. leptoporus* is not abundant the number of coccoliths along the transect (center-rim) of the filter have a more homogeneous distribution, the same trend is generally observed in the different replicas of the same sample (Fig. 2.3). Though differences have been observed in the different replicas, these are not larger than those observed between successive samples with very similar nannofossil composition, this result could suggest that the number of coccoliths counted in a transect is mainly affected by the preparation method, which bias the total number of coccoliths. The taxonomic bias, or the presence of larger coccoliths in the external part of the filter, could instead be easily minimized counting complete transects from the center to the rim of the filter.

2.3.2 Coccolith absolute abundances among replicas

Overall in the different replicas of the same sample, the maximum and minimum number of coccoliths have comparable values, what differs is the distribution along the transect. For example, in Fig. 2.1, 7.5-9 cm replicas are characterized by an average concentration value which is between 30-50 N/mm^2 but the distribution varies between repetitions. In sample7.5-9A the running average is 30-50 N/mm^2 with a maximum peak in center part of the filter. In 7.5-9B the initial value is of ca. 40-50 N/mm^2, but it then it decreases to20 N/mm^2 and finally displays an increasing peak (80 N/mm^2). In the replica 7.5-9C the number of coccoliths in the center of the filter is of ca. 40-50 N/mm^2 but toward the rim it shows a decrease (20 N/mm^2). The variability in the number of coccoliths counted in 1 mm^2 is quite constant (30-50 N/mm^2) and has been observed in most of the analyzed samples (Fig. 2.1), however samples with a lower variation have been also observed (Fig. 2.3). Finally, the replicas of sample 93-95 represent an anomaly with the number of coccoliths /mm^2 that are substantially different among the replicas (Fig. 2.3).

2.3.3 Species- specific absolute abundances

The repeatability of the counts among different replicas is important to test because it guarantees that the results are reliable. This is also important for our study samples from PS2498-1 core located in the Subantarctic South Atlantic Ocean. Preliminary results (Balestrieri et al., in preparation; see Chapter 4) have evidenced that the nannofossil abundances vary substantially between glacial- interglacial phases, from 20 to 40 10^7 CC/g sed respectively. This datum is

possibly caused by the absolute number of coccoliths but also by a change in the relative abundance of Noelaerhabdaceae, Coccolithaceae, Helicosphaeraceae, that typically represent the most common components of the assemblages. This is because the carbonate produced by different taxa can be substantially different. In the following we will analyze the variability of the most common taxa in order to understand the possible effect of the low repeatability on the estimation of carbonate secreted by different taxa. For this exercise, we decided to split *C. leptoporus* into two taxonomic units: *C. leptoporus* small and *C. leptoporus*. Each sample was analyzed among three different replicates (A, B, C).

2.3.3.1 Calcidiscus leptoporus small

High absolute abundances samples (≥ 1000 N/mm^2; samples 7.5-9 cm; 17.5-19 cm; 24-25 cm) show a standard deviation $\sigma = \sim \pm 100$ N/mm^2. It is worth noting that samples 77-80 cm (x_m= 397 N/mm^2) and 93-95 cm (x_m= 141.3 N/mm^2) show a twofold increase ($\sigma = \pm 2x_m$) from replicas A to B (sample 77-80 cm) and from A to C (sample 93-95 cm). These two samples are the only ones that show a doubling in the whole dataset. 97-100 cm and 103-105 cm samples are characterized by low absolute abundances (x_m=102 and 59 N/mm^2 respectively) and the lowest standard deviation ($\sigma = \sim \pm$ 10-20 N/mm^2). The other remaining samples do not show any specific variations (Fig. 2.4).

2.3.3.2 Calcidiscus leptoporus

Samples with low absolute abundances (7.5-9 cm; 17.5-19 cm; 24-25 cm; 77-80 cm; 97-100 cm; x_m= 20, 25, 60 N/mm^2) have an average standard deviation of $\sigma = \sim \pm$ 10-15 N/mm^2, among the different replicas of the same sample. In high absolute abundances samples, the $\sigma = \pm$ 50-100 N/mm^2 (42.5-44.5 cm; 55-57 cm; 71-72 cm; 74.5-76 cm; 93-95 cm; x_m= 600, 440, 290, 348, 115 N/mm^2). The order of magnitude in the different absolute values seem to be steady in its variations (Fig. 2.5).

2.3.3.3 Coccolithus pelagicus and *Helicosphaera carteri*

In all the study samples, we have found low abundances of *C. pelagicus* (10 to 70 N/mm^2). With very low absolute abundances (samples 7.5-9 cm; 17.5-19 cm; 24-25 cm; 42.5-44.5 cm; 55-57 cm; 71-72 cm; 74.5-76 cm; 77-80 cm; x_m= 15, 35 N/mm^2), the standard deviations are low, varying

from ± 5 or < 5, to ± 10-20 N/mm^2. For higher abundances (samples 93-95 cm; 97-100 cm; x_m= 70, 50 N/mm^2; Fig. 2.4) the standard deviation is σ = ± 25 N/mm^2. Worth noting is sample 103-105 cm, which is characterized by high absolute abundances (x_m = 67 N/mm^2) but a very low standard deviation: σ = ± 5 (Fig. 2.6).

The values analyzed from *H. carteri* absolute abundances (≥ 90 N/mm^2) show a regular trend in the standard deviation which is around σ = ± 10 N/mm^2. Two samples (7.5-9 cm and 97-100 cm; x_m= 155 and 82 respectively) are characterized by a higher standard deviation: σ = ± 20; 40 N/mm^2 (Fig. 2.7).

2.3.3.4 Emiliania huxleyi and Gephirocapsa muellerae

High *E. huxleyi* absolute abundances (≥ 300 N/mm^2; samples 7.5-9 cm; 17.5-19 cm; 24-25 cm; 42.5-44.5 cm; 55-57 cm; 71-72 cm; 74.5-76 cm; 77-80 cm) show a standard deviation of σ = ± 50-200 N/mm^2. Low absolute abundances (≤ 180 N/mm^2; samples 93-95 cm; 97-100 cm; 103-105 cm) exhibit a standard deviation that is around ± 5-20 N/mm^2 (Fig. 2.8).

G. muellerae low abundances (x_m= 40-60 N/mm^2; samples 7.5-9 cm; 17.5-19 cm; 24-25 cm) show low a standard deviation: σ = ± 5-20 N/mm^2. On the contrary, when the abundances are ≥ 200 N/mm^2, we calculated σ = ± 50-100 N/mm^2. However, this is not true for 42.5-44.5 cm, 77-80 cm and 97-100 cm samples which have high abundances (x_m ≥ 190 N/mm^2) but a low standard deviation (σ = ± 10-20 N/mm^2; Fig. 2.9).

2.4 Discussion

2.4.1 Sample preparation versus coccolith distribution

The filtration method (funnel system) sometimes lacks in accuracy because of uneven distribution of the material caused by air locking in part of the filter membrane, but also by steps in the procedure that might influence the particle distribution (Herrle and Bollmann, 2004; Bollmann et al., 2002).

Our data show that in different samples and among different replicas, the distribution of the material does not show a systematic trend (Figs. 2.1, 2.2 and 2.3). Bollmann et al. (2002) suggested that the inhomogeneity of the distribution of is likely related to one or more of these causes: the structure of the support sieve, the air locking of parts of the filter membranes, the improper filter

handling and/or the different flow velocities in the filter funnel. These authors have also noticed an increase in non- homogenous distribution of the material that is proportional to the increase in the cells content. Our data evidence that in the 61 of the study samples, there is direct relationship between the uneven distribution of the material on the filter and the absolute abundance of coccoliths. We also noticed that the distribution patterns along the transect are primarily controlled by the most abundant taxa of the assemblages, that could change among different samples. As an example, if *C. leptoporus* is the common species in the assemblage of the investigated sample (Fig. 2.1), the distribution of the coccoliths is higly inhomogeneous. By contrast, when *E. huxleyi* and *G. muellerae* show high absolute abundance, the distribution on the filter is much more homogeneous. These data indicate that the homogeneity of the distribution on the filter membrane is species- specific, with high inhomogeneity usually found in samples where large coccoliths (i.e., *C. leptoporus* and *H. carteri*) are the most important component of the assemblages. This is not the case for the large *C. pelagicus* but this anomaly is probably due to the fact that this taxon always remains an accessory component of the assemblage. This species-specific inhomogeneous distribution could be related to the shock waves originated by the change in the pressure in the rubber tubing, whose suction from the aspirator could produce a not ideal or permanent vacuum conditions. A possible alternative explanation is also that the lateral position of the water vacuum pump could create an asymmetrical suction that might cause the high concentration of large coccoliths but this mechanism would have produced an even stronger influence in small placolith, but this is not the case and thus the hypothesis.

2.5 Conclusions

We have performed replicas from samples retrived at PS2498-1 core in order to understand if the funnel filtration system, a procedure used to prepare calcareous nannofossil slides, could bias the absolute abundance data.

Our data suggest that: the distribution of coccoliths on the surface of the filter membrane is inhomogeneous, this could be related to the formation of shock waves as a response to a change in the rubber tubing pressure. This mechanims could affect the distribution of the large coccoliths especially when they represent an important component of the assembalges; among different replicas of the same sample we did not find any systematic trend in the distribution of coccoliths along a transect.

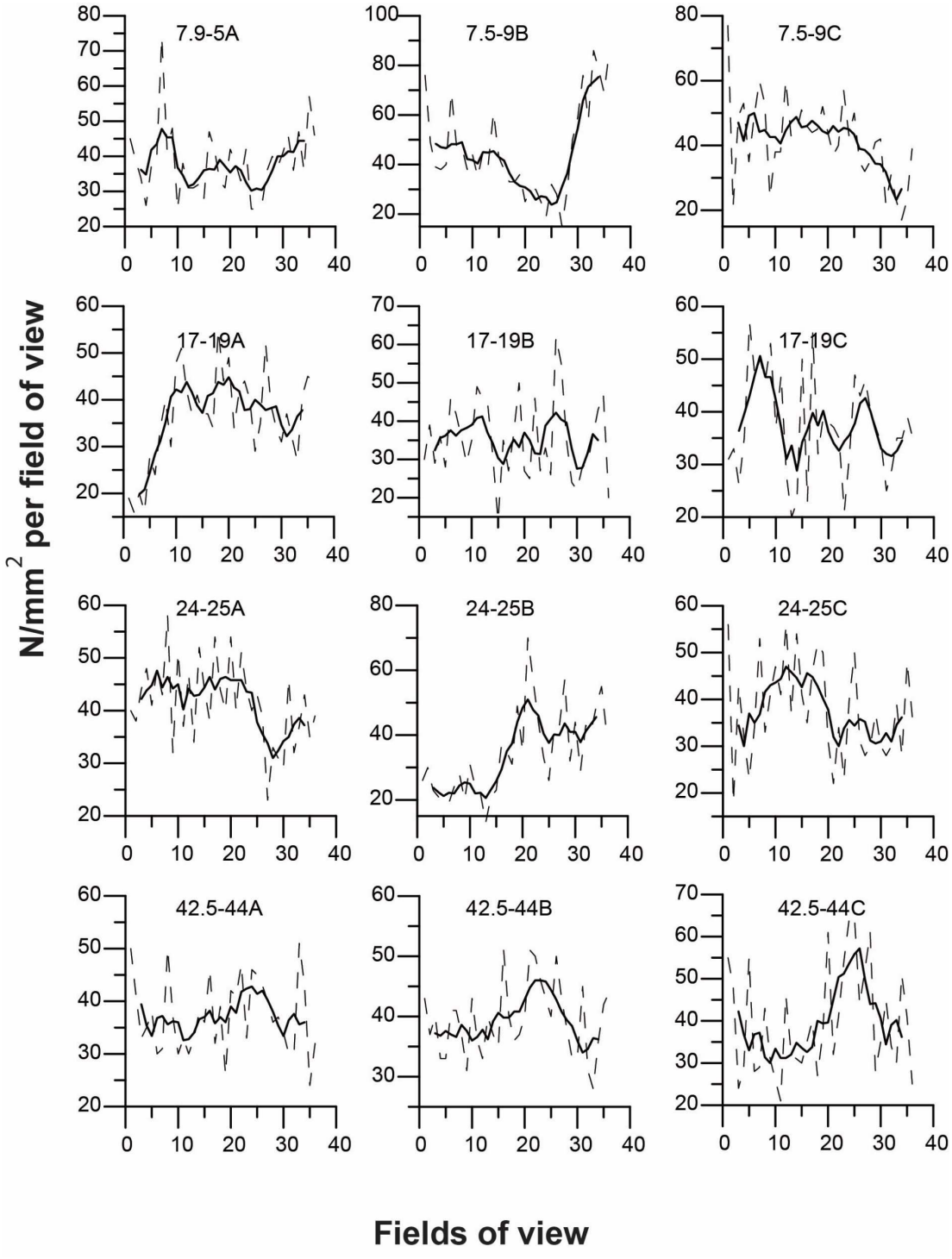

Figure 2.1: Variations per coccolith abundances (N/mm^2) counts per field of view in three replicates (A-B-C). Solid line is the running average (5 window points).

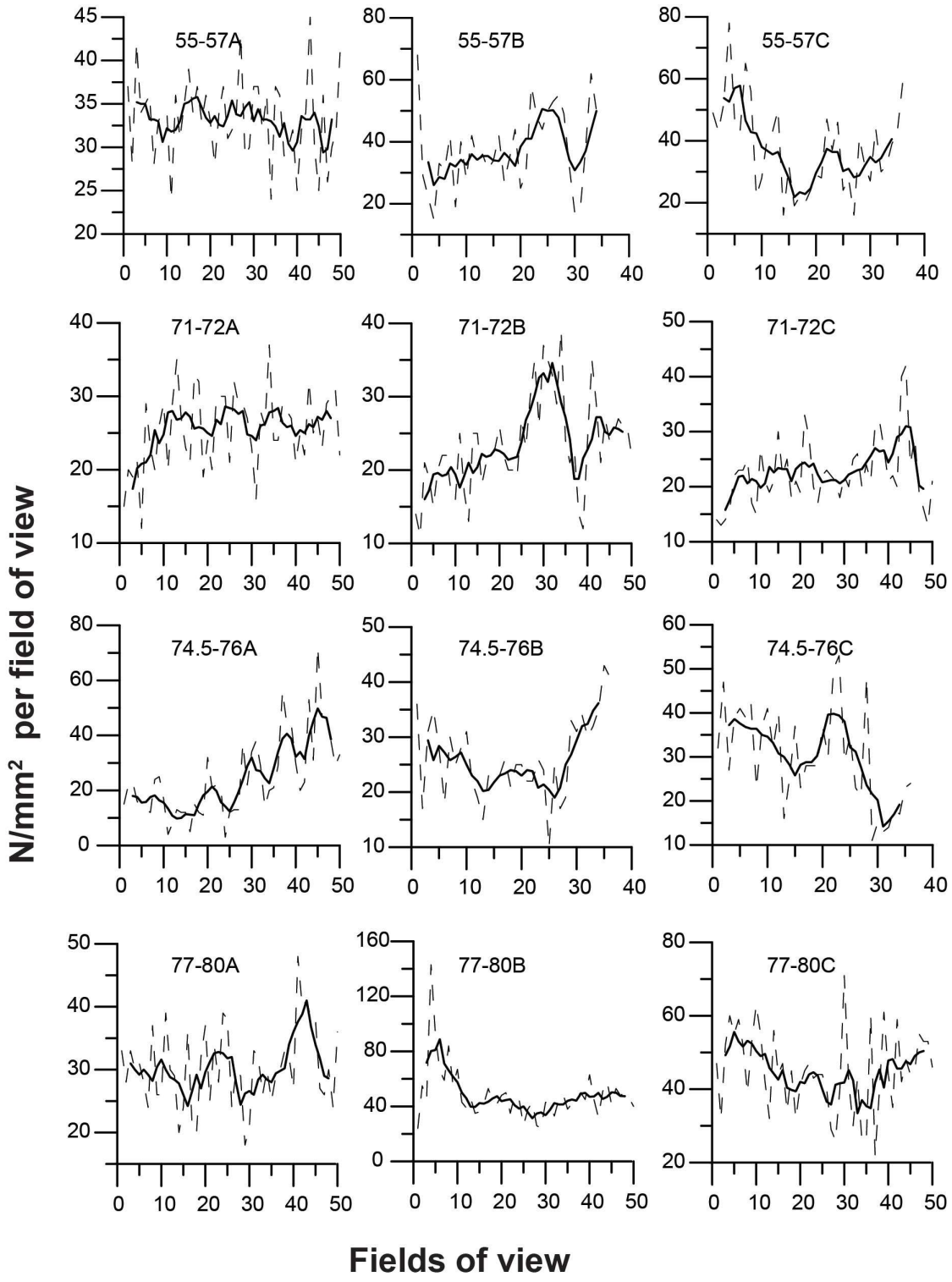

Figure 2.2: Variations per coccolith abundances (N/mm^2) counts per field of view in three replicates (A-B-C). Solid line is the running average (5 window points).

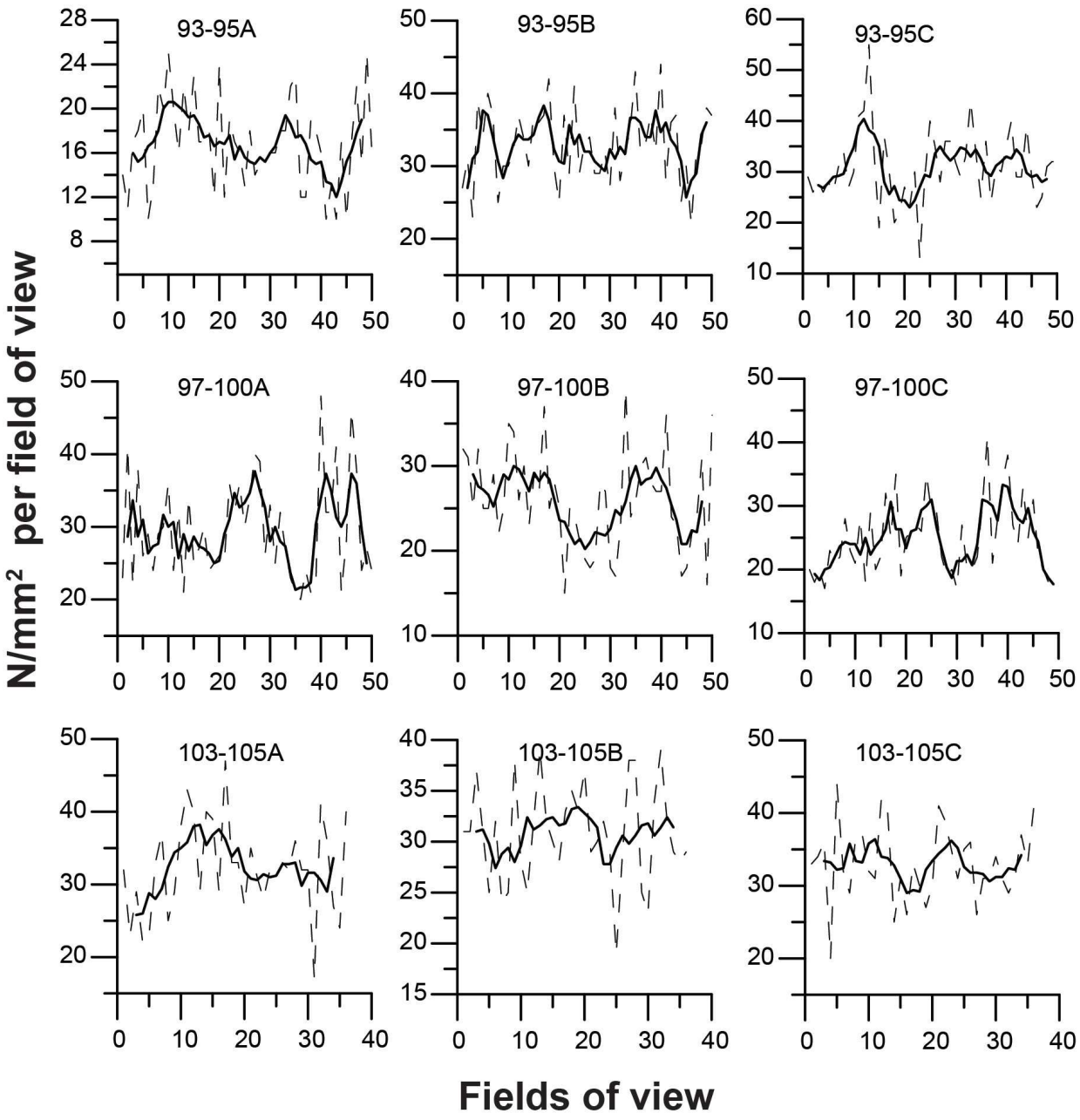

Figure 2.3: Variations per coccolith abundances (N/mm^2) counts per field of view in three replicates (A-B-C). Solid line is the running average (5 window points).

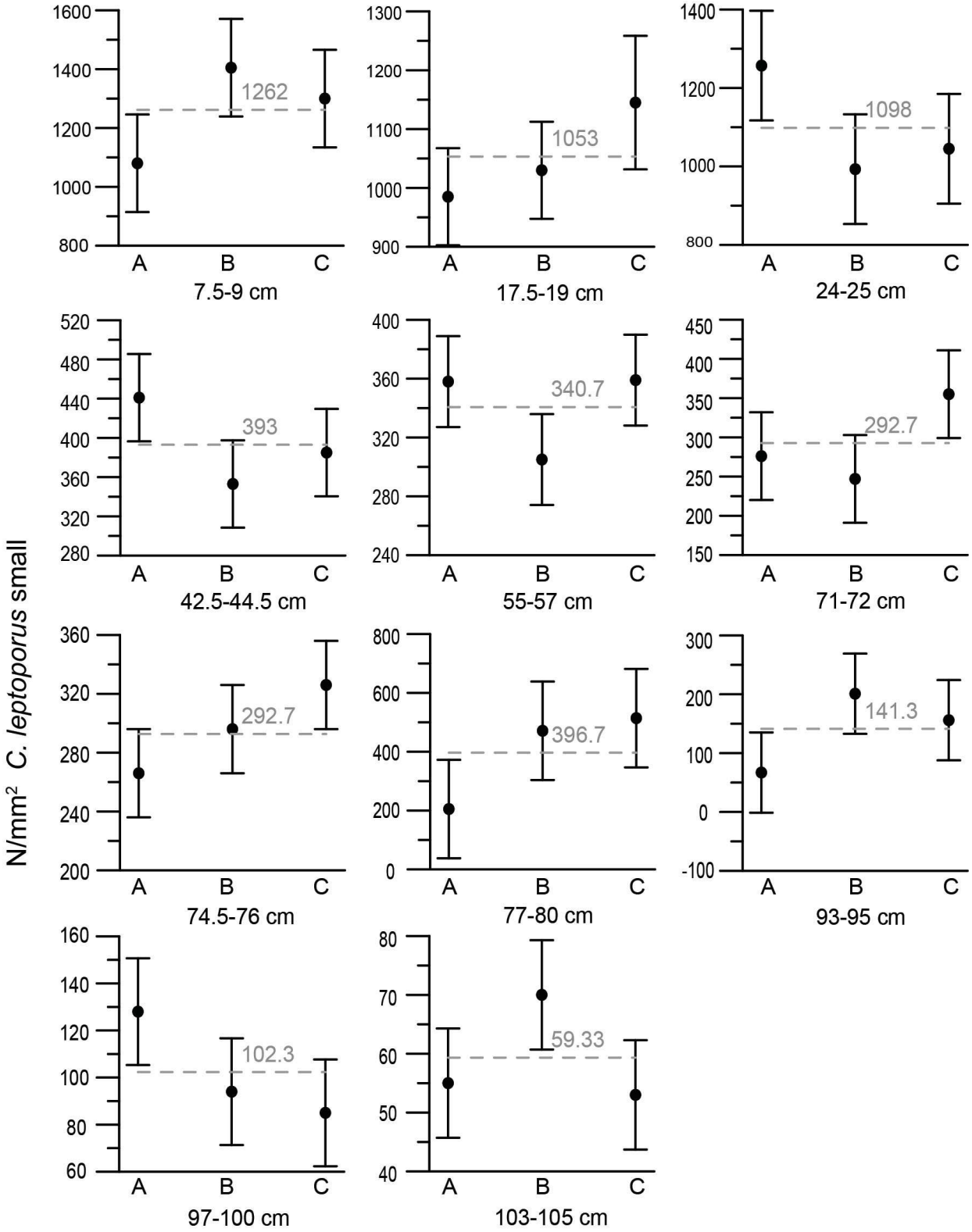

Figure 2.4: *Calcidiscus leptoporus* small coccolith abundances (N/mm^2) counts within the replicates (A-B-C). Grey dashed line represents the mean value for each sample, bars represent standard error of the mean.

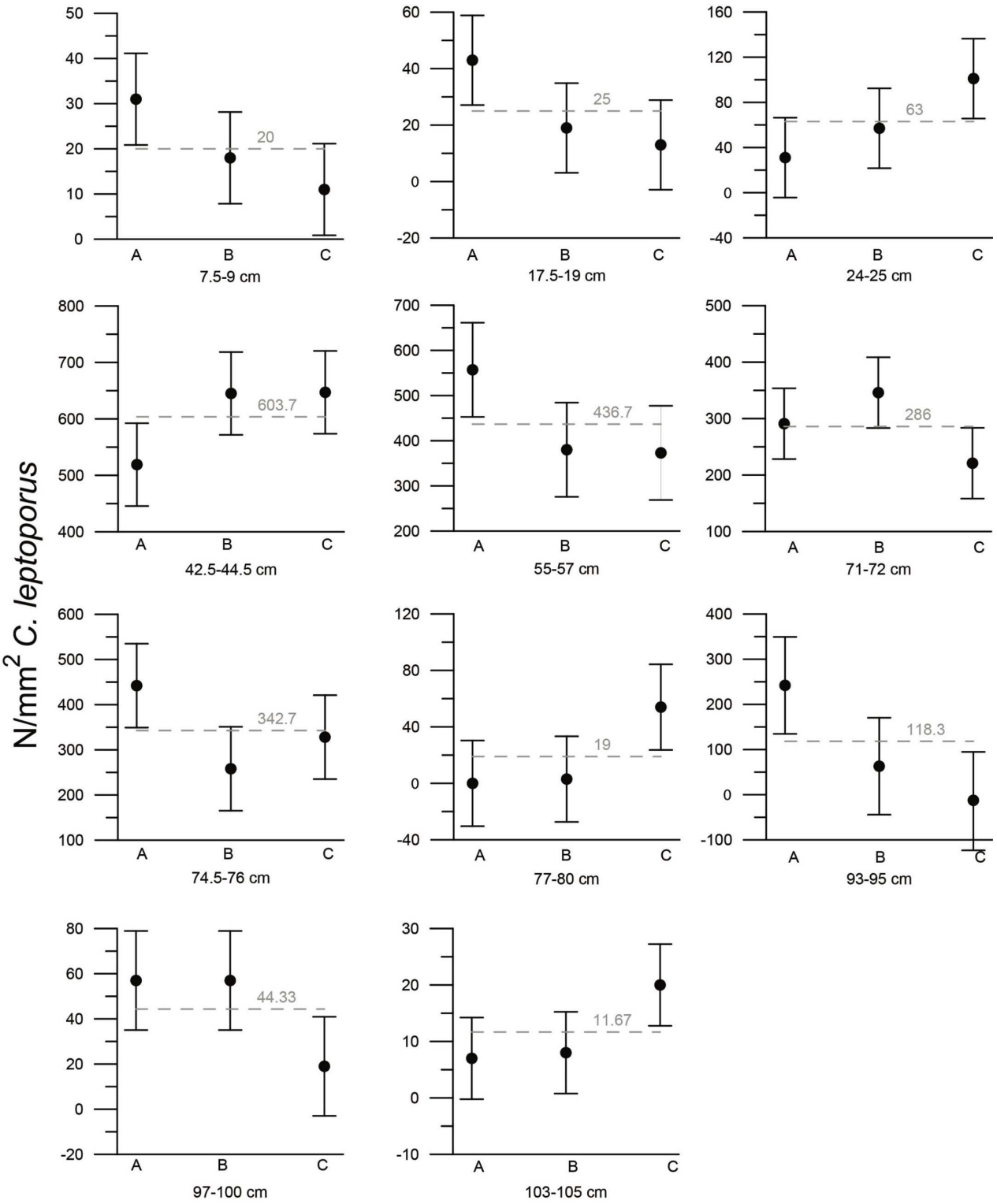

Figure 2.5: *Calcidiscus leptoporus* coccolith abundances (N/mm^2) counts within the replicates (A-B-C). Grey dashed line represents the mean value for each sample, bars represent standard error of the mean.

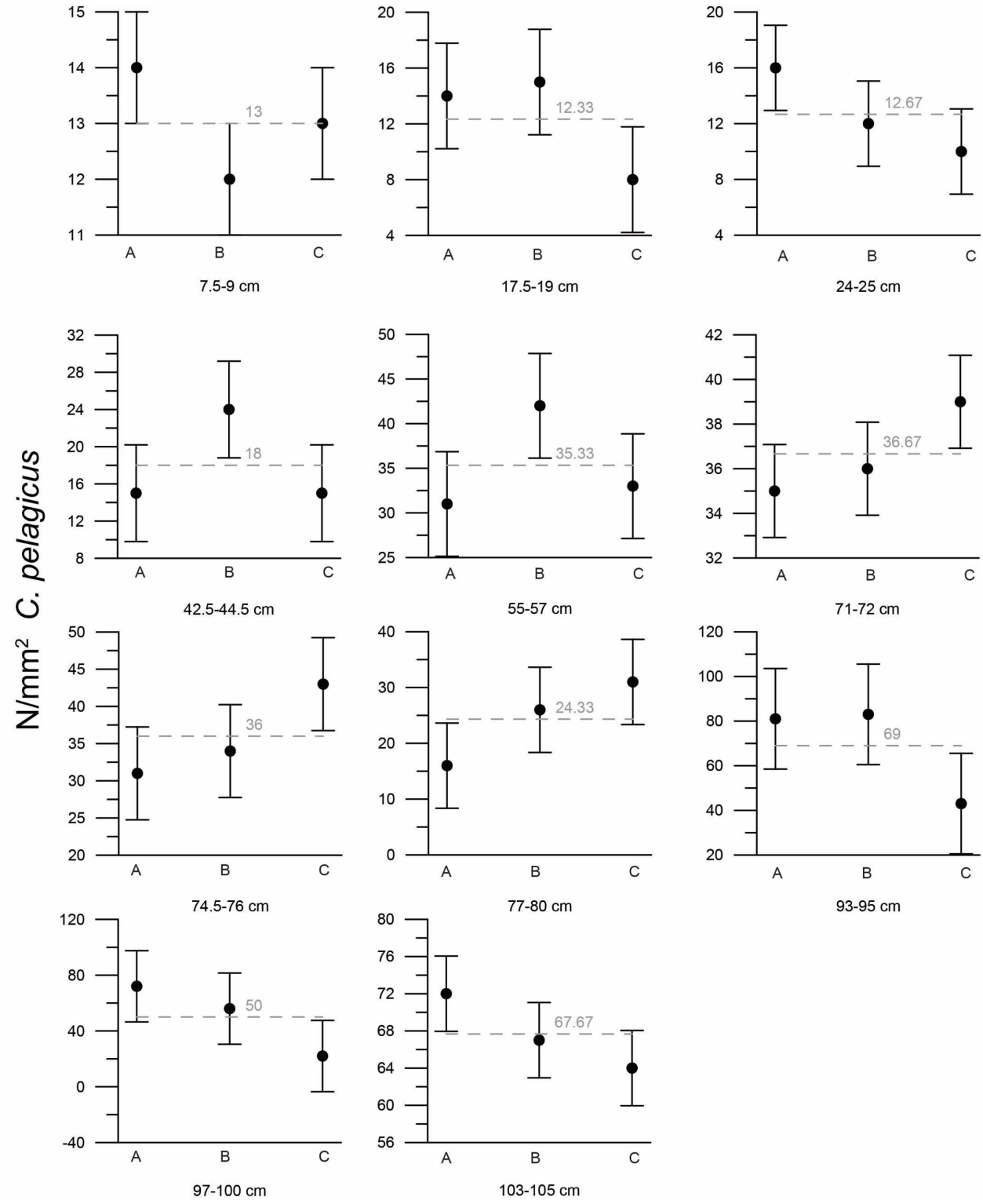

Figure 2.6: *Coccolithus pelagicus* coccolith abundances (N/mm^2) counts within the replicates (A-B-C). Grey dashed line represents the mean value for each sample, bars represent standard error of the mean.

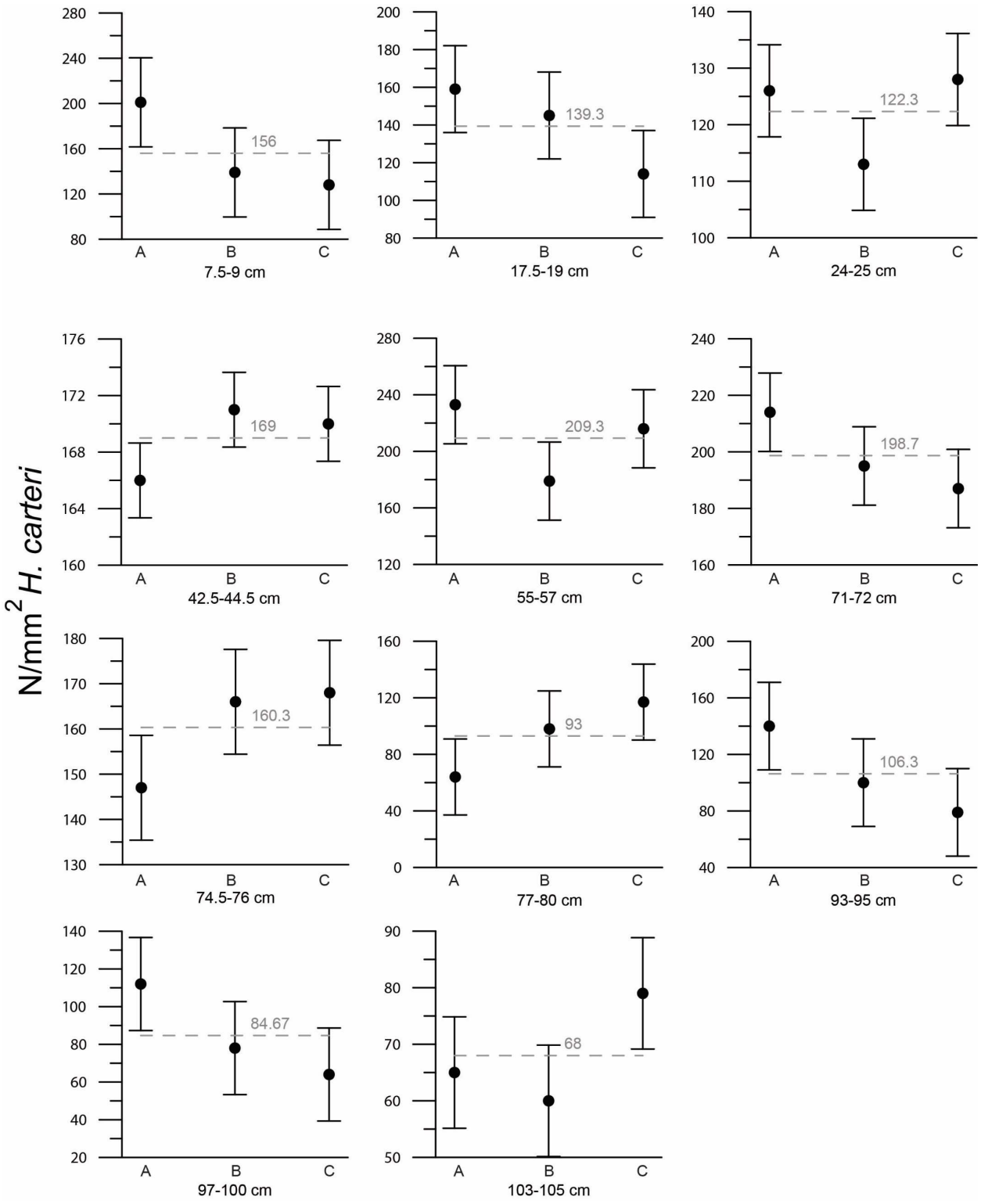

Figure 2.7: *Helicosphaera carteri* coccolith abundances (N/mm^2) counts within the replicates (A-B-C). Grey dashed line represents the mean value for each sample, bars represent standard error of the mean.

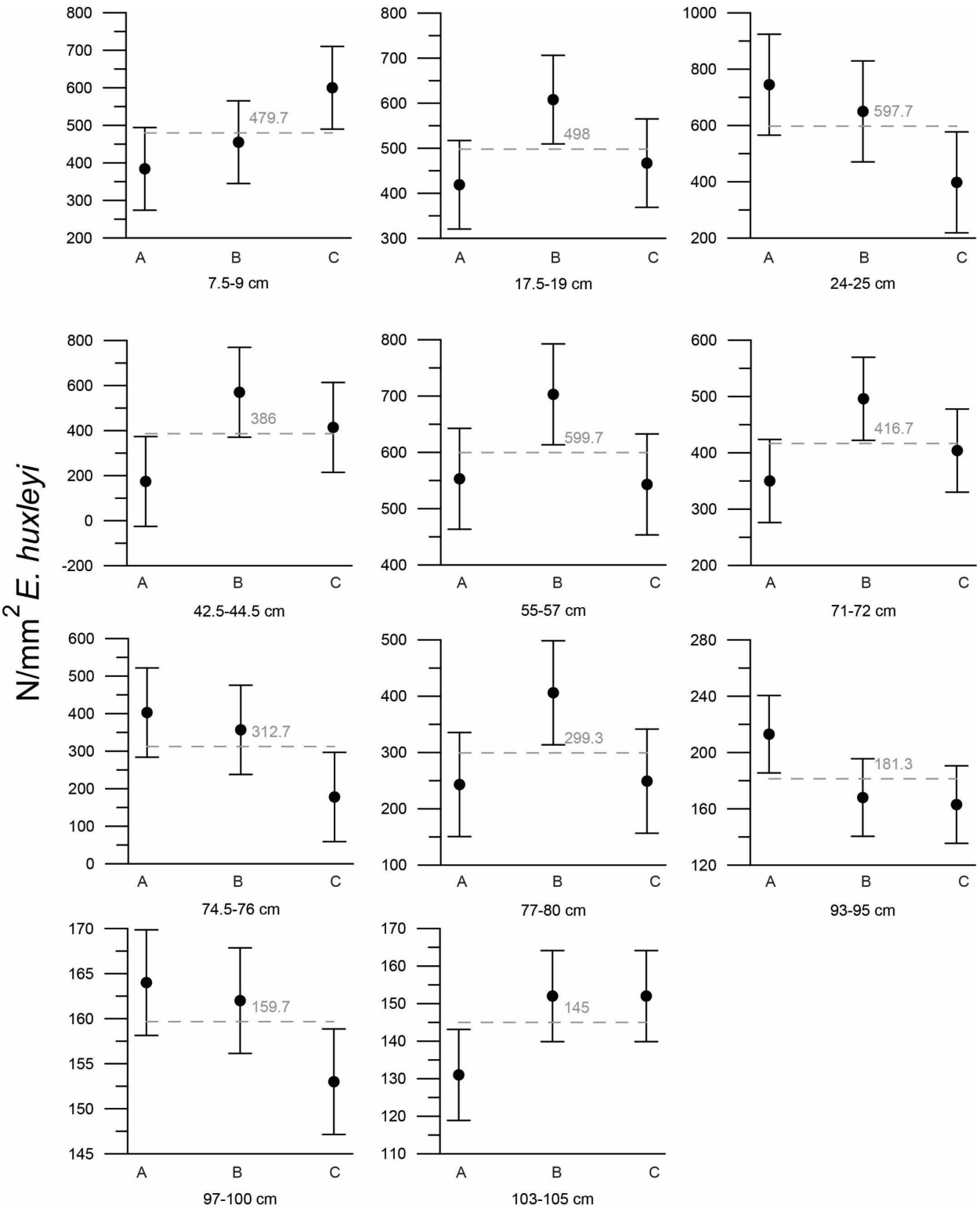

Figure 2.8: *Emiliania huxleyi* coccolith abundances (N/mm^2) counts within the replicates (A-B-C). Grey dashed line represents the mean value for each sample, bars represent standard error of the mean.

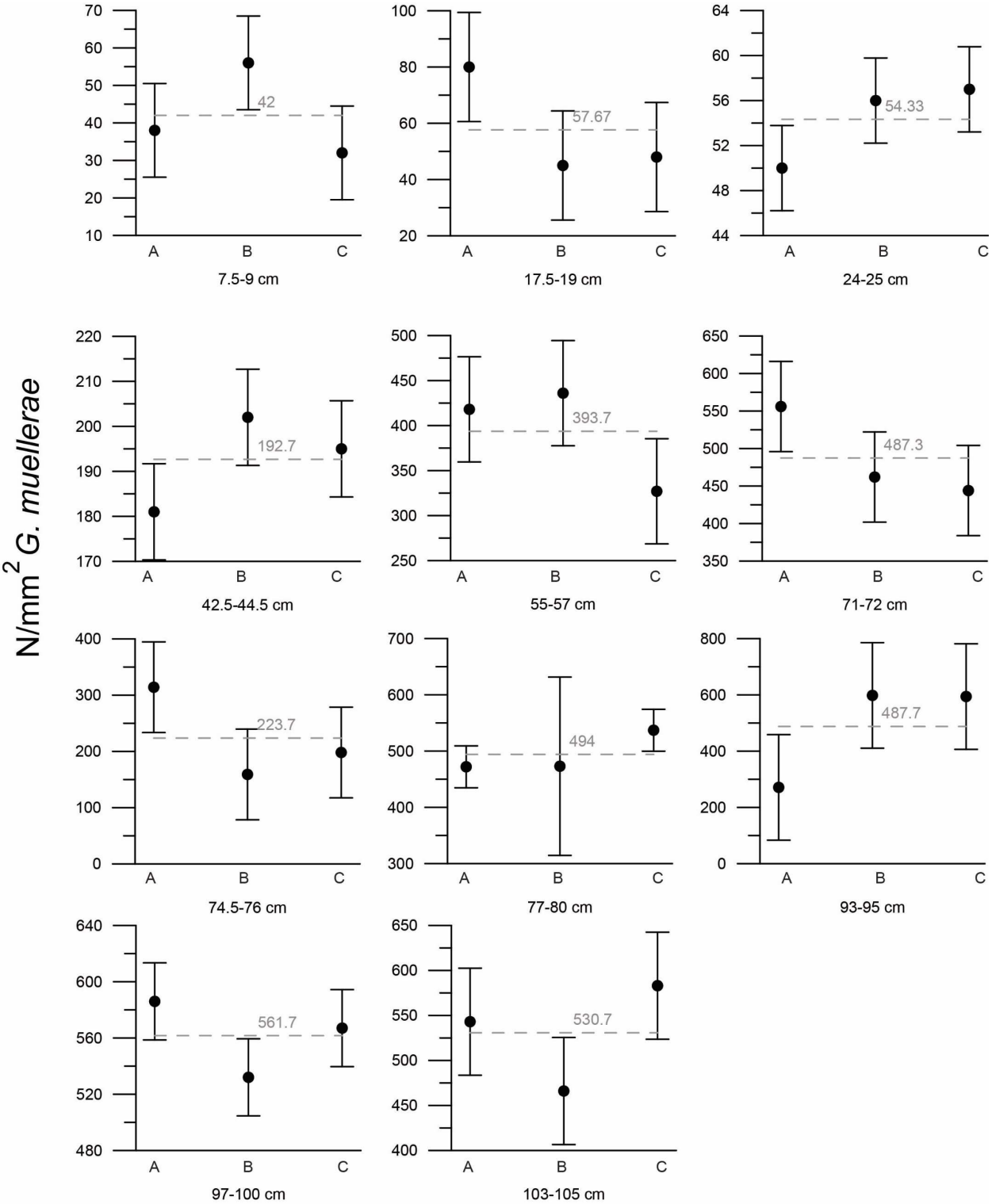

Figure 2.9: *Gephyrocapsa muellerae* coccolith abundances (N/mm^2) counts within the replicates (A-B-C). Grey dashed line represents the mean value for each sample, bars represent standard error of the mean.

References

Altman D.G. & Bland M.J., 2005 Standard deviations and standard errors. BMJ; 331-903.

Andruleit, H., 1996. A filtration technique for quantitative studies of coccoliths. Micropaleontology 42, 403–406.

Backman, J., Shackleton, N.J., 1983. Quantitative biochronology of Pliocene and Early Pleistocene calcareous nannofossils from the Atlantic, Indian and Pacific Oceans. Mar. Micropaleontol. 8, 141 – 170.

Beaufort, L. 1991. Adaptation of the Random Settling Method for Quantitative Studies of Calcareous Nannofossils. *Micropaleontology*, **37**(4): 415-418.

Bollmann J., Cortés M.Y., Haidar A.T., Brabec B., Close A., Hofmann R., Palma S., Tupas L., Thierstein H.R., 2002. Techniques for quantitative analyses of calcareous marine phytoplankton. Marine Micropaleontology 44, 163-185.

Bown, P.R. & Young, J.R. 1998. Techniques. *In:* P.R. Bown (Ed.). *Calcareous Nannofossil Biostratigraphy*. British Micropalaeontological Society Publications Series. Chapman & Hall/Kluwer Academic Press, London: 16-28.

Bradley E. & Copeland, M. D. (1957). Standard Deviation. A Practical Means for the Measurement and Control of the Precision of Clinical Laboratory Determinations. American Journal of Clinical Pathology, 27(5), 551–558. doi:10.1093/ajcp/27.5.551

Geisen, M., Bollmann, J., Herrle, J.O., Mutterlose, J., Young, J.R., 1999. Calibration of the random settling technique for calculation of absolute abundances of calcareous nannoplankton. Micropaleontology 45, 437–442.

Herrle J.O., Bollmann J., 2004, Accuracy and reproducibility of absolute nannoplankton abundances using the filtration technique in combination with a rotary sample splitter. Marine Micropaleontology 53 (2004) 389–404

Koch, C. and Young, J.R., 2007, A simple weighing and dilution technique for determining absolute abundances of coccoliths from sediment samples. J. Nannoplankton Res. **29** (1), pp.67-69, International Nannoplankton Association ISSN 1210-8049 Printed by Cambridge University Press, UK

Mejía, L. M., P. Ziveri, M. Cagnetti, C. Bolton, R. Zahn, G. Marino, G. Martínez-Méndez, and H. Stoll (2014), Effects of midlatitude westerlies on the paleoproductivity at the Agulhas Bank slope during the penultimate glacial cycle: Evidence from coccolith Sr/Ca ratios, *Paleoceanography*, 29,

697–714, doi:10.1002/2013PA002589.

Okada, H., Honjo, S., 1973. The distribution of oceanic coccolithophorids in the Pacific. Deep-Sea Res. 20, 55–374.

Okada, H., 2000. An improved filtering technique for calculation of calcareous nannofossil accumulation rates. J. Nannoplankton Res. 22, 203–204.

Young, J. R. and P. Ziveri (2000), Calculation of coccolith volume and its use in calibration of carbonate flux estimates, *Deep-Sea Research Part II,* 47, 1679-1700.

Ziveri, P., Rutten, A., de Lange, G.J., Thomson, J., Corselli, C., 2000. Present-day coccolith fluxes recorded in central eastern Mediterranean sediment traps and surface sediments. Palaeogeogr. Palaeoclimatol. Palaeoecol. 158, 175–195.

CHAPTER 3

Coccolith carbonate response to Southern Ocean iron fertilization during the last deglaciation

Balestrieri Chiara, Patrizia Ziveri, P. Graham Mortyn, Eliana Fornaciari, Michael Grelaud, Gianluca Marino, Heather Stoll, Claudia Agnini
Under review with *Quaternary Science Reviews, Elsevier.*

Keywords: Holocene, Paleoceanography, Southern Ocean, Micropaleontology, coccolithophores, Iron Fertilization, inorganic carbon pump, carbonate system.

Abstract

The increase in alkalinity hypothesized for the deep Southern Ocean (SO) during the Last Glacial Maximum (LGM) is likely related to the increase in pelagic carbonate export production and compensates the near elimination of shelf areas during the glacial. This along with changes in ventilation of deep ocean could partially account for a drawdown of oceanic atmospheric CO_2. Here, we present a record spanning the last 25 kyr of the coccolith carbonate production from the Subtropical Front in the South Atlantic zone at ODP Site 1089 (40°57'S; 9°53'E). The depth of this Site is 4,620 m, which lies below the lysocline that is presently positioned at 3,690 m in the Cape Basin. On glacial-interglacial scale, this site is characterized by a "Pacific-type" carbonate fluctuations, with high preservation of carbonate during glacial terminations. The coccolith dissolution index (CEX) reveals two intervals of carbonate dissolution coinciding with times of high iron dust, phosphorus delivery and primary production. The coccolithophore assemblages also indicate that the glacial phase is dominated by *Emiliania huxleyi,* an iron and phosphorus driven-opportunistic species and by larger and more heavily calcified taxa as waters become more alkaline. We also observe that the degree of *E. huxleyi* calcification mimics the carbonate saturation state of SO surface waters and that this area of the SO very likely was an alkalinity

source caused by the coccolithophore carbon pump which eventually acts as a trigger of the deglacial rise in pCO_2.

3.1 Introduction

Pleistocene glacial terminations constitute periods of large rises in atmospheric CO_2 concentrations and sea level, changes in ocean circulation and chemistry, and millennial-scale temperature changes that were asynchronous in the two hemispheres (Cheng et al., 2009; 2016). Therefore, these intervals provide valuable insight into the transition of Earth's climate from one climate state to another and into the interaction between orbital and millennial-scale climate processes (e.g., Wolff et al., 2009; Denton et al., 2010; Marino et al., 2015; Pérez-Mejías et al., 2017). Specifically, the patterns of ocean and climate change across the last glacial termination (Termination I [T-I], 18-12 ka BP) are overall well documented globally and well dated in the different palaeoclimate archives, which offers the opportunity to investigate in detail the different processes that characterize a glacial-interglacial transition. It has been shown that atmospheric CO_2 and CH_4 concentrations are nicely correlated with Antarctica and Greenland temperatures, respectively (Barnola et al., 1987; Chappellaz et al., 1990). These greenhouse gas variations, and particularly those in the atmospheric CO_2 concentrations, contribute to the overall glacial-interglacial radiative forcing of climate and are regraded to as an important amplifier of the orbital forcing that leads the termination of a glacial period (Rohling et al., 2012, Journal of Climate; IPCC, 2013). The causes of changing atmospheric CO_2 and past ocean carbon cycling can be inferred by analyzing the temporal $CaCO_3$ dissolution or preservation and the evolution of the calcite saturation horizon (Broecker, 1982a, 1982b; Archer, 1991; Marchitto et al., 2005). However, the role of the calcium carbonate production at the ocean surface and its subsequent export to the deep ocean in the exchange of carbon between the ocean and the atmosphere remains debated and not sufficiently well documented. Here, we want to address this problem and try to give further insight by studying coccolithophore assemblages and carbonate export production dynamics to yield paleoceanographic reconstructions (Klaas and Archer, 2002). Previous works, which focused on coccolith dynamics in the South Atlantic, analyzed the biogeographic distribution of coccolith species and morphotypes in relation to environmental changes (Boeckel et al., 2004, 2006; Cubillos et al., 2007; Mohan et al., 2008). Other authors investigated the contribution of coccoliths

to the carbonate export production to the sea floor during the glacial-interglacial cycles by pointing to the fact that this carbonate export proxy is controlled by productivity (Flores et al., 2012; Mejìa et al., 2014) and dissolution (Flores et al., 2003) harmonized by seawater carbonate chemistry dynamics (Beaufort et al., 2011). In this study we present new coccolith data from ODP Site 1089, located on the northern flank of the Agulhas Ridge, during the last glacial-interglacial transition, (between 25 and 5 ka) to reconstruct the export productivity of this area. ODP Site 1089 occupies a strategic position south of the Subtropical Front (STF) and north of the Antarctic Circumpolar Current (ACC); this allows for the documentation of the paleoceanograghic dynamics during the last deglaciation. We aim to reconstruct changes in coccolithophores carbonate export due to iron fertilization and high phosphorus delivery, which are important features to take into account in order to better understand changes in the carbonate system (Flores et al., 2012; Salter et al., 2014; Rembauville et al., 2016). In fact, an enhanced glacial soft tissue (organic) pump could have driven the high alkalinity documented in the SO, hence increasing carbonate dissolution events which in turn consequently raise the alkalinity budget (Martin and Fitzwater, 1989; Martin J.H.,1989, 1990, 1991; Rickaby et al., 2010). Additionally, the export of $CaCO_3$ as a result of an efficient carbonate pump under iron fertilization (Salter et al., 2014), draws down surface ocean alkalinity (De la Fuente et al., 2017) thus increasing sequestration of carbon and lowering the atmospheric CO_2. This is key for the dynamics of the partial pressure of dissolved CO_2 in surface waters. Specifically, this work elaborates on the changes in the oceanic carbonate system during the last 25 to 5 ka in the STF of the SO by (i) using coccolith assemblages to reconstruct the dynamics of the STF; (ii) reconstructing the productivity and coccolith carbonate export considering the alteration of the proxies by carbonate preservation; and (iii) analysing the influence of productivity and carbonate system on *Emiliania huxleyi* changes in term of morphotypes, mass and calcification.

3.2 Site Location and Oceanographic Setting

ODP Site 1089 was drilled in the southern Cape Basin near the Subtropical Front, at the northern flank of the Agulhas Ridge (40°57'S; 9°53'E; Fig. 3.1) on a sediment drift at 4,620 m water depth, which currently lies below the calcite saturation horizon (CSH, 4,175 m depth, Fig. 3.2). High terrigenous inputs increase the accumulation rate eventually favoring the rapid burial of sediments and preservation of carbonates (Gersonde et al., 2003). In this area, the surface water masses can be divided into two large-scale circulation systems: the anticyclonic motion controls the northern

to central South Atlantic around the South Atlantic high-pressure field (cross equatorial surface water transport of waters from the South Atlantic gyre into the North Atlantic Ocean) and the Southern South Atlantic with the adjoining Atlantic Sector of the SO in which the strong westerlies induce the eastward-directed Antarctic Circumpolar Current (ACC) that characterizes the Atlantic sector and the SO in general (Boeckel et al., 2006). The ACC has a complicated structure, which is bounded to the north by the Subtropical Front (STF). This front is defined by specific physico-chemical properties of the surface waters (temperature, salinity and nutrient concentration) that finally result in the strongest physicochemical gradients of the entire ocean (Fig. 3.1; Mizuki et al., 1994; Lutjeharms, 2006). The ocean currents forming the ACC create thermal and biological boundaries defining the progressive change from subtropical nutrient-depleted waters to nutrient-rich and highly productive polar waters (Orsi et al., 1995; Banse, 1996; Fig. 3.1). The bottom water masses at this Site are characterized by the intersection of the Weddell Sea waters (WS) and southern ACC passing through the Drake Passage as CDW by entering into the South Atlantic (Hodell et al., 2001; Boeckel et al., 2006; Rickaby et al., 2010; Fig. 3.2).

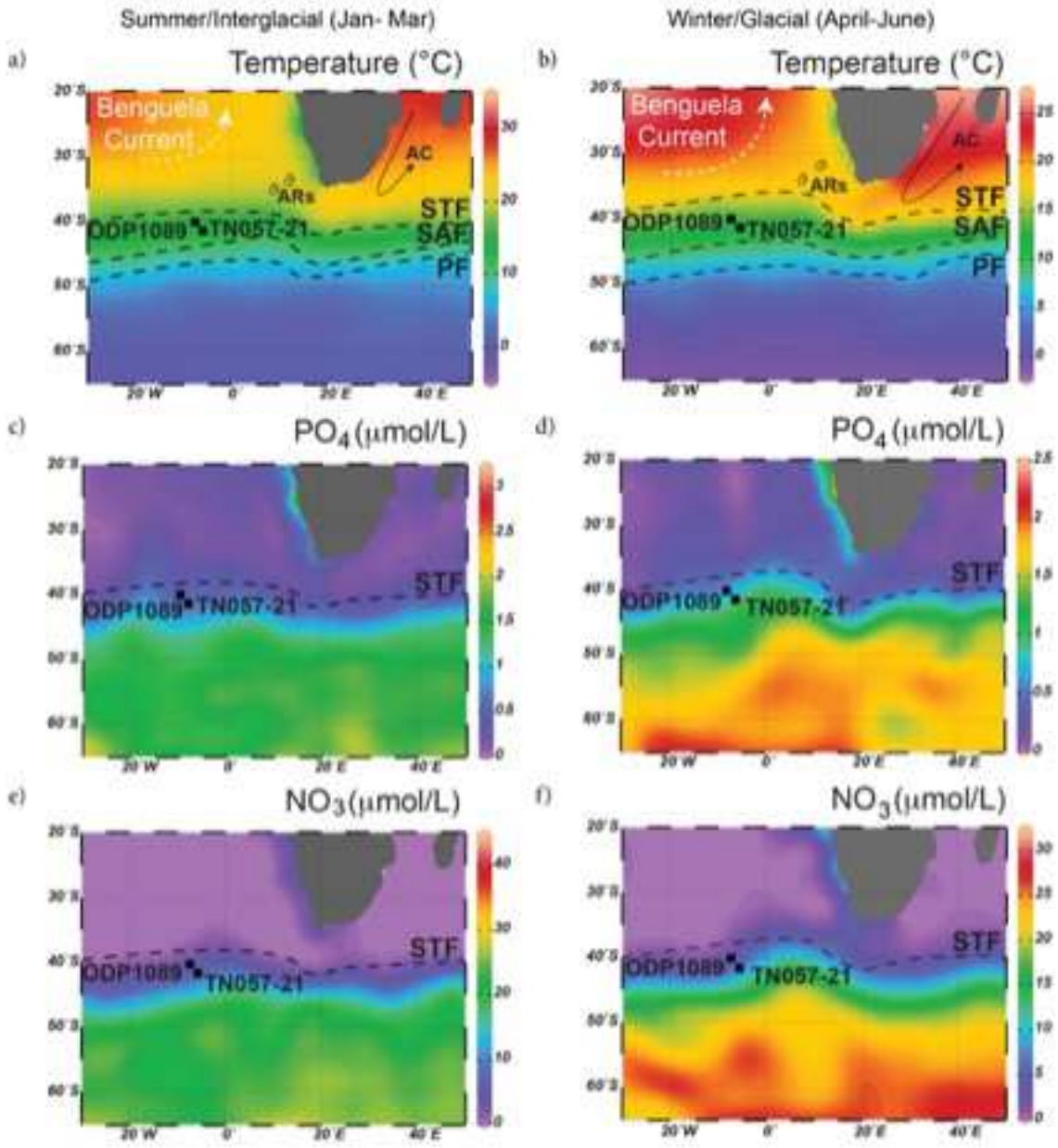

Figure 3.1: Location of Site ODP1089 and TN057-21, indicated as black squares. Site locations are overlain on a map of average monthly sea surface temperature (a;b), phosphate (c; d) and nitrate (e; f) from Jan.-March (Summer/Interglacial) to April-June (Winter/Glacial). Data have been compiled from World Ocean Atlas 2013 using the Software Ocean Data View 4® (R. Schlitzer, Ocean data view, 2009, http://gcmd.nasa.gov/records/ODV_AWI.html). The white arrows indicate the Benguela Current; the Agulhas Rings (ARs) and Agulhas Current (AC) are also shown. The average positions of the modern Subtropical Front (STF), Subantarctic Front (SAF) and Polar Front (PF) are shown as dashed lines (Mejía et al., 2014).

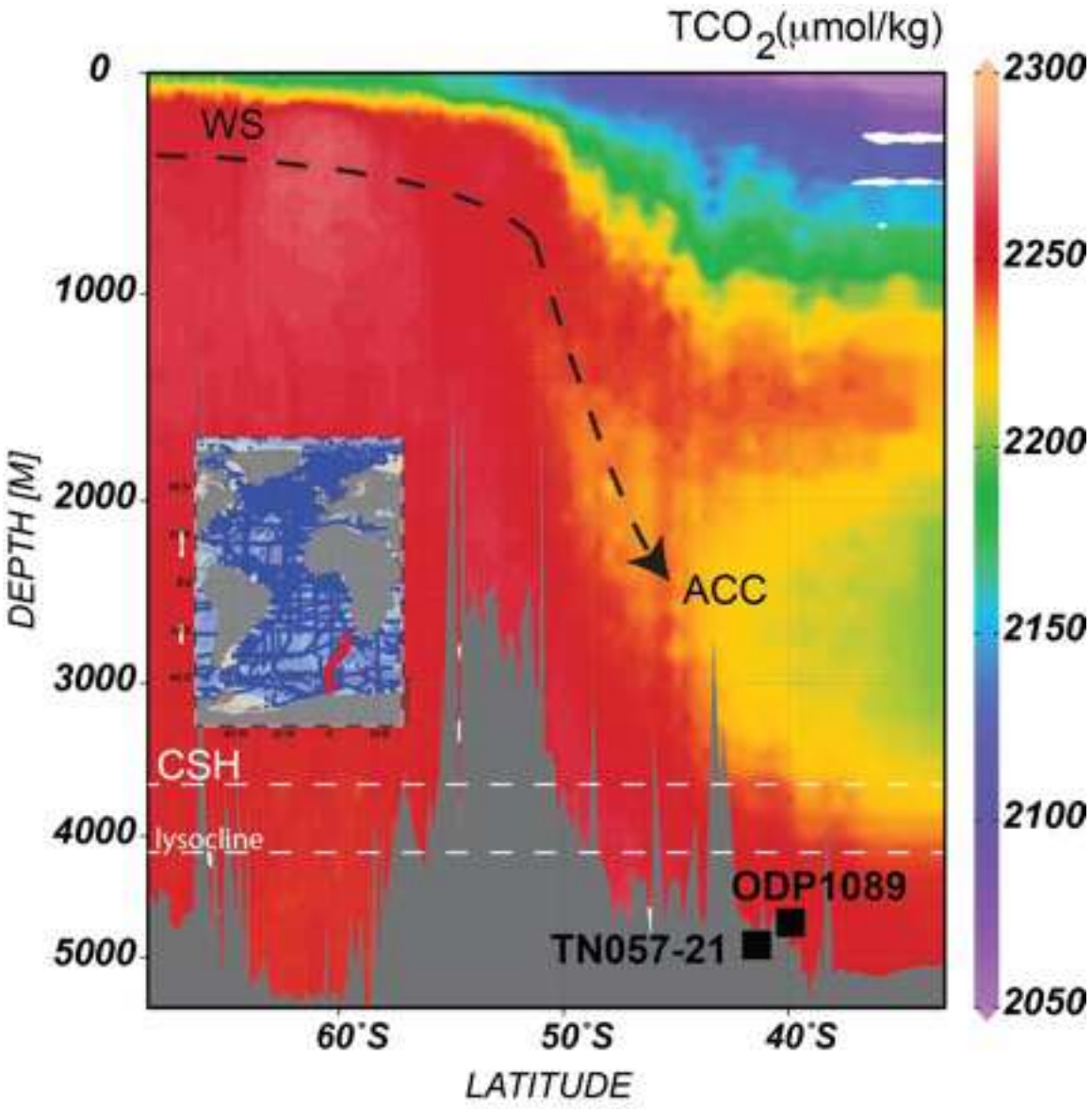

Figure 3.2: Hydrographic section of total carbon content (TCO_2 (µmol/kg)) from WOCE [Schlitzer, 2000] based on data from Global Alkalinity and Total Dissolved Carbon Estimates (Goyet, Healy and Ryan (2000); intersecting Weddell Sea (WS) and southern ACC zone with the location of ODP 1089 and TN057-21. The Calcite Saturation Horizon (3,690m; CSH, white dushed line) has been calculated based on modern salinity, temperature (°C), pressure (dbars), total alkalinity (µmol/kgSW) and pH data using CO_2Sys. The lysocline (4,175m) has been determined using the standard formula: 1-Ω=0.15, given by Thunell, (1982) for the Eastern Atlantic Ocean. A map showing the location of the transect is inset.

3.3 Materials and Methods

We analyzed 99 samples from ODP Site 1089 spanning a 292 cm interval (0.50-3.42 mbsf corresponding to 0.260- 3.180 mcd) at 3 cm resolution, which documents the time interval from 5 ka to 25 ka. The adopted age model is based on $\delta^{18}O$ values measured on *Globigerina bulloides* and *Globorotalia truncatulinoides* that was developed from the companion core TNO57-21 by Mortyn et al. (2002), which suggests an average resolution of ~200 years.

3.3.1 Sample preparation and coccolith analysis

Two different methodologies were followed for preparing samples from unprocessed material. Smear slides were prepared following standard procedures described by Bown and Young (1998), while for temporary wet mount slides we used the filtration method (Lototkaya et al., 1998; Ziveri et al., 1999). For the latter, 20–50 mg of dry bulk sediment were weighed and placed in a small vial. Samples were brought into suspension using tap water (45 ml) in the small vial. In order to disintegrate aggregates, the suspension was placed in an ultrasonic bath for 30 seconds. About 2-5 ml of solution was pipetted with a high-precision Eppendorf pipette, and placed in a beaker. The suspension was then filtered onto polycarbonate membranes (0.45 μm pore size, Millipore®). All membranes were stored in plastic Petri dishes and dried in an oven at 40 °C for 12 h. For light microscope analysis a portion of each filter was mounted onto a glass slide to make a temporary slide: the filter sample was made transparent by adding a drop of microscope oil (immersion oil with refraction index 1.515-1.517, viscosity 100-200 mPa.s), and then a glass plate was fixed to cover the filter. For the smear slide a sample was taken using a toothpick and placed on a slide.The sediment was then smeared out using the toothpick, making sure the sediment was well dispersed. The slide was then put on a hot plate to cool and a drop of Norland medium was applied on the sediment and covered by a cover slip. The slide was finally put under ultraviolet light to cure (10 minutes). These two procedures were used for each sample in order to estimate relative frequencies of different coccolith species and the number of coccoliths per gram of sediment, respectively. These samples were examined using a ZEISS transmitted light microscope at ×1250 magnification. After a preliminary qualitative analysis in order to evaluate the abundance and preservation state of calcareous coccolith assemblages, quantitative data were collected.

At least 500 coccoliths were counted per smear slide, in order to evaluate the relative abundance of the varius species. This method allows a confidence level of detecting a *taxon* greater than 99% when its relative abundance in the population is about 1% (Crow et al., 1960; Rio et al., 1990a, 1990b).

We counted the number of specimens ascribed to the same taxon on a pre-fixed area (total filter area is equal to 1735 mm^2) in order to estimate the coccolith carbonate contribution and the number of coccoliths per gram of dry sediment (coccolith concentration). For this counting ca. 500 coccoliths were quantified in each sample. The conversion of coccolith countings into coccoliths per gram of dry sediment followed the formula given by Ziveri et al. (1999).

Coccolith's absolute abundance (no. of coccoliths g^{-1} dry sediment) = (Nc x Sf) / (No x So x Ws) (eq. 1).

Nc= Number of coccoliths counted

Sf= Filtration area (mm^2)

No= Number of fields of view

So= Surface of the field of view (mm2)

Ws= Weight of sediment filtered (g).

3.3.1.1 Coccolith accumulation rate

The coccolith accumulation rate (ARc) has been obtained following the formula given by Ziveri et al. (1999). Dry bulk density values are available for eleven samples which allow to subdivide the study interval in eleven subintervals that are assumed to have a constant dry bulk density value throughout two successive tie points.

ARc= Dc × DBD × SR (eq. 2)

ARc= coccolith accumulation rates (number of coccoliths cm^{-2} ka^{-1})

Dc= coccolith density (number of coccoliths/gram of sediment)

DBD= dry bulk density (g cm^{-3}; data from Kuhn and Diekmann (2002))

SR= sedimentation rates (cm ka^{-1}; based on radiocarbon data from Mortyn et al., 2002 at TN057-21).

3.3.2 CEX index

In order to assess the effect of carbonate dissolution on the coccolith assemblages the relative abundance of two cosmopolitan and abundant species was used. The two species taken into consideration are: (i) *E. huxleyi,* which produces very delicate coccoliths with fragile t-shaped elements; and (*ii*) *Calcidiscus leptoporus* built of larger, strongly calcified coccoliths resistant to dissolution. The *C. leptoporus-E. huxleyi* dissolution index (CEX index; Boeckel and Baumann, 2004) is calculated as follows:

CEX= *E. huxleyi* (%) / [*E. huxleyi* (%) + *C. leptoporus* (%)]. (eq. 3)

CEX values close or equal to zero indicate a strongly dissolved assemblage, while values close or equal to one indicate perfect preservation of even the more fragile taxa (Boeckel and Baumann, 2004).

3.3.3 Coccolith carbonate mass estimate

To evaluate the coccolith mass we used two different methods: a) the coccolith mass estimate through an automated recognition system (SYRACO, Dollfus and Beaufort (1999); Beaufort and Dollfus (2004)) and b) the coccolith carbonate mass estimate based on the shape index (Young and Ziveri, 2000), both described hereafter.

a) Coccolith mass estimate through SYRACO

Smear slides of surface sediment samples were prepared following standard procedures as described in 3.1. The light microscope used is a Leica DM6000B cross-polarized with ×1000 magnification fitted with a SPOT Insight Camera. On average 40 pictures with an area of 15625 μm^2 were taken for each sample and analyzed with SYRACO that is able to distinguish between the different species present in the assemblages (Dollfus and Beaufort, 1999; Beaufort and Dollfus, 2004). The coccolith length in relation to the distal shield was converted from pixels to micrometers: 1 pixel corresponding to ~0.15 μm. The mass of each single coccolith was estimated using the method developed by Beaufort (2005) based on the brightness properties of calcite particles (thickness <1.55 μm) when viewed in cross-polarized light, following the recommendations of Horigome et al. (2014).

b) Coccolith carbonate mass based on shape index

Quantification of the coccolith $CaCO_3$ contribution to the bulk sediment was also determined using the mass equation of Young and Ziveri (2000), where the shape of a coccolith type (k_s), its average

length and calcite density are considered. Coccolith volumes were evaluated to determine the total carbonate fluxes produced by coccoliths and the relative contributions of each single taxon. This method has significant cumulative error (around 50%) principally due to the high variability in size observed in specimens ascribable to the same species (Young and Ziveri, 2000). An additional possible bias in the estimation of coccolith carbonate contribution is related to the presence of broken coccoliths that are not quantified in our counting but could represent a significant amount of carbonate. All this considered, the calculation of coccolith carbonate content could be significantly underestimated with respect to the total coccolith carbonate contribution (Young and Ziveri, 2000; Bordiga et al., 2014).

3.3.4 Calcification index

E. huxleyi calcification degree has been calculated using the calcification index given by D'Amario (2017). Coccolith mass depends on both length and degree of calcification; the latter has been independently calculated from *E. huxleyi* length following this formula:

$C_i = M_s/M_n$ (eq. 4).

C_i= Calcification index

M_s =mass measured with SYRACO

M_n= predicted normalized mass based on Young and Ziveri (2000).

3.4 Results

3.4.1 Coccolith data and CEX index

Throughout the study interval we identified a total of 17 species of coccoliths. The coccolith assemblage is overall dominated by *E. huxleyi*, *C. leptoporus*, *Florisphaera profunda, Gephyrocapsa muellerae, Gephyrocapsa oceanica, Coccolithus pelagicus* and *Helicosphaera* spp. (Fig. 3.3a). *E. huxleyi* and *C. leptoporus* have the highest relative abundances within the assemblage (Fig. 3.3b-f). *E. huxleyi* accounts for up to 60% of the entire coccolith assemblage during the glacial and decreases to 40% across the Holocene (Fig. 3.3d). *C. leptoporus* has an opposite trend, in that it increases from 10% to 30% across the study interval (Fig. 3.3f). Their absolute abundances, which follow the same trend of the relative abundances, are also the highest within the assemblage (4×10^9 coccolith/gram; Fig. 3.3c-e). The relative and absolute abundances of the low photic zone taxon *F. profunda* (Fig. 3.3g) show a general increase between ~25 ka and 9 ka with values ranging from 5 to 10% and from 0.4×10^9 ~0.7×10^9 coccolith/g. The species *C. pelagicus* shows an inverse trend with higher values (1.2×10^9 coccolith/gram; Fig. 3.3o) registered during the glacial interval. Finally, from the glacial, the other species (*G. muellerae, G. oceanica,* and *Helicosphaera* spp.) decrease from 5% to 2-3%.

The LGM is marked by 3 episodes of low CEX values at 22.3 ka (0.59), at 20.5-21 ka (0.61-0.62), and at 19-19.8 ka with values ranging from 0.34 to 0.43 (Fig. 3.3b). Low preservation intervals coincide with increases in coccolith accumulation rates (10, 14, and 18 $\times10^9$ n. of coccolith cm^{-2} ka^{-1}; Fig. 3.6g). From this point on, the CEX index varies in accordance with coccolith accumulation rates. At 15.5 ka, CEX decreases until 0.6 indicating a beginning of dissolution, while coccolith accumulation rate slightly increases up to 5 $\times10^9$ cm^{-2} ka^{-1} but still remaining relatively low with respect to glacial values. At 15.1 ka a low preservation peak (0.48) is associated with a decrease in the ARc (5 to 2×10^9 n. of coccolith cm^{-2} ka^{-1}). During MIS1 the coccolith accumulation rate is generally low with values ranging from 3 to 6×10^9 cm^{-2} ka^{-1}, between 7 and 6.2 ka the low values comprised of [CO_3^{2-}] and of ARc (3 n. of coccolith cm^{-2} ka^{-1}) suggest the presence of a dissolution event that is not evident if only the CEX index is considered (0.4-0.6).

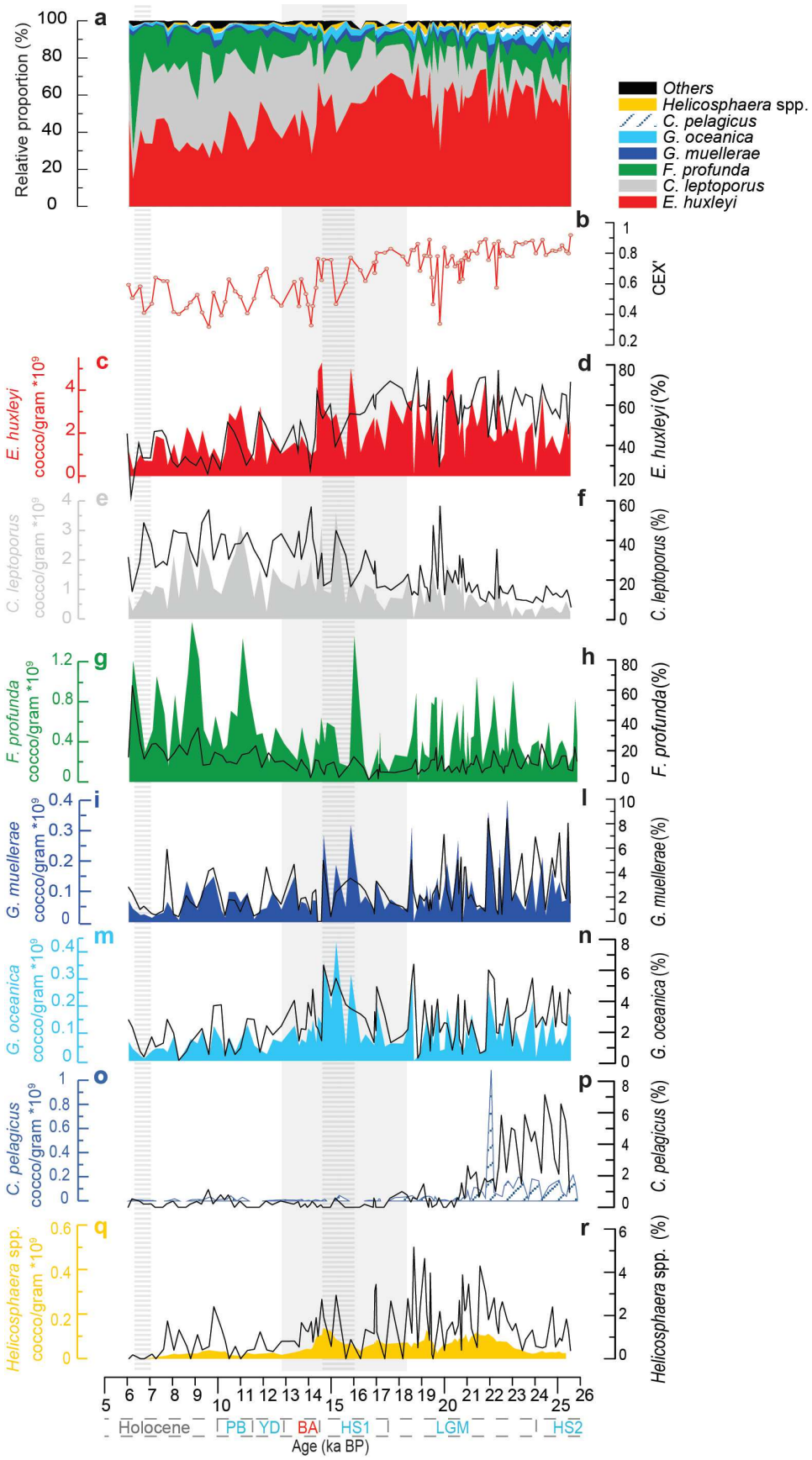
a
Relative proportion (%)
100
80
60
40
20
0
Others
Helicosphaera spp.
C. pelagicus
G. oceanica
G. muellerae
F. profunda
C. leptoporus
E. huxleyi
b
CEX'
1
0.8
0.6
0.4
0.2
c
E. huxleyi
cocco/gram *10⁹
d
E. huxleyi (%)
e
C. leptoporus
f
C. leptoporus (%)
g
F. profunda
h
F. profunda (%)
i
G. muellerae
l
G. muellerae (%)
m
G. oceanica
n
G. oceanica (%)
o
C. pelagicus
p
C. pelagicus (%)
q
Helicosphaera spp.
r
Helicosphaera spp. (%)
5 6 7 8 9 10 11 12 13 14 15 16 17 18 19 20 21 22 23 24 25 26
Holocene
PB
YD
BA
HS1
LGM
HS2
Age (ka BP)

Figure 3.3 (previous page): a) Coccolith cumulative proportion (%); b) coccolith dissolution index (CEX); c, e, g, i, m, o, q) Absolute abundances for each species (coccolith/ gram $\times 10^9$); d, f, h, l, n, p, r) Relative abundances for each species (%). The grey shaded area defines the last deglaciation (12.8-18.2 ka), the lined grey intervals show the dissolution intervals which have been defined throughout a multiproxy approach based on coccolith dissolution index, planktic foraminifera fragments, ions carbonate concentracions and coccolith accumulation rates. In red and blue, warm and cold intervals respectively. HS2-1, Heinrich stadial event 2-1; LGM, Last Glacial Maximum; BA, BØlling-AllerØd, YD, Younger Dryas, PB, Preboreal.

3.4.2 Coccolith carbonate content and *Emiliania huxleyi* calcification

Coccolith carbonate contribution to the fine fraction (%, <20 μm; Fig. 3.4f) shows high variability over the entire study period with an average value of 20 and 30% of the total carbonate of the fine fraction. These values may underestimate coccolith carbonate since they are based only on detectable coccolith specimens (not fragments). The contribution tends to increase through the study interval with higher values during the interglacial period. During the glacial period, the contribution of nannofossils to the carbonate contents of the fine fraction is dominated by *C. leptoporus* (almost 20%), *C. pelagicus* (4-7%, 37.22% at 21.8 ka), *Helicosphaera* spp. (4-7%) and *E. huxleyi* (2-3%) while the composition during the interglacial interval drastically changed with the dominance of *C. leptoporus* (30-40%) over all the other taxa.

In Fig. 3.4e during MIS2, the calcification index of *E. huxleyi* shows a relatively flat trend with an average value of 1.77± 0.0179, apart from a peak of 2 at 19.5 ka. During the glacial interval, the mass of *E. huxleyi* varies between ca. 3.5 and 4.5 pg while the length (maximum axis) has an average value of 2.45 μm (Fig. 3.4c-d). These two parameters show a strong positive correlation: smaller coccoliths (length) corresponding to lower coccoliths mass. At 18.9 ka, both the size and the mass of *E. huxleyi* temporarily decrease to 2.75 pg and 2.25 μm respectively but these parameters progressively return close to average values at around 14 ka. During MIS1, the size and mass of *E. huxleyi* gradually increase reaching high values of 2.58 μm and 4.7 pg respectively at ca. 12.1 ka. From this point upward, the mass of *E. huxleyi* decreases from ca. 4.5 pg to ca. 3.5 pg with the minimum value reached at 6.6 ka. In the same interval the size of *E. huxleyi* shows a relatively constant trend, positively correlated with the mass profile, which instead is slightly decreasing.

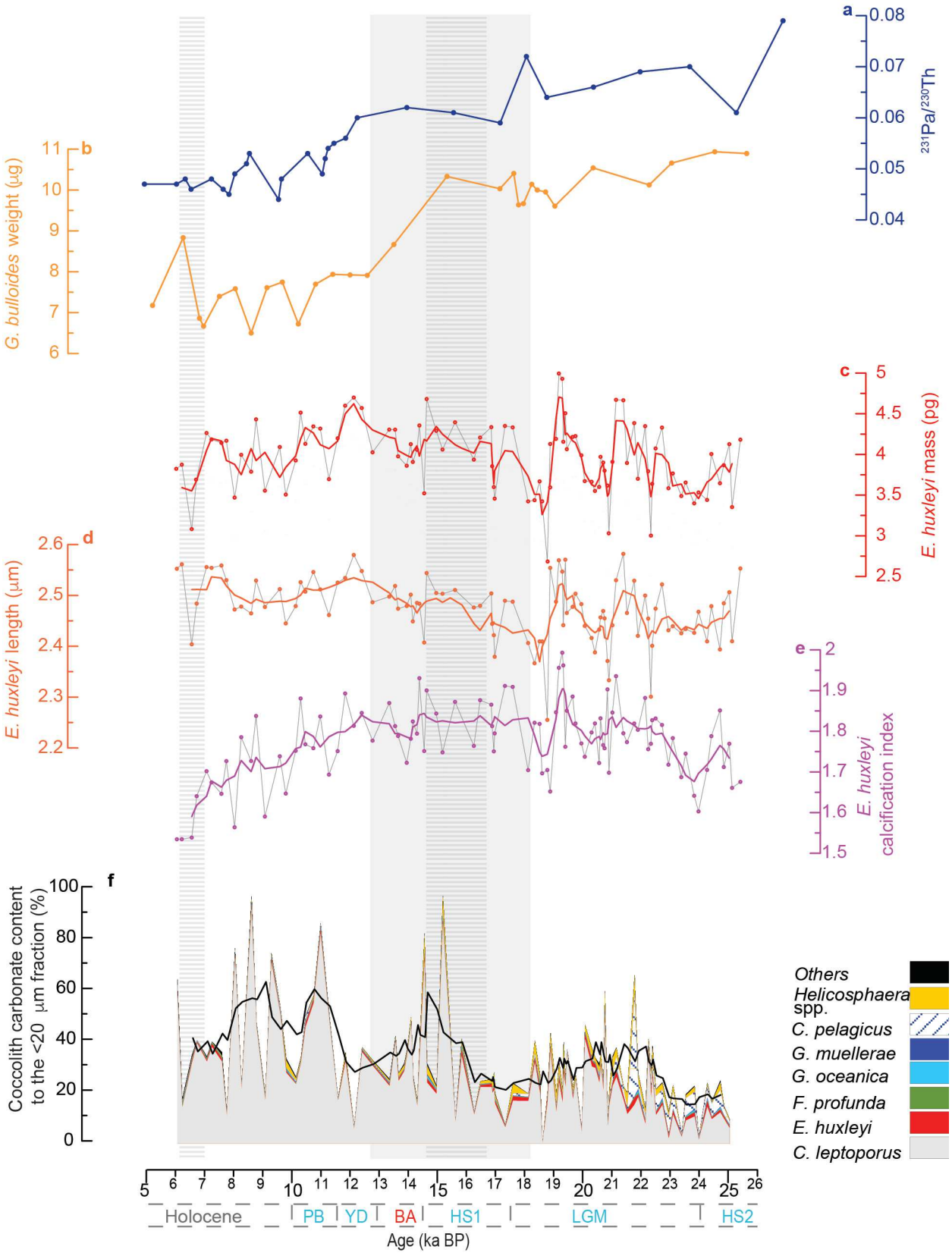
a
0.08
0.07
0.06
0.05
0.04
231Pa/230Th
b
11
10
9
8
7
6
G. bulloides weight (µg)
c
5
4.5
4
3.5
3
2.5
E. huxleyi mass (pg)
d
2.6
2.5
2.4
2.3
2.2
E. huxleyi length (µm)
e
2
1.9
1.8
1.7
1.6
1.5
E. huxleyi calcification index
f
100
80
60
40
20
0
Coccolith carbonate content to the <20 µm fraction (%)
Others
Helicosphaera spp.
C. pelagicus
G. muellerae
G. oceanica
F. profunda
E. huxleyi
C. leptoporus
5 6 7 8 9 10 11 12 13 14 15 16 17 18 19 20 21 22 23 24 25 26
Holocene
PB
YD
BA
HS1
LGM
HS2
Age (ka BP)

Figure 3.4 (previous page): a) $^{231}Pa/^{230}Th$ values reconstruction for ocean circulation at ODP1089 (Lippold et al, 2016); b) *G. bulloides* mass at MD96-2080 (μg; Martínez-Méndez et al., 2010); c) *E. huxleyi* mass (pg); d) length (μm) and e) calcification index with 5 points- running averages; f) coccolith carbonate contribution to the <20 μm fraction (%), others category consists of *Ceratolithus* spp. (%), *Syracosphaera* spp. (%), *Umbilicosphaera* spp. (%) and *D. tubifera* (%); in black the 5-window running average.

3.5 Discussion

3.5.1 Factors controlling surface water dynamics and coccolith record at ODP Site 1089

The importance of the SO globally relies on the different processes that occur both at surface and depth, which affect the general circulation (Hodell et al., 2003). This study is located in the present Subtropical region, south of the Subtropical Front (STF), and north of the Subantarctic Front (SAF). Surface ocean dynamics and biogeochemistry in this area are primarily driven by the position and intensity of the westerlies and the displacement of the upwelling cell of the Antarctic divergence due to the ice-sheet expansion/retreat (Mejìa et al., 2014; Flores et al., 2012), shaping also primary and carbonate production and seawater carbonate chemistry. In particular, westerly winds are responsible for delivering a high quantity of micronutrients (specifically iron) from South America (Anderson et al., 2014), which are meant to cause high efficiency of both carbon and carbonate counter pump by coccolithophores and foraminifera (Ziveri et al., 2007; Salter et al., 2014; Rembauville et al., 2016). Consequently, these winds are important to consider in order to understand the surface biological production dynamics. During MIS2, the SO was characterized by iron fertilization as evidenced by dust fluxes measured at EPICA Dome C (EDC; Fig. 3.5a; Lambert et al., 2012), suggesting an equatorward position of the westerlies. This westerlies' displacement caused also the surface upwelling cell to move towards the Subantarctic Zone (Flores et al., 2012), being responsible of an increase in the surface phosphorus budget of the ocean (Fig. 3.5g). Generally, the expected response to a naturally more iron-enriched surface ocean, from a biological point of view, is a rise in diatom export (Martin and Fitzwater, 1988; Martin J.H. ,1989, 1990, 1991; Anderson et al., 2014; Martinez-Garcia et al., 2014) with a consequent important carbon sequestration as a climate feedback. In fact, it has been shown that an intense soft tissue pump can be the main driver for the drawdown of atmospheric CO_2, also delivering a huge amount of carbon into the deep ocean (Watson et al., 2000; Blain et al., 2007; Pollard et al., 2009). Coccolithophore response, however, is known to be not so bloom-dependent to naturally-iron fertilized zones. In fact, recent works analyzing the effects of trace metals (particularly iron) on coccolithophore growth show that they are able to maintain growth at lower levels of inorganic

iron (Hartnett et al., 2012), and the enhanced degree of iron uptake depends not only on the type of grazer but also on the type of prey (Nuester et al., 2014). Additionally, the accessibility of the dissolved inorganic iron form to phytoplankton is reduced at lower pH because of redox chemistry of ligands (Marchetti & Maldonado, 2016). However, iron seems to be a key trace nutrient that is responsible for the growth of coccolithophores in the SO (Balch et al., 2011). As it has been proposed by Balch et al., 2016, when silicate is weak (and nitrate and phosphorus are high) non-silicate requiring coccolithophores can flourish and outcompete diatoms. Our data agree with this view, specifically, late glacial high phosphorus concentrations with high silicate consumptions and high iron delivery, may have induced high *E. huxleyi* biological production response. Specifically, we observe the highest peaks in *E. huxleyi* curve (%; Fig. 3.5f) in correspondence with an increase in the phosphorus content (Fig. 3.5g) and still high iron concentrations (between 22.3 to 17 ka; Fig. 3.5b). In fact, the linear correlation between *E. huxleyi* (%) and accumulation rate of iron ($mg/m^2/yr$) is relatively good (r^2= 0.297; p-value is 3.22e-06; see SI for calculations). Although, since iron is known to be bound to a wide variety of ligands (Tagliabue et al., 2017), the effect of the iron cycle on coccolithophore blooms is still complex to be clearly defined. In eutrophic conditions also, *E. huxleyi* is a relatively fast growth rate coccolithophore species likely to be r-strategy in ecological terms (Ziveri et al., 2000; Lototskaya et al., 1998; Flores et al., 2012). With *C. leptoporus* (%) response to iron fertilization, we get a negative linear correlation (r^2=0.322, p-value is 9.73e-07; SI), which suggests that iron ($mg/m^{-2}/a$) may have played an important role as a micronutrient delivered to the ocean. Furthermore, despite no significant correlation being observed between this *taxon* and the phosphorus content (g/g) (r^2=0.239, p-value is 0.0246; SI), a similar trend can be observed between these two latter parameters over the long-term (Fig. 3.5g-h). Taken together, these observations could suggest a species-specific productivity response of *E. huxleyi* to iron fertilization with phosphorus delivery and of *C. leptoporus* to the decrease of iron concentrations and the increase of phosphorus (Fig. 3.5), and the shifts in their biogeographic distribution following the STF system through the last 25-5 ka period. However, we cannot certainly say that this has been the main control on *E. huxleyi* and on *C. leptoporus* relative abundances, but it could have been possible that within the nutrients spectrum (Hallock, 1987), Fe and P are definitely playing a major role within the coccolith assemblage. The CEX index, which is usually used as a dissolution index, is instead unexpectedly related to coccolithophore productivity induced by iron fertilization and phosphorus content dynamics. This coccolith index

is defined by the ratio between delicate and resistant coccoliths and has been used for a long time to assess the preservation state of calcareous nannofossil assemblages (*e.g.* Dittert et al., 1999; Boeckel and Baumann, 2004; Marino et al., 2009; Amore et al., 2012). In this study, the CEX index is based on the two-driver species *E. huxleyi* (%) and *C. leptoporus* (%) and hence to both their iron fertilization and phosphorus content responses. During interglacials, a poleward shift of westerlies and STF positions (Martinez-Garcia et al., 2014) created mesotrophic zones in the Subtropical and Subantarctic zone. Under these conditions some coccolithophore species result in high export production such as *C. leptoporus*, as we discussed above. During MIS1, high surface water mixing and phosphorus content probably induced an increase in heavily calcified *C. leptoporus* relative concentrations. We suggest that our CEX index is then consistent with the displacement of the STF during the glacial-interglacial cycle (Fig. 3.5). In order to define and corroborate our STF migration, we also use the absolute concentration of *F. profunda* and *C. pelagicus* (Fig. 3.5d-e). *F. profunda* abundance increases north of the STF (Baumann et al., 2004), hence its low glacial concentrations reflect a northward shift of the boundary and viceversa during the interglacial (Fig. 3.5d; Martinez-Garcia et al., (2014)). *C. pelagicus* is widely used as a proxy for cold waters in palaeoceanographic studies (McIntyre et al., 1970; Raffi and Rio, 1981; Cachao and Moita, 2000), being well represented in cold waters at temperatures ranging from 1.7 to 15° C (Okada and McIntyre, 1979; Winter et al., 1994). Thus, its glacial increase reflects a STF shift towards the equator. Based on these data, high *F. profunda* reflect a southward shift of the STF and high *C. pelagicus* abundances a northward shift of the the same front. This observation fits well with the CEX index and westerlies' displacements that mirror the STF shifts over the glacial-interglacial cycle.

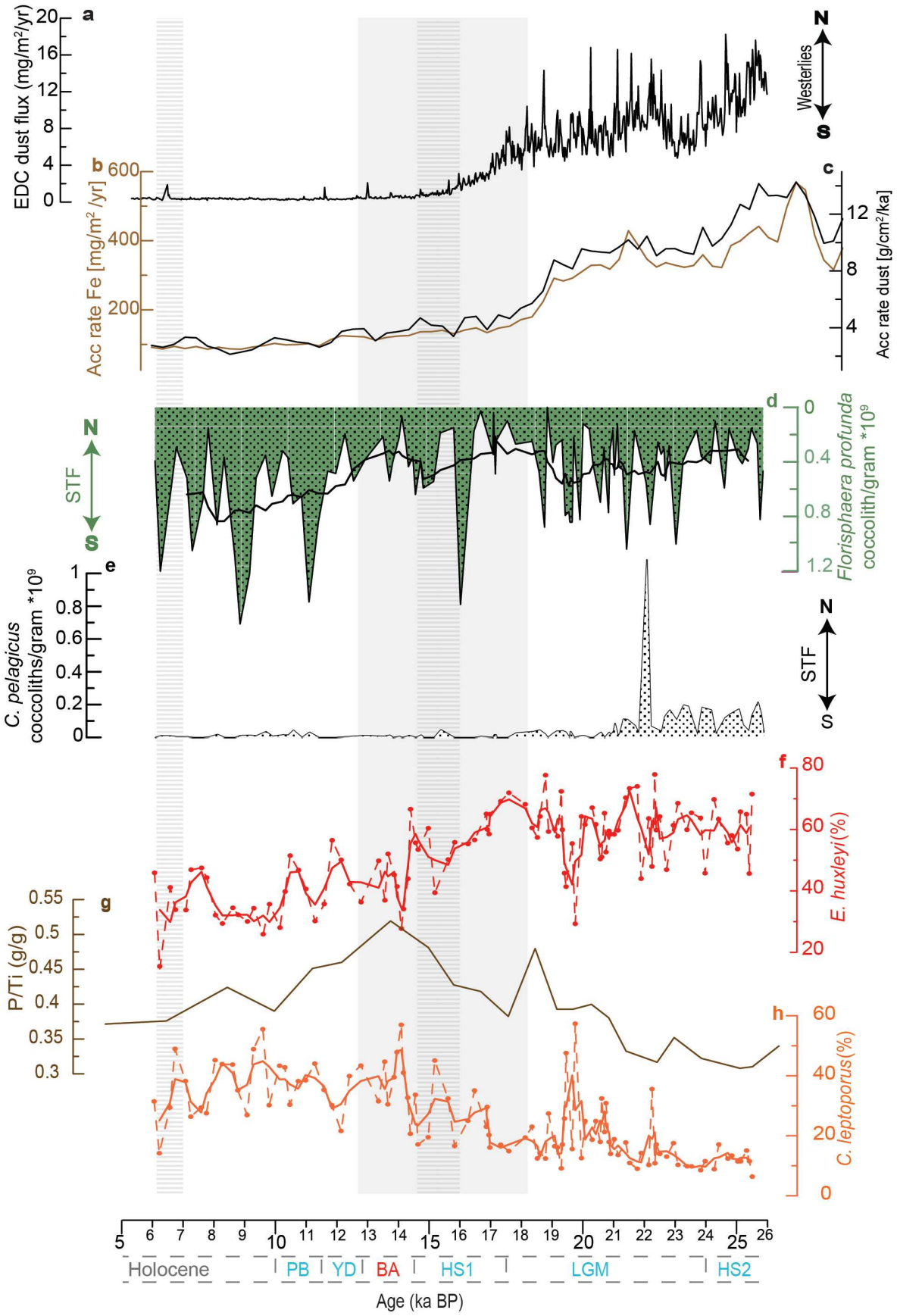
a
EDC dust flux (mg/m²/yr)
20
16
12
8
4
0
N
Westerlies
S
b
600
400
200
Acc rate Fe [mg/m² /yr]
c
12
8
4
Acc rate dust [g/cm²/ka]
d
N
STF
S
0
0.4
0.8
1.2
Florisphaera profunda coccolith/gram *10⁹
e
1
0.8
0.6
0.4
0.2
0
C. pelagicus coccoliths/gram *10⁹
N
STF
S
f
80
60
40
20
E. huxleyi(%)
g
0.55
0.5
0.45
0.4
0.35
0.3
P/Ti (g/g)
h
60
40
20
0
C. leptoporus(%)
5 6 7 8 9 10 11 12 13 14 15 16 17 18 19 20 21 22 23 24 25 26
Holocene
PB
YD
BA
HS1
LGM
HS2
Age (ka BP)

Figure 3.5 (previous page): a) EPICA Dome C dust flux (mg/m^2/yr; Lambert et al., 2012); b-c) Fe and dust accumulation rate at Site ODP1090 (g/cm^2/ka; Martinez-Garcia et al., 2011); d) *Florisphaera profunda* with running average (window:11) and e) *Coccolithus pelagicus* coccolith/gram ×10^9; f) *E. huxleyi* (%); g) P/Ti (g/g) ratio at ODP1089 (Flores et al., 2012); h) *C. leptoporus* (%).

3.5.2 Carbonate system and dissolution dynamics in the deep SO

Calcium carbonate analyses performed on the fine fraction (<20 μm; Fig. 3.6f) are of particular interest representing the calcareous nannofossil signature present in the sediments. Additionally at this location, a number of studies support the correlation between $CaCO_3$ and productivity due to coccolithophores (Flores et al., 2003; Moreno et al., 2005).

The carbonate content profile at the study site (average of 40 wt%; Fig. 3.6c) is shaped by export production and by the carbonate saturation depth considering that bioturbation and chemical erosion are minimized by the high sedimentation rates. The relatively high $CaCO_3$ content recorded during the glacial phases and the lower percentages documented in the interglacials are a peculiar characteristic of a 'Pacific-type' carbonate stratigraphy in the present interglacial-glacial regime (Hodell et al., 2001). During the terminations between glacial and interglacial periods, the amount of dissolved carbonate usually increases and, consequently the preservation of carbonate decreases (Hodell et al., 2001; Flores et al., 2012). However, the total carbonate content on the oceanic floors is the result of a complex interplay of processes rather than of a single process. Among these mechanisms the amount of $CaCO_3$ secreted by organisms in surface waters, the $CaCO_3$ solubility along the water column and at the seawater/sediment interface and the dilution derived by non-carbonate terrigenous sediments should be taken into account for a correct interpretation of data.

Since the variability of non-carbonate terrigenous material is negligible, in the way that it is high and constant enough to record the timing and amplitude of dissolution and preservation pulses with high fidelity (Hodell et al., 2001; Flores et al., 2003; Flores et al., 2012), the change in $CaCO_3$ content (Fig. 3.6c; Hodell et al., 2001) mainly reflects surface water carbonate production modulated by preservation. This means that the carbonate profile is free from the complexity that could limit the observation in other records (*e.g.* Indo-Pacific Ocean). During the interglacial stage, a decrease in $CaCO_3$ (Hodell et al., 2001) was observed and generally interpreted as caused by an enhanced input in terrigenous sediments due to an increased intensity of the westerly winds (Mejìa et al., 2014). Micropaleontological and geochemical analysis carried out in sediments at Site ODP1089 over the last 0.5 My reveals that most of the export productivity in the Subantarctic zone

was due to coccolithophores (Flores et al., 2012). Studies carried out in the North and South Atlantic show evidence for maxima in carbonate content coinciding with the first stages of the deglaciation (Bordiga et al., 2014). Fluxes of coccolith calcite to deep ocean sediments have been recognized as an important factor in the exchange of CO_2 between the ocean and the sediments (Sarmiento et al., 1988). High resolution records of changes in deep sea carbonate saturation state and carbonate dissolution may be useful to constrain the mechanism of deep-sea [CO_3^{2-}] variations and their implications on atmospheric pCO_2 changes (Hodell et al., 2001).

At Site TNO57-21, low values of bottom water [CO_3^{2-}] (Fig. 3.6f; Yu et al., 2014) are associated with high values in foraminifera fragmentation index (Fig. 3.6d; Hodell et al., 2003) and low values in CEX dissolution index (Fig. 3.6e) suggesting the presence of three low preservation intervals during the glacial; however, coccolith accumulation rates show a very high values that are usually indicative of better preservation (Fig. 3.6g). Coccolith and foraminiferal indices then suggest that bottom water dissolution overall increased across the deglaciation, with superimposed millennial-scale changes. During glacials, the undersaturated deep Weddell Sea water masses are supposed to better preserve the carbonate and then spread and influence the SO (Rickaby et al., 2010). An increase in high alkalinity Weddell Sea water will therefore exert an influence on carbonate preservation. During MIS2, Site ODP1089 was bathed by Weddell sea water and Low Circumpolar Deep Water (LCDW, low [CO_3^{2-}]), resulting in an enhanced preservation (Rickaby et al., 2010). During the last glacial, the SO was stratified and poorly ventilated (Martìnez-Botì et al*.,* 2015; Hodell et al., 2001), with a high deep-water alkalinity and high biomass production driven by iron fertilization and high phosphorus content. The carbonate balance is thus the result of the interplay of these two processes, which together should have triggered an increased alkalinity. We hypothesize that in order to buffer the high alkalinity of the sea waters, kinetic dissolution intervals (with durations of 5-10 ky each; Rickaby et al., 2010) may have occurred during MIS2; these events are recorded by [CO_3^{2-}] and CEX index but are not evident looking at ARc. The counterintuitive behavior between CEX and ARc curves may be explained, at least in part, by the assumption of a constant dry bulk density value within each of the eleven subintervals in which the study material was subdivided (see 3.1.1 paragraph in method). During the deglaciation low carbonate ion concentration (Fig. 3.6g), high coccolith accumulation rate (Fig. 3.6h) and high values in fragments of planktic foraminifera (Fig. 3.6e) provide multiple proxies that seem to give contradictory estimation of the carbonate production/preservation. However, a reconciliation of

these data is possible if we hypothesize that the carbonate saturation state has reached its maximum during Termination I (TI), as supported by the high coccolith accumulation rate (Fig. 3.6h) but the main mechanism that allows to maintain the steady state alkalinity balance of deep-water carbonate is dissolution, as evidenced by the low coccolith accumulation rate and the carbonate ion concentration (between 14.6-16 ka; Fig. 3.6f-g).

Alkalinity and dissolution played a synergistic role that is consistent with our coccolith accumulation rate. In particular, high coccolith accumulation rates are a response to the high saturation carbonate system with a low peak as a result of dissolution (Fig. 3.6).

During the interglacial, foraminifera fragmentation and CEX indices support an increased dissolution associated with a low coccolith accumulation rate, while [CO_3^{2-}] clearly indicates high alkalinity and thus good preservation (Fig. 3.6). In order to explain this discrepancy, we suggest that low surface pH (Fig. 3.6d; Martìnez-Botì et al., 2015), due to undersaturation of the carbonate system and strong water mixing conditions ($^{231}Pa/^{230}Th$ values as a proxy for ocean circulation, Fig. 3.4c, Lippold et al., 2016) could have caused low calcified shells and skeletons but also high grazing conditions on foraminifera and coccoliths, respectively. A line of evidence also comes from the mass of the planktic foraminifera *G. bulloides*, which interestingly decreases just after 15 ka (Fig. 3.4b; Martínez-Méndez et al., 2010).

At 15 ka, the resumption of the Meridional Overturning Circulation (MOC; Fig. 3.6f; McManus et al., 2004) caused an enhanced ventilation of deep waters, with a consequent release of CO_2 into the atmosphere and the return to more alkaline values (Rickaby et al., 2010). If this is the case, the calcification of foraminifera and coccolithophores has been controlled and possibly modified during their life cycles. Moreover, the dissolution indices based on foraminifera and nannofossils, which are usually used to evaluate the preservation state of the fossil assemblages, seem to provide clues on a different phenomenon, related to surface water conditions, as also evidenced by the high values of [CO_3^{2-}] in the bottom waters during the interglacial. During the final part of MIS1, microfossil indices and [CO_3^{2-}] concentrations both show an abrupt decrease that has been interpreted as a short-lived dissolution event. This result is consistent with the previous data that have demonstrated that the highest dissolution occurs at the interglacial-glacial transition, when the carbonate content reaches minimum values (Hodell et al., 2001).

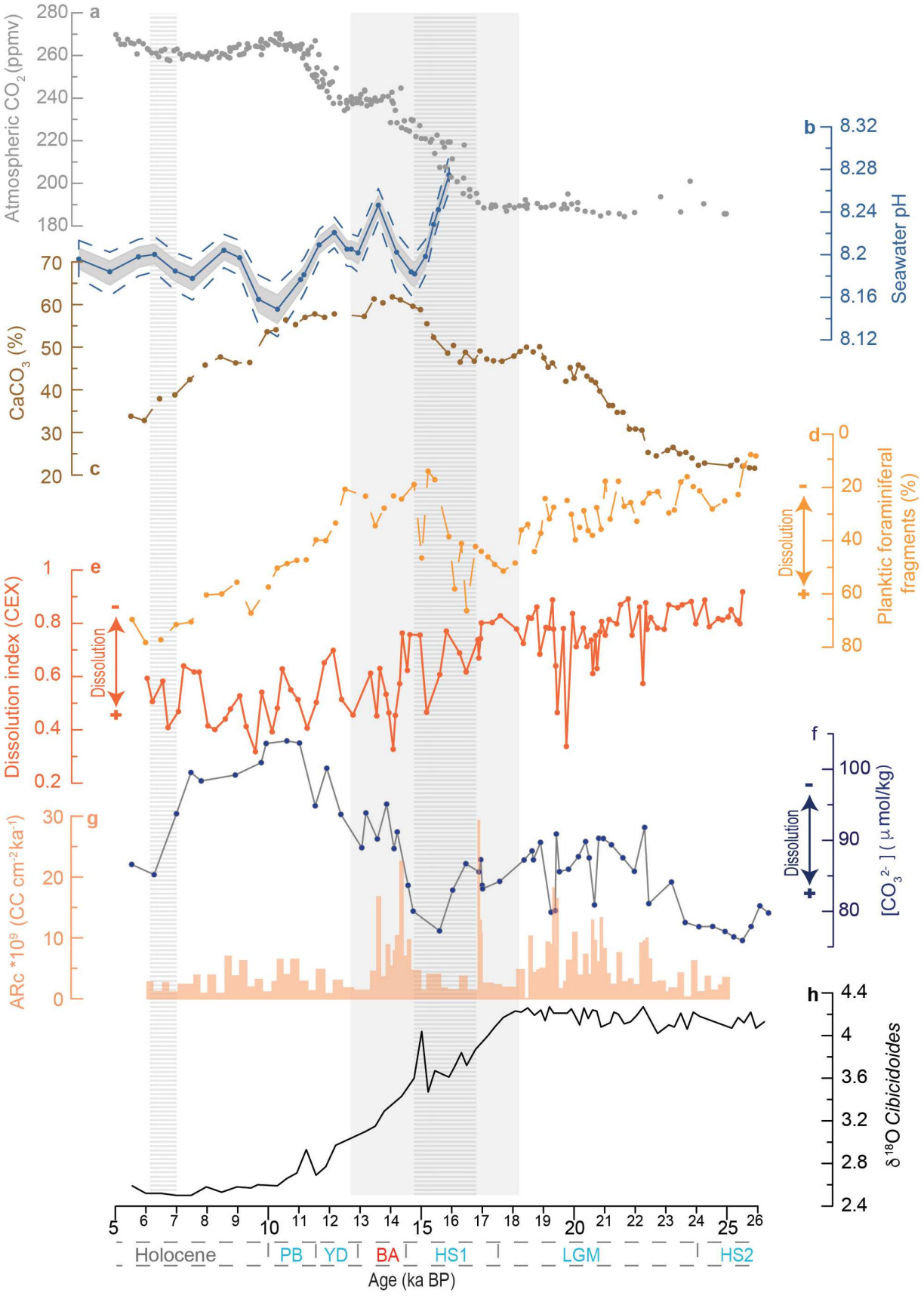
a
Atmospheric CO_2 (ppmv)
280
260
240
220
200
180
b
8.32
8.28
8.24
8.2
8.16
8.12
Seawater pH
70
60
50
40
30
20
$CaCO_3$ (%)
c
d
0
20
40
60
80
Dissolution
Planktic foraminiferal fragments (%)
1
0.8
0.6
0.4
0.2
e
Dissolution index (CEX)
Dissolution
f
100
90
80
$[CO_3^{2-}]$ (μmol/kg)
Dissolution
30
20
10
0
g
ARc *10^9 (CC cm^{-2} ka^{-1})
h
4.4
4
3.6
3.2
2.8
2.4
$\delta^{18}O$ *Cibicidoides*
5 6 7 8 9 10 11 12 13 14 15 16 17 18 19 20 21 22 23 24 25 26
Holocene
PB
YD
BA
HS1
LGM
HS2
Age (ka BP)

Figure 3.6 (previous page): a) Atmospheric CO_2 from Antarctic ice cores (Schmitt et al., 2012); b) superficial seawater pH reconstructed from salinity, temperature and boron isotopic data at PS2498-1 (Martìnez-Botì et al., 2015); c) $CaCO_3$ (%; Hodell et al., 2001); d) foraminifera planktic fragmentation index at TN057-21 (%; Hodell et al., 2003); e) coccolith dissolution index (CEX); f) [CO_3^{2-}] μmol/kg (TNO57-21; Yu et al., 2014); g) coccolith accumulation rates (n. of coccolith $\times 10^{10}$ cm^{-2} ka^{-1}); h) δ ^{18}O Cibicidoides (Hodell et al., 2003).

3.5.3 Coccolithophore carbonate response to surface and bottom water systems

3.5.3.1 Coccolith carbonate contribution to the carbonate sediments

In order to quantify the coccolith contribution to the total carbonate export and sedimentation it is important to take into account the total carbonate export production, the degree of dissolution and dilution with respect to the terrigenous inputs. To better evaluate the carbonate dynamics throughout the study interval, the contribution of coccolithophores to the < 20 μm $CaCO_3$ content has been investigated through the coccolith carbonate mass (Fig. 3.4f). These data display a low contribution to the fine fraction content (<20 μm), which mainly consists of 2-3% of *E. huxleyi* during MIS2, and 40 to 80% of *C. leptoporus* during MIS1 (Fig. 3.4f). Except for these two species, the assemblage is made up of other subtropical species (Mohan et al., 2008; Poulton et al., 2017) such as *F. profunda*, *G. oceanica*, *G. muellerae*, *C. pelagicus*, *Helicosphaera* spp., *Ceratholithus* spp., *Syracosphaera* spp., *Umbilicosphaera* spp., and *D. tubifera*. The low contribution to the total carbonate export is possibly related either to the grazing of coccoliths or in the evaluation of the coccolith size through light microscopy analysis that eventually result in an underestimation of the carbonate produced, due also to the impossibility to clearly identify all the different species. These three variables are not taken into account by the method adopted (Young and Ziveri, 2000), hence the role of calcareous phytoplankton in producing carbonate could have been underestimated. Mejìa et al. (2014) reported a higher contribution from sediments (Agulhas Bank, off South Africa) during MIS 6 and MIS 5, but Köbrich and Baumann (2009) estimated a contribution of ca. 18% from a one- year- moored sediment trap located off SW Africa. Finally, Flores et al. (2012) provided high values (80 to 90% during T1) in sediment samples at Site ODP 1089. The contribution of coccoliths to carbonate export in the fine fraction is thus highly variable and this result possibly depends on the abundance of both fragmented nannofossils and foraminifera. Additionally, Rembauville et al. (2016) presented data from the Kerguelen Plateau (Southern Ocean) under naturally-iron fertilized conditions, which highlight that in the <20μm the coccolithophore assemblage is made of >95% of *E. huxleyi* and *H. carteri*. Additionally the

foraminifera contribution to the annual PIC flux can be noticeable and this has to be taken into account in order to understand the inorganic carbon flux in relation to iron supply, mostly if an increased soft-tissue pump stimulated by iron availability in the glacial Subantarctic may have been accompanied by a strengthened carbonate counter pump (Salter et al., 2014). We suggest that the possibly dominant but also variable biological, hence carbonate export, response of foraminifer species to iron-fertilized production, can provide a good clue in order to quantify $CaCO_3$ fluxes.

3.5.3.2 *E. huxleyi* mass dynamics and calcification

Numerous studies analyzed *E. huxleyi* size, mass, calcification variations and different morphotypes in the South Atlantic considering different environmental factors (*e.g.* Horigome et al., 2014; Beaufort et al., 2011; Boeckel and Baumann, 2008; Riebesell et al., 2000; Cubillos et al., 2007; Mohan et al., 2008). Horigome et al. (2014) proposed that *E. huxleyi* calcification and geographic distribution of its morphotypes in the SO can be driven by nutrient availability and carbonate chemistry (pH and pCO_2). A modification of the relative abundance of *E. huxleyi* morphotypes allows for the identification of the shifting of the fronts in the South Atlantic zone (Cubillos et al., 2007; Mohan et al., 2008). In particular, types B and C (Young and Westbroek, 1991) are typically distributed south of the Subantarctic Front (SAF) while the overcalcified type A is found to occur north of the SAF. Since we observe maximum interglacial length values (Fig. 5f), we do not expect a geographic influence variation in our *E. huxleyi* assemblage but rather a response to the carbonate chemistry system changes. During the glacial, changes in the carbonate system could have played a key role in *E. huxleyi* calcification (Horigome et al., 2014). SEM analysis performed on calcareous nannofossil assemblages shows an increased degree in calcification for both glacial *E. huxleyi* type A and B. In particular, three different types of calcified *E. huxleyi* were defined based on morphometric parameters considering the ratio between slit length (SL) and tube width (TW) on the distal shield of the coccolith (Fig. 3.7a-b, D' Amario, 2017). Based on this ratio and the thickness of the tube, we distinguished: low calcified (A1, B1); medium calcified (A2, B2) and high calcified (A3, B3). A1 and B1 are characterized by long and larg coccoliths: SL> TW. A2 and B2 have slightly low SL with respect to the TW. Finally, A3 and B3 are the small ones with SL≈ TW. Furthermore, the glacial assemblage is mainly composed of heavily calcified forms such as *C. leptoporus*, *C. pelagicus* and *Helicosphaera* spp. (Fig. 3.4f). Rickaby et al. (2010), in accordance with the high alkalinity that occurred in the glacial ocean,

suggest an increased coccolithophore calcification as well as change toward assemblages dominated by larger and more heavily calcified forms. These data are consistent with our results (Fig. 3.2 in SI). During the deglaciation, before the dissolution interval, calcification reaches high values and this possibly represents the response to the carbonate saturation state (Fig. 3.6e). We suggest this is a direct response to the saturation point of the carbonate system as discussed above, which agrees also with high pH values in the surface waters (Fig. 3.6b). From this point, the *E. huxleyi* length trend seems to slightly increase during the interglacial (Fig. 3.6d), which could be due to the influence of *E. huxleyi* morphotype B2 on the average length, and could explain the increased interglacial length values. However, this would be in contrast with the biogeographic distribution of *E. huxleyi* morphotypes (Mohan et al., 2008) as explained above. Hence this following calcification decrease, driven by *E. huxleyi* length increase and mass decrease during the interglacial, could be a response to the undersaturation state with respect to carbonate in the surface waters. In fact, low surface pH values occurred during MIS1 in the Subantarctic zone (Martinez-Boti et al., 2015) at PS2498-1 site with a decrease also in *G. bulloides* weight at MD96-2080 site (µg; Martínez-Méndez et al., 2010). This surface undersaturation is in contrast with the high saturation state of bottom waters, due to MOC resumption (McManus et al., 2004). It has already been proposed that under low calcite saturation state, calcification may become energetically unfavorable for coccolithophores (Olson et al., 2017). We then propose that changes in the carbonate system are the main drivers in *E. huxleyi* calcification as already suggested by Horigome et al. (2014).

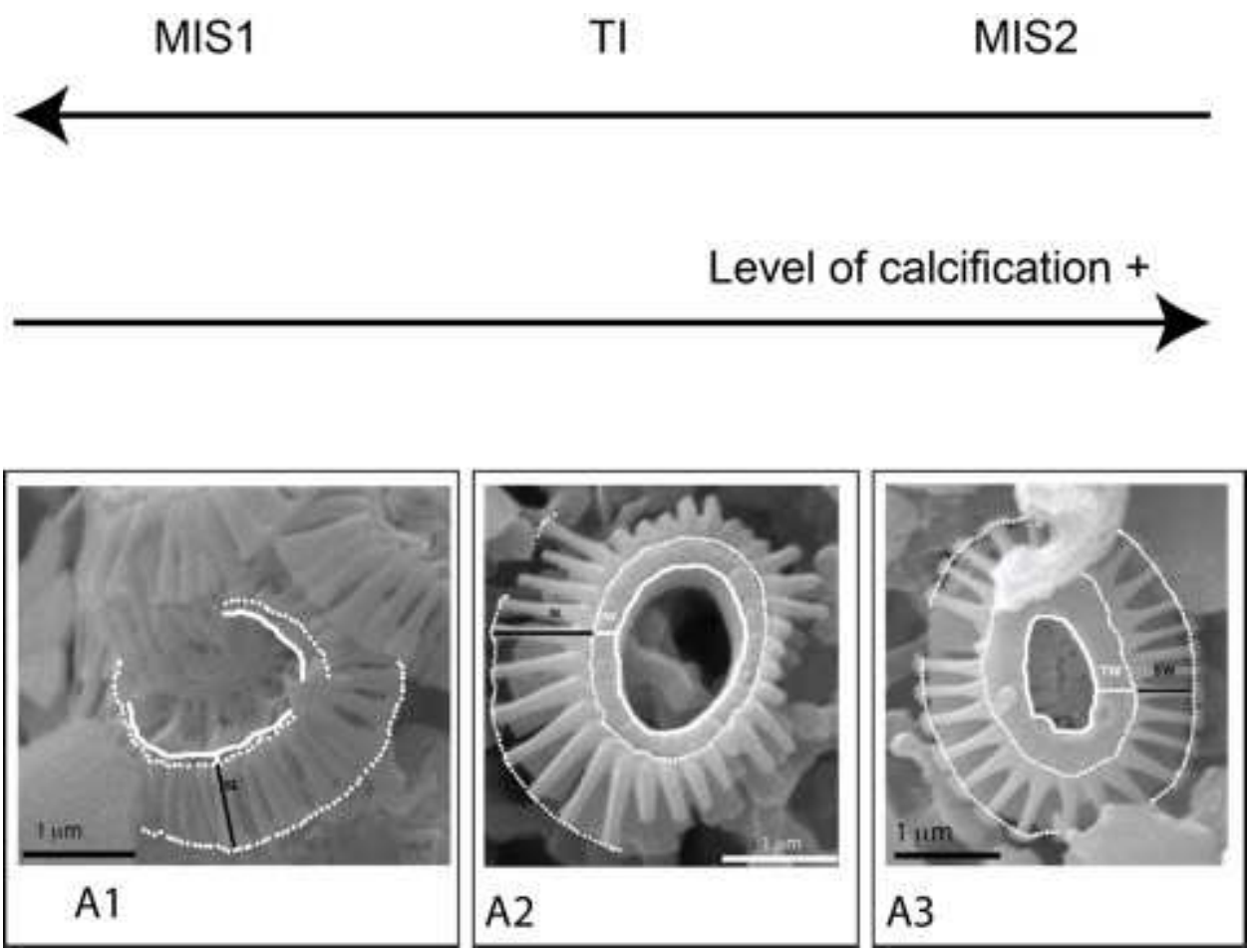

Figure 3.7a: Three different degrees of calcification in morphtoypes A of *E. huxleyi.*

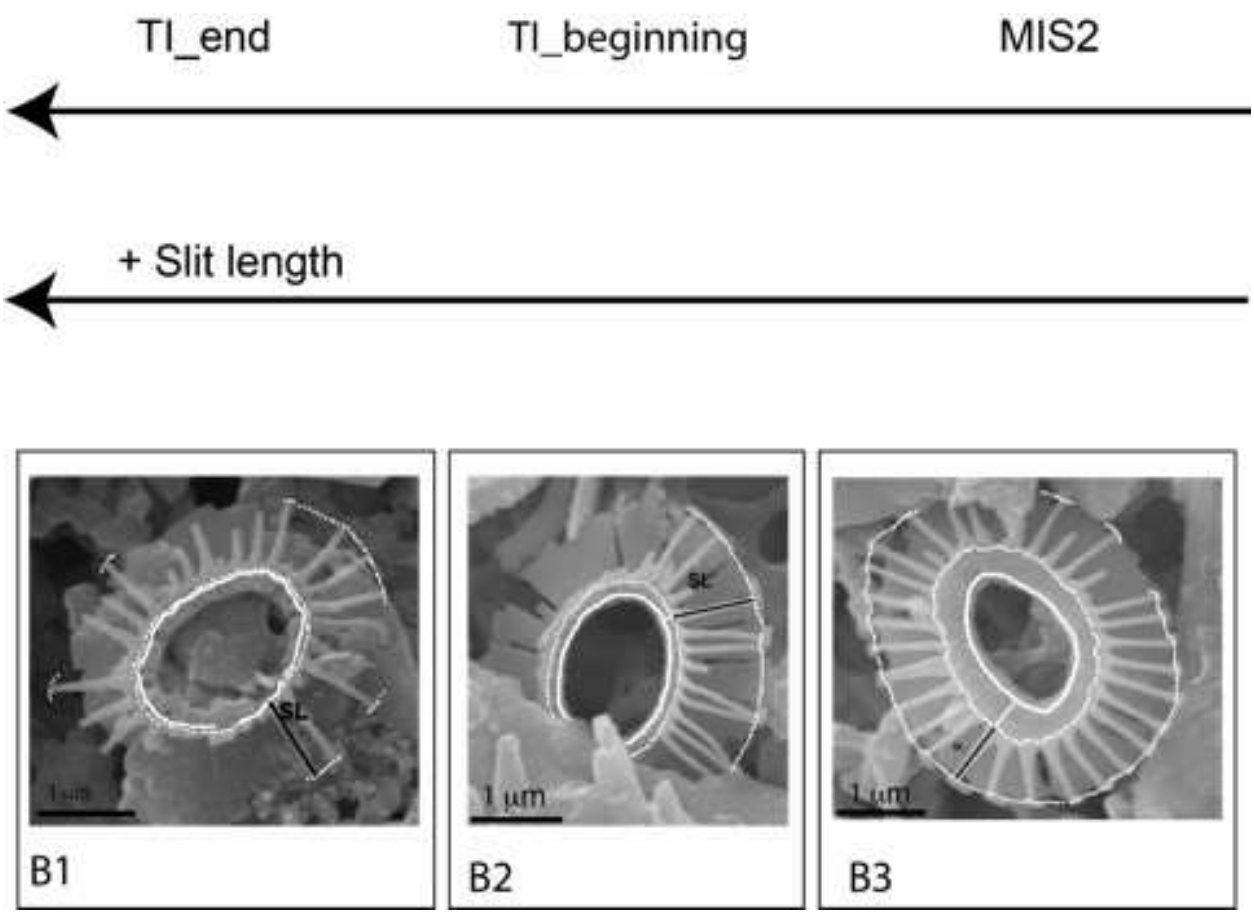

Figure 3.7b: Three different degrees of calcification in morphtoypes B of *E. huxleyi.*

3.6 Conclusions

The integration among different proxies, specifically the nannofossil CEX and foraminiferal dissolution indices, and inorganic carbon content, suggest the presence of two low preservation intervals at Site ODP 1089 in the interval comprised between 25 to 5 ka. These events mainly occur during the deglaciation as a response to lower alkalinity. During the glacial phase pelagic carbonate accumulation increases after the carbonate saturation interval, as a result of a decrease in deep ocean [CO_3^{2-}] and an increase in pCO_2, which triggered undersaturated conditions of the carbonate system in deep waters. This process would have in turn led to the rise of the CCD, in order to restore the carbonate saturation conditions, causing an increase in the alkalinity burial that outstripped the alkalinity system and triggered the deglacial dissolution as a buffer response. We also suggest that, as a response to glacial iron fertilization, there was an increase in the coccolithophore' strength of the carbonate counter pump. We suggest that during the glacial there was an increase in the carbonate counter pump and increased alkalinity at dissolution depths. An alternative counterbalancing mechanism could be related to the high magnitude of inorganic carbon accumulation secreted by foraminifera, which can be significant contributors to the production and export of PIC in certain ocean areas of the SO (*e.g.* Crozet, Kerguelen plateau).
Coccolith assemblages are mainly comprised by *E. huxleyi* and *C. leptoporus*, which seem to be highly influenced by iron fertilization and then by phosphorus content driven by westerlies' displacement. Specifically, low abundance of. *F. profunda* and high absolute concentrations of *C. pelagicus* represent the end members of their biogeographic distributions, which are controlled by equatorward STF movements. Moreover, highly calcified coccolith species in the assemblage and high *E. huxleyi* calcification values are a response to high alkalinity in the carbonate system.

Data availability

Data will be available on PANGAEA website.

Acknowledgments

This research used samples provided by the Integrated Ocean Drilling Program (IODP), which is sponsored by the U.S. National Science Foundation and participating countries under management of Joint Oceanographic Institutions, Inc. This research is part of the project PROductivity and

CARbonate dynamics in the Southern Ocean and impacts on atmospheric CO_2 (PROCARSO), 2010-2013. CA and CB are funded by University of Padova (SID 2016 - BIRD161002). G.M. acknowledges support from the University of Vigo programme to attract excellent research talent, and a generous start-up package. We are thankful to Richard Norris for his comments and suggestions, which have improved the manuscript.

Appendix A. Supplementary data

3.1 Taxonomy remarks and Coccolithophore biogeography in the Southern Ocean

Generally, the spatial distribution of the coccolithophore assemblages is controlled by water mass properties such as temperature, vertical mixing and nutrients (Boeckel and Baumann, 2008). The coccolithophore diversity (Shannon-Wiener diversity index) obtained for the Pacific sector of the SO is comparable to that observed in the Indian sector and the Drake passage (Saavedra Pellitero et al., 2014). Overall, *Emiliania huxleyi, Coccolithus pelagicus* and *Calcidiscus leptoporus* are the most abundant taxa in the modern SO (Baumann et al., 2004; Boeckel et al., 2006; Marino et al., 2009). South of 32° S and in the Benguela upwelling domain, *E. huxleyi* is a ubiquitous species and displays high abundances often over 50% of the entire assemblage. In the absence of *E. huxleyi, C. leptoporus* become the most abundant species. Additionally, the abundance of *F. profunda* decreases south of the STF (Baumann et al., 2004; Boeckel et al., 2006). As a taxonomic note, we emphasize that *Coccolithus* includes two species that are the Sub-Arctic *C. pelagicus* producing coccoliths <10 μm long, and a temperate sub-species *C. braarudii* producing larger coccoliths >10 μm long. *Calcidiscus leptoporus* consists of three sub-taxa, variously described as large, intermediate and small morphotypes or as separate sub-species, or species (Ziveri et al., 2004). The larger subspecies form of *C. leptoporus* tends to be more abundant in the equatorial region and is absent at higher latitudes; this is an indicator of meso-eutrophic conditions; the intermediate form has a wide distribution in cool, nutrient-poor waters. The ecology of the smaller form is unclear, since it seems to have a very patchy distribution (Ziveri et al., 2004). Boeckel et al. (2006) found that *F. profunda* and specimens ascribable to *Gephyrocapsa* are the most common taxa in the lower photic zone (LPZ) of the SO. However, among gephyrocapsids, small *Gephyrocapsa* (<4 μm) represents the major component (Marino et al., 2009).

3.2 Nutrient control on the coccolith assemblage

E. huxleyi shows a negative correlation with high P(g) hence increased upwelling; on the contrary *C. leptoporus* shows a good correlation with increase phosphorus budget. The nutrient primary control on coccolithophores seems to be exerted by iron for both *E. huxleyi* and *C. leptoporus*.

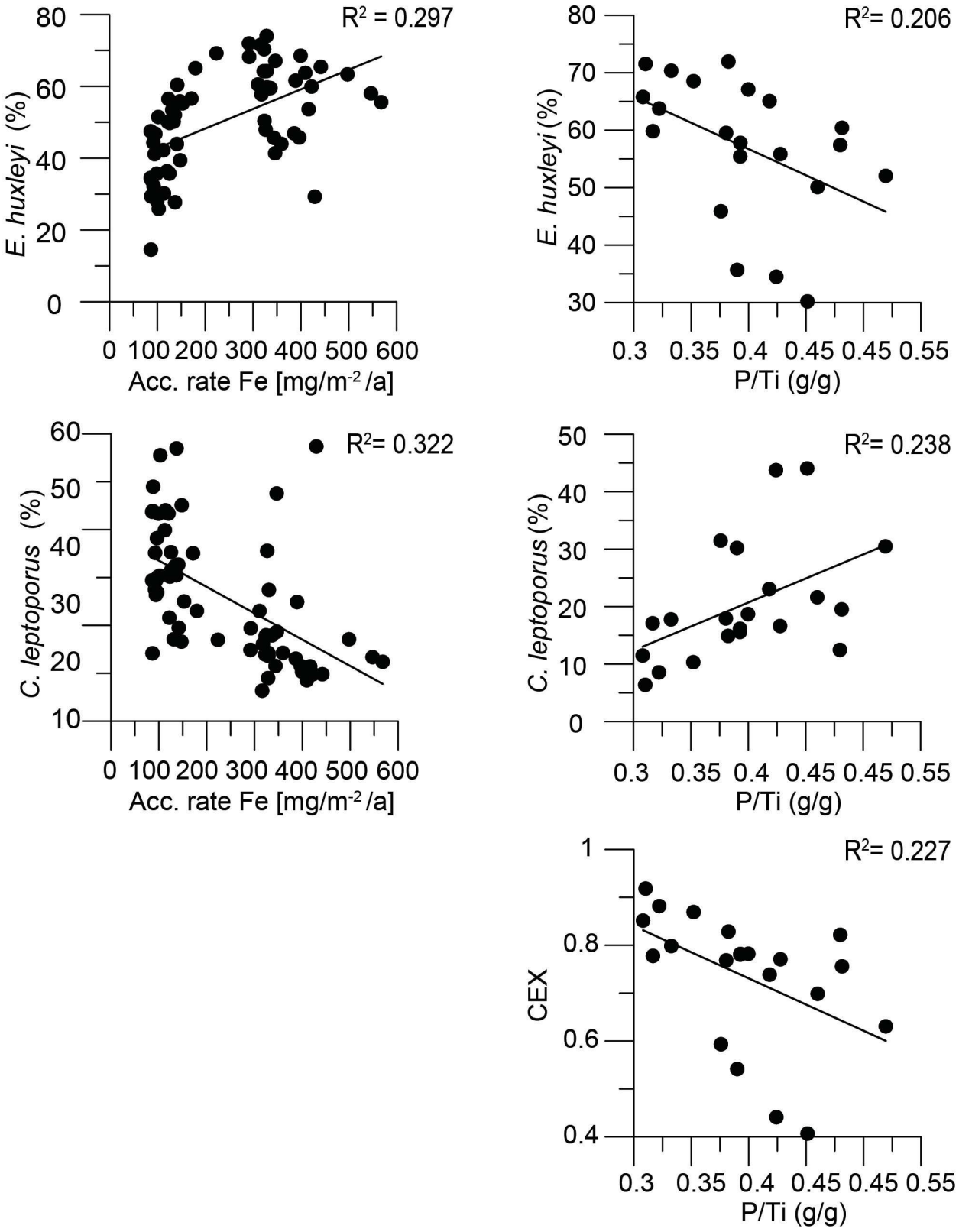

Figure S2: Correlation between *E. huxleyi* (%) and *C. leptoporus* (%) with Acc. Rate Fe [mg/m^{-2}/a] and P/Ti (g/g) and, CEX index is correlated with P/Ti (g/g).

Statistical results have been computed on MATLAB:

Fe_Ehux_p =

Linear regression model:

y ~ 1 + x1

Estimated Coefficients:

	Estimate	SE	tStat	pValue
(Intercept)	37.325	2.9301	12.738	5.7829e-19
x1	0.054606	0.010669	5.118	3.2237e-06

Number of observations: 64, Error degrees of freedom: 62

Root Mean Squared Error: 11.6

R-squared: **0.297**, Adjusted R-Squared 0.286

F-statistic vs. constant model: 26.2, **p-value = 3.22e-06**

Fe_Clep_p =

Linear regression model:

y ~ 1 + x1

Estimated Coefficients:

	Estimate	SE	tStat	pValue
(Intercept)	39.051	2.7815	14.04	6.4196e-21
x1	-0.055063	0.010128	-5.4366	9.7276e-07

Number of observations: 64, Error degrees of freedom: 62

Root Mean Squared Error: 11

R-squared: **0.323**, Adjusted R-Squared 0.312

F-statistic vs. constant model: 29.6, **p-value = 9.73e-07**

P/Ti_Ehux_p =

Linear regression model:

y ~ 1 + x1

Estimated Coefficients:

	Estimate	SE	tStat	pValue

(Intercept)	93.307	16.466	5.6667	1.8342e-05
x1	-91.47	41.122	-2.2244	0.038441

Number of observations: 21, Error degrees of freedom: 19

Root Mean Squared Error: 11.1

R-squared: **0.207**, Adjusted R-Squared 0.165

F-statistic vs. constant model: 4.95, **p-value = 0.0384**

P/Ti_Clep_p =

Linear regression model:

y ~ 1 + x1

Estimated Coefficients:

	Estimate	SE	tStat	pValue
(Intercept)	-12.745	13.718	-0.92912	0.36448
x1	83.624	34.259	2.441	0.024609

Number of observations: 21, Error degrees of freedom: 19

Root Mean Squared Error: 9.23

R-squared: **0.239**, Adjusted R-Squared 0.199

F-statistic vs. constant model: 5.96, **p-value = 0.0246**

P/Ti_CEX_p =

Linear regression model:

y ~ 1 + x1

Estimated Coefficients:

	Estimate	SE	tStat	pValue
(Intercept)	1.168	0.18525	6.305	4.7279e-06
x1	-1.0929	0.46264	-2.3624	0.028981

Number of observations: 21, Error degrees of freedom: 19

Root Mean Squared Error: 0.125

R-squared: **0.227**, Adjusted R-Squared 0.186

F-statistic vs. constant model: 5.58, **p-value = 0.029**

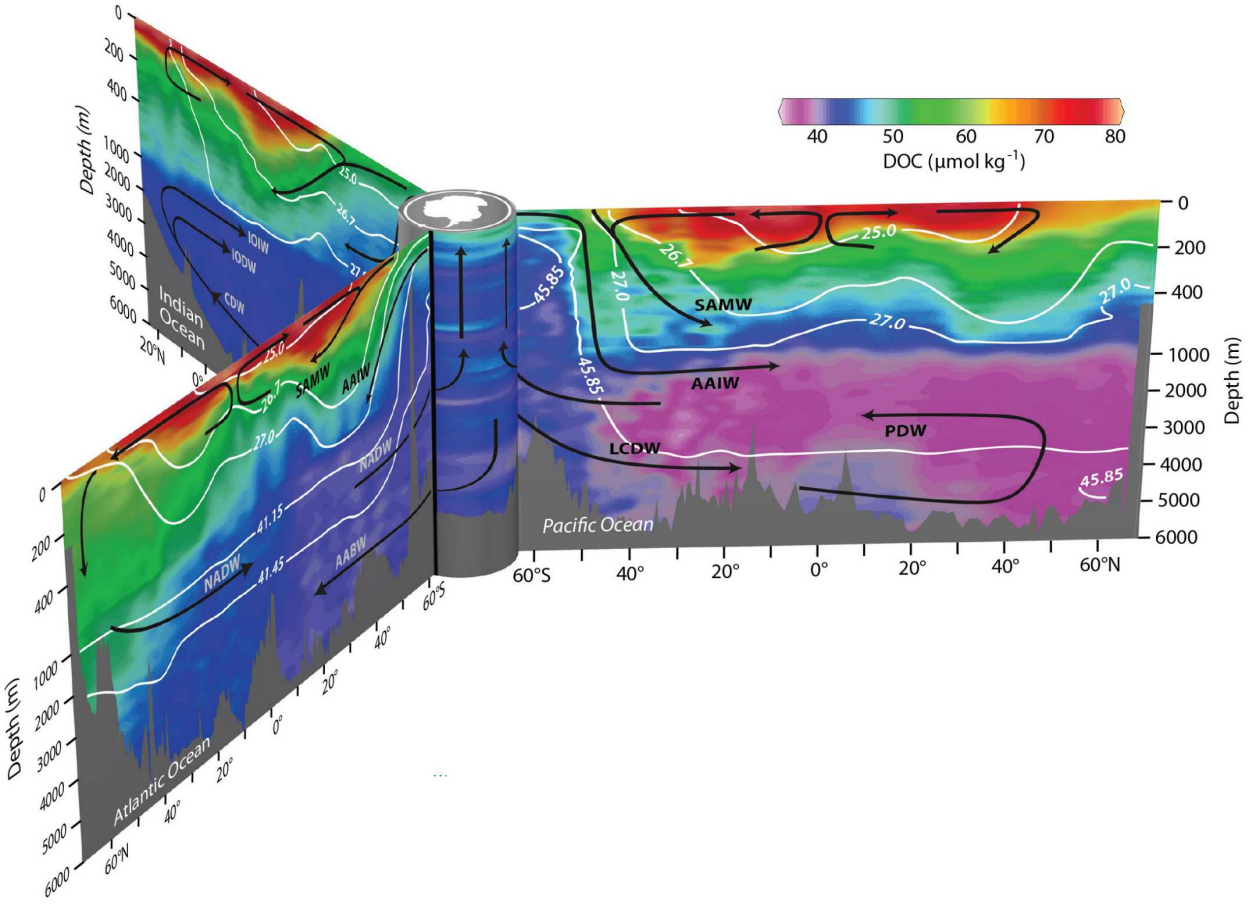

Figure S3: Distribution of DOC (µmol/kg) in the central Atlantic, Pacific and eastern Indian oceans with surface, intermediate and deep waters from all lines connected via the Antarctic circumpolar currents. White lines show constant density surfaces; black lines indicate water masses renewal. AABW, Antarctic Bottom Water; AAIW, Antarctic Intermediate Water; CDW, Circumpolar Deep Water; IODW, Indian Ocean Deep Water; IOIW, Indian Ocean Intermediate Water; LCDW, Lower Circumpolar Deep Water; NADW, North Atlantic Deep Water; PDW, Pacific Deep Water; SAMW, Subantarctic Mode Water. From Hansell et al., 2015.

References

Archer, D. (1991), Modeling the calcite lysocline, J. Geophys. Res., 96(C9), 17,037–17,050, doi:10.1029/91JC01812

Amore, F. O. et al. (2012). A Middle Pleistocene Northeast Atlantic coccolithophore record: Paleoclimatology and paleoproductivity aspects. *Marine Micropaleontology,* 90-91, 44–59. doi:10.1016/j.marmicro.2012.03.006.

Anderson, R. F. et al. (2009). Wind-Driven Upwelling in the Southern Ocean and the Deglacial Rise in Atmospheric CO_2 . *Science*, 323(1443). doi:10.1126/science.1167441.

Anderson R. F. et al. (2014). Biological response to millennial variability of dust and nutrient supply in the Subantarctic South Atlantic Ocean. *Philosphical Transaction of the Royal Society* A, 372, 20130054. DOI: 10.1098/rsta.2013.0054.

Balch, W. M. et al. (2016). Factors regulating the Great Calcite Belt in the Southern Ocean and its biogeochemical significance. *Global Biogeochemical Cycles*, 30, 1124–1144, doi:10.1002/ 2016GB005414.

Balch, W. M. et al. (2011). The contribution of coccolithophores to the optical and inorganic carbon budgets during the Southern Ocean Gas Experiment: new evidence in support of the "Great Calcite Belt" hypothesis. *J. Geophys. Res.* 116:C00F06. https://doi.org/10.1029/2011JC006941

Banse, K. (1996). Low seasonality of low concentrations of surface chlorophyll in the Subantarctic water ring: underwater irradiance, iron, or grazing? *Progress in Oceanography*, Volume 37, Issues 3–4, Pages 241–291, doi:10.1016/S0079-6611(96)00006-7.

Barber, R. T. et al. (1996). Primary productivity and its regulation in the equatorial Pacific during and following the 1991-1992 El Niño. *Deep-Sea Research Part II*, Vol.43, No. 4-6, pg.933-969. DOI: 10.1016/0967-0645(96)00035-5, 0.84.

Barnola, J. M., Raynaud, D., Korotkevich, Y. S. & Lorius, C. (1987). Vostok ice cores provides 160,000-year record of atmospheric CO_2. Nature 329, 408–414. doi: 10.1038/329408a0

Baumann, K.-H, Boeckel B. & Frenz M. (2004). Coccolith contribution to South Atlantic carbonate sedimentation, in: Thierstein H. R. and J. R. Young (Eds.). *Coccolithophores, From Molecular Processes to Global Impact, Springer*, doi:10.1007/978-3-662-06278-4.

Beaufort, L. (2005). Weight estimates of coccoliths using the optical properties (birefringence) of calcite. *Micropaleontol*ogy, 51, 289–298. DOI: 10.2113/gsmicropal.51.4.289.

Beaufort, L. & Dollfus D. (2004). Automatic recognition of coccoliths by dynamical neural networks. *Marine Micropaleontology*, 51(1):57-73. doi:10.1016/j.marmicro.2003.09.003.

Beaufort, L. et al. (1997). Insolation Cycles as a Major Control of Equatorial Indian Ocean Primary Production. *Science*, Vol. 278, no. 5342, pp. 1451-1454, doi:10.1126/science.278.5342.1451.

Beaufort, L. et al. (2011). Sensitivity of coccolithophores to carbonate chemistry and ocean acidification. *Nature* 476, 80–83. doi:10.1038/nature10295.

Beucher, C. P., Brzezinski M. A. & Crosta X. (2007). Silicic acid dynamics in the glacial sub-Antarctic: Implications for the silicic acid leakage hypothesis. *Global Biogeochemical Cycles*, vol. 21, gb3015. doi:10.1029/2006gb002746.

Blain S. et al. (2007). Effect of natural iron fertilization on carbon sequestration in the Southern Ocean. *Nature* 446: 1070–1074. DOI:10.1038/nature05700.

Boeckel, B. & Baumann K.-H. (2004). Distribution of coccoliths in surface sediments of the south-eastern South Atlantic Ocean: ecology, preservation and carbonate contribution, *Marine Micropaleontology,* 51, 301– 320, doi:10.1016/j.marmicro.2004.01.001.

Boeckel, B. & Baumann K.-H. (2008). Vertical and lateral variations in coccolithophore community structure across the subtropical frontal zone in the South Atlantic Ocean. *Marine Micropaleontology*, Volume 67, Issues 3–4, Pages 255–273. doi:10.1016/j.marmicro.2008.01.014.

Boeckel, B. et al. (2006). Coccolith distribution patterns in South Atlantic and Southern Ocean surface sediments in relation to environmental gradients. *Deep-Sea Research Part I,* 53 1073–1099. doi:10.1016/j.dsr.2005.11.006.

Bollmann, J. et al. (2002). Techniques for quantitative analyses of calcareous marine phytoplankton. *Marine Micropaleontology*, 44, 163-185. DOI: 10.1016/S0377-8398(01)00040-8

Bordiga, M. et al. (2014). Coccolithophore carbonate during the last 450 ka in the NW Pacific Ocean (ODP site 1209B, Shatsky Rise). *Journal of Quaternary Science*, 29(1) 57–69, doi:10.1002/jqs.2677.

Bown, P.R. & Young J. R. (1998). Introduction, in: Bown P.R. (ed). *Calcareous Nannofossil Biostratigraphy,* Chapman & Hall, London, pp 1–15.

Broecker, W. S. (1982a), Glacial to interglacial changes in ocean chemistry, Prog. Oceanogr., 11, 151–197.

Broecker, W. S. (1982b), Ocean chemistry during glacial time, Geochim. Cosmochim. Acta, 46, 1689–1705.

Broecker, W. S. & Peng T.-H. (1987), The role of $CaCO_3$ compensation in the glacial to interglacial atmospheric CO_2 change, *Global biogeochemical cycles*, vol. 1, no. 1, pages 15-29. https://doi.org/10.1029/GB001i001p00015.

Broerse, A. T. C. et al. (2000b). Export production, species composition, and coccolith-$CaCO_3$ fluxes in the NE Atlantic (34N 21W and 48N 21W). *Deep- Sea Res. II*, 47, 1877–1905.

Burckle, L. H. (1984). Diatom distribution and paleoceanographic reconstruction in the Southern Ocean — Present and last glacial maximum. *Marine Micropaleontology*, Volume 9, Issue 3, Pages 241–261. https://doi.org/10.1016/0377-8398(84)90015-X

Cachão M. & Moita M.T. (2000). *Coccolithus pelagicus*, a productivity proxy related to moderate fronts off Western Iberia, *Marine Micropaleontology,* 39 (1–4), pp. 131-155. 10.1016/S0377-8398(00)00018-9

Chappellaz, J., Barnola, J.-M., Raynaud, D., Korotkevich, Y. S. & Lorius, C. (1990). Ice-core record of atmospheric methane over the past 160,000 years. Nature 127 – 131. 10.1038/345127a0

Cheng, H. et al., (2016). Climate variations of central Asia on orbital to millennial timescales. Scientific Reports volume 6.

Cheng, H. et al., (2009). Ice Age Terminations. Science, vol. 326, pp. 248-252. DOI: 10.1126/science.1177840

Cermeño, P. et al. (2008). The role of nutricline depth in regulating the ocean carbon cycle. 20344–20349, *PNAS*, vol. 105, no. 51. https://doi.org/10.1073/pnas.0811302106.

Crow, F. L. et al. (1960). *Statistics manual:* New York (Dover Publ., Inc.).

Cubillos J.C., et al. (2007). Calcification morphotypes of the coccolithophorid *Emiliania huxleyi* in the Southern Ocean: changes in 2001 to 2006 compared to historical data. *Marine Ecology Progress Series* 348: 47–54. https://doi.org/10.3354/meps07058

D' Amario B. (2017). Coccolithophore calcification, life- cycle dynamics and diversity in a warming and acidifying Mediterranean Sea, (Doctoral Dissertation). Depòsit digital de documents de la UAB. Universitat Autònoma de Barcelona.

Denton G. H. et al. (2010). The last Glacial Termination. Vol. 328, Issue 5986, pp. 1652- 1656. DOI: 10.1126/science.1184119

De la Fuente M. et al. (2017). The evolution of the deep ocean chemistry and respired carbon in the eastern equatorial pacific over the last deglaciation. Paleoceanography, 32, 12, 1371-1385. https://doi.org/10.1002/2017PA003155

Dickson, A.J., et al. (2008). Mid-depth South Atlantic Ocean circulation and chemical stratification during MIS-10 to 12: implications for atmospheric CO_2, *Climate of the Past*, doi:10.5194/cp-4-333-2008.

Dittert N. et al. (1999). Carbonate dissolution in the deep-sea: methods, quantification and paleoceanographic application. G. Fischer, G. Wefer (Eds.), *Use of Proxies in Paleoceanography — Examples from the South Atlantic, Springer, Berlin* (1999), pp. 255-284.

Dollfus, D. & Beaufort L. (1999). Fat neural network for recognition of position-normalised object, *Neural Netw*, 12, 553–560.

Flores, J.-A. et al. (2012). The "White Ocean" Hypothesis: A Late Pleistocene Southern Ocean Governed by Coccolithophores and Driven by Phosphorus. *Frontiers in Microbiol*ogy 2012; 3: 233, doi: 10.3389/fmicb.2012.00233.

Flores J. et al. (2000). Southern Ocean pleistocene calcareous nannofossil events: Calibration with isotope and geomagnetic stratigraphies. *Marine Micropaleontology*, 40, 4, 377-402. 10.1016/S0377-8398(00)00047-5.

Franzese, M. A. (2008). Paleoceanography of the Agulhas Current and Retroflection determined by radiogenic isotopes in deep-sea sediments, (Doctoral dissertation). Graduate School of Arts and Sciences, University of Columbia, New York, USA.

Gersonde, R. et al. (2003). Last glacial sea surface temperatures and sea-ice extent in the Southern Ocean (Atlantic-Indian sector): A multiproxy approach. *Paleoceanography*, 18(3). Doi:1061, 10.1029/2002PA000809.

Gottschalk, J. et al. (2015). Abrupt changes in the southern extent of North Atlantic Deep Water during Dansgaard-Oeschger events. *Nature Geoscience*, 8(12), 950 - 954. https://doi.org/10.1038/ngeo2558.

Hallock, P. (1987). Fluctuations in the trophic resource continuum : a factor in global diversity cycles? Paleoceanography, 2, 5 457-471.

Hansell, D.A., C.A. Carlson, D.J. Repeta, and R. Schlitzer. 2009. Dissolved organic matter in the ocean: A controversy stimulates new insights. *Oceanography* 22(4):202–211, https://doi.org/10.5670/oceanog.2009.109.

Hartnett, A. et al. (2012). Iron transport and storage in the coccolithophore: *Emiliania huxleyi. Metallomics* 4:1160–66.

Hodell, D.A., Charles C. D. & F. J. Sierro (2001). Late Pleistocene evolution of the ocean's

carbonate system, *Earth and Planetary Science Letters,* 192 109-124. 10.1016/s0012-821x(01)00430-7

Hodell, D. A. et al. (2003). The Mid-Brunhes Transition in ODP Sites 1089 and 1090 (Subantarctic South Atlantic), Earth's Climate and Orbital Eccentricity: The Marine Isotope Stage 11. *Question Geophysical Monograph 137*, Copyright by the American Geophysical Union. doi: 10.1029/137GM09.

Horigome, M.T. et al. (2014). Environmental controls on the *Emiliania huxleyi* calcite mass. *Biogeosciences*, 11, 2295–2308. doi:10.5194/bg-11-2295-2014

IPCC (2013), Summary for Policymakers, in Climate Change 2013: *The Physical Science Basis. Contribution of Working Group I to the Fifth Assessment Report of the Intergovernmental Panel on Climate Change*, edited by T. F. Stocker et al., Cambridge Univ. Press, Cambridge, U.K., and New York.

Jansen, E. et al. (2007). Paleoclimate. In: *Climate Change 2007: The Physical Science Basis. Contribution of Working Group I to the Fourth Assessment Report of the Intergovernmental Panel on Climate Change* [Solomon, S., D. Qin, M. Manning, Z. Chen, M. Marquis, K.B. Averyt, M. Tignor and H.L. Miller (eds.)]. Cambridge University Press, Cambridge, United Kingdom and New York, NY, USA.

Kanfoush, S.L. (2013). Correlation of Ice-Rafted Detritus in South Atlantic Sediments with Climate Proxies in Polar Ice over the Last Glacial Period, *Reprinted from International Journal of Ocean and Climate Systems*, Volume 4, Number 1.

Klaas, C. & Archer, D.E., (2002). Association of sinking organic matter with various types of mineral ballast in the deep sea: implications for the rain ratio. Global Biogeochem. Cycles 16, 63-1–63-14. http://dx.doi.org/10.1029/2001GB001765. 1116.

Keeling, C. D. & Whorf T. P. (2004). Atmospheric CO_2 records from sites in the SIO air sampling network, in *Trends*: A Compendium of Data on Global Change, Carbon Dioxide Inf. Anal. Cent., Oak Ridge Natl. Lab., U.S. Dep. of Energy, Oak Ridge, Tenn.

Köbrich, M.I. & Baumann K.-H. (2008). Coccolithophore flux in a sediment trap off Cape Blanc (NW Africa). *Journal of Nannoplankton Research*, 30 (2), 83-96.

Lippold, J. et al. (2016). Deep water provenance and dynamics of the (de)glacial Atlantic meridional overturning circulation. *Earth and Planetary Science Letters*, 445, 68-78. https://doi.org/10.1016/j.epsl.2016.04.013.

Lototskaya, A. et al. (1998). Calcareous nannoflora response to Termination II at 45° N, 25° W (northeast Atlantic), *Marine Micropaleontology,* 34: 47-70.

Marchetti A. & Maldonado M.T. (2016). Iron. In *The Physiology of Microalgae*, ed. MA Borowitzka, J Beardall, JA Raven, pp. 233–79. Cham, Switz.: Springer.

Marchitto, T. M., J. Lynch-Stieglitz, & S. R. Hemming (2005). Deep Pacific $CaCO_3$ compensation and glacial-interglacial atmospheric CO2, Earth Planet. Sci. Lett., 231, 317–336, doi:10.1016/j.epsl.2004.12.024.

Marino G. et al., (2015). Bipolar seesaw control on last interglacial sea level. Nature volume 522, pages 197–201. doi: 10.1038/nature14499.

Marino, M. et al. (2009). Response of calcareous nannofossil assemblages to paleoenvironmental changes through the mid-Pleistocene revolution at Site 1090 (Southern Ocean). *Palaeogeography, Palaeoclimatology, Palaeoecology*, 280 333–349. doi:10.1016/j.palaeo.2009.06.019

Martínez-Botí, M. A. et al. (2015). Boron isotope evidence for oceanic carbon dioxide leakage during the last deglaciation. *Nature* 518, 219–222. doi:10.1038/nature14155.

Martínez-García, A. et al. (2014). Iron Fertilization of the Subantarctic Ocean During the Last Ice Age, *Science*, 343, 1347. doi: 10.1126/science.1246848.

Martínez-Méndez, G., et al. (2010). Contrasting multiproxy reconstructions of surface ocean hydrography in the Agulhas Corridor and implications for the Agulhas Leakage during the last 345,000 years. *Paleoceanography*, Vol. 25, pa4227, doi:10.1029/2009PA001879.

Martin, J. H., et al. (1989). VERTEX:phytoplankton/iron studies in the Gulf of Alaska.*Deep-SeaRes*.,36649-680.

Martin, J. H., Gordon R. M., Fitzwaterand S. & Broenkow W. W. (1990). Glacial-Interglacial CO_2 change: the iron hypothesis. *Paleoceanography*. 5. 1- 13.

Martin, J.H., Gordon R. M. & Fitzwater S. E. (1990). Iron in Antarctic waters. Nature. 345. 156-158.

Martin, J. H., Gordon R. M. & Fitzwater S. E. (1991). The case for iron. *Limnology Oceanogr*aphy, 36(8), 1793-1802© 1991, by the *American Society of Limnology and Oceanography*, Inc.

McIntyre, A., Bé A. W. H., & Roche M. B. (1970). MODERN PACIFIC COCCOLITHOPHORIDA: A PALEONTOLOGICAL THERMOMETER. *Transactions of the New York Academy of Sciences*, 32: 720–731. doi:10.1111/j.2164-0947.1970.tb02746.

McManus, J.F. et al. (2004). Collapse and rapid resumption of Atlantic meridional circulation linked to deglacial climate changes: *Nature*, v. 428, p. 834–837. doi: 10.1038/nature02494.

Mejía, L. M. et al. (2014). Effects of midlatitude westerlies on the paleoproductivity at the Agulhas Bank slope during the penultimate glacial cycle: Evidence from coccolith Sr/Ca ratios. *Paleoceanography*, 29, 697–714, doi:10.1002/2013PA002589.

Mohan R. et al. (2008). Ecology of coccolithophores in the Indian sector of the Southern Ocean. Volume 67, Issues 1–2, April 2008, *Pages* 30-45.

Moreno A., et al. (2005). Links between oscillation at the millennial time-scale. A multi-proxy study of the last 50,000 from the Alboran Sea (Western Mediterranean Sea). *Quat. Sci. Rev.* 24, 1623–163610.1016/j.quascirev.2004.06.018.

Mortyn, P.G. & Charles C. D. (2003). Planktonic foraminiferal depth habitat and $\delta^{18}O$ calibrations: Plankton tow results from the Atlantic sector of the Southern Ocean, *Paleoceanography*, Vol. 18, no. 2, 1037, doi:10.1029/2001PA000637.

Mortyn, P. G., Charles C. D. & Hodell D. A. (2002). Southern Ocean upper water column structure over the last 140 kyr with emphasis on the glacial terminations, *Global and Planetary Change 34*, 241–252.

Nuester, J. et al. (2014). The regeneration of highly bioavailable iron by meso- and microzooplankton. *Limnol. Oceanogr.* 59:1399–409.

Okada H. & McIntyre A. (1979). Seasonal distribution of modern Coccolithophores in the Western North Atlantic Ocean. *Marine Biology,* 54 (1979), pp. 319-328.

Olson, M. B., et al. (2017). Ocean acidification effects on haploid and diploid *Emiliania huxleyi* strains: Why changes in cell size matter*, J. Exp. Mar. Biol. Ecol*., 488, 72-82, doi: 10.1016/j.jembe.2016.12.008, 2017.

Oppo, D.W. & Fairbanks R. G. (1987). Variability in the deep and intermediate water circulation of the Atlantic Ocean during the past 25,000 years: Northern Hemisphere modulation of the Southern Ocean. *Earth and Planetary Science Letters*. Volume 86, Issue 1, Pages 1-15.

Orsi, A. H., Whitworth T. & Nowlin Jr. W. D. (1995). On the meridional extent and fronts of the Antarctic Circumpolar Current, *Deep-Sea Research I,* Vol. 42, No. 5, pp. 64-673, *Elsevier Science* Ltd Printed in Great Britain.

Parrenin, F., et al. (2013). Atmospheric carbon dioxide, methane, deuterium, and calculated Antarctic temperature of EPICA Dome C ice core, *Science*, Vol. 339, Issue 6123, pp. 1060-1063. doi: 10.1126/science.1226368.

PÉrez-Mejías, C. et al., (2017). Abrupt climate changes during Termination III in Southern Europe. PNAS. Vol. 114, Issue 38, pp. 10047 LP – 10052.

Pollard R.T., et al. (2009). Southern Ocean deep-water carbon export enhanced by natural iron fertilization. *Nature* 457: 577–580.

Poulton, A.J., et al. (2017). Coccolithophore ecology in the tropical and subtropical Atlantic Ocean: New perspectives from the Atlantic meridional transect (AMT) programme, *Progress in Oceanography*, 10.1016/j.pocean.2017.01.003.

Rembauville, M., et al. (2016). Planktic foraminifer and coccolith contribution to carbonate export fluxes over the central Kerguelen Plateau, *Deep Sea Research,* Part I, 111, 91–101. http://dx.doi.org/10.1016/j.dsr.2016.02.017

Rickaby, R. E. M., et al. (2010). Evidence for elevated alkalinity in the glacial Southern Ocean, *Paleoceanography*, 25, PA1209, doi:10.1029/2009PA001762.

Raffi, I., & Rio D., (1981). *Coccolithus pelagicus* (Wallich): a paleotemperature indicator in the late Pliocene Mediterranean deep sea record. *In* Wezel, F.C. (Ed.), *Sedimentary Basins of Mediterranean Margins:* C.N.R. Italian Project of Oceanography, Bologna (Tecnoprint), 187–190.

Riebesell, U., et al. (2000). Reduced calcification of marine plankton in response to increased atmospheric CO_2, *Nature*, 407, 364-367.

Rio, D., Fornaciari E. & Raffi I. (1990a). Late Oligocene through early Pleistocene calcareous nannofossils from western equatorial Indian Ocean (Leg 115), in *Duncan*, R.A., Backman, J., L. C. Peterson et al., Proc. ODP, Sci. Results, 115: College Station, TX (Ocean Drilling Program), 175-235.

Rio, D., Raffi I. & Villa G. (1990b). Pliocene-Pleistocene calcareous nannofossil distribution patterns in the western Mediterranean, *in* Kastens, K.A., J. Mascle, et al*., Proc. ODP, Sci. Results,*107: College Station, TX (Ocean Drilling Program), 513-533.

Rohling E.J., et al., (2012). Making sense of paleoclimate sensitivity, *Nature*, 491 (7426), 683-691. doi:10.1038/nature11574

Saavedra-Pellitero, et al. (2014). Biogeographic distribution of living coccolithophores in the Pacific sector of the Southern Ocean, *Marine Micropaleontology* 109, 1–20. https://doi.org/10.1016/j.marmicro.2014.03.003

Salter, I., et al. (2014). Carbonate counter pump stimulated by natural iron fertilization in the Polar Frontal Zone, *Nature Geosciences,* letters, 7, 885-889. doi: 10.1038/NGEO2285.

Sarmiento, J.L., Toggweiler J. R. & Najjar R. (1988). Ocean carbon-cycle dynamics and atmospheric pCO_2. Philos T Roy Soc London 325: 3–21.

Schmitt J., et al. (2012). Carbon isotope constraints on the deglacial CO_2 rise from ice cores. Science 336, 711–714.

Shemesh, A., et al. (2002). Sequence of events during the last deglaciation in Southern Ocean sediments and Antarctic ice cores, *Paleoceanography*, doi: 10.1029/2000PA000599.

Shevenell, A.E. & Bohaty S. M. (2012). Southern exposure: New paleoclimate insights from Southern Ocean and Antarctic margin sediments, *Oceanography* 25(3):106–117, http://dx.doi.org/10.5670/oceanog.2012.82.

Schulz, K.G., et al. (2004). Effect of trace metal availability on coccolithophorid calcification. *Nature*, 430, 673–676.

Shipboard Scientific Party, (1999). Site 1088. *In* Gersonde R, Hodell DA, Blum, P., et al., *Proc. ODP, Init. Repts.,* 177, 1-66 [Online].

Skinner, L. C., et al. (2010). Ventilation of the Deep Southern Ocean and Deglacial CO_2 Rise, *Science*, DOI: 10.1126/science.1183627.

Thunell, R.C., (1982). Carbonate dissolution and abyssal hydrography in the Atlantic Ocean. Marine Geology, 47: 165-180.

Toggweiler, J.R. (1999), Variation of atmospheric CO_2 by ventilation of the ocean's deepest water. *Paleoceanography*, Vol. 14, No. 5, Pages 571-588.

Watson, A.J., et al. (2000). Effect of iron supply on Southern Ocean CO_2 uptake and implications for glacial atmospheric CO_2. Nature 407, 730-733 (2000). doi:10.1038/35037561.

Winter A., Jordan R. & Roth P. (1994). Biogeography of living Coccolithophores in ocean waters. A. Winter, W. Siesser (Eds.), Coccolithophores, *Cambridge University Press, Cambridge* (1994), pp. 13-37.

Wolff E. W., Fischer H. & Röthlisberger. (2009). Glacial terminations as southern warmings without northern control. Nature Geoscience, 2, pages 206- 209. DOI: 10.1038/NGEO442

Young, J. R. & Ziveri P. (2000), Calculation of coccolith volume and its use in calibration of carbonate flux estimates, *Deep-Sea Research Part II,* 47, 1679-1700.

Yu, J., et al. (2014). Deep South Atlantic carbonate chemistry and increased interocean deep water exchange during the last deglaciation. *Quat. Sci. Rev.* 90, 80–89.

Ziveri, P., et al. (2004). Present day coccolithophore-biogeography in the Atlantic Ocean. In: Thierstein, H. & Young J. R. (Eds.), Coccolithophores: from Molecular Processes to Global Impact. Springer Verlag, pp. 403-428.

Ziveri, P., et al. (2004). Biogeography of selected Holocene coccoliths in the Atlantic Ocean. Edition: Coccolithophores: From Molecular Processes to Global Impact, Publisher: Springer Verlag, Editors: Thierstein, H. and Young, J., pp.403-428. DOI: 10.1007/978-3-662-06278-4_15.

Ziveri, P., et al. (2007). Sinking of coccolith carbonate and potential contribution to organic carbon ballasting in the deep ocean, *Deep-Sea Research II* 54, 659–675, doi: 10.1016/j.dsr2.2007.01.006.

Ziveri, P., Young J. R. & van Hinte J. E. (1999). Coccolithophore export production and accumulation rates, In: On determination of sediment accumulation rates, *GeoResearch Forum, Trans Tech Publications LTD*, Switzerland, Volume 5: 41-56.

CHAPTER 4

Coccolithophore carbonate production and carbon cycle implications in the Subantarctic South Atlantic Ocean (PS2498-1) during the last 19 ky

Abstract

Reconstructions of past changes in the marine biological carbon pumps have become an important issue in order to understand the ocean-atmosphere CO_2 exchanges, especially in the Southern Ocean. Coccolithophore assemblages at Site PS2498-1, in the Subantarctic South Atlantic Ocean (44°15' S, 14°23' W, 3.783 m water depth), were used to reconstruct paleoproductivity variations during the last deglaciation (Marine Isotope Stage (MIS) 2-1). Site PS2498-1 is located at 3.783 m, below the calcite saturation horizon (CSH; 3.690 m), above the lysocline (4.175 m) and it is characterized by an 'Atlantic type' carbonate stratigraphy, where high carbonate production are recorded during interglacials. Coccolithophore assemblages were overwhelmingly dominated by *Emiliania huxleyi* and *Calcidiscus leptoporus*. Absolute coccolith concentrations, coccolith accumulation rates and coccolith carbonate contribution showed highest productivity throughout MIS1, which allows us to infer changes in the concentration of past atmospheric CO_2. We also suggest that the decrease in the surface ocean pH, that occurred during the Holocene, could have resulted in a change in the coccolithophores community structure, and a decrease in *C. leptoporus* and *E. huxleyi* coccolith size. The decrease in *E. huxleyi* coccolith mass (pg) observed during the Holocene is possibly related to an evolutionary adaptation in response to undersaturated water conditions.

4.1 Introduction

Coccolithophores are unicellular pelagic algae which are very abundant in the whole ocean's nannophytoplankton. Coccolithophore assemblages are diagnostic for understanding physical and chemical photic zone conditions, consequently they can be used as proxies for paleoecological and paleoceanographic recunstructions (McIntyre and Be, 1967; Giraudeau et al., 1993; Andruleit and

Baumann, 1998; Nederbragt et al., 2008; Okada and McIntyre, 1979). They produce a carbonate skeleton which is characterized by calcareous plates (< 20 μm) that are called coccoliths. Because of their small size and large abundance, it is possible to sample marine sediment cores at very high resolution. We analyzed coccolith assemblage in dated sediment samples from Site PS2498-1 which is located in the Subantarctic South Atlantic Ocean spanning the last deglaciation (19 ky). The Holocene is particularly useful to consider because it provides a reliable basis to anticipate any future climate evolution caused by global warming (Sabine, 2004; Tzedakis et al., 2009; Rohling et al., 2012, Journal of Climate; IPCC, 2013). This region is hydrographically dominated by the eastward flux of the Antarctic Circumpolar Current (ACC), which is modulated by the Antarctica's ice sheet fluctuations and westerlies' position (Mejìa et al., 2014; Martìnez-Garcìa et al., 2014), and by saturated and undersaturated in carbonate content deep waters throughout glacial-interglacial cycles (Martínez-Botí et al., 2015; Yu et al., 2016; Gottschalk et al., 2016; Warratz et al., 2017). These millenial-scale climate changes have accompanied the last glacial period and deglaciation, but it is still a matter of dibate which are the 'control valves'. Site PS2498-1 is characterized by an 'Atlantic type' carbonate stratigraphy, being defined by low carbonate sedimentation during glacials and then enhanced carbonate during the interglacials (Hodell et al., 2001). Coccolithophores can alter the inorganic carbon system and alkalinity of the seawater because of two processes, photosynthesis and calcification, which consume and produce respectively CO_2 (Calvo et al., 2004; Rost and Riebesell, 2004). Shift in the dominant plankton type (from carbonate to siliceous producing) could have decrease the production of $CaCO_3$ hence increasing the seawater carbonate ion content and then causing enhanced drawdown of atmospheric CO_2 values during the glacial time. This along with changes in ventilation of deep sea waters could account, in part, for a sequestering of atmospheric CO_2 into the ocean. Many authors propose the SO as a pool for sequestring and releasing carbon dioxide during the last deglaciation (Broeker, 1982; Martinez-Boti et al., 2015; Yu et al., 2016). High biological production, through the biological pump, is meant to play a crucial role in the air-sea gas exchange (Candell et al., 2007; Anderson et al., 2017); mostly if responding to iron fertilization (diatoms) and phosphorus delivery (coccolithophores) through the shift of the glacial upwelled Antarctic cell (Martin, 1990; Flores et al., 2012; Martinez-Garcia et al., 2014; Lorenzo et al., 2018; Balestrieri et al., in review). Past works have showed high levels of dust influx that could have stimulated the biological productivity in the Subantarctic South Atlantic during the last Glacial (Kumar et al., 1995;

Martinez-Garcia et al., 2009; 2011; Anderson et al., 2017). Specifically, iron seems to be crucial for phytoplankton growth because of its association to some fundamental physiological processes, such as photosynthesis, respiration and nitrate assimilation (Beherenfeld and Milligan, 2013). Moreover, since the last Glacial Maximum (LGM), atmospheric CO_2 emissions have risen from 180 to 370 ppm (Langer et al., 2006), and it has been largely absorbed by the oceans leading to a reduction in surface pH and carbonate saturation (Feely, 2004; Martinez-Boti et al., 2015). The decrease in seawater pH in response to Ocean Acidification (OA) may also increase or decrease iron solubility depending on the nature of the strong organic iron ligands (Millero et al., 2009; Shi et al., 2010), hence affecting positively or negatively ocean productivity and CO_2 drawdown based on iron bioavailability. Marine ecosystems are influenced by changes in the seawater pH due to OA because pH affects chemical and physiological reactions (Hoffman et al., 2012). Specifically, increasing or decreasing phytoplankton productivity, calcification, nitrogen and phosphorus acquisition (Hutchins et al., 2009; Riebesell and Tortell, 2011; Mackey et al., 2015).

In a rapidly changing global environment, it is fundamental to gain more insights about ecosystem responses. Hence, the analysis of coccolithophore assemblages is a useful tool for infering changes in the reconstruction of some of this features, such as productivity. Some studies have demonstrated the importance of coccolithophores in the reconstruction of productivity conditions in order to understand the relationship between these primary producers and surface ocean dynamics (Flores et al., 2012; Cabarcos et al., 2014). OA, warming and hence stratification (which lead to nutrient-deplete waters) with other environmental parameters, are meant to influence biogeochemical cycling of nutrients (Hutchins et al., 2009), coccolithophore community structure, morphology and calcification degree by controlling their distribution in the ocean (Winter et al., 1994). We evaluate coccolith absolute abundances, accumulation rates and burial of $CaCO_3$ to the sediments in order to understand coccolith carbonate contribution through the carbonate counterpump. In the present work we also evaluate the analysis of coccolith mass dynamics in relation to calcification and length dynamics throughout the study period with the aim to analyse the coccolith response to the carbonate system parameters and dynamics. Previous studies in the context of ocean acidification and coccolith calcification in sediment samples indicate controversial results (Fig. 4.3) (Beaufort et al., 2011; McClelland et al., 2016). The goals of this study are then: (i) to reconstruct changes in the paleoproductivity by the response of coccolith assemblage; (ii) to infer changes in the carbonate system; (iii) to speculate possible causes on how

Emiliania huxleyi and *Calcidiscus leptoporus* coccolithophores' size and weight have been infuenced by oceanographic global changes.

4.2 Site Location and Oceanographic Setting

Core PS2498-1 is located in the Subantarctic Atlantic Ocean and it was recovered by the RV Polastern vessel from the eastern flank of the mid-Atlantic Ridge (44°15' S, 14°23' W, 3.783 m water depth; Fig. 4.1). The Subantarctic zone of the South Atlantic is an area dominated by the extensive eastward stream of the Antarctic Circumpolar Current which consists of three zonal belts of water masses and fronts (Orsi et al., 1995; Mejía et al., 2014; Patil et al., 2017). The prevailing winds of this region (i.e., westerlies) drive the eastward deflection of the Brazil current (BC) into the South Atlantic current (SAC). This surface water system is controlled by the interaction between high-subtropical and low-subpolar pressure fields that are in turn related to the Subtropical front (STF), the Subantarctic front (SAF) and the Polar front (PF). These fronts differ by having different temperatures, salinity and nutrient concentrations (Fig. 4.1; Orsi et al., 1995; Mejía et al., 2014). Today the PF is located about 6° South to core PS2498-1 but the position of the PF was inverted with the study site during the glacials (Schmidt et al., 2003). At present, the depth of the study site is below the calcite carbonate saturation horizon (CSH; Ω= 0.99 at 3.690 m) and above the lysocline (4.175m). The study area is presently bathed by the Lower Circumpolar Deep water in the passage between corrosive (low [CO_3^{2-}]) southern- sourced Antarctic Bottom water (AABW) and more alkaline (higher [CO_3^{2-}]) northern- sourced North Atlantic Deep water (NADW, Fig. 4.2; Gottschalk et al., 2015).

4.3 Material and Methods

A total of 32 samples have been analyzed from Core PS2498-1 spanning a 132 cm-thick interval, which documents the time interval from 2 ka to 19 ka. The adopted age model is based on ^{14}C radiometric dating (Martínez-Botí et al., 2015). The sample was prepared following the filtration method (Andruleit, 1996). This procedure requires the use of about 30 mg of dry bulk sediment of the sample that were weighed and placed in small glass vials. An amount of ca. 40 ml of tap water were added in each small glass vial. In order to dissolve aggregates, the solution was placed in an ultrasonic bath for 30 seconds. 5 ml of solution were extracted then filtered onto a polycarbonate membrane (0.45 μm pore size, Millipore®) and oven-dried at 40 °C for 12 hours. For light

microscope analysis a portion of each filter was cut, mounted onto a glass slide and finally secured with Canada balsam glue (density at 20°C: 0.99; ROTH) and a cover slip. The sample slides were then analyzed using a ZEISS Axioskop40 transmitted light microscope at 1250X magnification. Species identification was based on the taxonomy provided by Nannotax 3, an electronic guide to the biodiversity and taxonomy of coccolithophores (http://www.mikrotax.org/Nannotax3/index.php?dir=Coccolithophores3).
In order to evaluate the relative abundance of taxa, at least 300 coccoliths were counted; absolute abundances are estimate counting the number of specimens of the analysed taxa present in specific area (1mm^2; Crow et al., 1960; Backman and Shackleton, 1983) and in the total filtered area (706.5 mm^2). The absolute abundance of coccoliths (no. of coccoliths g^{-1} dry sediment) are calculate with following formula:

(Nc x Sf) / (No x So x Ws) (eq. 1).

Nc= Number of coccoliths counted
Sf= Surface of the filter
No= Number of fields of view
So=Surface of the field of view
Ws= Weight of sediment filtered

To evaluate the length of major axis of *Emiliania huxleyi*, the slides were analyzed with a Leica DM6000B cross polarized light microscope fitted to a SPOT Insight Camera, at 1000X magnification. Fourthy pictures were taken for each sample and were processed using the SYRACO (SYstème de Reconnaissance Automatique de COccolithes), a software developed for the automatic recognition of coccolihs (Dollfus and Beaufort, 1999; Beaufort and Dollfus, 2004).

4.3.1 CEX' index

The CEX' index is used to estimate the effect of carbonate dissolution on coccoliths. The calculation of this index is based on the relative abundance of selected species: *E. huxleyi*, *Gephyrocapsa muellerae* and *Calcidiscus leptoporus* (Dittert et al., 1999; Boeckel and Baumann, 2004). The first two species are relatively fragile while *C. leptoporus* is high resistant taxon.

The CEX' dissolution index is calculated using this formula:

CEX'= *E. huxleyi* (%) + *G. muellerae* (%) / [*E. huxleyi* (%) + *G. muellerae* (%) + *C. leptoporus* (%)] (2)

Overall, low CEX' values indicate high dissolution while high values designate no or little dissolution. A threshold of 0.6, estimated for South Atlantic sediments, is used to detect dissolved samples (Boeckel and Baumann, 2004).

4.3.2 *Emiliania huxleyi* and *Calcidiscus leptoporus* Length index

We calculated a length index (L_i) for the two most abundant species within the assemblage. For *E. huxleyi*; by using the results obtained from SYRACO and knowing that coccolith mass depends both on length and its degree in calcification, we calculated a length index (L_i), considered independently from coccolith calcification degree, following eq. 4; (D' Amario 2017):

$L_i = \frac{Ls}{Ln}$ (4)

Where L_s is the length measured with SYRACO, L_n is the corrected length for a coccolith of a certain length (μm) based on D' Amario et al 2017 equation.

For *C. leptoporus* we also used eq. (4), measuring the different diameters at the SEM and then normalizing them by the mean value. For this type of analysis we considered 14 out of 32 samples.

4.3.3a Coccolith accumulation rates

We calculated the coccolith accumulation rate (ARc; Ziveri et al., 1999) as follows:

ARc= Dc × DBD × SR (eq. 5)

ARc= coccolith accumulation rates (number of coccoliths cm^{-2} ka^{-1})

Dc= coccolith density (number of coccoliths/gram of sediment)

DBD= dry bulk density (g cm^{-3}; data from Anderson et al., 2014)

SR= sedimentation rates (cm ka^{-1}; based on radiocarbon data from Gersonde et al., 2003).

4.3.3b Coccolith $CaCO_3$ accumulation rate

Coccolith carbonate burial (g; $CaCO_3$) was calculated based on Suchéras-Marx and Henderiks (2014) and Saavedra-Pellitero et al., (2017), as follows:

$CoccolithCaCO_3 = [\Sigma(C \times mass_{taxa})]$ (eq. 6)

C= number of coccoliths per gram of sediment

$mass_{taxa}$=species-specific coccolith carbonate (in picogram per coccolith).

Average individual coccolith species- specific masses were taken from Young and Ziveri (2000), and calculations followed Suchéras-Marx and Henderiks (2014). Coccolith carbonate estimates (%) were evaluated within the $CaCO_3$ (%, wt) content, assuming that coccolith carbonate constitutes 60 to 90% of bulk carbonate (Bordiga et al., 2014).

4.3.4 Definition of the morphotypes

C. leptoporus is characterised by large morphological variability. We distinguished three different morphotypes based on a quantitative approach by considering the definition of size boundaries between the coccolith diameter of the morphotypes (Knappertsbuch et al., 1997; Renaud et al., 2002). Being aware of the overlap within the different morphotypes, in particular between *C. leptoporus* and *C. quadriperforaturs,* we defined *C. leptoporus* small and *C. leptoporus* which are the two morphotypes we found in our samples. We analysed the shape of the suture and central area (Klejine, 1993; Renaud et al., 2002; Baumann et al., 2016) at the SEM in 14 samples, in order to understand the occurrence of the main morphotype and to measure the diameter of the external shield. SEM pictures were taken using a Zeiss Sigma HD FE-SEM. The SEM was operated at 5 kV for a spot-size of less than 5 nm. Images were formed by collecting secondary electrons using an InLens detector. Morphotypes are defined as follows: *C. leptoporus* small, the sutures are angular and serrated lines (diameter < 5 μm); *C. leptoporus*, the sutures are smoothed and angular (5 μm < diameter > 8.5 μm); *C. quadriperforatus*, the sutures are curved (diameter > 8.5 μm).

4.4 Results

4.4.1 Coccolith absolute abundances, accumulation rates and carbonate burial

Throughout the study interval we identified a total of 17 species but the assemblage is dominated by four species (*E. huxleyi*, *C. leptoporus*, *Gephyrocapsa muellerae* and *Helicosphaera carteri;* Fig. 4.4- 4.5c). *E. huxleyi* and *C. leptoporus* show the highest Holocene absolute abundances (ca.

40 10^7 CC/ g sed) of the entire assemblage (Fig. 4.5c; 4.4c-d-h). Specifically, *E. huxleyi* increases its absolute abundances from 4 to 38 10^7 CC/ g sed throughout the whole interval by having a steep increase after 9 ky (Fig. 4.4h). *Calcidiscus leptoporus* trend can be divided into three different parts. The lowest part shows low values (2-8 10^7 CC/g sed.). The second part, which is comprised between the Last Glacial Period (LGP) and 11 ka, displays an increase from 6 to 20 10^7 CC/g sed., followed by a sudden collapse (2 10^7 CC/g sed.) recorded at 7 ka. The third part, from mid to late Holocene, is characterized by an interval with low values (0 to 4 10^7 CC/g sed). If we move to *Calcidiscus leptoporus* subsp. small, this taxon shows a slight increase trend from the Last Glacial Period up to 8 ka (0 to 10 10^7 CC/g sed.), when a shift toward higher values is observed (37 10^7 CC/g sed), values remains high for the rest of the study interval. *Gephyrocapsa muellerae* records high abundances (12 10^7 CC/g sed) during the cold part of the whole study period. At 12.8 ka these absolute abundances start decreasing until the end of the Holocene (2-4 10^7 CC/g sed; Fig. 4.4f). The lower- photic zone dwelling taxon *Helicosphaera carteri* shows low abundances (0-2 10^7 CC/g sed) during glacial water conditions period, and then it starts increasing for the rest of the Holocene (3-5 10^7 CC/g sed). A general increasing trend is observed through the study interval in the coccolith accumulation rate, from 20 to 40 10^7 (number of coccoliths cm^{-2} ka^{-1}; Fig. 4.5e). It is possible to observe three positive prominent peaks that reach the maximum values within the trend at 7 ka (60 10^7 n. of coccoliths cm^{-2} ka^{-1}), at 6 ka (51 10^7 n. of coccoliths cm^{-2} ka^{-1}) and at 4 ka (58 10^7 n. of coccoliths cm^{-2} ka^{-1}).

The coccolith carbonate contribution (%) to the carbonate content (%) is characterized by high values, ranging from 60% (10 ky to 12.8 ky) to 100% during the study interval (Fig. 4.5c).

During the deglaciation, the assemblage is almost composed in equal proportions by *C. leptoporus*, *C. pelagicus*, *E. huxleyi*, *G. muellerae*, *H. carteri*, and *Florisphaera profunda* with minor percentages of minor taxa's presence (*Ceratholithus* spp., *Discosphaera tubifera*, *G. oceanica*, *Helicosphaera* spp., *Pontosphaera* spp., *Siracosphaera* spp., *Umbilicosphaera* spp.). From the Younger Dryas upwards the coccolithophore assemblage contribution to the carbonate sediments increases up to ca 100% and it is mainly composed by highly calcified coccoliths such as *C. leptoporus* and *H. carteri* (Fig. 4.5c). Interestingly, the coccolith carbonate burial (g; Fig. 4.5d) follows the same trend showed by the coccolith accumulation rate, with higher values recorded (40g of $CaCO_3$) between the final part of the deglaciation and the beginning of the Holocene.

4.4.2 Dissolution index (CEX')

CEX' dissolution index shows a gradual decrease troughout the study succession (Fig. 4.5g). From the base of the section to ca. 15 ka, CEX' index displays values of around 0.8-1 that indicate high preservation /low dissolution. The minimum value of CEX' index is reached at 8.5 ka (0.39) and indicate high dissolution/low preservation. The final part of the study succession displays values of CEX' index that are around the threshold value (0.6).

4.4.3 *E. huxleyi* mass

E. huxleyi mass ranges between 1.2 and 2.2 pg (Fig. 4.7d). The mass of *E. huxleyi* displays minimum values during the glacial and then increases up to the Younger Drias event. From 12 ka, the values seem to reach a steady state centered around ca. 1.9. In the last 6 ky, the *E. huxleyi* mass gradually decreases.

4.4.4 *Calcidiscus leptoporus* and *Emiliania huxleyi* length index (L_i)

Calcidiscus leptoporus Length index is at its maximum value (1.10) at 14.8 ka, consequently it decreases until the value of 0.96 and from that point it reaches the minimum value of the trend (0.94) at 4 ka. During the Late Holocene the value sharply increases until 1 (Fig. 4.7a). *E. huxleyi* Length index tendency shows a general decrease by starting from a positive peak at 17.3 ka (0.745) and other two remarking peaks at 16 ka (0.738) and 14 ka (0.734). Afterward it adjusts at about 0.723 with a final increase in the Late Holocene (0.735; Fig. 4.7b).

4.5 Discussion

4.5.1 Coccolithophore response to paleoproductivity changes in the Subantarctic zone

Core PS2498-1 is located in the eastern part of the Mid-Atlantic Ridge on elevated topography, being dissociated from turbidites and eventually dilution caused by bottom currents delivering sediments (Anderson et al., 2017). Since in this region the terrigenous fluxes are possibly related to either aeolian transport or ocean currents such as the Antarctic Circumpolar Current (ACC), we can exclude the the second option because of the elevated location of our study site. The terrigenous component (%, Fig. 4.4a) is thus transported by the Westerlies, which are the dominant driver in the biosiliceous production. Conversely coccolithophores are, better adapted to oligotrophic conditions (Longhurst et al., 1995; Oviedo et al., 2016; Saavedra-Pellitero et al., 2017)

and in fact their production, as recorded by the coccolith accumulation rates (number of coccoliths cm^{-2} ka^{-1}), is low during the glacial when the terrigeous input is higher, and high, during the deglaciation and the Holocene, when the terrigenous content is low (%; Fig. 4.5e with 4.4a). During the glacial period, it has been shown by many authors (Mohan et al., 2008; Martinez-Garcia et al., 2014; Mejía et al., 2015; Patil et al., 2017; Balestrieri et al., in review) that the ACC shifts toward the equator, due to Antarctica's ice expansion. The shift to the North of the oceanic frontal regimes also plays a prominent role in the pattern of productivity variations, which is what we observe with the phosphorus delivery due to the shift of the upwelling cell of the Antarctic divergence (Flores et al., 2012). Coccolithophore productivity is linked to nutrient availability, salinity, temperature, light intensity and carbonate system changes which are combined to the regional surface hydrography (Saavedra-Pellitero et al., 2017). Our data of coccolith ascribable to *Gephyrocapsa muellerae* show affinity for cold and eutrophic water conditions (Grelaud et al. 2009). In fact, *G. muellerae* progressively replace *G. ericsonii* toward higher latitude (Baumann et al., 1999). *G. muellerae's* trend shows a good correlation with opal fluxes (Fig. 4.4f with g) which has been demostrated to be a good proxy for upwelling dynamics in this area of the Subantarctic zone (Anderson et al., 2009; Anderson et al., 2014; Martinez-Botì et al., 2015). On the contrary, *Helicosphaera carteri* exhibits the preference for deeper water during the stratification period of surface waters, elevated temperature, salinity and low NO_3 and PO_4 concentrations (Fig. 4.4e; Cros i Miguel, 2001; Patil et al., 2017). We propose that the high abundances of this taxon are related to nutrients distribution of the deep nutricline rather than controlled by biogeographic limits. In fact, Baumann et al. (2004) showed that *H. carteri* has a widespread distribution within the Subantarctic zone (SAZ), the Subtropical zone (STZ) and even Noorth to this area. Conversely, *Florisphaera profunda* a taxon that is usually abundant in the lower photic zone (Okada and Honjo, 1973; Honjo and Okada 1974; Grelaud et al., 2012) in these conditions is instead very rare and virtually excluded because the study area is at the boundary of its biogeographic areal (Baumann et al., 2004). It is thus possible that *H. carteri* has replaced *F. profunda* as a deep dwelling species during phases of warm and stratified waters (Fig. 4.4e with 4.4f). *Calcidiscus leptoporus* is considered an oligotrophic taxon which better thrives in stratified waters (Renaud et al., 2002; Saez et al., 2003; Balestrieri et al., in review). Other authors have proposed different ecological affinities for the three subspecies of this taxon: *Calcidiscus leptoporus* subsp. *leptoporus, Calcidiscus leptoporus* subsp. *quadriperforatus and Calcidiscus*

leptoporus subsp. *small* (Renaud et al., 2002 and Baumann et al., 2016). Renaud et al. (2002) assumed that *C. leptoporus* preferentially inhabits cold/oligotrophic waters, this is quite in agreement with what we have found at PS2498-1, though our data better fit with an affinity for temperate/oligotrophic conditions (Fig. 4.3 a-b with c). With regard to the different morphotypes, Renaud et al. (2002) suggested that high abundances of *Calcidiscus leptoporus* subsp. *small* depend on the decresead fitness of the other two morphotypes. Our data show a dominance of *Calcidiscus leptoporus* subsp. *small* at the expense of the larger morphotypes which howewer, display (i.e. *Calcidiscus leptoporus* subsp. *quadriperforatus*) a very sporadic occurrence throughout the study section.

4.5.2 Coccolithophore carbonate productivity and carbon cycle implications

Lately, many authors have proposed that, during the last deglaciation, the SO played a key role in regulating the ocean-atmosphere CO_2 balance due to changes in ocean circulation and biological productivity (*e.g.* Sigman and Boyle, 2000; Kohfeld et al., 2005; Martínez-Botí et al., 2015). Generally, in the SO the biological productivity is limited because of the low availability of the micronutrient iron. According to the iron fertilization hypothesis this phytoplankton growth limitation must have been relieved during glacial periods by a great delivery of iron through the aeolian dust input (Martin et al., 1990; Martínez-García et al., 2014). This wind-driven high biological production during the Last Glacial Period would have promoted marine productivity, and then enhanced carbon fluxes to the deep ocean, causing partially of the atmCO_2 drawdown during glacials (Martin et al., 1990). Increased nutrients content from high latitude and wind-iron supply during glacials drive a shift from carbonate to siliceous primary producers, resulting in an increase in seawater carbonate ions due to the decrease in carbonate production relative to the organic carbon ratio, hence drawing down atmCO_2 (Saavedra- Pellittero et al., 2017). Coccolith rich sediments at Site PS2498-1 dominated the whole interval being at its maximum during the Holocene (Fig. 4.5c), and being charcterized by highly calcified species. On the contrary, siliceous fluxes are at their maximum during the glacial (Anderson et al., 2009), and this could suggest a change in the marine biological carbon pumps that affected the atmospheric CO_2, probably in combination with other physical processes. The coccolith carbonate burial and accumulation rates indicate rather high coccolithophore production throughout the deglaciation and the interglacial (Fig. 4.5d-e). In the South Atlantic ocean at Site ODP1090 and 1089, coccolithophore production

has been shown to be highest during the glacial (Flores et al., 2012 and Balestrieri et al., in review) due to the increase in the inventory of phosphorus and iron in the ocean. Instead, in the South Pacific ocean, coccolith carbonate production has been maxima during the interglacials (Saavedra-Pellittero et al., 2017). According to Hodell et al., 2001, Atlantic sites above ~4200 m in the Cape Basin all exhibit the 'Atlantic- type' carbonate pattern, as our coccolith data (ARc and coccolith $CaCO_3$ production, Fig. 4.6) show for site PS2498-1. The ARc and coccolith carbonate contribution (%) are highly correlated to atmCO_2 values (r^2= 0.66, p-value = 1.25e-08, and r^2= 0.75, p-value = 3.41e-09, respectively; Fig. 4.6 and see SI for statistical calculations) measured in air trapped in Antarctic ice cores (Monnin et al., 2001 and Perrenin et al., 2013). This can indicate a relationship between coccolitophore production and atmCO_2, even if these types of correlations have not been unvarying in different sites in the South Atlantic (Martínez-Garcia et al., 2009). Our data are in agreement with coccolith data evaluated in the South Pacific Ocean by Saavedra-Pellittero et al., 2017. They discuss this increased coccolithophore carbonate counterpump, either through calcification or an abundance shift toward heavily calcified specimens, as a strong contribution to the observed rise in atmospheric CO_2 concentration during Termination V. Our data strongly agree with this statement, in fact *E. huxleyi* mass has an increasing trend starting from the deglaciation (Fig. 4.7d) and the coccolith carbonate assemblage is mainly composed by highly calcified coccolith during the interglacial (Fig. 4.5c). We support then the idea that coccolithophore, through increased calcification and/or highly calcified growth species played a central role in the outgassing of high amount of CO_2 from the surface ocean into the atmosphere. Considering the average coccolith carbonate contribution (36.81 g) at the seafloor during the last deglaciation gives us a rough estimate of the carbonate accumulation rate at the seafloor of 0.3677 mol $CaCO_3$. Since only 16% of the $CaCO_3$ sink out of the surface ocean at 100 m water depth reaching the sea-floor at ~3700 m (Saavedra-Pellittero et al., 2017), the strenght of the carbonate counterpump 2.10×10^{10} mol $CaCO_3$ or 0.47 Pg C (as $CaCO_3$). Based on the assumption that a $CaCO_3$ export at 100m of 0.3 Pg in the SO during interglacials corresponds to a rise in atmospheric CO_2 concentrations of about 8ppm (Köhler et al., 2010), we calculated an increase of 11.61 ppm of atmCO_2 during the Holocene due to coccolithophore calcification/production. However, it has to be taken into account that every export of hard shells into the deep ocean is coupled with the production of the organic carbon through the soft tissue pump, which then takes part in the glocal carbon cycle dynamic.

4.5.3 Do high *Emiliania huxleyi* abundances respond to high pCO_2?

Most of the Southern Ocean is a High Nutrient Low chlorophyll region (HNLC; Venables et al., 2010). Phytoplankton community do not fully utilize these macro-nutrient because of iron limitations (Martin, 1990). Several experiments in these HNLC areas and some recently results show how iron fertilization can induce phytoplankton biomass and productivity (Boyd et al., 2000, 2004). In particular, the state of knowledge about coccolithophores assemblage structure is that they are mostly associated with nutrient poor environments, even if some species are unrestricted (Oviedo et al., 2016). Moreover some species have different growth strategies, being typical of oligotrophic or of eutrophic conditions, in fact, if the latter is the case they are considered "opportunistic species" (Ziveri et al., 2004; de Vargas, 2007). In response to the last Glacial iron fertilization in the SO, induced by dust input, it has been already discussed (Balestrieri et al., in review) the high abundant presence of *E. huxleyi* as the "opportunistic species" within the coccolith assemblage. These blooms have already been reported in turbulent regimes (Schiebel et al., 2011). In this study we expected the same results, however this is not what we see (Fig. 4.5e). We believe that this is due to the high dissolution process that occurred at that time (Gottschalk et al., 2015; Warratz et al., 2017). In this way, *E. huxleyi* absolute abundances should have been higher than what we are actually observing. As we discussed in the previous paragraph, in the glacial-interglacial surface water change, we observe a shift from siliceous to carbonate phytoplankton realm, primarly related to nutrient availability but which has also been suggested to be driven by more acidified waters (Rost and Riebesell., 2004). This latter hypothesis could be a co-driver for our results. In fact, in Holocene nutrient-depleted and undersaturated waters we detect high *E. huxleyi* absolute abundances, even higher than the oligotrophic adapted species *C. leptoporus* and *C. leptoporus* small (Fig. 4.5e with 4.4c-d). *E. huxleyi* is the most common and abundant species in the ocean thank to its high capacity to live in wide ranges of environmental conditions (Paasche, 2002; Bach et al., 2012). Under high irradiance, pCO_2 and temperature, it has been observed high *E. huxleyi* photosynthesis and growth rate (Aloisi, 2015). Instead, macronutrients limitations induce a decrease in the growth rate, in particular phosphorus limitations cause an 'overproductions' of coccoliths (Müller et al., 2008). Müller et al, 2017 demonstrated the independence effects of pCO_2 and macronutrient limitations on *E. huxleyi* ecotype A in the Southern Ocean, proposing *E. huxleyi* physiological changes coupled with micronutrient

limitations. The case for our *E. huxleyi* (10^7 CC/g sed.) high presence during interglacial waters, could be primarly linked to the increase in pCO_2 (r^2= 0.58; p-value = 1.04e-06, Fig. 4.6 and see SI for statistical calculations) coupled with low phosphorus concentrations. Since we are analysing a fossil record, which cannot give information about coccosphere final structure (one or more layers), we could also think of a possible 'overproduction' of *E. huxleyi* coccoliths stirred by low surface phosphorus concentrations coupled with a well adapted *E. huxleyi* population in acidified waters. Dissolution here is not driving the assemblage due to the influence of north saturated waters that are bathing the Site and hence preserving coccoliths (Gottschalk et al., 2015; Warratz et al., 2017; more details in the next paragraph).

4.5.4 Post-depositional effects on the coccolith assemblage

Post-depositional effects on coccoliths, such as dissolution and dilution, are important processes to consider in order to understand the significance and reliability of our paleoceanographic proxies. Site PS2498-1 is positioned on elevated topography, being isolated from counter currents. It is also located (3.783 m) below the CSH (3.690 m) and above the lysocline (4.175 m; Fig. 4.3). Although calcite becomes thermodynamically unstable just below the CSH, dissolution proceeds extremely slowly, only at calcite lysocline depth the dissolution impacts become noticeable (Ridgwell & Zeebe, 2005). Warratz et al., 2017 and Gottschalk et al., 2015 show that, at Site MD07-3076Q, which is adjacent to Site PS2498-1 (Fig. 4.3), during the late LGM and early deglacial period, the carbonate content has been essentially low (%; Fig. 4.5a). In fact, fragmented planktonic foraminifera index (%; Fig. 4.5b) shows high values (highly fragmented foraminifera) during this time of period. It is proposed that this low and not well preserved carbonate content was due to a weak North Atlantic Deep Water's influence (well- ventilated and CO_3^{2-} saturated) dominated by deep Antarctic Bottom Water (undersaturated CO_3^{2-}), hence enhancing carbonate dissolution in the deep Subantarctic (Gottschalk et al., 2015; Warratz et al., 2017). *E. huxleyi* is the most fragile coccolithophore species and in fact its absolute abundances are low during the late LGP, HS1 and BA, being in good harmony with the fragmented planktonic foraminifera trend (Fig. 4.4h with 4.5h). Additionally, SEM pictures show the bad preservation of the coccoliths belonging to this *taxon* (Fig. 4.8). On the contrary, *C. leptoporus* does not seem to be highly affected, in terms of quality data, by dissolution (Fig. 4.9). However, CEX' dissolution index seems to have an opposite trend with respect to the fragmented planktonic foraminfera during the study interval (Fig. 4.5f-

4.5g). It has been previously observed that the absolute abundances of these two taxa are highly correlated with iron fertilization and phosphorus delivery changes in the surface water of the SO (Balestrieri et al., in review). We put forth the idea that glacial low *C. leptoporus* absolute abundances, responding to eutrophic waters (Fig. 4.4c-d with 4.4a -b), coupled with highly dissolved *E. huxleyi,* could be leading to an artifact by hiding the real glacial dissolution signal which is instead represented by planktonic foraminifera. Since dissolution was pervasive, we believe that during the Glacial, the fragile *G. muellerae* species's abundances (10^7 CC/g sed.) could have been much higher than what we counted. On the other hand, most individuals of *H. carteri*, due to their strong calcified skeleton could have been prevented by being dissolved. During the Holocene, Site PS2498-1 was bathed by northern currents sources, due to the resumption of the Atlantic Meridional Overturning Circulation (AMOC; McManus et al., 2004; Toggweiler et al., 2010; Gottschalk et al., 2015; Martinez-Boti et al., 2015; Warratz et al., 2017). These northern mid-depth water sources were well- ventilated and CO_3^{2-} saturated, being able to preserve all the pelagic snow production under oligotrophic water conditions. In this way, we explain the high carbonate content (%; Fig. 4.5a) related to phytoplankton producers found in these Subantarctic sites (Warratz et al., 2017).

4.5.5 Has surface ocean acidification been driven coccolith size?

One of the challanges of this last decade has been to reconstruct and understand the carbonate system dynamics both at surface and deep water, and to understand its role as a major influent on carbonate producers export (such as coccolithophores; Hodell et al., 2001; Rickaby et al., 2010; Beaufort et al., 2011; Horigome et al., 2014; Martinez-Boti et al., 2015; Gottschalk et al., 2016). Generally, environmental parameters such as seawater temperature, salinity, nutrient availability and carbonate system are proposed to have a synergistic effect on coccolith calcification and dimensions (Horigome et al., 2014). In particular, ongoing ocean acidification (due to ocean uptake of anthropogenic carbon emissions) is expected to primarly influence coccolith mass and size (Riebesell et al., 2000; Beaufort et al., 2011; Bach et al., 2012; Mejer et al., 2014). Previous works have showed different results, for example Beaufort et al., 2011 found smaller and lighter coccoliths with high pCO_2, instead Grelaud et al., 2009 show the opposite. We investigated the variations of *C. leptoporus* and *E. huxleyi* lengths (L_i), and *E. huxleyi* mass dynamic in the South Atlantic for the last 19 ky. The geographical distribution of these two species, which is controlled

by environmental conditions, is well- represented in this area of the Southern Ocean (Baumann et al., 2004; Horigome et al., 2014; Baumann et al., 2016). But the physiological role of key factors (*e.g.* pCO_2 and pH) for both of them is still controversial, as we previously mentioned. *E. huxleyi* mass trend, in this area, has been already been discussed by other authors (Beaufort et al., 2011; Müller et al., 2017; Balestrieri et al., in review), by proposing its shifts coupled with change in the carbonate system. It is known that coccolith mass depends both on coccolith length and on the degree of calcification. According to our data, *E. huxleyi* mass values (pg) are increasing and length values are decreasing, hence the degree of calcification should be positively growing (Fig. 4.7d-b with 4.6c); being in contrast with some cultures' results. In fact, in coccolithophore cultures it has been showed that under ocean acidification, coccolithophores (in particular *E. huxleyi* strains) tend to be less calcified and highly malformed (Riebesell et al., 2000; Langer et al., 2009; Müller et al., 2017). This happens because under ocean acidification scenarios, calcification is generally reduced due to the high energetic costs of the process (Müller et al., 2017). We then expected a variation in *E. huxleyi* length (μm) that should have increased instead of what we observe (Fig. 4.6d). Additionally, since the LGP, CO_2 levels have risen from 180 to 370 ppm and within the fossil record we do not find any malformed individual of either *E. huxleyi* or *C. leptoporus* as it is instead suggested by cultures' results (Langer et al., 2006). They propose that this lack in malformed nannofossil, could be explained by preferentially dissolution effect of incomplete coccoliths; or an evolutionary process adaptation developed in a possible time- window of almost 18000 kyr. This last theory has been also proposed by Saez et al., 2003 based on genetic analyses. They suggest a possible sympatric speciation linked to a gradualistic evolution to just explain *C. leptoporus* morphological differences. Aftermath, based on Holocene environmental conditions, increased atmospheric CO_2 coupled with the AMOC resumption could have lead to light, delicate and preserved coccoliths, if this is the case we should have been able to measure low mass values (pg), which is not. Therefore, we could hypothesize the idea of an evolutionary adaptation of the formation/calcification of the coccoliths in balance with the undersaturated surface waters, as Langer et al., 2006 proposed. Another hypothesis could be related to Aloisi et al., 2015's model based on biological metabolic theory in order to understand coccolith size variability coupled with metabolic rates. In particular, both high temperatures and pCO_2 cause fast coccolithophores growth rate (Aloisi, 2015) which could be more affected than maturity rate within one generation time, leading to a decrease in cell size (thus coccosphere and coccolith size proportionally). During the

Holocene, high temperature and high pCO_2 could have increased coccolithophores growth rate over maturity rate (Fig. 4.4), hence heading to a decrease in cell size (coccolith size).

4.6 Conclusions

We present new coccolith records from Site PS2498-1 in the Subantarctic South Atlantic Ocean for the last deglaciation, that document change in primary productivity in response to high phosphorus delivery and low surface ocean pH. In particular, cold- eutrophic *G. muellerae* absolute abundances supports the enhanced glacial biological productivity (high iron and phosphorus delivery). On the other hand, *H. carteri*, *C. leptoporus* small and *C. leptoporus* absolute abundances support warm- oligotrophic water conditions. In particular, we speculate the increase of *E. huxleyi* abundances (10^7 CC/sed.) is coupled with the increase in surface pCO_2. A surface ocean coccolith calcification burial of 0.47 Pg C was estimated considering typical $CaCO_3$ dissolution rates in the water column, and hence it has been estimated a rise in $atmCO_2$ of 11.61 ppm due to the carbonate counterpump (we neglected the related organic carbon export rates). Comparison of our coccolith record with other dissolution proxies reveals that the Site was affected by dissolution during the LGP, HS1, BA. Instead, the AMOC resumption induced high carbonate preservation at this Site during the interglacial. Analyses on *E. huxleyi* (mass and length) and *C. leptoporus* (length) reveal the complexity of understanding the relationship between coccolith size, morphology and physiological response sensitivity to environmental conditions. We speculate that the increase in *E. huxleyi* calcification with the decrease in its length and in *C. leptoporus* size could be a response to an evolutionary adaptation of coccolith calcification in undersaturated water. Another option could be that high temperature and pCO_2 caused fast growth rate over maturity rate within a population inducing a decrease in coccolith size.

Acknowledgments

CA and CB are funded by University of Padova (SID2016 - BIRD161002). We thank Dr. Leonardo Tauro and Dr. Niccolò Tomaso for the SEM analysis.

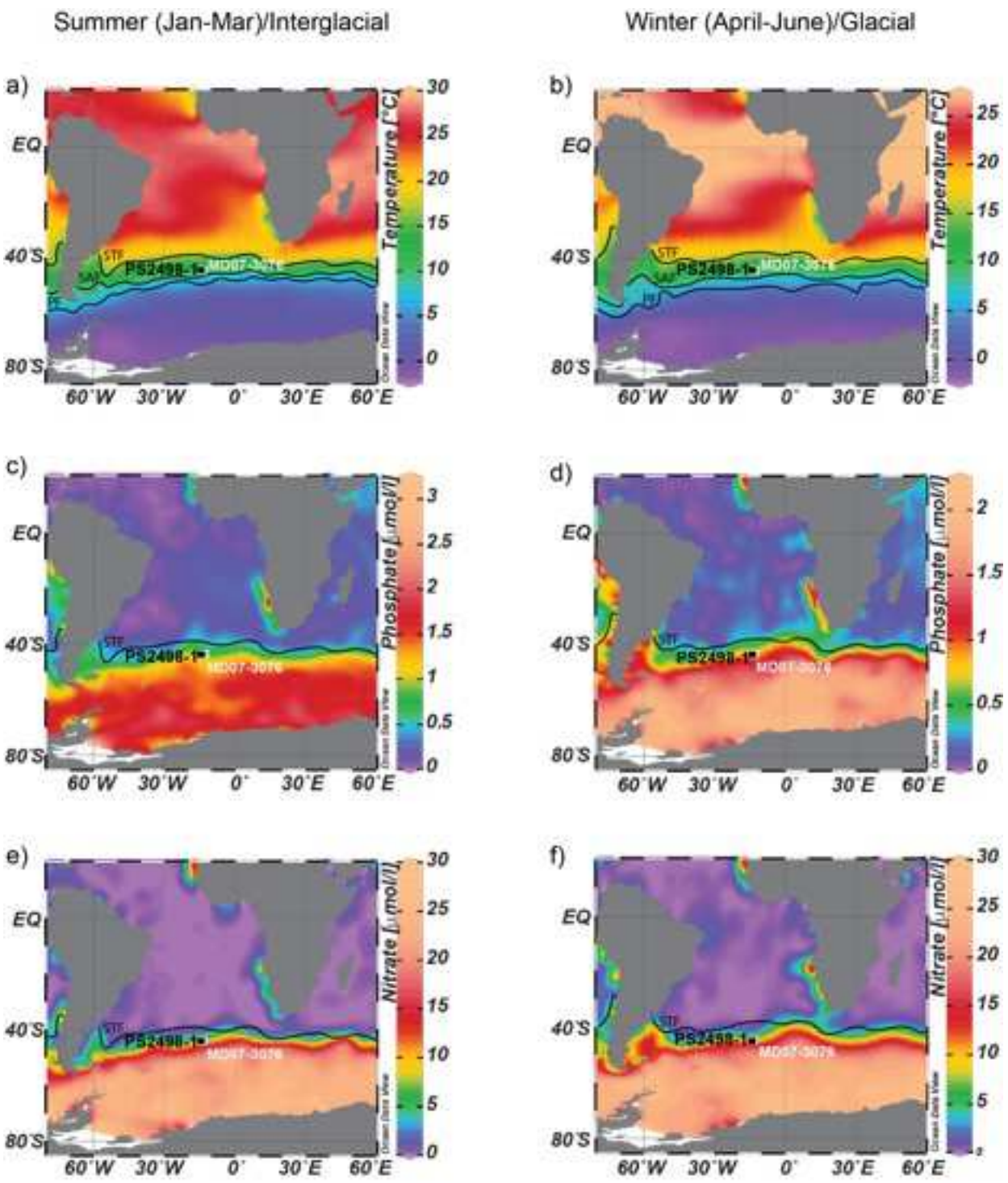
Summer (Jan-Mar)/Interglacial
Winter (April-June)/Glacial
a)
b)
c)
d)
e)
f)
EQ
40°S
80°S
60°W
30°W
0°
30°E
60°E
STF
SAF
PF
PS2498-1
MD07-3076
Temperature [°C]
Phosphate [µmol/l]
Nitrate [µmol/l]

Figure 4.1 (previous page): Site locations of PS2498-1 (black square; this study) and MD07-3076Q (white square). They are overlain on a map of average monthly sea surface temperature (a;b), phosphate (c; d) and nitrate (e; f) from Jan-March (Summer/Interglacial) to April-June (Winter/Glacial). Data have been compiled from World Ocean Atlas 2013 using the Software Ocean Data View 4® (R. Schlitzer, Ocean data view, 2009, http://gcmd.nasa.gov/records/ODV_AWI.html). The average positions of the modern Subtropical Front (STF), Subantarctic Front (SAF) and Polar Front (PF) are shown as black lines (Mejía et al., 2014).

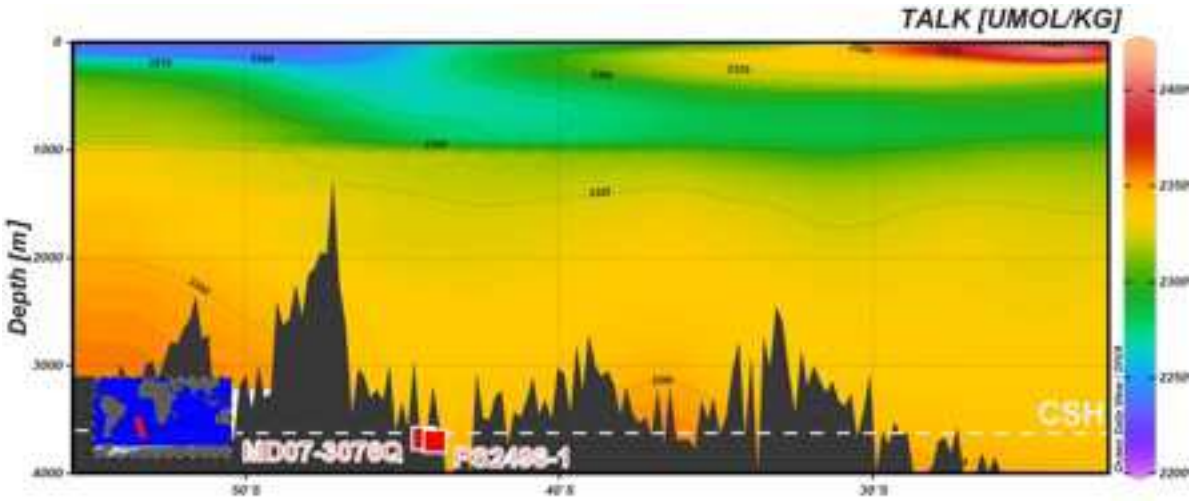

Figure 4.2: Hydrographic section of total carbon content (TALK(µmol/kg)) from WOCE [Schlitzer, 2000] based on data from Total Alkalinity and Total Dissolved Carbon Estimates (Goyet, Healy and Ryan, 2000) crossing the central Sub-Antarctic Atlantic Ocean with the location of PS2498-1 (this site) and MD07-3076Q (marked by red squares). White dashed line is showing the Carbonate Saturation Horizon calculated with CO_2Sys.

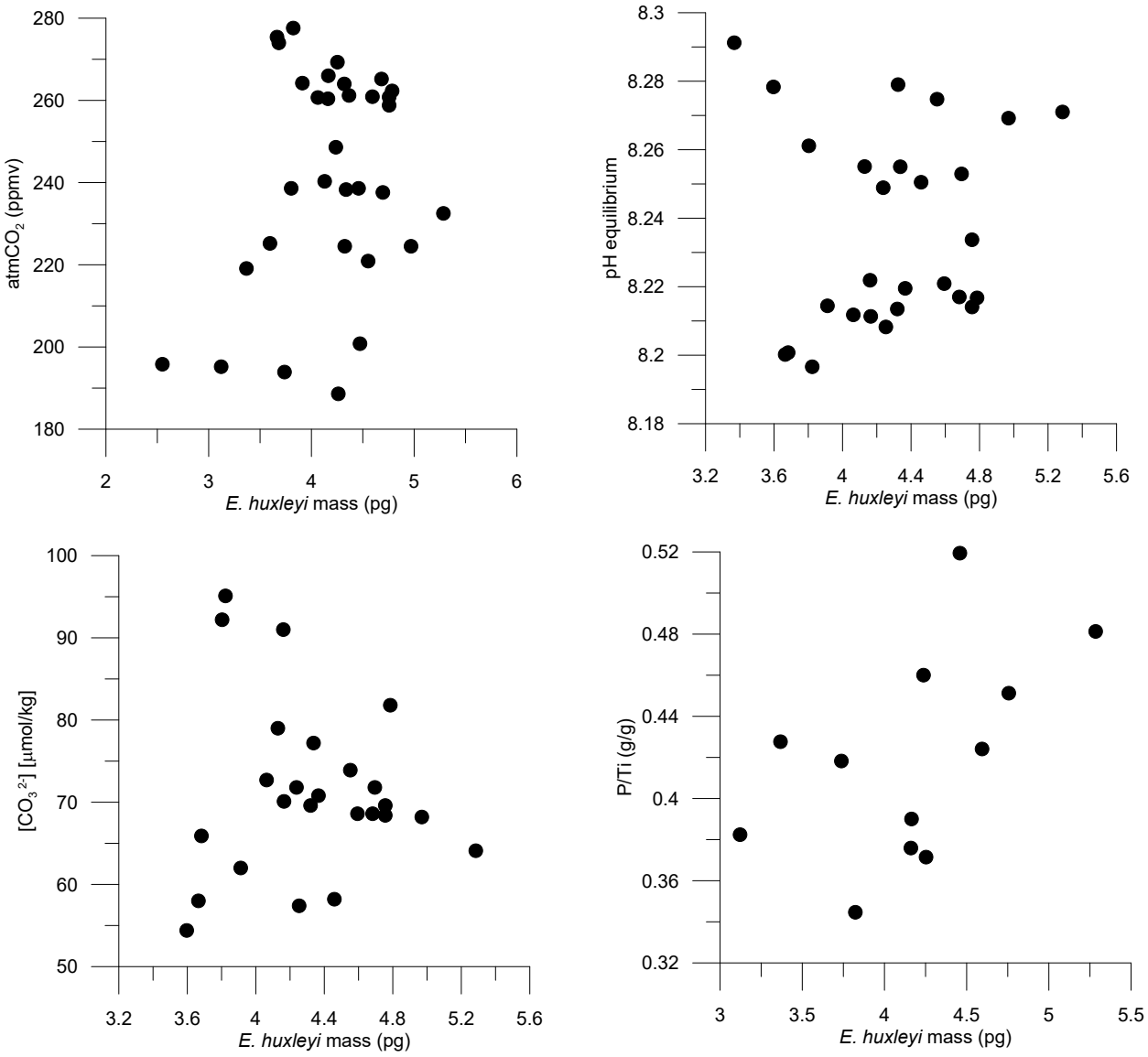

Figure 4.3: Conceptual model analyzing all the different principal variables ($atmCO_2$, pH, $[CO_3^{2-}]$ and P) that are considered to influence *E. huxleyi* mass (pg) dynamics.

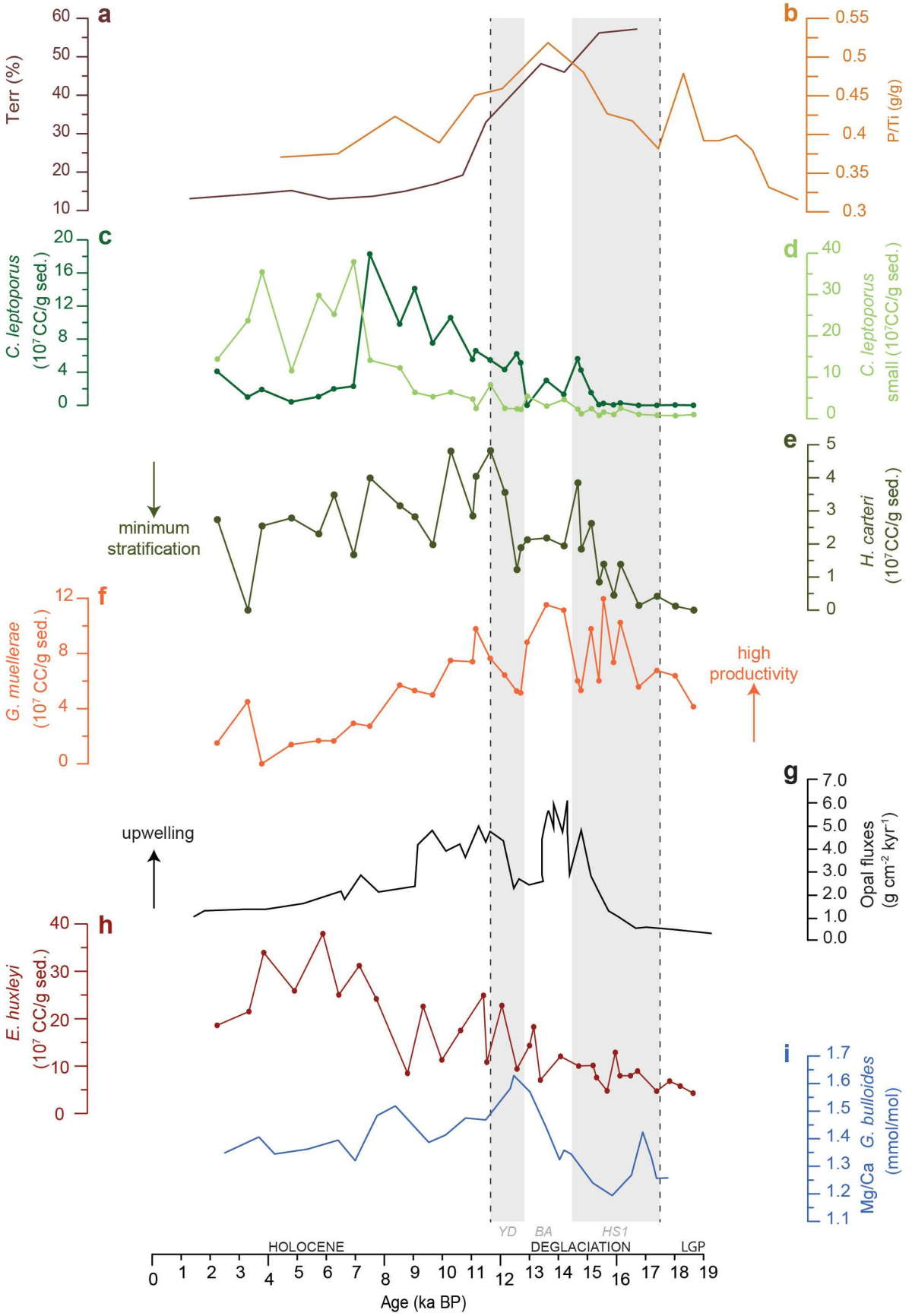
a
Terr (%)
b
P/Ti (g/g)
c
C. leptoporus (10⁷CC/g sed.)
d
C. leptoporus small (10⁷CC/g sed.)
e
H. carteri (10⁷CC/g sed.)
minimum stratification
f
G. muellerae (10⁷ CC/g sed.)
high productivity
upwelling
g
Opal fluxes (g cm⁻² kyr⁻¹)
h
E. huxleyi (10⁷ CC/g sed.)
i
Mg/Ca G. bulloides (mmol/mol)
YD
BA
HS1
HOLOCENE
DEGLACIATION
LGP
Age (ka BP)

Figure 4.4 (previous page): a) Terrigenous content (%; PS2498-1; Anderson et al., 2014); b) P/Ti (g/g) ratio at ODP1089 (Flores et al., 2012); c, d) *C. leptoporus* and small (10^7 CC/g sed); e) *H. carteri* (10^7 CC/g sed); f) *G. muellerae* (10^7 CC/g sed); g) opal fluxes (g cm^{-2} kyr^{-1}; TN057-13-4PC; Anderson et al., 2009); h) *E. huxleyi* (10^7 CC/g sed); i) Mg/Ca on *G. bulloides* (PS2498-1; Martinez-Boti et al., 2015). Vertical dashed lines delimit the deglaciation (11.7-17.5 ka), and light grey vertical bands highlight the coldest periods of the last 19kyr. Last Glacial Period (LGP); Heinrich stadials (HS1); Bølling-Allerod (BA) and Younger Dryas (YD).

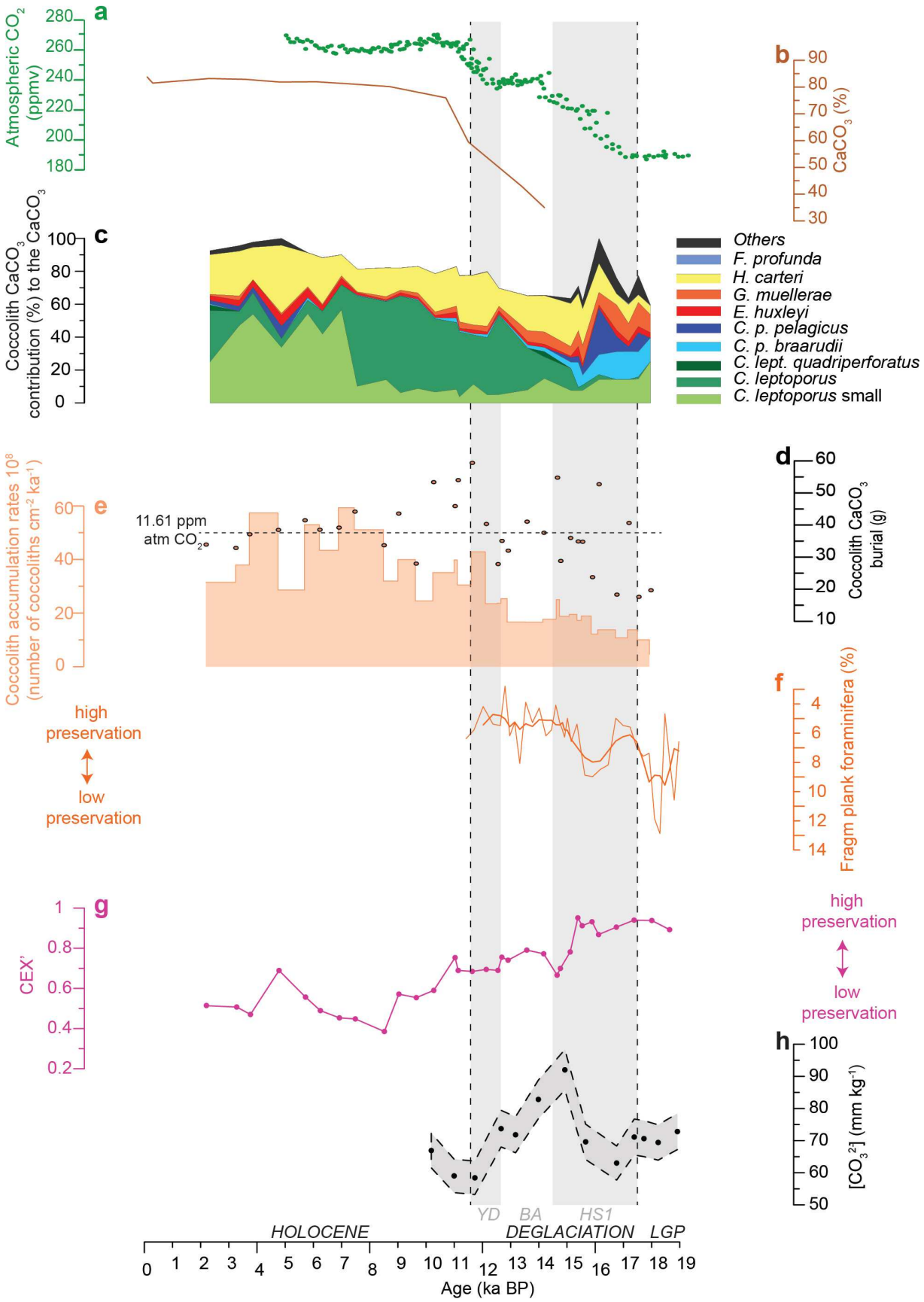
a
Atmospheric CO2 (ppmv)
280
260
240
220
200
180
b
CaCO3 (%)
90
80
70
60
50
40
30
c
Coccolith CaCO3 contribution (%) to the CaCO3
100
80
60
40
20
0
Others
F. profunda
H. carteri
G. muellerae
E. huxleyi
C. p. pelagicus
C. p. braarudii
C. lept. quadriperforatus
C. leptoporus
C. leptoporus small
d
Coccolith CaCO3 burial (g)
60
50
40
30
20
10
e
Coccolith accumulation rates 10^8 (number of coccoliths cm^-2 ka^-1)
60
40
20
0
11.61 ppm atm CO2
high preservation
low preservation
f
Fragm plank foraminifera (%)
4
6
8
10
12
14
high preservation
low preservation
g
CEX'
1
0.8
0.6
0.4
0.2
h
[CO3 2-] (mm kg-1)
100
90
80
70
60
50
YD
BA
HS1
HOLOCENE
DEGLACIATION
LGP
0 1 2 3 4 5 6 7 8 9 10 11 12 13 14 15 16 17 18 19
Age (ka BP)

Figure 4.5 (previous page): a) Atmospheric CO_2 from Antarctic ice cores (Schmitt et al., 2012); b) $CaCO_3$ content (%; PS2498-1; Anderson et al., 2014); c) Coccolith carbonate contribution (%) to the $CaCO_3$ (%); d) Coccolith $CaCO_3$ burial (g), grey dashed line shows the mean value (36.81 g of $CaCO_3$) which corresponds to 11.61 ppm rise of atmCO_2; e) Coccolith accumulation rate 10^8 (number of coccoliths cm^{-2} ka^{-1}); f) Fragmented planktic foraminifera (%; MD07-3076Q; Gottschalk et al., 2015); g) CEX' (ratio between *E. huxleyi- Gephyrocapsa muellerae* and *Calcidiscus leptoporus*); h) Carbonate ions concentration (µm kg^{-1}; MD07-3076Q; Gottschalk et al., 2015).

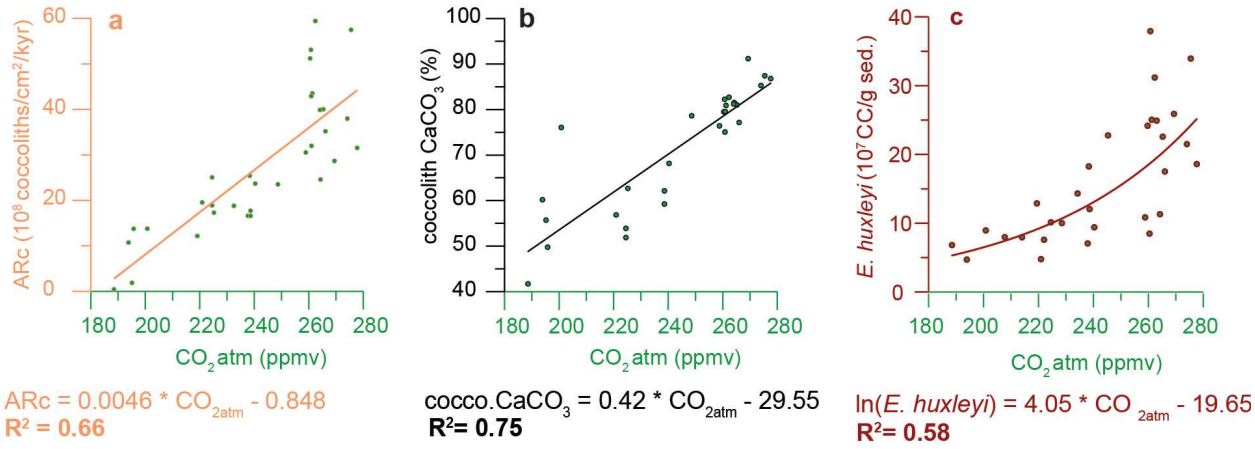

Figure 4.6: Coccolithophore productivity and CO_2. a) Atmospheric CO_2 (ppmv; Monnin et al., 2001 and Perrenin et al., 2013) versus coccolith accumulation rate (ARc; coccoliths/cm^2/kyr). The coefficient of determination (r^2) and the equation are indicated; b) Atmospheric CO_2 versus coccolith carbonate contribution (%) to the carbonate fraction of the sediments (%), with linear regression line and r^2; c) Atmospheric CO_2 versus *Emiliania huxleyi* (10^7 CC/ g sed.), with exponential equation line and r^2. Statistical calculations details are described in the SI.

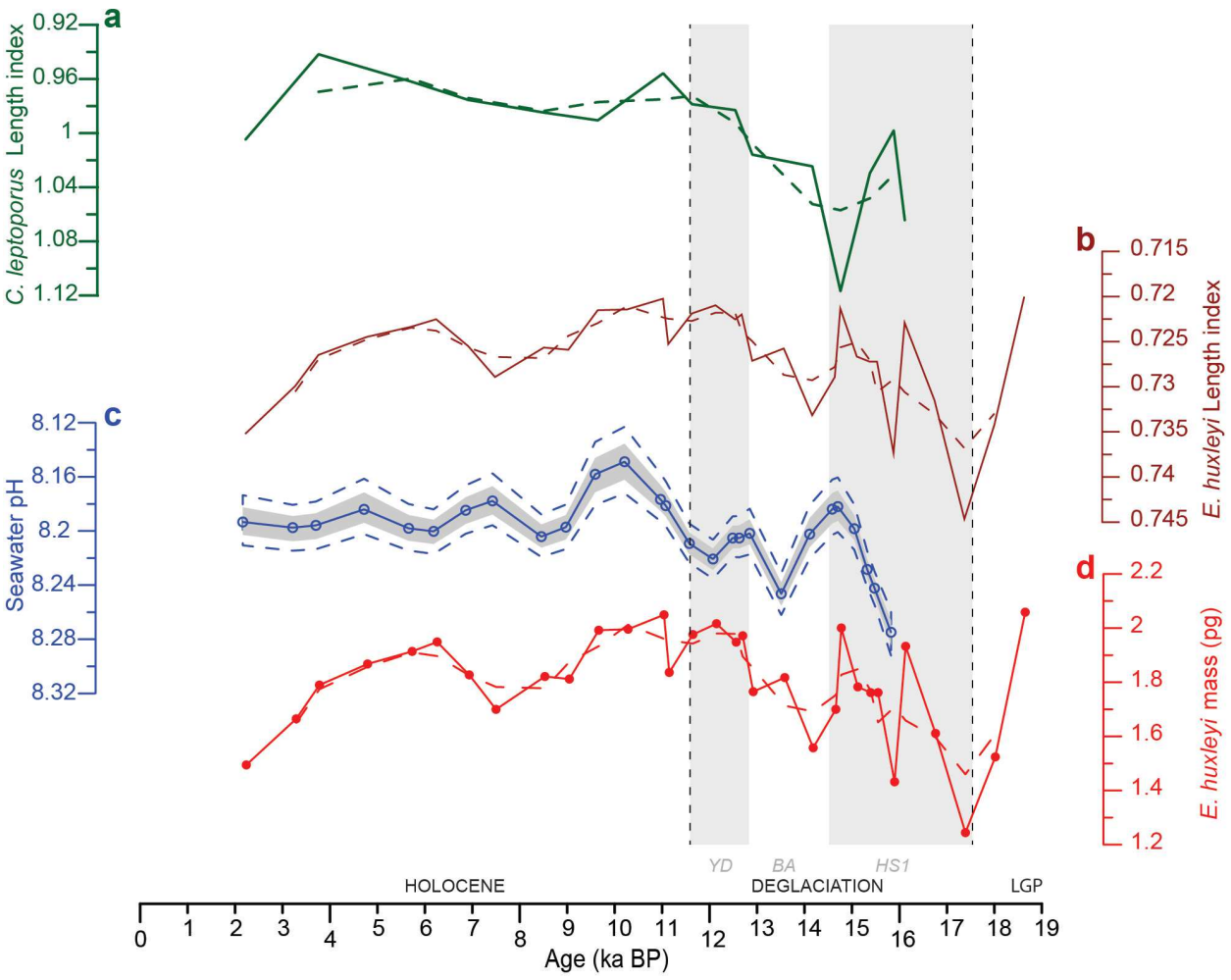

Figure 4.7: a) *C. leptoporus* length index; b) *E. huxleyi* length index; c) surface seawater pH, based from reconstructed salinity, temperature and boron isotopic data at PS2498-1 (Martìnez-Botì et al., 2015); d) *E. huxleyi* normalized mass (pg; D' Amario et al., 2018).

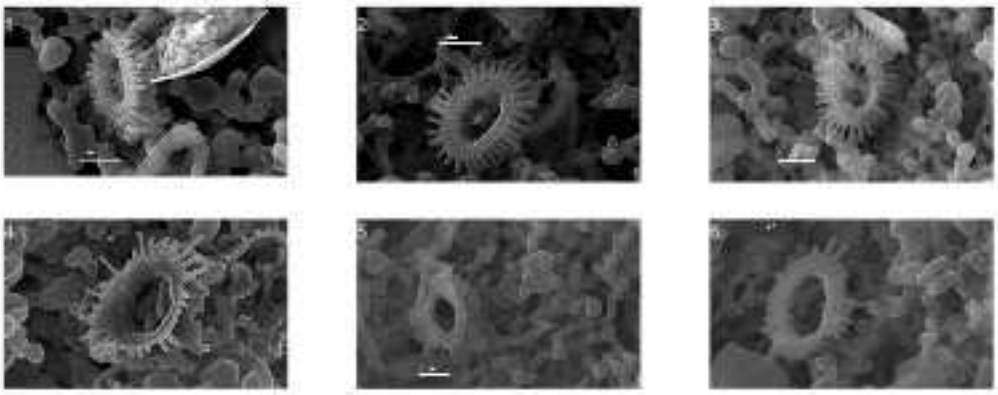

Figure 4.8: *E. huxleyi*. 1) 7.5-9 cm (3.28 ka); 2) 11-12 cm (3.77ka); 3) 24-25 cm (5.73 ka); 4) 74.5-76.5 cm (12.55 ka); 5,6) 93-95 cm (14.65 ka).

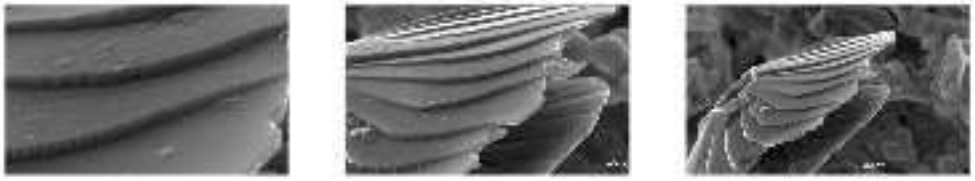

Figure 4.9: *C. leptoporus* small with angular and serrated suture lines (87-90 cm; 14.18 ka).

Appendix A. Supplementary Information

Statistical results have been computed on MATLAB:

CO_2_ARc_p =

Linear regression model:
y ~ 1 + x1

Estimated Coefficients:

	Estimate	SE	tStat	pValue
(Intercept)	-0.84781	0.14611	-5.8024	2.4249e-06
x1	0.0046435	0.00060028	7.7356	1.2481e-08

Number of observations: 32, Error degrees of freedom: 30
Root Mean Squared Error: 0.0889
R-squared: **0.666**, Adjusted R-Squared 0.655
F-statistic vs. constant model: 59.8, **p-value = 1.25e-08**

CO_2_coccoCaCO$_3$_p =

Linear regression model:
y ~ 1 + x1

Estimated Coefficients:

	Estimate	SE	tStat	pValue
(Intercept)	-29.546	11.678	-2.5301	0.017799
x1	0.41551	0.047665	8.7171	3.408e-09

Number of observations: 28, Error degrees of freedom: 26
Root Mean Squared Error: 6.95
R-squared: **0.745**, Adjusted R-Squared 0.735
F-statistic vs. constant model: 76, **p-value = 3.41e-09**

CO_2_Ehuxleyi(10^7 CC/g sed.)_p=

Nonlinear regression model:

Var2 ~ b1*x + b2

Estimated Coefficients:

	Estimate	SE	tStat	pValue
b1	4.0598	0.6538	6.2096	1.0431e-06
b2	-19.656	3.5868	-5.4802	7.4757e-06

Number of observations: 30, Error degrees of freedom: 28
Root Mean Squared Error: 0.386
R-Squared: **0.579**, Adjusted R-Squared 0.564
F-statistic vs. constant model: 38.6, **p-value = 1.04e-06**

References

Aloisi G. (2015). Covariation of metabolic rates and cell-size in coccolithophores. Biogeosciences 10: 4665–4692.

Anderson R. F., Barker S, Fleisher M, Gersonde R, Goldstein SL, Kuhn G, Mortyn PG, Pahnke K, Sachs JP. (2014) Biological response to millennial variability of dust and nutrient supply in the Subantarctic South Atlantic Ocean. *Phil. Trans. R. Soc. A* 372: 20130054. http://dx.doi.org/10.1098/rsta.2013.0054

Anderson R. F., Ali S., Bradtmiller L. I., Nielsen S. H. H., Fleisher M. Q., Anderson B. E. & Burckle L. H. (2009). Wind- driven upwellingin the Southern Ocean and the Deglacial Rise in Atmospheric CO_2. Science, 323.

Andruleit, H. A. and Baumann, K. H. (1998). History of the Last Deglaciation and Holocene in the Nordic seas as revealed by coc- colithophore assemblages, Mar. Micropaleontol., 35, 179–201.

Bach, L.T., Bauke, C., Meier, K.J.S., Riebesell, U., Schulz, K.G., (2012). Influence of changing carbonate chemistry on morphology and weight of coccoliths formed by Emiliania huxleyi. Biogeosciences 9, 3449-3463.

Baumann, K.-H., Pellittero-Saavedra M., Böckel B., Ott C., (2016). Morphometry, biogeography and ecology of *Calcidiscus* and *Umbilicosphaera* in the South Atlantic. Revue de micropaléontologie, http://dx.doi.org/10.1016/j.revmic.2016.03.001

Baumann, K.-H., Bockel, B., Frenz, M., (2004). Coccolith contribution in the South Atlantic carbonate sedimentation. In: Thierstein, H.R., Young, J.R. (Eds.), Coc- colithophoreseFrom Molecular Processes to the Global Impact. Springer, pp. 367-402.

Baumann K.-H., Cepek M., and Kinkel H., (1999). Coccolithophores as indicators of ocean water masses, surface water temperature, and paleoproductivity- examples from the South Atlantic. In Use of Proxies in Paleoceanography: examples from the South Atlantic (Fisher G. and Wefer G.).

Beaufort L., I. Probert, T. de Garidel-Thoron, E. M. Bendif, D. Ruiz-Pino, N. Metzl, C. Goyet, N. Buchet, P. Coupel, M. Grelaud, B. Rost, R. E. M. Rickaby & C. de Vargas. (2011). Sensitivity of coccolithophores to carbonate chemistry and ocean acidification. Nature, volume 476.

Beaufort, L. and D. Dollfus, (2004). Automatic recognition of coccoliths by dynamical neural networks, *Marine Micropaleontology*, 51(1):57-73, doi:10.1016/j.marmicro.2003.09.003.

Bordiga, M., M. Cobianchi, C. Lupi, N. Pelosi, N. L. Venti, and P. Ziveri (2014). Coccolithophore carbonate during the last 450 ka in the NW Pacific Ocean (ODP site 1209B, Shatsky Rise), J. Quat. Sci., 29(1), 57–69, doi:10.1002/jqs.2677.

Boyd, P. W., et al. (2000). A mesoscale phytoplankton bloom in the polar Southern Ocean stimulated by iron fertilization, Nature, 407, 695 – 702, doi:10.1038/35037500.

Boyd, P. W., et al. (2004). The decline and fate of an iron-induced subarctic phytoplankton bloom, Nature, 428, 549 – 553, doi:10.1038/nature02437.

Broecker, W. (1982). Glacial to interglacial changes in ocean chemistry. *Prog. Oceanogr.* 2, 151–197.

Calvo, E., C. Pelejero, G. A. Logan, and P. De Deckker (2004). Dust-induced changes in phytoplankton composition in the Tasman Sea during the last four glacial cycles, Paleoceanography, 19, PA2020, doi:10.1029/2003PA000992.

Canadell J.G., Quéré C., Raupach M.R., Field C.B., Buitenhuis E.T., Ciais P., Conway T.J., Gillet N.P., Houghton R.A., Marland G., (2007). Contributions to accelerating atmospheric CO2 growth from economic activity, carbon intensity, and efficiency of natural sinks. Proc. Natl. Acad. Sci. USA 104, 18886- 18870.

Cros I Miguel Di M. Luisa, (2001). Planktonic Coccolithophores of the NW Mediterranean (PhD thesis).

de Vargas, C., Aubry, M.P., Probert, I., Young, J., (2007). Origin and evolution of coccolithophores: from coastal hunters to oceanic farmers. In: Falkowski, P.G., Knoll, A. (Eds.), Evolution of Primary Producers in the Sea. Elsevier Academic Press, Amsterdam, Boston, pp. 251-285.

D' Amario B. (2017). Coccolithophore calcification, life- cycle dynamics and diversity in a warming and acidifying Mediterranean Sea, (Doctoral Dissertation). Depòsit digital de documents de la UAB. Universitat Autònoma de Barcelona.

Dittert N., K.-H. Baumann, T. Bickert, R. Henrich, R. Huber, H. Kinkel and H. Meggers (1999). Carbonate dissolution in the deep-sea: methods, quantification and paleoceanographic application**,** G. Fischer, G. Wefer (Eds.), *Use of Proxies in Paleoceanography — Examples from the South Atlantic, Springer, Berlin* (1999), pp. 255-284.

Dollfus, D. and L. Beaufort (1999). Fat neural network for recognition of position-normalised object, *Neural Netw*, 12, 553–560.

Feely, R. A. et al. (2004). Impact of anthropogenic CO_2 on the $CaCO_3$ system in the oceans. Science 305, 362–366.

Flores, J.-A. et al. (2012). The "White Ocean" Hypothesis: A Late Pleistocene Southern Ocean Governed by Coccolithophores and Driven by Phosphorus. *Frontiers in Microbiol*ogy 2012; 3: 233, doi: 10.3389/fmicb.2012.00233.

Gersonde, R, A. Abelmann, U. Brathauer, S. Becquey; C. Bianchi, G. Cortese, G. Hannes, G. Kuhn, H.-S. Niebler, M. Segl, R. Sieger, U. Zielinski and D. K. Fütterer, (2003). Last glacial sea surface temperatures and sea-ice extent in the Southern Ocean (Atlantic-Indian sector): A multiproxy approach. *Paleoceanography*, 18(3)**,** 1061, 10.1029/2002PA000809.

Giraudeau, J., Monteiro, P. M. S., and Nikodemus, K. (1993). Distribution and malformation of living coccolithophores in the Northern Benguela upwelling system off Namibia, Mar. Micropaleontol., 22, 93–110.

Gottschalk J., Skinner L.C., Misra S., Waelbroek C., Menviel L., Timmeramnn A., (2015). Abrupt changes in the southern extent of North Atlantic Deep Water during Dansgaard-Oeschger events. Nat. Geosci. 8, 950–955.

Gottschalk J., Skinner L.C., Lippold J., Vogel H., Frank N., Jaccard S.L., Waelbroek C., 2015. Biological and physical controls in the Southern Ocean on past millennial-scale atmospheric CO_2 changes. Nature. DOI: 10.1038/ncomms11539.

Grelaud, M., G. Marino, P. Ziveri, and E. J. Rohling, (2012). Abrupt shoaling of the nutricline in response to massive freshwater flooding at the onset of the last interglacial sapropel event, Paleoceanography, 27, PA3208, doi:10.1029/ 2012PA002288.

Hodell, D. A., Charles, C. D. & Sierro, F. J. (2001). Late Pleistocene evolution of the ocean's carbonate system. *Earth Planet. Sci. Lett.* 192, 109–124.

Hoffmann L.J., Breitbarth E., Boyd P.W., Hunter K.A., (2012). Influence of ocean warming and acidification on trace metal biogeochemistry. Mar. Ecol. Prog. Ser. 470-191-205.

Honjo, S., and H. Okada, (1974). Community structure of coccolithophores in the photic layer of the mid-Pacific, Micropaleontology, 20(2), 209–230, doi:10.2307/1485061.

Horigome, M. T., Ziveri, P., Grelaud, M., Baumann, K.-H., Marino, G., and Mortyn, P. G. (2014). Environmental controls on the Emiliania huxleyi calcite mass, Biogeosciences, 11, 2295–2308, doi:10.5194/bg-11-2295-2014.

Hutchins D., Mulholland M., Fu F., (2009). Nutrient cycles and marine microbes in a CO_2-

enriched ocean. Oceanography 22-128-145.

IPCC (2013), Summary for Policymakers, in Climate Change 2013: *The Physical Science Basis. Contribution of Working Group I to the Fifth Assessment Report of the Intergovernmental Panel on Climate Change*, edited by T. F. Stocker et al., Cambridge Univ. Press, Cambridge, U.K., and New York.

Jaccard, T. I. Eglinton, and G. H. Haug, (2014). Iron fertilization of the subantarctic ocean during the last ice age. *Science* 343, 1347–1350. Martínez-Garcia A, Rosell-Mele A, Jaccard SL, Geibert W, Sigman DM, Haug GH., (2011). Southern Ocean dust–climate coupling over the past four million years. *Nature* 476, 312–315. doi:10.1038/nature10310

Kohfeld, K. E., C. L. Quéré, S. P. Harrison, and R. F. Anderson, (2005). Role of marine biology in glacial-interglacial CO_2 cycles, Science, 308(5718), 74–78. doi:10.1126/science.1105375

Kumar N, Anderson RF, Mortlock RA, Froelich PN, Kubik P, Dittrich-Hannen B, Suter M., (1995). Increased biological productivity and export production in the glacial Southern Ocean. *Nature* 378, 675–680. doi:10.1038/378675a0

Langer, G., Geisen, M., Baumann, K.-H., Kläs, J., Riebesell, U., Thoms, S., Young, J.R., (2006). Species-specific responses of calcifying algae to changing seawater car- bonate chemistry. Geochem. Geophys. Geosyst. 7, Q09006. http://dx.doi.org/ 10.1029/2005GC00122

Langer, G., Benner, I., (2009). Effect of elevated nitrate concentration on calcification in *Emiliania huxleyi*. J. Nannoplankton Res. 30, 77–80.

Longhurst, A., Sathyendranath, S., Platt, T., Caverhill, C., (1995). An estimate of global primary production in the ocean from satellite radiometer data. J. Plankton Res. 17, 1245e1271.

Mackey K.R.M., Morris J.J., Morel F.M.M. (2015). Response of photosynthesis to ocean acidification. Oceanography 28, 74- 91.

Martínez-Botí, M. A., Marino G., Foster G. L., Ziveri P., Henehan M.J., Rae J.B.W., Mortyn P.G., Vance D. (2015). Boron isotope evidence for oceanic carbon dioxide leakage during the last deglaciation. *Nature* 518, 219–222. doi:10.1038/nature14155

Martin JH. 1990 Glacial–interglacial CO_2 change: the iron hypothesis. *Paleoceanography* 5, 1–13. doi:10.1029/PA005i001p00001

Martin, J. H., R. M. Gordon, and S. E. Fitzwater, (1990). Iron in Antarctic waters, Nature, 345(6271), 156–158, doi:10.1038/345156a0

Martínez-Garcia, A., D. M. Sigman, H. Ren, R. F. Anderson, M. Straub, D. A. Hodell, S. L.

Martínez-Garcia A, Rosell-Mele A, Geibert W, Gersonde R, Masque P, Gaspari V, Barbante C., (2009). Links between iron supply, marine productivity, sea surface temperature, and CO_2 over the last 1.1 Ma. *Paleoceanography* 24, PA1207. doi:10.1029/2008PA001657

McClelland, H. L. O., N. Barbarin, L. Beaufort, M. Hermoso, P. Ferretti, M. Greaves, and R. E. M. Rickaby, (2016). Calcification response of a key phytoplankton family to millennial-scale environmental change, Sci Rep., 6,34263, doi:10.1038/srep34263

McManus, J.F., R. Francois, J.-M. Gherardi, L.D. Keigwin, and S. Brown-Ledger, (2004). Collapse and rapid resumption of Atlantic meridional circulation linked to deglacial climate changes: *Nature*, v. 428, p. 834–837, doi: 10.1038/nature02494

McIntyre, A. and Be, A. W. H. (1967). Modern Coccolithophoridae of Atlantic Ocean-I. Placoliths and Cyrtoliths, Deep-Sea Res., 14, 561–597.

Meier, K.J.S., Beaufort, L., Heussner, S., Ziveri, P. (2014). The role of ocean acidification in *Emiliania huxleyi* coccolith thinning in the Mediterranean Sea. Biogeosciences 11, 2857-2869.

Millero F.J., Woosley R., Ditrolio B., Waters J., (2009). Effect of ocean acidification on the speciation of metals in seawater. Oceanography 22: 72-85.

Mohan R., L.P. Mergulhao, M.V.S. Guptha, A. Rajakumar, M. Thamban, N. Anilkumar, M. Sudhakar and R. Ravindra (2008). Ecology of coccolithophores in the Indian sector of the Southern Ocean. Volume 67, Issues 1–2, April 2008, *Pages* 30-45.

Müller M.N., Trull T.V. and Hallegraef G.M., (2017). Independence of nutrient limitation and carbon dioxide impacts on the Southern Ocean coccolithophore *Emiliania huxleyi*. The ISME Journal. 1777–1787.

Müller, M. N., Antia, A. N., and LaRoche, J., (2008). Influence of cell cycle phase on calcification in the coccolithophore *Emiliania huxleyi*, Limnol. Oceanogr., 53, 506–512.

Nederbragt, A. J., Thurow, J. W., and Bown, P. R., (2008). Paleoproductivity, ventilation, and organic carbon burial in the Santa Barbara Basin (ODP Site 893, off California) since the last glacial, Paleoceanography, 23, PA1211, doi:10.1029/2007PA001501

Okada H. and A. McIntyre, (1979). Seasonal distribution of modern Coccolithophores in the Western North Atlantic Ocean**.** *Mar. Biol.,* 54 (1979), pp. 319-328.

Okada, H. and Honjo, S. (1973). The distribution of oceanic coccolithophorids in the Pacific, Deep-Sea Res. Pt. I, 20, 355–374.

Orsi, A. H., T. Whitworth and Jr. W.D. Nowlin, (1995). On the meridional extent and fronts of the Antarctic Circumpolar Current, *Deep-Sea Research I,* Vol. 42, No. 5, pp. 64-673, *Elsevier Science* Ltd Printed in Great Britain.

Oviedo A.M., Ziveri P., Gazeau F., (2016). Coccolithophore community response to increasing pCO_2 in Mediterranean oligotrophic waters. Estuarine, Coastal and Shelf Science 186, 58-71.

Paasche E. (2002). A review of the coccolithophorid *Emiliania huxleyi* (Prymnesiophyceae), with particular reference to growth, coccolith formation, and calcification-photosynthesis interactions. Phycologia 40: 503–529.

Patil S.M., Mohan R., Shetye S.S., Gazi S., Baumann K.-H., Jafar S., (2017). Biogeography distribution of extant coccolithophores in the Indian sector of the Southern Ocean. Marine Micropaleontology, Volume 137, pages 16-30.

Renaud S., Ziveri P., Broerse A.T.C., (2002). Geographical and seasonal differences in morphology and dynamics of the coccolithophore Calcidiscus leptoporus. Mar Micropaleontol. 46:363–385.

Rickaby, R. E. M., H. Elderfield, N. Roberts, C.-D. Hillenbrand, and A. Mackensen, (2010). Evidence for elevated alkalinity in the glacial Southern Ocean, Paleoceanography, 25, PA1209, doi:10.1029/2009PA001762

Riebesell U., Tortell P.D. (2011). Effects of ocean acidification on pelagic organisms and ecosystems. In: Gattuso J-P, Lansson (eds) Ocean acidification. Oxford University Press., Oxford, p. 99-121.

Riebesell, U., Zondervan, I., Rost, B., Tortell, P.D., Zeebe, R.E., Morel, F.M., (2000). Reduced calcification of marine plankton in response to increased atmospheric CO_2. Nature 407, 364-367.

Rio, D., E. Fornaciari and I. Raffi, (1990a). Late Oligocene through early Pleistocene calcareous nannofossils from western equatorial Indian Ocean (Leg 115), in *Duncan*, R.A., Backman, J., L. C. Peterson et al., Proc. ODP, Sci. Results, 115: College Station, TX (Ocean Drilling Program), 175-235.

Rio, D., I. Raffi and G. Villa (1990b). Pliocene-Pleistocene calcareous nannofossil distribution patterns in the western Mediterranean, *in* Kastens, K.A., J. Mascle, et al*., Proc. ODP, Sci. Results,*107: College Station, TX (Ocean Drilling Program), 513-533.

Rohling E.J., et al., (2012). Making sense of paleoclimate sensitivity, *Nature*, 491 (7426), 683-691. doi:10.1038/nature11574

Rost, B., Riebesell, U., (2004). Coccolithophores and the biological pump: responses to environmental changes. In: Thierstein, H., Young, J. (Eds.), Coccolithophores: From Molecular Processes to Global Impact. Springer, Berlin, pp. 99-125.

Saavedra-Pellitero, M., K.-H. Baumann, F. Lamy, and P. Köhler, (2017). Coccolithophore variability across Marine Isotope Stage 11 in the Pacific sector of the Southern Ocean and its potential impact on the carbon cycle, Paleoceanography, 32, 864–880, doi:10.1002/2017PA003156

Saavedra-Pellitero M., Baumann K.-H., Ullermann J., Lamy F., 2017. Marine Isotope Stage 11 in the Pacific sector of the Southern Ocean; a coccolithophore perspective. 2017. Quaternary Science Reviews 158, 1-14.

Sáez AG, Probert I, Geisen M, Quinn P, Young JR, Medlin LK, (2003). Pseudo-cryptic speciation in coccolithophores. Proc Natl Acad Sci USA 100:7163–7168.

Schiebel, R., Brupbacher, U., Schmidko, S., Nausch, G., Waniek, J. J., and Thierstein, H.-R.: Spring coccolithophore production and dispersion in the temperate eastern North Atlantic Ocean, J. Geophys. Res., 116, C08030, doi:10.1029/2010JC006841, 2011

Schmidt D.N., Renaud S. and Bollmann J. (2003). Response of planktic foraminiferal size to late Quaternary climate change. PALEOCEANOGRAPHY, VOL. 18, NO. 2, 1039, doi:10.1029/2002PA000831

Shi D., Xu Y., Hopkinson B.M., Morel F.M.M., (2010). Effect of Ocean acidification on iron availability to marine phytoplankton. Science 327, 676-679.

Sigman, D. M., and E. A. Boyle, (2000). Glacial/interglacial variations in atmospheric carbon dioxide, Nature, 407(6806), 859–869, doi:10.1038/ 35038000

Suchéras-Marx, B., and J. Henderiks, (2014). Downsizing the pelagic carbonate factory: Impacts of calcareous nannoplankton evolution on carbonate burial over the past 17 million years, Global Planet. Change, 123, 97–109, doi:10.1016/j.gloplacha.2014.10.015

Toggweiler, J. R., and D. W. Lea, (2010). Temperature differences between the hemispheres and ice age climate variability, Paleoceanography, 25, PA2212, doi:10.1029/2009PA001758

Tzedakis, P. C., D. Raynaud, J. F. McManus, A. Berger, V. Brovkin, and T. Kiefer, (2009). Interglacial diversity, Nat. Geosci., 2(11), 751–755, doi:10.1038/ngeo660

Venables, H. and Moore, M., (2010). Phytoplankton and light limitation in the southern ocean: learning from high-nutrient, high-chlorphyll areas, J. Geophys. Res., 115, C02015,

doi:10.1029/2009JC005361.

Warratz G., Henrich R., Voigt I., Chiessi C.M., Kuhn G., Lantzsch H., (2017). Deglacial changes in the strength of deep southern component water and sediment supply at the Argentine continental margin. DOI: 10.1002/2016PA003079

Winter, A., Jordan, R.W., Roth, P.H., (1994). Biogeography of living coccolithophores in ocean waters. In: Winter, A., Siesser, W.G. (Eds.), Coccolithophores. Cambridge University Press, Cambridge, pp. 161–178.

Ziveri,P., Baumann,K.H., Boeckel,B., Bollmann,J., Young,J., (2004). Presentday coccolithophore-biogeography in the Atlantic Ocean. In: Thierstein, H., Young, J. (Eds.), Coccolithophores: from Molecular Processes to Global Impact. Springer Verlag, pp. 403-428.

Ziveri, P., J.R. Young and J.E. van Hinte (1999). Coccolithophore export production and accumulation rates, In: On determination of sediment accumulation rates. In book: On the Determination of Sediment Accumulation Rates, Edition: GeoResearch Forum vol. 5, Chapter: Coccolithophore export production and accumulation rates, In: On determination of sediment accumulation rates, Publisher: *Trans Tech Publications LTD, Switzerland, Editors: P. Bruns* (Editor, H. Christian Hass, pp.41-56).

CHAPTER 5

Enhanced *E. huxleyi* carbonate production as a positive feedback to increase deglacial pCO_{2sw} in the Eastern Equatorial Pacific

Abstract

The modern Eastern Equatorial Pacific (EEP) ocean is a high nutrient low chlorophyll (HNLC) region with the potential to be a large oceanic source of carbon for the atmosphere. During the last deglaciation, the EEP has played a major role in the outgassing of carbon dioxide from the upwelling surface water system coming from the Southern Ocean to the atmosphere through a mechanism likely related to an enhanced biological pump. Here we present data spanning the last 30 ky on the mass and calcification dynamics of the coccolithophore species *Emiliania huxleyi* obtained from samples located at Site ODP 1238 (1°52.310´S, 82°46.934´W; 2203 m) in the EEP. Our results show an increased coccolith calcification rate during times of high pCO_2 and low surface water pH conditions; this unexpected result is tentatively explained as related to changes in homeostasis equilibrium between cell and the environment. We also calculated the particulate inorganic to organic carbon ratio (PIC:POC) in order to detect changes in the carbonate to carbon pump activity, which can act as either a positive or negative feedback to ocean-atmospheric CO_2 changes. Our study indicates an enhanced coccolithophore biological pump during the last glacial that could have buffered, at least partially, the excess of $atmCO_2$ via absorption into the ocean. Finally, during the last deglaciation, the enhanced carbonate counter pump was a major source of high pCO_{2sw} in the EEP surface ocean.

5.1 Introduction

The Eastern Equatorial Pacific (EEP) is a high-nutrient low-chlorophyll region (HNLC); in these areas iron and silica concentrations do not permit a fully efficient utilization of these nutrients by plankton communities (Pichevin et al., 2009; Costa et al., 2016). The EEP is also characterized by

extended coastal and equatorial upwelling areas, which have surface waters with high pCO_2 values (Mekik and Raterink, 2008). As the atmospheric CO_2 concentrations are experiencing a continuous increase due to anthropogenic emissions, we would expect three main consequences in ocean environments: the increase in seawater temperatures, an enhanced sea water stratification, which would cause a decrease in nutrient availability to the surface (Krumhardt et al., 2017) and a high CO2 input into the ocean that will produce an increase in dissolved inorganic carbon (DIC). During the last deglaciation, the Earth experienced a prominent increase in atmospheric CO_2, temperatures and ocean stratification, which we want to investigate to capture the response of coccolithophores. In the last 15 years, a vast amount of research has been done on coccolithophores in order to understand their response/adaptation to high temperatures, low pH and highly stratified and oligotrophic conditions (*e.g.* Riebesell et al., 2000; Iglesias-Rodriguez et al., 2008; Feng et al., 2008; Grelaud et al., 2009; Feng et al., 2016; Krumhardt et al., 2017). Coccolithophores are a main component of the phytoplankton community, representing ca. 20% of the phytoplankton carbon pool in the open ocean regions (Poulton et al., 2007; Krumhardt et al., 2017). They are particularly important in oceanic carbon cycles because they lie at the base of the marine food web; they also play a fundamental role in the global carbon cycle performing both photosynthesis and calcification and they enter in the ocean-atmosphere CO_2 exchange through the export of organic and inorganic carbon (Klaas and Archer, 2002). Some recent studies hypothesized a decrease in calcification of coccolithophores as a response to increased CO_2 concentrations (e.g. Beaufort et al., 2011; Freeman and Lovenduski, 2015; Krumhardt et al., 2017), however other works (Grelaud et al., 2009; Smith et al., 2012; Balestrieri et al., in review.) indicated an increased calcification rate in response to enhanced CO_2 values. Finally, data based on laboratory studies on living organisms showed contradictory results, a decrease or increase in the calcification rate at high CO_2 level (Riebesell et al., 2000; Iglesias-Rodriguez et al., 2008; Langer et al., 2012). Here we present fossil data on the ubiquitous species *Emiliania huxleyi* collected from IODP Site 1238 sediments spanning the last deglaciation to monitor and understand the coccolithophore response to changes in the pCO_2, surface water pH and nutrient availability. *Emiliania huxleyi* is the most abundant and widely distributed coccolithophore species (Paasche, 2001; Iglesias-Rodríguez, 2002; Winter et al., 2013). Recent studies have suggested that it has a strong genetic and morphologic differentiation, and variable degree of calcification (Aloisi et al., 2015). In addition, we evaluated the particulate inorganic carbon (PIC) and particulate organic carbon (POC) following McClelland

et al. (2016) using *E. huxleyi* mass (pg) in order to infer changes of the coccolithophore organic pump that could have had a substantial impact on physical ocean dynamics during the last deglaciation in the EEP. Both PIC and POC production may have been affected by the ongoing anthropogenic climate change via calcification and photosynthesis respectively. This ratio is commonly calculated in studies that focus on the physiology of coccolithophores because it gives clues on how much calcium carbonate is secreted by coccolithophores relative to photosynthetically derived organic carbon (Findlay et al., 2011). In open ocean areas, the ratio of $CaCO_3$ to organic carbon sinking to the deep-sea floor is the result of the carbon produced by three major classes of organisms: corals, foraminifera and coccolithophores.

The importance of coccolithophores in this complicated part of the oceanic carbon cycle is of great relevance because they are responsible for roughly half of the exported oceanic $CaCO_3$ (Broecker and Clark, 2009; Schiebel, 2002), and they thus play an important role in the global PIC:POC ratio. However, further complications to take into consideration are that the PIC:POC ratio in coccolithophores is species-specific (Blanco-Ameijeiras et al., 2016) and this proxy is influenced by environmental conditions (Müller et al., 2017). Nevertheless, quantifying POC production rate and the relative PIC values would allow monitoring of possible changes in the global carbon cycle and, even more interestingly, the response of coccolithophores under specific carbonate system conditions. The primary goal of this study is to shed light on the changes in the mass and calcification of *E. huxleyi* that have occurred in such a crucial area of the ocean (EEP) during the last deglaciation; this would allow us to ascertain the role played by this group of microfossils in a more global perspective and better understand the positive or negative feedback mechanisms related to coccolithophores that may have affected the ocean- atmosphere CO_2 exchanges.

5.2 Site Location and Oceanographic Setting

ODP Site 1238 is located on the southern flank of Carnegie Ridge (1°52.310´S, 82°46.934´W; Fig. 5.1) ~200 km off the coast of Ecuador in the Eastern Equatorial Pacific (EEP) at a water depth of ca 2200 meters (Fig. 5.2). The EEP is a highly productive area characterized by cold waters and high nutrient concentrations. This is because of (i) the contribution from high latitude waters, (ii) the presence of a shallow nutricline, (iii) and the exchange with the coastal upwelling (Cabarcos et al., 2014). The EEP surface circulation is characterized by a complex system of surface and subsurface currents that are primarily controlled by the local wind field and the advection to the

surface of intermediate waters (Wyrtki, 1966; Fiedler and Talley, 2006; Bova et al., 2015). In detail, surface currents are driven by southeast trade winds and Ekman divergence along the Equator and the South American coast (Wyrtki, 1966). The South Pacific subtropical circulation is directly connected to the equatorial circulation through upwelling and advection of the Peru Current (PC) along Peru Margin (Fiedler and Talley 2006; Bova et al., 2015). This upwelling current is a branch of the Antarctic Circumpolar Current and transports heat and nutrients from the Southern Ocean (SO; Cabarcos et al., 2014; Mekik and Raterink, 2008). Between the PC and its coastal branch (Peru Coastal Current; Fig. 5.1) but in an opposite direction the Peru-Chile Countercurrent (PCCC) flows. This current is characterized by intermediate surface temperatures (Cabarcos et al., 2014). On the contrary, the North Pacific domain is separated from the equatorial region by the North Equatorial Countercurrent (NECC) that has a consequently lower influence on the surface waters in the Pacific Basin (Fig. 5.1; Fiedler and Talley, 2006). This current is then deflected to the north feeding the Costa Rica Coastal Current (CRCC) and the North Equatorial Current (NEC). At ~80 m depth, below the South Equatorial Current (SEC), the subsurface Equatorial Undercurrent (EUC) flows eastward into the Pacific Basin by transporting modified Subantarctic Waters (SAAW; Bova et al., 2015; de la Fuente et al., 2017). At deeper water depths, a mixture of Upper Circumpolar Deep Water (UCDW) and Pacific Deep Water (PDW) dominates the EEP (Fig. 5.2; Fiedler and Talley, 2006; de la Fuente et al., 2017). PDW is related to water masses coming from the North Pacific, while UCDW represents the upper layer of the deep Antarctic Circumpolar Current (ACC; Mantyla & Reid, 1983; You, 2000). These deep-water masses are characterized by the same density and depth range in the Pacific (Talley et al., 2011), and though they have different origins they are both part of the extremely weak deep circulation in the Pacific Ocean.

5.3 Materials and Methods

Sixty-six samples were analyzed from ODP Site 1238 along a 192 cm-thick interval with a sampling resolution of ca. 3 cm (0.01-1.92 mbsf), spanning from 0.33 to 29.49 ka. The adopted age model is based on AMS ^{14}C dates from ODP Site 1238 (Martínez-Botí et al., 2015). The ages of the study samples were calculated applying a linear interpolation between the available tie-points.

Samples were prepared using the decanting method proposed by Beaufort et al. 2014. About 30

mg of dry bulk sediment were weighed and placed in a small glass vial (50 ml); sediment was brought into suspension using 45 ml of tap water in the vial. In order to dissolve aggregates, the suspension was placed in an ultrasonic bath for 5 seconds; at this point 5 ml of solution was poured into a flat beaker in which we previously placed a cover slip. We drained the water out from the top with an Eppendorf pipette in order to leave only a slight amount over the cover slip. Then, the beaker was placed in an oven at 70°C for 12 hours in order to dry the cover slip. Finally, the cover slip was mounted on a slide using the Canada balsam glue (density at 20°C: 0.99; ROTH).

To evaluate the coccolith mass, we used the SYRACO automated recognition system (Dollfus and Beaufort, 1999; Beaufort and Dollfus, 2004). We used a Leica DM6000B transmitted light microscope with ×1000 magnification fitted with a SPOT Insight Camera. On average 40 pictures with an area of 15625 μm^2 were taken for each sample and analyzed with SYRACO, a system able to distinguish between the different species present in the assemblages (Dollfus and Beaufort, 1999; Beaufort and Dollfus, 2004). The coccolith length in relation to the distal shield was converted from pixels to micrometers: 1 pixel corresponding to ~0.15 μm. The mass of each single coccolith was estimated using the method developed by Beaufort (2005) based on the brightness properties of calcite particles (thickness <1.55 μm) when viewed in cross-polarized light and following the recommendations of Horigome et al. (2014). In order to correct the overestimation of coccolith mass detected by SYRACO, we corrected the obtained values following D'Amario (2017).

5.3.1 Calcification index

We calculated the *E. huxleyi* calcification index (D'Amario 2017) in order to evaluate the calcification degree of *E. huxleyi* . The length of the main axis of *E. huxleyi* has been independently calculated taking into account that coccolith mass depends both on length and degree of calcification:

$C_i = M_s/M_n$ (eq. 1).

C_i= Calcification index

C_i= Calcification index

M_s =cossolith mass measured with SYRACO

M_n= predicted normalized mass based on Young and Ziveri (2000).

5.3.2 Derived PIC:POC ratio

We calculated the molar ratio of particulate inorganic carbon to particulate organic carbon (PIC:POC) of the biomass obtained from SYRACO using formulas proposed by McClelland et al. (2016):

$PIC:POC_{coccolith}=e^{3.5\pm0.2}AR_L^{1.12}$ (eq. 2)

$AR_L = \frac{T_L}{\sqrt{A_L}} = \frac{ML}{A_L^{3/2}}$ (eqs. 3 and 4)

T_L= coccolith thickness

A_L= coccolith surface (μm^2)

M_L= coccolith mass from SYRACO (pg)

Here, we adopt the threshold value of ~1.86 pg suggested by McClelland et al. (2016) and considered valid under typical modern carbonate system conditions, in order to define photosynthesis versus calcification activity in individuals of *Emiliania huxleyi*.

5.4 Results

5.4.1 *Emiliania huxleyi* mass, calcification index and derived PIC:POC ratio

The mass of *E. huxleyi* shows a general increasing trend from the glacial into the interglacial period by developing in two different steps. The first (glacial) part is characterized by the average value of 2.16 pg ($\sigma \pm 0.25$) with higher and lower values around this mean and a particularly high peak at 18.9 ka (2.78 pg) and three minimum values (1.8 pg) reached at 26 ka, 18.2 ka and 15.3 ka. At 15 ka, the trend increases, reaching its maximum value of 2.83 pg (14 ka); from this point on, there is a decreasing trend up to 9.8 ka and it eventually stabilizes for the rest of the Holocene around the average value of 2.3 pg. Overall, the *E. huxleyi* calcification index (Ci) displays an increasing trend. In detail, during the glacial the Ci values are relatively constant around 1.7, except for a brief interval from 23 to 20 ka in which Ci values show a temporary decrease reaching a minimum of 0.45 at ca.21 ka. From this point, the Ci curve is characterized by a continuous increasing trend that does not seem to stabilize around a certain value, and it finally ends during the final part of the late Holocene at ca 3 ka (1.9). The PIC:POC ratio reflects well the changes

observed in the *E. huxleyi* mass and can be divided into two different intervals: the glacial and the interglacial. During the glacial, the PIC:POC ratio shows a decreasing trend from 1.95 recorded at 29.5 ka up to 1.78 at 18.3 ka. From 18.4 ka to 15 ka, the ratio increases up to at 1.95 but in the following 5 ky the PIC:POC ratio decreases up to 1.81 while at ca. 9 ka the ratio tends to remain constant for the rest of the study interval with values of ca 1.93; an expection is the positive spike observed (2.00) at 4 ka.

5.5 Discussion

5.5.1 Biological production and carbonate system dynamics

5.5.1.1 The carbonate system at Site ODP1238

For many decades it has been challenging to accurately quantify the deep marine $CaCO_3$ dissolution (e.g. Arrhenius, 1952; Pedersen, 1983). In the EEP it has been recognized that the increase in biological productivity, which directly correlates with the $CaCO_3$ concentration in sediments, outweighed the dissolution effects, showing a net increase during glacial periods (Pedersen, 1983; Costa et al., 2016). By contrast, dissolution processes have instead been recognized during interglacial periods in sediments at or below the lysocline (Luz and Shackleton, 1975). In the Equatorial Pacific Ocean, sediments located above the lysocline are characterized by cyclic fluctuations in productivity that primarily result in variations of the carbonate content (Adelseck and Anderson, 1978). According to our carbonate system estimations, calculated from Total Alkalinity (TALK, μmol/kg; WOCE [Schlitzer, 2000], the calcite saturation horizon and the lysocline are positioned below the depth of the study site (2203 m) (Ridgwell and Zeebe, 2005). If this is correct, ODP Site 1238 should not be subject to dissolution, or if so, to a very low degree. However, it should be taken into account that local processes other than dissolution, such as winnowing and variable calcite production, may also be important (Pedersen, 1983).

Recent studies have shown that at the end of the last glacial period the deep waters of the EEP have been poorly ventilated compared to modern conditions (Bova et al., 2015; Martìnez-Botì et al., 2015; de la Fuente et al., 2017). In fact, a more active circulation began before the onset of the deglaciation at ~17.5 ka; (Martìnez-Botì et al., 2015; de la Fuente et al., 2017; Skinner et al., 2015), which allowed the outgassing of a large amount of CO_2 to the atmosphere, (Fig. 5.3a). The increase in CO_2 observed during the deglaciation might be related either to the deglacial evolution of the

deep ocean ventilation, but also to the emission of high quantity of respired CO_2 that acted as a source of carbon to the atmosphere (de la Fuente et al., 2017). Our results indicate an outgassing of CO_2 from the ocean to the atmosphere during the last deglaciation; this process could have been partially induced by enhanced dissolution and/or coccolithophore calcification activity (Fig. 5.3c-d with Fig. 5.4e). In the absence of major ocean carbon sources, the calcium carbonate ($CaCO_3$ % at ODP1240; Fig. 5.3c) related to other proxies (*e.g.* Fig. 5.3b-d-g) behaves as a semi-conservative tracer that allows inference of changes in the post-depositional effects on microfossils. The position of Site ODP Site 1240 (2921 m water depth) is very close the present Carbonate Saturation Horizon (Fig. 5.2) and below the lysocline, which offers a good evaluation of the carbonate system dynamics. We use here the *E. huxleyi* mass (pg) trend as a microfossil proxy to detect changes in the carbonate system along the study period. *E. huxleyi* is one of the most delicate species with respect to dissolution processes within coccolithophores, because it produces very delicate coccoliths with fragile t-shaped elements (Young and Ziveri, 2000). It also has to be taken into account that the mass of *E. huxleyi* is sensitive to various environmental parameters such as temperature, [CO_3^{2-}], nutrient and light availability (*e.g.* Riebesell et al., 2000; Cubillos et al., 2007; Boeckel and Baumann, 2008; Mohan et al., 2008; Beaufort et al., 2011; Horigome et al., 2014;); but analyzing the same sediment samples with a multiproxy approach is, at least presently, a monitor of the dynamics of the deep-sea carbonate system (Mekik and Raterink, 2008).

5.1.1.2 *E. huxleyi* mass as a phytoplankton carbonate production proxy

The high $CaCO_3$ content (~ 60%; Fig. 5.3c) observed at ODP Site 1240 during the last glacial period matches well with stable high *E. huxleyi* mass values, high organic carbon (C_{org}) and low [CO_3^{2-}] values (Fig. 5.3), indicating a high calcium carbonate preservation. This is related to the fact that when calcium carbonate is not dissolved throughout the water column, carbonate ions are not released into sea water, which in turn implies low alkalinity values (Ridgwell and Zeebe, 2005). The high C_{org} (%) is usually associated either with higher biological productivity or higher preservation of organic compounds in deep waters with low oxygen content (Pedersen, 1983; Pichevin, 2009; de la Fuente et al., 2017). The good preservation of the sediments extends for the whole glacial interval and up to the onset of the deglaciation. From 11.8 ka to 9 ka, a decrease in the calcium carbonate content (%), nannofossil-based CEX' index, *E. huxleyi* mass (pg), and C_{org} (%) are associated with an increase in carbonate ion content (Fig. 5.3); the occurrence of all these

changes are usually related to enhanced dissolution but the good preservation of nannofossils suggests it may not be the case (Fig. 5.3b) (Cabarcos et al., 2014). A possible alternative explanation is that relatively low values of carbonate are related to low carbonate production (11.8-9 ka, 45% in Fig. 5.3c). This hypothesis is supported by the decrease observed in *E. huxleyi* mass (pg), which eventually resulted in an increase of deep-water alkalinity or, in other words high [CO_3^{2-}]. The low coccolithophore production is possibly caused by diatoms that would be able to outcompete calcareous phytoplankton because of an increase in nutrients delivered from the SO waters (Cabarcos et al., 2014). The final part of the middle Holocene is characterized by high values of $CaCO_3$, *E. huxleyi* mass and relatively lower values of the CEX' index and [CO_3^{2-}]. CEX' values lower than 0.6 are considered to be indicative of dissolution events (according to Boeckel and Baumann, 2004 for the South Atlantic). During the late Holocene (6-4 ka), we detect a negative peak in all proxies considered, though they are not perfectly synchronized. This general decrease has been interpreted in terms of low nannofossil carbonate production, which is possibly caused by El Niño like variability (Cabarcos et al., 2014).

5.5.2 Oligotrophic water conditions and enhanced coccolithophore PIC production

The EEP is a high-nitrate low-chlorophyll region (Beherenfeld and Kobler, 1999; Pennington et al., 2006) and nutrients are never fully utilized by plankton because of iron and silica limitation (Mekik and Raterink, 2008; Pichevin et al., 2009). During the glacial, these conditions likely enhanced the diatom carbon pump that could have contributed to the glacial carbon dioxide drawdown (Pichevin et al.,2009). The iron concentrations instead are not sufficient for an iron fertilization even if a delivery of iron has occurred from the Subantarctic zone (SAZ) of the SO through SAAW, (Costa et al., 2016). These authors observed a glacial decrease in opal accumulation that does not reflect a decline in carbon rain-rate ratio and the biological carbon pump (Fig. 5.4b). The unexpected glacial decline in silica accumulation has been explained as an increased silicic acid supply from the SO that occurred at the time the demand for this nutrient declined locally in the EEP (Pichevin et al., 2009). The eutrophic water conditions in the EEP during the glacial should have stimulated an increase in the biosiliceous production, which has not been observed (Pichevin et al., 2009). In fact, the siliceous production shows minimum values and this anomaly could have made high carbonate production possible, though coccolithophores are usually better adapted to oligotrophic conditions (Cabarcos et al., 2014). During the glacial, *E.*

huxleyi photosynthesis activity (POC production; <1.86) prevailed over calcification, hence playing a role in the CO_2 sequestration from the atmosphere to the ocean (Fig. 5.4e) and this is consistent with the absence of iron fertilization and relatively low coccolithophore carbonate activity (Salter et al. 2014; Rembauville et al., 2016; Balestrieri et al., in review). The derived PIC:POC ratio pattern is also in good agreement with ΔpCO_2 (p^{sw}_{CO2}-p^{atm}_{CO2}, Martínez-Botí et al., 2015), which shows that the EEP region has been a region of sinking during the last glacial.

On the contrary, interglacial PIC:POC ratio values are characterized by an enhanced carbonate counter pump (>1.86), which becomes a source of CO_2 that is released from the ocean into the atmosphere (Fig. 5.4e). During the Holocene, surface waters in the EEP were characterized by low nutrient concentrations and high stratification (El Niño; Cabarcos et al., 2014). Hence, under phosphate and nitrate limitation there is an increase in the ratio of calcite to particulate organic carbon (Zondervan, 2007).

5.5.3 Factors controlling *E. huxleyi* calcification

5.5.3.1 Is pH primarily controlling *E. huxleyi* calcification activity?

A number of environmental factors such as nutrient availability, water temperatures and water stratification have changed over the last 30 ky in the EEP, (Pichevin et al., 2009; Cabarcos et al., 2014). Most importantly, atmospheric CO_2 critically increased (Fig. 5.3a) and the EEP was an expanded area characterized by high sea surface CO_2 level derived from the exchange with the atmosphere (Mekik and Raterink, 2008). As discussed, the EEP also played a fundamental role in outgassing the oceanic glacial reservoir of CO_2 to the atmosphere. The absorption and outgassing of oceanic CO_2 are able to induce changes in surface seawater pH (Martínez-Botí et al., 2015). Since coccolithophores are one of the major calcifying groups they can be highly affected by changes in the carbonate system, which is why we try to evaluate the factors influencing the carbonate system using nannofossil-based indices. Variations in coccolith thickness both within different species and in different strains of the same species depends on the cellular calcification per surface area, as well as changes in the PIC/POC ratio. The key mechanism that controls the biomineral amount for a given cell volume is correlated with the degree of calcification of a cell, leading to a variable thickness of the individual coccolith (Bolton et al., 2016). Though we are aware that several factors are able to drive cells to adjust calcite per cell surface area, here we discuss the changes observed in the PIC:POC ratio extrapolated by *E. huxleyi* in order to interpret

changes in the photosynthesis versus calcification activity (P:C); this has been done comparing the PIC:POC ratio with *E. huxleyi* calcification index (Fig. 5.4d- e).

Generally, phytoplankton growth is optimal at constant pH (Flynn et al., 2016). As mentioned above, the carbonate system critically changed during the last deglaciation and modifications in calcification and photosynthesis activities performed by *E. huxleyi* possibly caused changes in the cell because of the sensitivity of the organisms increases at higher values in seawater [H^+] (Bach et al., 2011). In particular, the pH homeostasis performed by coccolithophores in order to maintain stable pH conditions can be related to the P:C ratio (Flynn et al., 2016). During the last glacial the ocean absorbed small amounts of CO_2 and this resulted in high surface seawater pH (8.35; Fig. 5.4b). As a response to these alkaline seawater conditions, coccolithophores show values of P:C ratio (1.85) very close to the threshold value. As T1 approaches, the P:C ratio increases and this change may have produced a sequestration of CO_2 in the ocean and would have eventually reduced the atm pCO_2. Moreover, the photosynthetic activity is able to modify the carbonate chemistry in the microenvironment around the phytoplankton cell, thus increasing seawater pH (Flynn et al., 2016), but unfortunately we do not have any evidence for this (Fig. 5.4b). In fact, as photosynthetic activity increases (until 17.5 ka), the surface seawater pH decreases due to the absorption of CO_2 from the atmosphere.

Our question is then, is the carbon pump working as a buffer for the acidification of the surface seawater? If so, how could this be a trigger in terms of homeostatic regulation in the coccolithophore cell? And then, why did this buffer activity stop just when CO_2 values started to increase more dramatically? Photosynthesis consumes CO_2 and, as a result it increases seawater pH values and acts as buffer for ocean acidification (Riebesell et al., 2000; Flynn et al., 2016). At high pCO_2 levels, the photosynthesis performed by coccolithophores is more active (Aloisi, 2015) until the seawater [H^+] starts to drive the homeostatic mechanisms in coccolithophores that become the main factor to balance the internal cell and external pH by increasing calcification. If this is a realistic explanation, the sharp and fast increase in PIC:POC ratio observed when CO_2 values almost reached their maximum can be interpreted as related to a pH homeostasis mechanism. The low PIC:POC ratio values during the glacial is also consistent with the low values in the calcification index (Fig. 5.4d-e), DpCO_2 and seawater pH (Martínez-Botí et al., 2015). Additionally, Brownlee et al. (1994) proposed that at pH values around 8.3, in a high-calcifying

strain such as *E. huxleyi*, both photosynthesis and calcification were dependent on the presence of external Ca^{2+} to a similar degree. We can indeed propose a 1:1 ratio (P:C) possibly variable toward a more photosynthetic activity driven by nutrient availability.

5.5.3.2 Is pCO_2 being controlled by *E. huxleyi* calcification activity?

During the second part of T1, when pCO_2 and pH start to increase and decrease respectively the PIC:POC ratio has a prominent increase that is also reflected in the calcification index; we hence infer an increased calcification activity within *E. huxleyi* (Fig. 5.4). Laboratory studies have reported contradictory responses of coccolithophores calcification to increasing CO_2 (*e.g.* Riebesell et al., 2000; Iglesias- Rodriguez et al., 2008) within one single strain of *E. huxleyi*. In particular, Beaufort et al. (2011) reported the presence of less calcified *E. huxleyi* (morphotype R) in CO_2-rich waters along the Patagonian shelf and the Chilean upwelling waters. Our data show an increase in calcification activity with increasing CO_2.

We suggest that there could be a threshold value in the CO_2 levels that is not reached during this time interval, and above which calcification starts decreasing due to too high energetic costs (Flynn et al., 2016). AtmCO_2 values in the Holocene increased up to 280 ppmv, which is the starting value considered in culture experiments by Riebesell et al. (2000) in order to analyze variations possibly occurring in *E. huxleyi* calcification. One possible hypothesis is that coccolithophores start to decrease calcification rates only when CO_2 values exceed a threshold level, as for an instance 280 ppmv. If this is the case, there could be a possible spectrum of CO_2 levels in which the response of *E. huxleyi* varies in terms of calcification rate. Through the cell membrane, coccolithophores absorb HCO_3^- and CO_2 (Berry et al., 2002; McClelland et al., 2017) but only external HCO_3^- is used for calcification (Sekino and Shiraiwa, 1994; Berry et al., 2002). Under high seawater pCO_2 conditions pH drastically decreases, thus producing an electrochemical and homeostatic disequilibrium between the extracellular and intracellular $[H^+]$ (McClelland et al., 2017). In order to buffer the seawater acidification and maintain the pH neutrality between the cytosol cell and the exterior environment, calcification (through this reaction in the coccolith vesicle: $HCO_3^- + Ca^{2+} \rightarrow CaCO_3 + H^+$) may have acted to adjust the cytosol pH through the release of H^+(Quiroga and Gonzalez., 1993). High calcification rates could be a response to buffer the difference in pH between the environment and the cytosol of the organism. Hence, a possible mechanism to maintain the internal cell carbonate system in equilibrium with the external one is an enhanced

calcification activity at high seawater pCO_2.

High calcification activity could have acted as a negative feedback on atmospheric CO_2 levels playing an important role in increasing seawater pCO_2 and thus allowing for the release to the atmosphere during the deglaciation. The rapid change in PIC:POC ratio between glacial and interglacial states could be explained by a dramatic change in the P:C strategy, primarily driven by high pCO_2 pressures and successively by the pH homeostatic mechanism. In the past, several explanations have been proposed to justify decreased calcification rates at low seawater pH, including the theory that the outward transport of protons may have become a high cost process (Zondervan et al., 2002), and hence photosynthesis activity would have had priority over calcification. It could be possible that with pCO_{2atm} values lower than 280 ppm, coccolithophores would have had an adaptive advantage by enhancing calcification rather than photosynthesis; however, with pCO_{2atm} values higher than 280 ppm, coccolithophores would have decreased calcification in favor of photosynthesis.

5.6 Conclusions

We present a high-resolution dataset of the mass and calcification dynamics of the most abundant and common coccolith species in the modern ocean, *E. huxleyi*. We show increased calcification degree evidenced by an increase in *E. huxleyi* mass from the glacial into the Holocene as a response to low surface pH and increased CO_2 values, due to the natural homeostasis regulation between the cytosol cell and the seawater environment. We also infer changes in the calcification versus photosynthesis activity based on reconstructed PIC:POC ratios. Finally, we point out an enhanced coccolith carbonate counter pump during the last deglaciation that has likely played a major role in increasing sea water pCO_2that was successively released into the atmosphere.

Acknowledgments

This research used samples provided by the Integrated Ocean Drilling Program (IODP), which is sponsored by the U.S. National Science Foundation and participating countries under management of Joint Oceanographic Institutions, Inc. CA and CB are funded by University of Padova (SID2016 - BIRD161002).

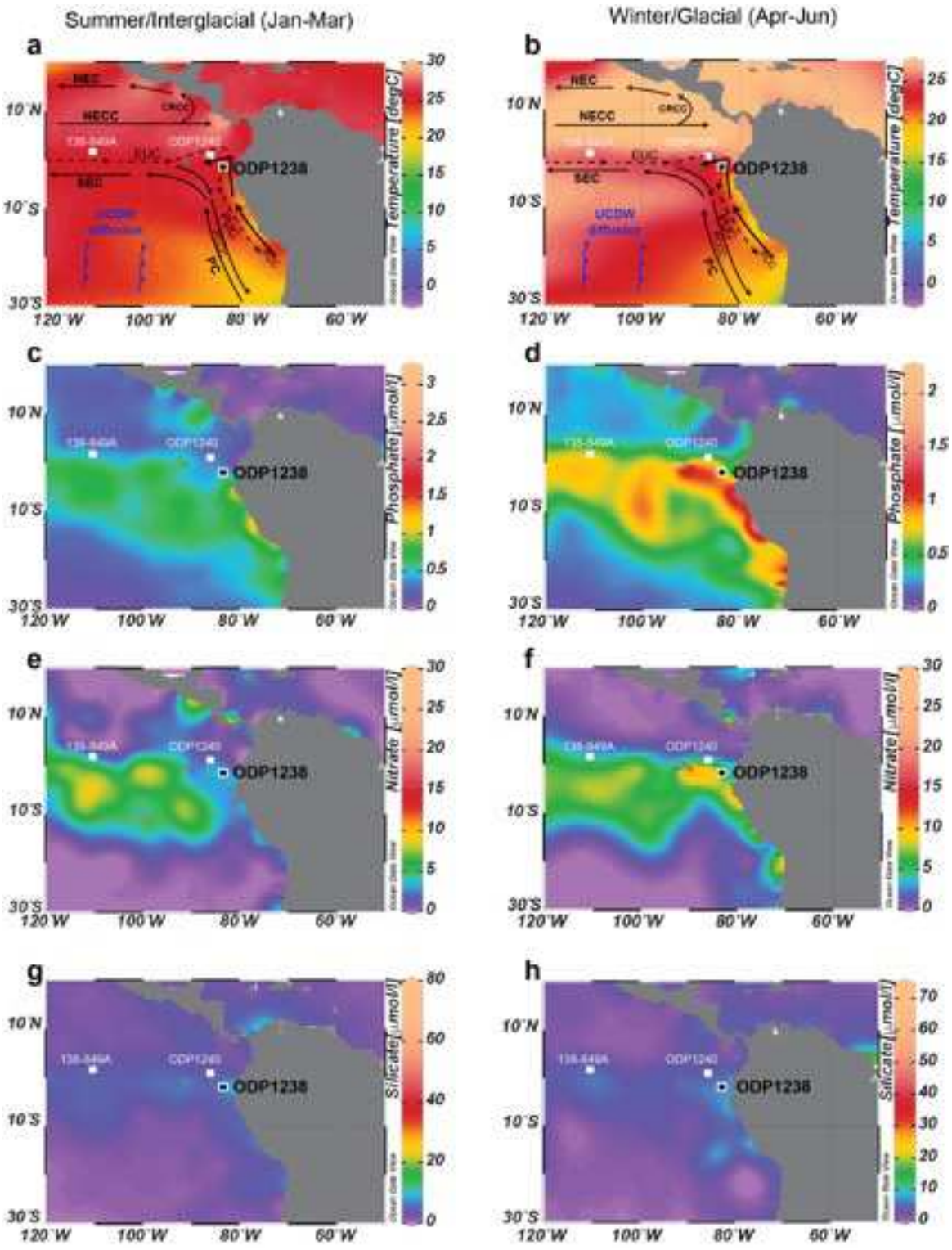
Summer/Interglacial (Jan-Mar)
Winter/Glacial (Apr-Jun)
a
b
c
d
e
f
g
h
NEC
NECC
CRCC
SEC
EUC
PC
UCDW
ODP1238
ODP1240
10°N
10°S
30°S
120°W
100°W
80°W
60°W
Temperature [degC]
Phosphate [µmol/l]
Nitrate [µmol/l]
Silicate [µmol/l]

Figure 5.1(previous page): EEP oceanography. The map of the study area with locations of Site IODP 1238 (in black, this study), IODP 1240 and 138-849A, indicated as white squares. Site locations are superimposed on a map of average monthly sea surface temperature (a; b), phosphate (c; d), nitrate (e; f) and silicate (g; h) of Jan-March (Summer/Interglacial) and April-June (Winter/Glacial). Data have been compiled from World Ocean Atlas 2013 using the Software Ocean Data View 4® (R. Schlitzer, Ocean data view, 2009, http://gcmd.nasa.gov/records/ODV_AWI.html). In a and b a scheme for surface currents (black arrows): PC (Peru Current); PCC (Peru Coastal Current); PCCC (Peru-Chile Countercurrent; SEC (South Equatorial Current); NEC (North Equatorial Current); NECC (North Equatorial Countercurrent; CRCC (Costa Rica Coastal Current); subsurface currents (dush black arrows): EUC (Equatorial Undercurrent); PUC (Perù Undercurrent) and deep (blue) ocean circulation: UCDW (Upper Circumpolar Deep water mass).

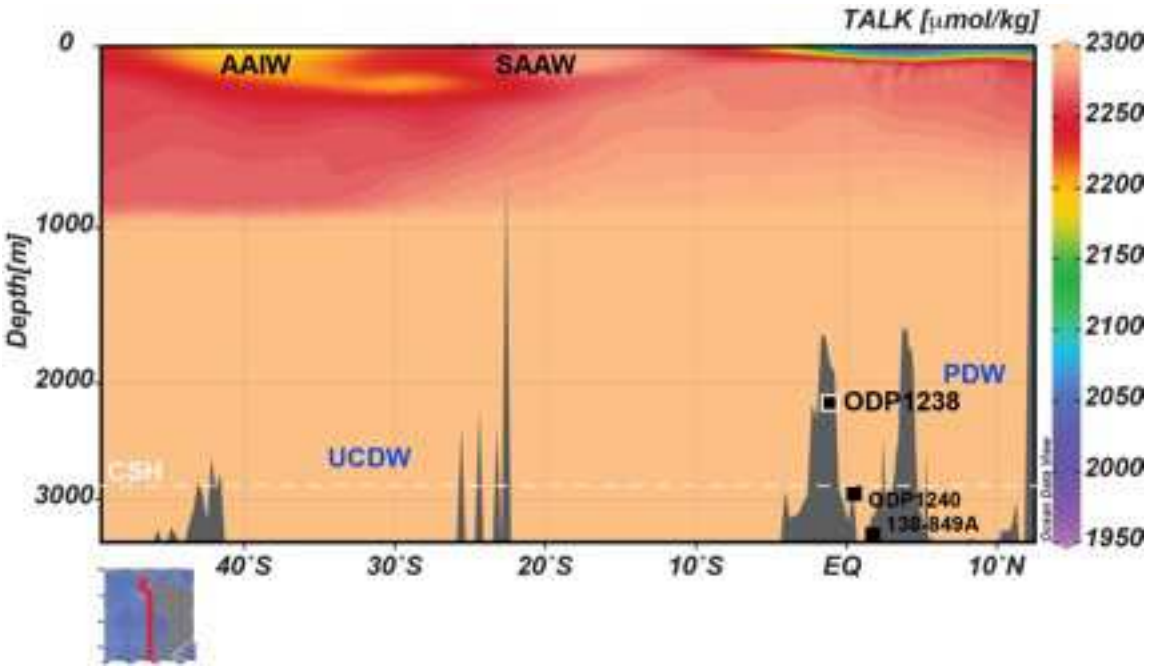

Figure 5.2: Latitudinal depth profile map displaying Total Alkalinity (TALK, µmol/kg) data from WOCE [Schlitzer, 2000] based on Global Alkalinity and Total Dissolved Carbon Estimates (Goyet, Healy and Ryan (2000). The Calcite Saturation Horizon (CSH, 2997m; white dashed line) has been calculated based on modern salinity, temperature (°C), pressure (dbars), total alkalinity (µmol/kg) and pH data using CO_2Sys. A map showing the location of the transect is at the bottom left. Sea surface (black) water circulation is characterized by high latitude Antarctic Intermediate water (AAIW) that arrives at low latitudes through Subantarctic Water (SAAW). Deep (blue) water circulation is characterized by Upper Circumpolar Deep Water (UCDW) that merges into the Pacific Deep Water (PDW).

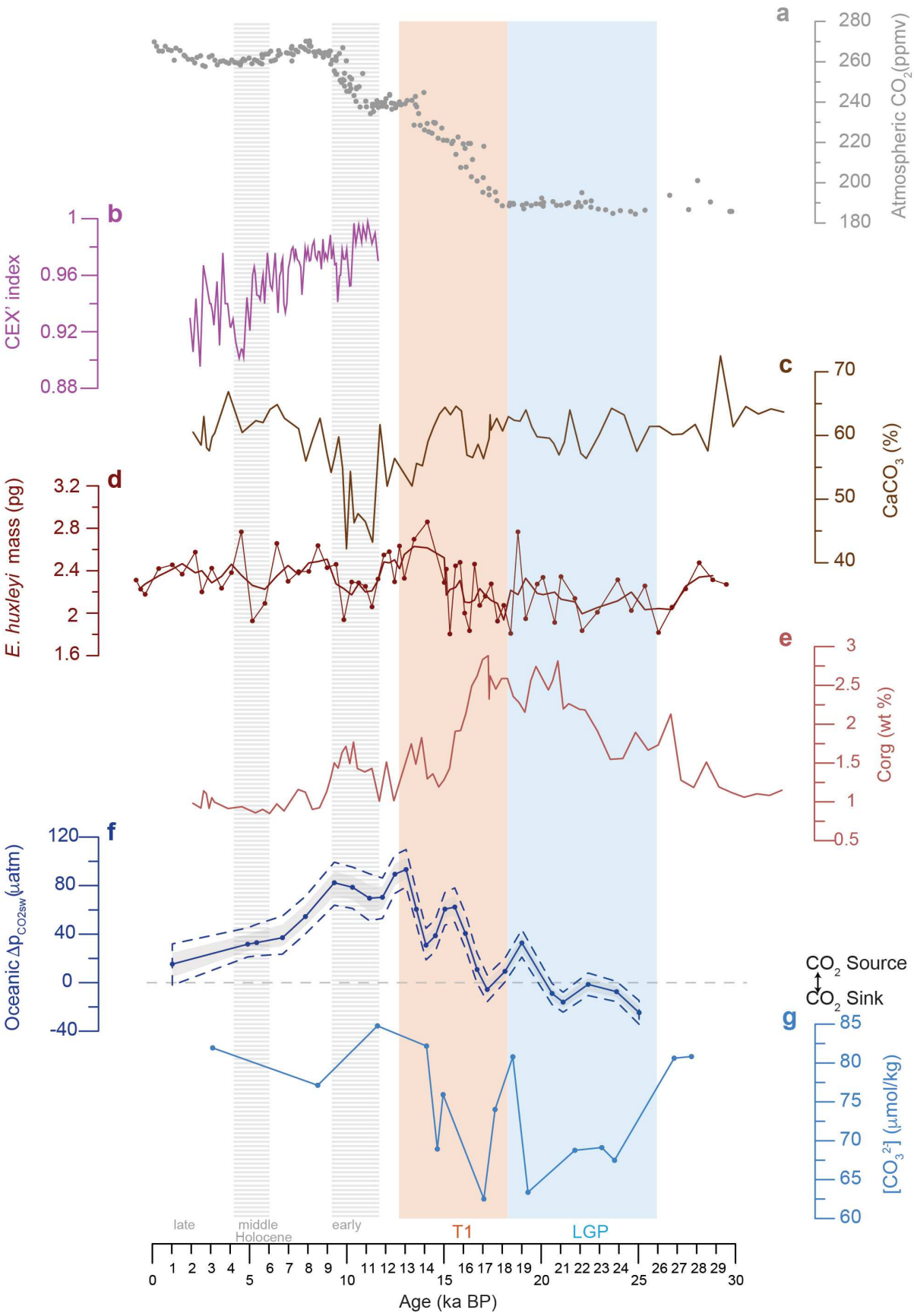
a
Atmospheric CO2(ppmv)
280
260
240
220
200
180
b
CEX' index
1
0.96
0.92
0.88
c
CaCO3 (%)
70
60
50
40
d
E. huxleyi mass (pg)
3.2
2.8
2.4
2
1.6
e
Corg (wt %)
3
2.5
2
1.5
1
0.5
f
Oceanic ΔpCO2sw (µatm)
120
80
40
0
-40
CO2 Source
CO2 Sink
g
[CO3 2-] (µmol/kg)
85
80
75
70
65
60
late
middle Holocene
early
T1
LGP
0 1 2 3 4 5 6 7 8 9 10 11 12 13 14 15 16 17 18 19 20 21 22 23 24 25 26 27 28 29 30
Age (ka BP)

Figure 5.3 (previous page): Data and proxies from IODP Sites 1238 and 1240. a) Atmospheric CO_2 (ppmv) concentrations from Antarctic ice cores (Schmitt et al., 2012); b) CEX' index or dissolution index at ODP1240 (Cabarcos et a., 2014); c) $CaCO_3$ (wt%) at Site ODP 1240 (Pichevin et al., 2009); d) *E. huxleyi* mass (pg); e) organic C (wt%) at Site ODP 1240 (Pichevin et al., 2009); f) ΔpCO_2 derived for IODP1238 (Martínez-Botí et al., 2015); g) $[CO_3^{2-}]$ (μmol/kg) at IODP1240 (de la Fuente et al., 2017). Blue band represents the Last Glacial Period; red band represents Termination 1 (T1); in grey we define the early (12-8 ka), middle (8-4 ka) and late (4-0 ka) Holocene. Grey bands represent low coccolithophore production.

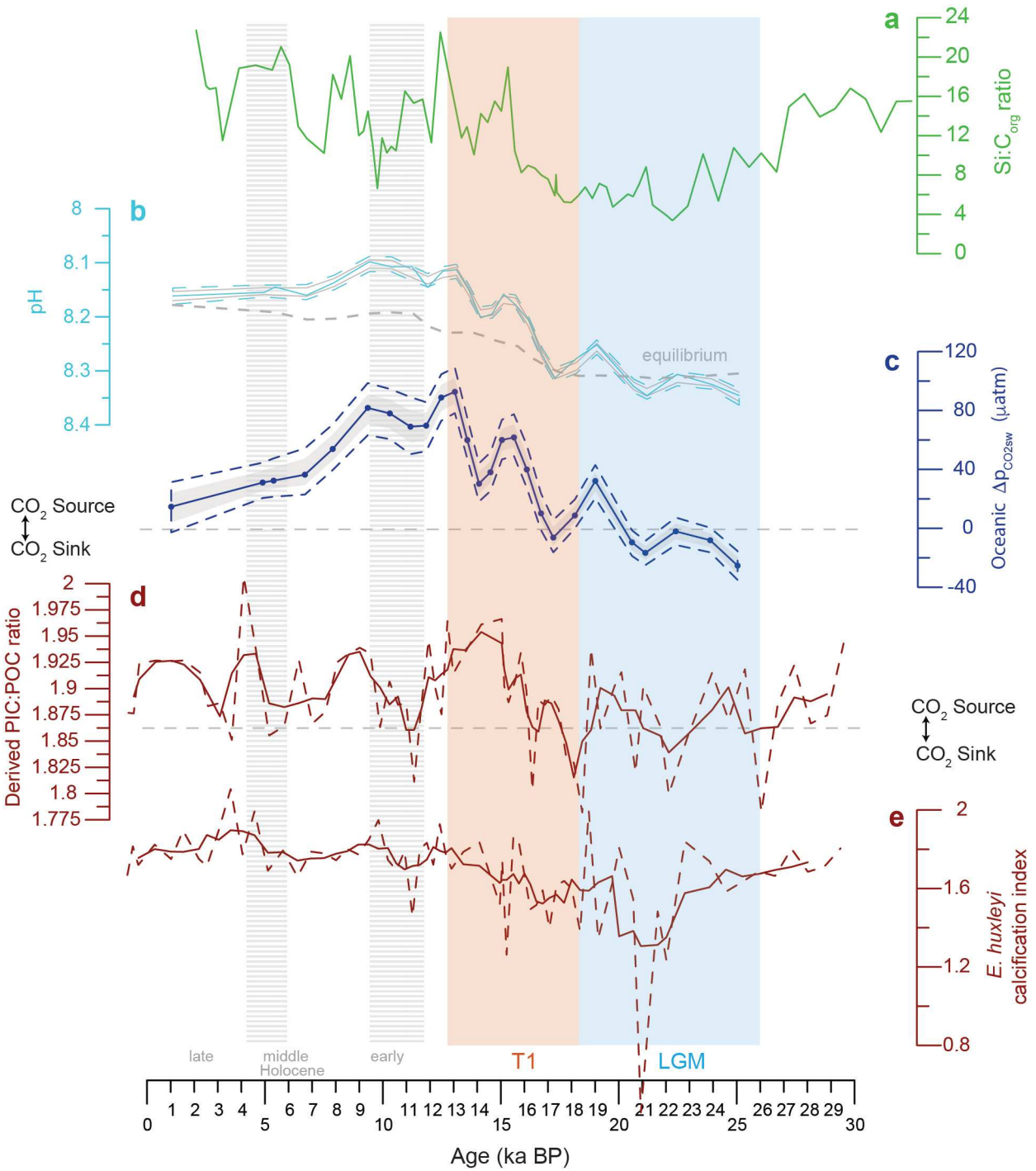

Figure 5.4: Data and proxies from IODP Sites 1238 and 1240. a) Si:C ratio at Site ODP 1240 (Pichevin et al., 2009); b) surface water pH reconstruction for IODP1238 and calculated surface pH in equilibrium with atmospheric pCO_2 (Martínez-Botí et al., 2015); c) ΔpCO_2 derived for IODP1238 (Martínez-Botí et al., 2015); d) derived PIC:POC ratio from *E. huxleyi* mass (pg); e) *E. huxleyi* calcification index. Blue band represents the Last Glacial Period; red band represents Termination 1 (T1); in grey we define the early (12-8 ka), middle (8-4 ka) and late (4-0 ka) Holocene. Grey bands represent low coccolithophores production.

References

Adelseck, C. G., Jr., and Anderson, T. F. (1978). The late Pleistocene record of productivity fluctuations in the eastern equatorial Pacific Ocean: Geology, v. 6, p. 388-391.

Aloisi, G. (2015). Covariation of metabolic rates and cell size in coccolithophores, Biogeosciences, 12, 4665-4692, https://doi.org/10.5194/bg-12-4665-2015

Arrhenius, G. (1952), Sediment cores from the east Pacific, Rep. Swed. Deep Sea Exped. 1947–1948, 5, 1–228.

Bach LT, Riebesell U, Schulz KG. 2011 Distinguishing between the effects of ocean acidification and ocean carbonation in the coccolithophore Emiliania huxleyi. Limnol. Oceanogr. 56, 2040 – 2050. https://doi.:10.4319/lo.2011.56.6.2040

Balestrieri C., Ziveri P., Mortyn P.G. et al. (2018). Coccolith carbonate export responses to Southern Ocean iron fertilization during the last deglaciation. Subm. to Quaternary Science review. Elsevier.

Beaufort L., Barbarin N. & Gally Y. (2014). Optical measurements to determine the thickness of calcite crystals and the mass of thin carbonate particles such as coccoliths. *Nature Protocols* volume 9, pages 633–642.

Beaufort L et al. 2011 Sensitivity of coccolithophores to carbonate chemistry and ocean acidification. Nature 476, 80–83. https://doi.:10.1038/nature10295 .

Beaufort, L. (2005). Weight estimates of coccoliths using the optical properties (birefringence) of calcite. *Micropaleontol*ogy, 51, 289–298. https://doi.:10.2113/gsmicropal.51.4.289

Beaufort, L. & Dollfus D. (2004). Automatic recognition of coccoliths by dynamical neural networks. *Marine Micropaleontology*, 51(1):57-73. **https://doi.:10.1016/j.marmicro.2003.09.003**

Berry, L., Taylor, A. R., Lucken, U. et al. (2002) Calcification and inorganic carbon acquisition in coccolithophores. Funct.Plant Biol., 29, 289 – 299.

Blanco-Ameijeiras, S., Lebrato, M., Stoll, H.M., Iglesias-Rodriguez, D., Müller, M.N., Méndez-Vicente, A., Oschlies, A., 2016. Phenotypic variability in the coccolithophore Emiliania huxleyi. PLOS ONE 11, 1–17. https://dx.doi.org/10.1371/journal.pone. 0157697

Bova C. S., Hebert T., Rosenthal Y., Kalansky J., Altabet M., Chazen C. et al., (2015). Links between eastern equatorial Pacific stratification and atmospheric CO_2 rise during the last deglaciation. https://doi.org/10.1002/2015PA002816

Broecker, W.S. and Clark E. (2009). Ratio of coccolith $CaCO_3$ to foraminifera $CaCO_3$ in late Holocene deep sea sediments. Paleoceanography, 24(3), PA3205, https://doi.org/10.1029/2009PA001731

Cabarcos E., Flore J-A and Sierro F. (2014). High resolution productivity record and reconstruction of ENSO dynamics during the Holocene in the Eastern Equatorial Pacific using coccolithophores. The Holocene. Vol. 24(2) 176–187.

Costa K.M., MvManus J.F., Anderson R.F. et al. (2016). No iron fertilization in the equatorial Pacific Ocean during the last ice age. Nature 519. Vol. 529.

D' Amario B. (2017). Coccolithophore calcification, life- cycle dynamics and diversity in a warming and acidifying Mediterranean Sea, (Doctoral Dissertation). Depòsit digital de documents de la UAB. Universitat Autònoma de Barcelona.

De la Fuente M., Calvo E., Skinner L., Pelejero C., Evans D., Müller W. Et al. (2017). The evolution of the deep ocean chemistry and respired carbon in the eastern equatorial pacific over the last deglaciation. Paleoceanography, 32, 12, 1371-1385.

Dollfus, D. & Beaufort L. (1999). Fat neural network for recognition of position-normalised object, *Neural Netw*, 12, 553–560.

Feng, Y., Roleda, M.Y., Armstrong, E., Boyd, P.W., Hurd, C.L., 2016. Environmental controls on the growth, photosynthetic and calcification rates of a Southern Hemisphere strain of the coccolithophore Emiliania huxleyi. Limnol. Oceanogr. https://doi.org/10.1002/lno.10442

Feng, Y., Warner, M.E., Zhang, Y., Sun, J., Fu, F.X., Rose, J.M., Hutchins, D.A., 2008. Interactive effects of increased pCO_2, temperature and irradiance on the marine coccolithophore Emiliania huxleyi (Prymnesiophyceae). Eur. J. Phycol. 43, 87–98. https://doi.org/10.1080/09670260701664674

Fiedler, P. C., and L. D. Talley (2006), Hydrography of the eastern tropical Pacific: A review, Prog. Oceanogr., 69(2–4), 143–180. https://doi.:10.1016/ j.pocean.2006.03.008

Findlay, H.S., Calosi, P., Crawfurd, K., 2011. Determinants of the PIC:POC response in the coccolithophore Emiliania huxleyi under future ocean acidification scenarios. Limnol. Oceanogr. 56, 1168–1178. http://dx.doi.org/10.4319/lo.2011.56.3.1168

Flores J. A. and Sierro F. (1997). Revised technique for calculation of calcareous nannofossil accumulation rates. Micropaleontology 43(3):321-324.

Flynn K.J., Clark D.R. and Wheeler G. (2016). The role of coccolithophore calcification in

bioengeneering their environment. Proc. R. Soc. B 283: 20161099. https://doi.org/10.1098/rspb.2016.1099

Freeman, N.M. and Lovenduski, N.S., 2015. Decreased calcification in the Southern Ocean over the satellite record. Geophys. Res. Lett. 42, 1834–1840. https://doi.org/10. 1002/2014GL062769

Iglesias-Rodriguez, M.D., Halloran, P.R., Rickaby, R.E.M., Hall, I.R., Colmenero-Hidalgo, E., Gittins, J.R., Green, D.R.H., Tyrrell, T., Gibbs, S.J., von Dassow, P., Rehm, E., Armbrust, E.V., Boessenkool, K.P., (2008). Phytoplankton calcification in a high-CO_2 world. Science 320, 336–340.

Goyet, C., Healy, R., and Ryan, J. (2000) Estimated alkalinity and total dissolved inorganic carbon, available at: https://https://doi..org/odv.awi.de/en/data/ocean/global_alkanity_tco2

Grelaud M.; Beaufort L.; Cuven S.; Buchet N. (2009). Glacial to interglacial primary production and El Niño-Southern Oscillation dynamics inferred from coccolithophores of the Santa Barbara Basin. Paleoceanography, 24(1), PA1203. https://doi.org/10.1029/2007PA001578

Klaas, C., and D. E. Archer (2002), Association of sinking organic matter with various types of mineral ballast in the deep sea: Implications for the rain ratio, Global Biogeochem. Cycles, 16(4), 1116. https://doi.org/:10.1029/2001GB001765

Krumhardt K.M., Lovenduski N., Iglesias-Rodriguez et al. (2017). Coccolithophore growth and calcification in a changing ocean. Progress in Oceanography. 159. 276-295.

Langer G.; Oetjen K.; Brenneis T. (2012): Calcification of Calcidiscus leptoporus under nitrogen and phosphorus limitation. Journal of Experimental Marine Biology and Ecology, 413, 131-137, https://doi.org/10.1016/j.jembe.2011.11.028

Luz, B. & Shackleton, N. J. (1975) in Dissolution of Deep-Sea Carbonates, Cushman Fdn Foraminifera Res. Spec. Publ. 13, 142–150.

Mantyla, A. W., & Reid, J. L. (1983). Abyssal characteristics of the World Ocean waters. Deep-Sea Research Part A: Oceanographic Research Papers, 30(8), 805–833. https://doi.org/10.1016/0198-0149(83)90002-X

Martínez-Botí, M. A., Marino G., Foster G. L., Ziveri P., Henehan M.J., Rae J.B.W., et al. (2015). Boron isotope evidence for oceanic carbon dioxide leakage during the last deglaciation. *Nature* 518, 219–222. https://doi.org:10.1038/nature14155

McClelland H.L.O., Bruggeman J., Hermoso M. & Rickaby (2017). The origin of carbon isotope vital effects in coccolith calcite. Nature Communications volume 8.

McClelland H. L. O., Barbarin N., Beaufort L., Hermoso M., Ferretti P., Greaves et al., (2016). Calcification response of a key phytoplankton family to millenial- scale environmental change. *Scientific Reports* volume 6, Article number: 34263.

Mekik F., Raterink L. (2008). Effects of surface ocean conditions on deep- sea calciate dissolution proxies in the tropical Pacific. PALEOCEANOGRAPHY, VOL. 23, PA1216, https://doi.org:10.1029/2007PA001433

Müller, M.N., Trull, T.W., Hallegraeff, G.M., (2017). Independence of nutrient limitation and carbon dioxide impacts on the Southern Ocean coccolithophore Emiliania huxleyi. ISME J. https://doi.org: 10.1038/ismej.2017.53

Paasche E. (*2001*) A review of the coccolithophorid Emiliania huxleyi (Prymnesiophyceae), with particular reference to growth, coccolith formation, and calcification-photosynthesis interactions. Phycologia. Vol. 40, No. 6, pp. 503-529. https://doi.org/10.2216/i0031-8884-40-6-503.1

Pedersen, T. F. (1983). Increased productivity in the eastern equatorial Pacific during the last glacial maximum (19,000 to 14,000 yr B.P). Geology, 11(1), 16–19.

Pichevin L.E., Reynolds B.C., Ganeshram R. S. et al. (2009). Enhanced carbon pump inferred from relaxation of nutrient limitation in the glacial ocean. Nature. Vol. 459.

Poulton, A.J., Adey, T.R., Balch, W.M., Holligan, P.M. (2007). Relating coccolithophore calcification rates to phytoplankton community dynamics: regional differences and implications for carbon export. Deep Sea Res. Part II 54, 538–557. (the Role of Marine Organic Carbon and Calcite Fluxes in Driving Global Climate Change, Past and Future). https://doi.org/10.1016/j.dsr2.2006.12.003

Riebesell, U., Zondervan, I., Rost, B., Tortell, P.D., Zeebe, R.E., Morel, F.M.M., 2000. Reduced calcification of marine plankton in response to increased atmospheric CO_2. Nature 407, 364–367. https://doi.org/10.1038/35030078

Ridgwell, A., and R. E. Zeebe (2005). The role of the global carbonate cycle in the regulation and evolution of the Earth system, Earth Planet. Sci. Lett., 234, 299–315. https://doi.org:10.1016/j.epsl.2005.03.006

Schiebel, R., (2002). Planktic foraminiferal sedimentation and the marine calcite budget. Global Biogeochem. Cycles 16, 3-1–3-21. https://dx.doi.org/10.1029/ 2001GB001459. 1065

Sekino K. and Shiraiwa Y. (1994). Accumulation and utilization of dissolved inorganic carbon by a marine unicellular coccolithophorid, Emiliania huxleyi. Plant Cell Physiol. 35, 353–361.

Smith, H.E., Tyrrell, T., Charalampopoulou, A., Dumousseaud, C., Legge, O.J., Birchenough, S., Pettit, L.R., Garley, R., Hartman, S.E., Hartman, M.C., Sagoo, N., 2012. Predominance of heavily calcified coccolithophores at low $CaCO_3$ saturation during winter in the Bay of Biscay. Proc. Natl. Acad. Sci. 109 (23), 8845–8849. https://doi.org/10.1073/pnas.1117508109

Quiroga, O. and Gonzalez, E.: Carbonic anhydrase in the chloroplast of a coccolithophorid (Prymnesiophyceae), J. Phycol., 29, 321–324, 1993.

Skinner L., McCave I.N., Carter L. et al. (2015). Reduced ventilation and enhanced magnitude of the deep Pacific carbon pool during the last glacial period. Earth and Planetary Science letters. Volume 411. Pg. 45- 52.

Talley, L. D., G. L. Pickard,W. J. Emery, and J. H. Swift (2011). Descriptive PhysicalOceanography: An Introduction, 6th ed., 560 pp., Elsevier, Boston.

Winter A., Henderiks J., Beaufort L., Rickaby R.E.M., Brown C.W. (2014). Poleward expansion of the coccolithophore *Emiliania huxleyi*, *Journal of Plankton Research*, Volume 36, Issue 2, 1 March 2014, Pages 316–325, https://doi.org/10.1093/plankt/fbt110

Wyrtki, K., 1966. Oceanography of the eastern equatorial Pacific Ocean. Oceanography and Marine Biology Annual Review 4, 33–68.

You, Y. (2000). Implications of the deep circulation and ventilation of the Indian Ocean on the renewal mechanism of North Atlantic Deep Water. Journal of Geophysical Research, 105(C10), 23,895–23,926. https://doi.org/10.1029/2000JC900105

Young, J. R. & Ziveri P. (2000), Calculation of coccolith volume and its use in calibration of carbonate flux estimates, *Deep-Sea Research Part II,* 47, 1679-1700.

Zondervan, I. (2007). The effects of light, macronutrients, trace metals and CO2 on the production of calcium carbonate and organic carbon in coccolithophores - A review, Deep-sea research part ii-topical studies in oceanography, 54 (5), pp. 521-537. https://doi.org:10.1016/j.dsr2.2006.12.004

Zondervan, I., Rost, B. & Riebesell, U. (2002). Effect of CO_2 concentration on the PIC/POC ratio in the coccolithophoreEmilianiahuxleyi grownunder light-limiting conditions and different daylengths. J. Exp. Mar. Biol. Ecol. 272, 55–70.

CHAPTER 6

Conclusions and future research perspective

This PhD thesis contributes to the general understanding of the role played by an abundant phytoplankton community, the coccolithophores, in the Southern and Eastern Equatorial Pacific Oceans during the last deglaciation. Microfossil assemblages have been analyzed from sediment samples recovered at ODP Sites 1089 (Subtropical zone of the South Atlantic), 1238 (Eastern Equatorial Pacific), and PS2498-1 (Subantarctic zone of the South Atlantic). In the following paragraphs the main results and conclusions of the thesis with suggestions on future research are summarized.

In Chapter 2, we discussed the repeatability of our results on samples prepared with the filtration method, which is the most commonly used method to prepare samples in order to obtain coccolith absolute abundances (CC g/dry sed.). This method is based on the assumption that coccoliths are homogenously distributed on the filter membrane. We discuss the repeatability of samples (from Site PS2498-1), in order to evaluate coccolith distribution on the filter surface. Some degree of inhomogeneity is found in the different replicas and an increase in the numbers of individuals, when *C. leptoporus*, *C. pelagicus* and *Helicosphaera* spp. are abundant, are also observed.

In Chapter 3, the coccolith assemblages of the Subtropical South Atlantic (ODP Site 1089) are mainly composed by *E. huxleyi* and *C. leptoporus* and the results obtained from this site are possibly emphasized by episodes of iron fertilization and high phosphorus delivery due to the equatorward displacements of the westerlies and the upwelling Antarctic cell, respectively. The dissolution proxy (CEX) evidences for two low preservation intervals during the deglaciation (17 to 15 ka) and the final part of the Holocene (7 to 6 ka). We use other coccolith species within the assemblage, such as *F. profunda* and *C. pelagicus,* to detect changes in the shifts of the Subtropical front over the glacial/interglacial cycle. Specifically, low absolute abundances of the former taxon are related to the shift of the optimal biogeographic areal of this species which was driven by a displacement of the surface water boundary (STF). The latter taxon shows high absolute abundances during the glacial and this is possibly related to its affinity with cold and temperate waters, as expected during the Antarctic ice-sheet expansion.

Data obtained from the coccolith assemblages reflect the carbonate system dynamics that are, in this case, driven by changes in surface and deep water masses. During the glacial more alkaline conditions allow the increase of highly calcified coccolith species. On the contrary, during the Holocene, low surface water pH caused a decrease in the mass of coccolith species. We also suggest an enhanced strength of the coccolithophore carbonate counter pump as a response to iron fertilization, which would have resulted in a decrease of the ion carbonate concentrations of the deep waters eventually leading the rise of the CCD. Finally, our data on *E. huxleyi* mass and calcification dynamics allow to propose a relationship between changes in the carbonate system and modifications in coccolithophore mass and calcification. Specifically, high calcification in *E. huxleyi* is likely the response to the saturation state condition of the carbonate system.

Similar data have been acquired from Site PS2498-1 where coccolith assemblages are mainly constituted by *E. huxleyi* and *C. leptoporus* (Chapter 4). However, *E. huxleyi* trend seems to have a different response at Site PS2498-1 if compared with Site 1089. At this site, the possible undersaturation of surface waters coupled with high pCO_2 values may explain the growth rates recorded in *E. huxleyi*. The changes observed in other taxa within the assemblage seem instead related to changes in the paleoproducivity conditions of surface waters. Specifically, the absolute abundances of *G. muellerae* are used to recognize the position of the nutricline during high Fe and P deliveries. The high absolute abundances of *C. leptoporus* small, *C. leptoporus* and *H. carteri* are instead in good agreement with oligotrophic water conditions characterizing the Holocene. We finally analyze coccolith mass and length for both *E. huxleyi* and *C. leptoporus* in order to better understand their relationship with environmental parameters. The increase in *E. huxleyi* mass and in both *E. huxleyi* and *C. leptoporus* coccolith length observed under high temperatures and pCO_2, are possibly explained by an evolutionary adaptation in undersaturated waters.

In Chapter 5, at Site ODP1238, we focus on analyzing *E. huxleyi* mass and calcification degree in order to reconstruct the PIC:POC ratio and evaluate the photosynthesis versus calcification activity. We propose an enhanced coccolith carbonate counter pump during the Holocene which has likely played a major role in enhancing the sea water pCO_2 thus favoring the outgassing of CO_2 from the ocean into the atmosphere. Finally, we propose an increased calcification degree in *E. huxleyi* mass from the glacial into the Holocene as a response to low surface pH and increased CO_2 values, possibly due to the natural homeostasis regulation between the cytosol cell and the seawater.

Overall our results indicate that the coccolith response to environmental parameters strongly depends on the paleoproductivity and carbonate chemistry of both surface and bottom waters. In the case of the Subtropical community dominated by *E. huxleyi* and *C. leptoporus*, nutrient concentrations and carbonate system are likely the main control factors on absolute abundances. Interestingly, in the Subantarctic community, *E. huxleyi* seems to be primarily driven by ocean acidification.

Future investigations on the response of coccolithophores communities to the combined effects of changes in different environmental parameters are needed in order to quantify and better define the response of this group and provide solid bases for projections on the role that coccolithophores will play on ongoing climate change (*e.g.* Gerecht et al., 2018; Segovia et al., 2018).

BIBLIOGRAPHY

Amore, F. O. et al. (2012). A Middle Pleistocene Northeast Atlantic coccolithophore record: Paleoclimatology and paleoproductivity aspects. *Marine Micropaleontology,* 90-91, 44–59. doi:10.1016/j.marmicro.2012.03.006.

Arrhenius G. O. (1952). Sediment cores from the East Pacific, in Petterson, H., ed. Reports of the Swedish Deep- Sea Expedition, v. 5. Fasc. I, 227 p.

Balch W.M. (2018). The Ecology, Biogeochemistry, and Optical Properties of Coccolithophores. Annu. Rev. Mar. Sci. 2018. 10:71–98.

Balch WM, Bates NR, Lam PJ, Twining BS, Rosengard SZ, et al. (2016). Factors regulating the Great Calcite Belt in the Southern Ocean and its biogeochemical significance. *Glob. Biogeochem. Cycles* 30:1124–44

Balch WM, Drapeau DT, Bowler BC, Booth ES, Lyczskowski E, Alley D. (2011). The contribution of coc- colithophores to the optical and inorganic carbon budgets during the Southern Ocean Gas Experiment: new evidence in support of the "Great Calcite Belt" hypothesis. *J. Geophys. Res.* 116:C00F06

Balch WM, Drapeau DT, Bowler BC, Booth ES. (2007). Prediction of pelagic calcification rates using satellite- measurements. *Deep-Sea Res. II* 54:478–95

Balch WM. (2004). Re-evaluation of the physiological ecology of coccolithophores. In *Coccolithophores: From Molecular Processes to Global Impact*, ed. HR Thierstein, JR Young, pp. 165–90. Berlin: Springer-Verlag.

Balch WM, Drapeau DT, Bowler BC, Booth ES. (2007). Prediction of pelagic calcification rates using satellite- measurements. *Deep-Sea Res. II* 54:478–95.

Balestrieri C., Ziveri P., Mortyn P.G., Fornaciari E., Grelaud M., Marino G., Agnini C. Coccolith carbonate response to Southern Ocean iron fertilization during the last deglaciation. Submitted to Quaternary Science Reviews. Elsevier.

Barnola, J. M., Raynaud, D., Korotkevich, Y. S. & Lorius, C. (1987). Vostok ice cores provides 160,000-year record of atmospheric CO_2. *Nature* 329, 408–414.

Beaufort L, Probert I, de Garidel-Thoron T, Bendif EM, Ruiz-Pino D, et al. (2011). Sensitivity of coccolithophores to carbonate chemistry and ocean acidification. *Nature* 476:80–83.

Bereiter, B., S. Eggleston, J. Schmitt, C. Nehrbass-Ahles, T. F. Stocker, H. Fischer, S. Kipfstuhl, and J. Chappellaz (2015), Revision of the EPICA Dome C CO2 record from 800 to 600 kyr before present, Geophys. Res. Lett., 42, 542–549, doi:10.1002/2014GL061957.

Berger, A. L. (1978). Long-term variations of daily insolation and Quaternary climatic change. *J. Atmos. Sci.* 35**,** 2362 – 2367.

Billard, c. & Inouye, i. (2004). What is new in coccolithophore biology? In Coccolithophores – from Molecular Processes to Global Impact (Thierstein, H.R. & Young, J.R., editors), 1–29. Springer-Verlag, Berlin.

Bown, P. R., Lees, J. A. and Young, J. R. (2004). Calcareous nannoplankton evolution and diversity through time, in Coccolithophores: from molecular processes to global impact, pp. 481–508, Springer.

Boeckel, B. & Baumann K.-H. (2004). Distribution of coccoliths in surface sediments of the south-eastern South Atlantic Ocean: ecology, preservation and carbonate contribution, *Marine Micropaleontology,* 51, 301– 320, doi:10.1016/j.marmicro.2004.01.001.

Broecker, W. and Clark, E. (2009). Ratio of coccolith $CaCO_3$ to foraminifera $CaCO_3$ in late Holocene deep sea sediments, Paleoceanography, 24(3), 1–11, doi:10.1029/2009PA001731.

Broecker, W.S. (2003) The Oceanic $CaCO_3$ Cycle. In Holland, H. D., and Turekian, K. K. (eds.), Treatise on Geochemistry. Amsterdam: Elsevier, Vol. 6, pp. 529–549. DOI: 10.1016/B0-08-043751-6/06119-3

Broecker, W. S., (1984). Terminations, in Milankovitchand Climate,Part 2, edited by A. Bergeretal, pp. 687-698, D. Reidel, Norwell, Mass.

Brussaard CPD. (2004). Viral control of phytoplankton populations—a review. *J. Eukaryot. Microbiol.* 51:125–38.

Brzezinski M. A., S. B. Baines, W. M. Balch, C. P. Beucher, et al., (2011). Co- limitation of diatoms by iron and silicic acid in the equatorial Pacific. Deep-Sea Research II 58 (2011) 493–511.

Chappell J. and Shackleton N.J. (1986). Oxygen isotopes and sea level. Nature 324, 137-140.

Chappellaz, J., Barnola, J.-M., Raynaud, D., Korotkevich, Y. S. & Lorius, C. (1990). Ice-core record of

atmospheric methane over the past 160,000 years. *Nature* 127 – 131.

Charles, C. D., Froelich, P. N., Zibello, M. A., Mortlock, R. A., and Morley, J. J. (1991). Biogenic

opal in Southern Ocean sediments over the last 450,000 years: implications for surface water chemistry and circulation. Paleoceanography 6, 697–728.

de Baar H. J. W., Buma A.G.J., R.F. Nolting, G.C. Cadée. (1990). On iron limitation of the Southern Ocean: experimental observations in the Weddell and Scotia Seas. *Marine Ecology Progress Series*. Vol. 65, No. 2, pp. 105-122.

Dittert N. et al. (1999). Carbonate dissolution in the deep-sea: methods, quantification and paleoceanographic application**.** G. Fischer, G. Wefer (Eds.), *Use of Proxies in Paleoceanography — Examples from the South Atlantic, Springer, Berlin*, pp. 255-284.

De Vargas C., Aubry M.-P., Probert I., Young J. (2007). Origin and Evolution of coccolithophores: From Coastal Hunters to Oceanic Farmers. Evolution of primary producers in the sea. Chapter 12, 251-285.

Durak GM, Taylor AR, Walker CE, Probert I, et al. (2016). A role for diatom-like silicon transporters in calcifying coccolithophores. *Nat. Commun.* 7:10543.

Emiliani, C. (1995). Two revolutions in the Earth Sciences. Terra Nova, 7, 587-597, The Ocean Floor Spec. Issue (ed. By E. Bonatti and F.C. Wezel).

Findlay H.S., Calosi P., Crawfurd K. (2011). Determinants of the PIC:POC response in the coccolithophore *Emiliania huxleyi* under future ocean acidification scenarios. Limnology and Oceanography. Vol. 56, Issue 3., pages 1168-1178.

Fine, R. A., Lukas, R., Bingham, F. M., Warner & M. J.&Gammon, R. H. (1994). The western equatorial Pacific: a water mass crossroads. J. Geophys. Res. 99, 25063–25080.

Flores, J.-A., Filippelli G.M., Sierro F.J. & Latimer J. (2012). The "White Ocean" Hypothesis: A Late Pleistocene Southern Ocean Governed by Coccolithophores and Driven by Phosphorus. *Frontiers in Microbiol*ogy 2012; 3: 233, doi: 10.3389/fmicb.2012.00233

Flores, J.-A., Marino, M., Sierro, F. J., Hodell, D. A., and Charles, C. D. (2003). Calcareous plankton disso- lution pattern and coccolithophore assemblages during the last 600 kyr atODPSite 1089 (Cape Basin, South Atlantic): paleoceanographic impli- cations. Palaeogeogr. Palaeoclimatol. Palaeoecol. 196, 409–426.

Frada, M. J., Probert, I., Allen, M. J., Wilson, W. H. and de Vargas, C. (2008). The "Cheshire Cat" escape strategy of the coccolithophore *Emiliania huxleyi* in response to viral infection, Proc. Natl. Acad. Sci. U. S. A., 105(41), 15944–15949, doi:10.1073/pnas.0807707105.

Frada, M. J., Bidle, K. D., Probert, I. and de Vargas, C. (2012). In situ survey of life cycle phases

of the coccolithophore Emiliania huxleyi (Haptophyta), Environ. Microbiol., 14(6), 1558– 1569, doi:10.1111/j.1462-2920.2012.02745.x

Gerecht A.C., Šupraha L., Langer G., and Henderiks J. Phosphorus limitation and heat stress decrease calcification in *Emiliania huxleyi.* Biogeosciences, 15, 833–845, 2018. https://doi.org/10.5194/bg-15-833-2018

Gottschalk J., Skinner L.C., Lippold J., Vogel H., Frank N., Jaccard S., & Waelbroeck C. (2016). Biological and Physical controls in the Southern Ocean on past millennial-scale atmospheric CO_2 changes. Nature Communications volume 7. Doi: 10.1038/ncomms11539

Grelaud M.; Beaufort L.; Cuven S.; Buchet N. (2009). Glacial to interglacial primary production and El Niño-Southern Oscillation dynamics inferred from coccolithophores of the Santa Barbara Basin. Paleoceanography, 24(1), PA1203. https://doi.org/10.1029/2007PA001578

Hart TJ (1934). On the phytoplankton of the southwest Atlantic and the Bellingshausen Sea. Discovery Rept 8: 1-268.

Harvey E. L., Kay D. Bidle, Matthew D. Johnson. (2015). Consequences of strain variability and calcification in *Emiliania huxleyi* on microzooplankton grazing, *Journal of Plankton Research*, Volume 37, Issue 6, 1. Pages 1137- 1148, https://doi.org/10.1093/plankt/fbv081

Howard W. R., W.L. Prell. (1994). Late Quaternary $CaCO_3$ production and preservation in the Southern Ocean: implications for oceanic and atmospheric carbon cycling. Paleoceanography, 9, pp. 453-482.

Ikehara, M., Kawamura, K., Ohkouchi, N., Murayama, M., et al., (2000). Variations of terrestrial input and marine productivity in the South- ern Ocean (48˚S) during the last two deglaciations. Paleoceanography 15, 170–180.

Imbrie J. et al., Boyle E.A., Clemens S.C., Duffy A., et al., (1993). On the structure and origin of major glaciation cycles, 2, the 100000-year-cycle. Paleoceanography, 8, 699-736.

Imbrie, J., Boyle E.A., Clemens S.C., Duffy A., et al., (1992). On the structure and origin of major glaciation cycles. 1. Linear responses to Milankovich forcing. *Paleoceanography* **7,** 701–738.

Imbrie, J., J. D. Hays, D. G. Martinson, A. McIntyre, et al., (1984). The orbital theory of Pleistocene climate: Support from a revised chronology of the marine $\delta^{18}O$ record, in Milankovitch and Climate, Part I, edited by A. L. Berger, pp. 269 – 305, D. Reidel, Norwell, Mass.

Imbrie, J. and J. Z. Imbrie (1980). Modeling the climatic response to orbital variations, Science, 207, 943-952.

Intergovernmental Panel on Climate Change (IPCC) (2013), Climate Change 2013: The Physical Science Basis. Contribution of Working Group I to the Fifth Assessment Report of the Intergovernmental Panel on Climate Change, 1535 pp., Cambridge Univ. Press, Cambridge and New York.

Keeling, R. F. & Visbeck, M. (2001). Palaeoceanography: Antarctic stratification and glacial CO2. Nature 412, 605–606.

Köbrich, M.I. & Baumann K.-H. (2008). Coccolithophore flux in a sediment trap off Cape Blanc (NW Africa). *Journal of Nannoplankton Research*, 30 (2), 83-96.

Keeling, R. F. & Visbeck, M. (2001). Palaeoceanography: Antarctic stratification and glacial CO2. Nature 412, 605–606.

Kumar, N., Anderson, R. F., Mortlock, R. A., Froelich, P. N., et al., (1995). Increased biological productivity and export production in the glacial Southern Ocean. Nature 378, 675–680.

Krumhardt K.M., Lovenduski N. S., Iglesias-Rodriguez M.D., Kleypas J.A. (2017). Coccolithophore growth and calcification in a changing ocean. Progress in Oceanography 159, 276-295.

Latimer, J. C., and Filippelli, G. M. (2001). Terrigenous input and paleoproductivity in the Southern Ocean. Paleoceanography 16, 627–693.

Lisiecki, L. E., and M. E. Raymo (2005), A Pliocene-Pleistocene stack of 57 globally distributed benthic delta O-18 records, Paleoceanography, 20, PA1003, doi:10.1029/2004PA001071.

Liu, Z. Y. & Yang, H. J. (2003). Extratropical control of tropical climate, the atmospheric bridge and oceanic tunnel. Geophys. Res. Lett. 30, 1230.

Lukas, R. (1986). The termination of the equatorial undercurrent in the eastern Pacific. Prog. Oceanogr. 16, 63–90.

Lüthi, D., M. Le Floch, T. F. Stocker, B. Bereiter, T. Blunier, J. M. Barnola, U. Siegenthaler, D. Raynaud, and J. Jouzel (2008), High-resolution carbon dioxide concentration record 650,000-800,000 years before present, Nature, 453, 379–382.

Marchetti A, Maldonado MT. (2016). Iron. In *The Physiology of Microalgae*, ed. MA Borowitzka, J Beardall, JA Raven, pp. 233–79. Cham, Switz.: Springer

Margalef, R. (1978). Life-forms of phytoplankton as survival alternatives in an unstable environment. Oceanol. Acta 1, 493–509.

Marino, M., Maiorano P., Lirer F. & Pelosi N. (2009). Response of calcareous nannofossil assemblages to paleoenvironmental changes through the mid-Pleistocene revolution at Site 1090 (Southern Ocean). *Palaeogeography, Palaeoclimatology, Palaeoecology*, 280 333–349. doi:10.1016/j.palaeo.2009.06.019

Martin, J. H., R. M. Gordon & S. E. Fitzwater, (1990). Iron in Antarctic waters, Nature 345, 156-158.

Martin H.H., Coale K.H, Johnson K.S., Fitzwater S.E., et al., (1994). Testing the iron hypothesis in ecosystems of the equatorial Pacific Ocean. Nature, vol. 371.

Martin, J.H. & Fitzwater, S.E. (1989). Iron deficiency limits phytoplankton growth in the north-east Pacific Subarctic Nature, 331, 314-343.

Martínez-Botí, M. A., Marino G., Foster G.L., Ziveri P., et al. (2015). Boron isotope evidence for oceanic carbon dioxide leakage during the last deglaciation. *Nature* 518, 219–222. doi:10.1038/nature14155.

Martínez-Garcia, A. et al. (2009). Links between iron supply, marine productivity, sea surface temperature, and CO2 over the last 1.1 Ma. Paleoceanography 24, PA1207.

Meyer J. & Riebesell U., (2015). Reviews and syntheses: responses of coccolithophores to ocean acidification: a meta-analysis. *Biogeosciences* 12:1671–82.

Mejía, L. M., Ziveri P., Cagnetti M., Bolton C. et al. (2014). Effects of midlatitude westerlies on the paleoproductivity at the Agulhas Bank slope during the penultimate glacial cycle: Evidence from coccolith Sr/Ca ratios. *Paleoceanography*, 29, 697–714, doi:10.1002/2013PA002589.

Milankovitch, M., 1941: Canon of Insolation and the Ice-Age Problem (in German). Special Publications pf the Royal Ser- bian Academy, Vol. 132, Israel Program for Scientific Trans-lations, 484 pp.

Moreno, A.,Cacho, I.,Canals, M., Prins, M. A., Sánchez-Goñi, M. F., Grimalt, J. O., & Weltje, G. J. (2002). Saharan dust transport and high- latitude glacial climatic variability: the Alboran Sea record. Quat. Int. 58, 318–328.

Mortlock, R., A., Charles, C.D., Froelich, P. N., Zibello, M. A., et al., (1991). Evidence for lower produc- tivity in the Antarctic Ocean during the last glaciations. Nature 351, 220–223.

Nöel, M.-H., Kawachi, M. & Inouye, I. (2004). Induced dimorphic life cycle of a coccolithophorid, Calyptrosphaera sphaeroidea (Prymnesiophyceae, Haptophyta), J. Phycol., 40(1), 112–129, doi:10.1046/j.1529-8817.2004.03053

Parkin, D. W. & Shackleton N. J. (1973). Trade wind and temperature correlations down deep-sea core off the Sahara Coast. Nature, Lond. 245, 455-457.

Past Interglacials Working Group of PAGES (2016), Interglacials of the last 800,000 years, Rev. Geophys., 54, doi:10.1002/2015RG000482.

Pedersen T. F. (1983). Increased productivity in the eastern equatorial Pacific during the last glacial maximum (19000 to 14000 yr B.P.). GEOLOGY, v. 11, p. 16-19.

Peterson L. C. & Prell W. L. (1985). Carbonate preservation and rates of climatic change: an 800 kyr record from the Indian Ocean. In The Carbon Cycle and Atmospheric CO_2: Natural Variations Archean to Present, Geophys. Monogr. Ser. 32 (eds. E. T. Sundquist and W. S. Broecker) pp. 251–270.

Poulton A. J., Holligan P. M., Charalampopoulou A., Adey T. R. (2017). Coccolithophore ecology in the tropical and subtropical Atlantic Ocean: New perspectives from the Atlantic meridional transect (AMT) programme. Progress in Ocenaography 158, 150-170.

Raven J., Falkowski P., Oceanic sinks for atmospheric CO2. (1999). Pant, Cell and Environment. Vol. 22, 6, pages 741-755.

Rembauville, M., Meilland J., Ziveri P., Schiebel R., et al. (2016). Planktic foraminifer and coccolith contribution to carbonate export fluxes over the central Kerguelen Plateau, *Deep Sea Research,* Part I, 111, 91–101.

Renaud, S., Ziveri, P., & Broerse, A. T. C. (2002). Geographical and seasonal differences in morphology and dynamics of the coccolithophore Calcidiscus leptoporus. *Marine Micropalaeontology*, *46*(3-4), 363-385. DOI: 10.1016/S0377-8398(02)00081-6

Rickaby, R. E. M., et al. (2010). Evidence for elevated alkalinity in the glacial Southern Ocean, *Paleoceanography*, 25, PA1209, doi:10.1029/2009PA001762.

Rio, D., Fornaciari E. & Raffi I. (1990a). Late Oligocene through early Pleistocene calcareous nannofossils from western equatorial Indian Ocean (Leg 115), in *Duncan*, R.A., Backman, J., L. C. Peterson et al., Proc. ODP, Sci. Results, 115: College Station, TX (Ocean Drilling Program), 175-235.

Rio, D., Raffi I. & Villa G. (1990b). Pliocene-Pleistocene calcareous nannofossil distribution patterns in the western Mediterranean, *in* Kastens, K.A., J. Mascle, et al*., Proc. ODP, Sci. Results,*107: College Station, TX (Ocean Drilling Program), 513-533.

Rost, B. & Riebesell, U.: Coccolithophores and the biological pump: responses to environmental

changes, in Coccolithophores From Molecular Processes to Global Impact, edited by H. R. Thierstein and J. R. Young, pp. 99–125, Springer-Verlag, Berlin Heidelberg, Germany., 2004.

Salter, I., Schiebel R., Ziveri P., Movellan A., et al., (2014). Carbonate counter pump stimulated by natural iron fertilization in the Polar Frontal Zone, *Nature Geosciences,* letters, 7, 885-889. doi: 10.1038/NGEO2285.

Sarmiento J.L., Dunne J., Gnanadesikan A., Key R.M., Matsumoto K., Slater R. (2002). A new estimate of the CaCO3 to organic carbon export ratio. *Glob. Biogeochem. Cycles* 16:1107.

Segovia M., Lorenzo M.R., Iniguez C., Garcia-Gomez C. (2018). Physiological stress response associated with elevated CO2 and dissolved iron in phytoplankton community dominated by the coccolithophore *Emilania huxleyi*. Mar. Ecol. Prog. Ser. 586:73-89. https://doi.org/10.3354/meps12389

Sett S., Bach L.T., Schulz K.G., Koch-Klavsen S., Lebrato M., Riebesell U. (2014) Temperature Modulates Coccolithophorid Sensitivity of Growth, Photosynthesis and Calcification to Increasing Seawater *p*CO. PLoS ONE 9(2): e88308. https://doi.org/10.1371/journal.pone.0088308.

Shackleton, N. J., Backmann J., Zimmermann H., Kent D. V., et al. (1984), Oxygen isotope calibration of the onset of ice-rafting and history of glaciation in the North Atlantic region, Nature, 307(5952), 620–623.

Shackleton, N. J., A. Berger & W. R. Peltier, (1990). An alternative astronomical calibration of the lower Pleistocene timescale based on ODP site 677, Trans. R. Soc. Edinburgh: Earth Sci., 81, 251–261.

Sigman D.M., Hain M.P. and Haug G.H. (2010). The polar ocean and glacial cycles in atmospheric CO(2) concentration. Nature. 466(7302):47-55.

Smith S.V.& Gattuso J.P. (2011). Balancing the oceanic calcium carbonate cycle: consequences of variable water column. *Aquat. Geochem.* 17:327–37.

Smith S.V., Mackenzie F.T. (2016). The role of CaCO3 reactions in the contemporary oceanic CO_2 cycle. *Aquat. Geochem.* 22:153–75.

Stephens B.B., Keeling R.F. (2000). The influence of Antarctic sea ice on glacial-interglacial CO2 variations. Nature. 2000. 404(6774):171-4.

Takahashi, T. Sutherland S.C., Wanninkhof R., Sweeney C. et al. (2009). Climatological mean and decadal change in surface ocean pCO2, and net sea-air CO2 flux over the global oceans. Deep-Sea Res. I 56, 2075–2076.

The Royal Society (2005). Ocean acidification due to increasing atmospheric carbon dioxide.

Thierstein, H. R., Geitzenauer, K. R., and Molfino, B., 1977. Global synchroneity of late Quaternary coccolith datum levels: validation by oxygen isotopes. Geol. Soc. Am. Bull., 5:400-404.

Toggweiler, J. R., Dixon, K. & Broecker, W. S. (1991). The Peru upwelling and the ventilation of the South Pacific thermocline. J. Geophys. Res. 96, 20467–20497.

Tsuchiya, M., Lukas, R., Fine, R. A., Firing, E. & Lindstrom, E. (1989). Source waters of the Pacific equatorial undercurrent. Prog. Oceanogr. 23, 101–147.

Watson A.J., Law C.S., Van Scoy K.A., Millero F.J., Yao., W., Friederich G.E., Liddicoat R.H. Wanninkhof R.H., Barber R.T., Coale K.H. (1994). Minimal effect of iron fertilization on sea-surface carbon dioxide concentrations. Nature volume 371, pages 143–145.

Wu G. & Berger W. H. (1989) Planktonic foraminifera: differential dissolution and the quaternary stable isotope record in the west equatorial Pacific. Paleoceanography 4, 181 – 198.

Yamamoto- Kawai M., McLaughin F. A., Carmack E. C., Nishino S., Shimada K. (2009). Aragonite undersaturation in the Arctic Ocean: effects of ocean acidification and sea ice melt. Science;
326(5956):1098-100. doi: 10.1126/science.1174190

Young JR, Geisen M, Cros L, Kleijne A, et al. (2003). A guide to extant coccolithophore taxonomy. *J. Nannoplankton Res.* Spec. Issue 1, Int. Nannoplankton Assoc.

Young, J. R. & Ziveri P. (2000), Calculation of coccolith volume and its use in calibration of carbonate flux estimates, *Deep-Sea Research Part II,* 47, 1679-1700.

Zachos, J. C., G. R. Dickens, & R. E. Zeebe (2008), An early Cenozoic perspective on greenhouse warming and carbon-cycle dynamics, Nature, 451(7176), 279–283, doi:10.1038/nature06588.

Ziveri, P., Thunell, R.C. & Rio, D., (1995). Export production of coccolithophores in an upwelling region: results from San Pedro Basin, Southern California borderlands. Mar. Micropa- leontol., 24: 335-358.

Ziveri P., Young J.R. & van Hinte J.E. (1999). Coccolithophore export production and accumulation rates. GeoResearch Forum 5: 41–56.

SUPPLEMENTARY MATERIAL

INPUT CONDITIONS												
Salinity	**t(°C) in**	**P (dbars) in**	**TA in (mmol/kgSW)**	**TCO2 in (mmol/kgSW)**	**pH in**	**fCO2 in (matm)**	**pCO2 in (matm)**	**HCO3 in (mmol/kgSW)**	**CO3 in (mmol/kgSW)**	**CO2 in (mmol/kgSW)**	**B Alk in (mmol/kgSW)**	**OH in (mmol/kgSW)**
34.40	10.726	9	2281.99	2082.36	8.07	359.9	361.3	1922.6	144.3	15.47	68.94	1.85
34.31	9.972	38	2276.37	2081.66	8.07	355.9	357.3	1925.2	140.8	15.69	67.88	1.72
34.22	8.486	89	2276.20	2097.58	8.06	366.1	367.6	1950.2	130.4	16.98	63.80	1.43
34.12	7.016	129	2274.78	2108.77	8.05	369.6	371.0	1968.6	122.2	18.03	60.68	1.21
34.45	7.712	249	2284.87	2138.14	7.98	437.7	439.4	2006.2	111.1	20.81	55.34	1.13
34.36	6.503	339	2282.65	2153.30	7.96	464.3	466.2	2029.7	100.5	23.03	50.92	0.94
34.24	4.653	536	2282.54	2162.79	7.95	454.7	456.6	2044.5	94.1	24.11	48.96	0.78
34.25	3.611	742	2290.63	2182.84	7.93	474.2	476.2	2069.6	87.1	26.12	46.15	0.66
34.38	3.108	992	2312.34	2220.34	7.87	528.5	530.7	2111.9	78.8	29.63	42.28	0.57
34.50	2.770	1255	2326.52	2239.54	7.85	544.9	547.2	2132.6	76.0	30.91	41.36	0.53
34.59	2.701	1413	2331.89	2240.19	7.86	525.4	527.6	2132.1	78.2	29.87	42.85	0.55
34.70	2.546	1680	2338.67	2241.42	7.87	501.7	503.9	2132.2	80.6	28.67	44.78	0.56
34.76	2.542	1974	2340.04	2228.70	7.90	451.2	453.2	2115.6	87.3	25.78	49.18	0.61
34.81	2.520	2221	2339.15	2225.58	7.89	442.2	444.1	2112.3	88.0	25.28	50.23	0.62
34.82	2.417	2466	2340.78	2216.56	7.91	407.1	408.9	2100.0	93.2	23.36	53.76	0.66
34.83	2.312	2709	2342.18	2213.47	7.92	391.6	393.3	2095.8	95.1	22.56	55.51	0.67
34.83	2.204	2956	2345.11	2215.34	7.91	386.3	387.9	2097.8	95.2	22.34	56.23	0.67
34.82	2.013	3201	2349.33	2220.92	7.90	386.1	387.8	2104.4	94.1	22.49	56.21	0.65
34.79	1.738	3445	2353.89	2230.21	7.88	393.7	395.4	2116.0	91.1	23.18	55.18	0.62
34.76	1.379	3690	2360.81	2242.74	7.86	403.1	404.8	2131.0	87.7	24.06	53.86	0.58
34.75	1.178	3931	2364.46	2249.28	7.85	407.2	409.0	2139.0	85.8	24.50	53.36	0.56
34.73	1.056	4175	2365.82	2252.42	7.83	409.1	410.9	2143.3	84.4	24.73	53.18	0.54
34.73	1.027	4419	2365.84	2253.55	7.82	410.6	412.4	2145.3	83.4	24.85	53.19	0.54
34.73	1.038	4647	2366.28	2254.31	7.81	410.8	412.6	2146.6	82.9	24.85	53.40	0.53

RESULTS (Output Conditions)												
t(°C) out	**P (dbars) out**	**pH out**	**fCO2 out (matm)**	**pCO2 out (matm)**	**HCO3 out (mmol/kgSW)**	**CO3 out (mmol/kgSW)**	**CO2 out (mmol/kgSW)**	**B Alk out (mmol/kgSW)**	**OH out (mmol/kgSW)**	**WCa out**	**WAr out**	**xCO2 out (dry at 1 atm) (ppm)**
10.726	9	8.07	359.9	361.3	1922.6	144.32	15.47	68.94	1.85	3.44	2.19	365.8
9.972	38	8.07	355.9	357.3	1925.2	140.82	15.69	67.88	1.72	3.34	2.13	361.6
8.486	89	8.06	366.1	367.6	1950.2	130.37	16.98	63.80	1.43	3.07	1.95	371.6
7.016	129	8.05	369.6	371.0	1968.6	122.16	18.03	60.68	1.21	2.86	1.81	374.7
7.712	249	7.98	437.7	439.4	2006.2	111.08	20.81	55.34	1.13	2.53	1.61	443.9
6.503	339	7.96	464.3	466.2	2029.7	100.54	23.03	50.92	0.94	2.25	1.43	470.6
4.653	536	7.95	454.7	456.6	2044.5	94.14	24.11	48.96	0.78	2.03	1.29	460.4
3.611	742	7.93	474.2	476.2	2069.6	87.10	26.12	46.15	0.66	1.80	1.14	479.9
3.108	992	7.87	528.5	530.7	2111.9	78.79	29.63	42.28	0.57	1.55	0.98	534.7
2.770	1255	7.85	544.9	547.2	2132.6	76.01	30.91	41.36	0.53	1.41	0.90	551.2
2.701	1413	7.86	525.4	527.6	2132.1	78.18	29.87	42.85	0.55	1.41	0.90	531.5
2.546	1680	7.87	501.7	503.9	2132.2	80.59	28.67	44.78	0.56	1.37	0.88	507.5
2.542	1974	7.90	451.2	453.2	2115.6	87.34	25.78	49.18	0.61	1.40	0.90	456.4
2.520	2221	7.89	442.2	444.1	2112.3	88.02	25.28	50.23	0.62	1.35	0.87	447.3
2.417	2466	7.91	407.1	408.9	2100.0	93.18	23.36	53.76	0.66	1.36	0.88	411.8
2.312	2709	7.92	391.6	393.3	2095.8	95.11	22.56	55.51	0.67	1.32	0.86	396.1
2.204	2956	7.91	386.3	387.9	2097.8	95.22	22.34	56.23	0.67	1.26	0.82	390.6
2.013	3201	7.90	386.1	387.8	2104.4	94.05	22.49	56.21	0.65	1.18	0.78	390.4
1.738	3445	7.88	393.7	395.4	2116.0	91.08	23.18	55.18	0.62	1.09	0.72	398.0
1.379	3690	7.86	403.1	404.8	2131.0	87.71	24.06	53.86	0.58	1.00	0.66	407.5
1.178	3931	7.85	407.2	409.0	2139.0	85.78	24.50	53.36	0.56	0.93	0.62	411.6
1.056	4175	7.83	409.1	410.9	2143.3	84.43	24.73	53.18	0.54	0.87	0.58	413.5
1.027	4419	7.82	410.6	412.4	2145.3	83.43	24.85	53.19	0.54	0.82	0.55	415.1
1.038	4647	7.81	410.8	412.6	2146.6	82.90	24.85	53.40	0.53	0.79	0.52	415.3

TABLE S1 (previous page). Carbonate system (output conditions, bottom table) calculated based on modern salinity, temperature (°C), pressure (dbars), total alkalinity (μmol/kgSW) and pH data (Input conditions, top table) using CO2Sys at ODP Site 1089 and PS2498-1.

INPUT CONDITIONS					
Salinity	**t(°C)**	**P (dbars)**	**TA (mmol/kgSW)**	**TCO2 (mmol/kgSW)**	**pH**
34.98	22.580	8.10	2327	2023.7	8.076
34.93	16.333	23.80	2326	2181.9	7.843
34.79	13.909	49.50	2298	2233.9	7.668
34.73	12.389	98.70	2302	2246.9	7.648
34.73	11.597	150.20	2299	2260.9	7.613
34.74	11.044	200.70	2300	2271	7.588
34.71	10.300	252.80	2302	2278	7.575
34.70	9.847	297.80	2302	2280	7.561
34.61	8.476	400.90	2303	2283	7.579
34.52	7.128	497.40	2301		
34.49	6.305	599.30	2306		
34.51	5.752	701.90	2319	2300	7.607
34.51	5.079	798.80	2328	2304	7.632
34.52	4.616	901.40	2340	2311	7.646
34.53	4.248	998.60	2350	2316	7.662
34.55	3.958	1102.10	2359	2321	7.675
34.56	3.677	1203.60	2367	2326	7.687
34.57	3.426	1300.90	2372	2326	7.705
34.59	3.095	1449.70	2384	2334	7.714
34.61	2.809	1597.60	2391	2337	7.731
34.62	2.585	1747.60	2396	2335	7.745
34.64	2.278	2000.20	2406	2338	7.760
34.66	2.061	2247.90	2412	2337	7.775
34.67	1.917	2500.20	2412	2329	7.794
34.67	1.831	2739.70	2414	2329	7.791
34.68	1.795	2997.50		2334	7.787
34.68	1.779	3251.20		2331	7.783
34.69	1.758	3506.60	2410	2320	7.788
34.69	1.728	3753.80	2406	2311	7.787
34.69	1.737	3992.90	2408	2311	7.780
34.69	1.742	4247.80	2408	2312	7.762
34.69	1.744	4492.70	2407	2311	7.756
34.69	1.746	4743.10	2407	2310	7.744
34.69	1.769	4989.20	2410	2309	7.739
34.69	1.791	5260.90	2405	2310	7.719
34.69	1.795	5302.00	2405	2310	7.720

RESULTS (Output Conditions)													
t(°C) out	**P (dbars) out**	**pH out**	**fCO2 out (matm)**	**pCO2 out (matm)**	**HCO3 out (mmol/kgSW)**	**CO3 out (mmol/kgSW)**	**CO2 out (mmol/kgSW)**	**B Alk out (mmol/kgSW)**	**OH out (mmol/kgSW)**	**Revelle out**	**WCa out**	**War out**	**xCO2 out (dry at 1 atm) (ppm)**
22.58	8.10	8.07	362.08	363.28	1796.91	215.84	10.94	92.55	5.86	9.64	5.17	3.39	373.16
16.33	23.80	7.84	669.66	672.04	2043.21	114.58	24.11	51.73	1.92	13.99	2.72	1.75	684.34
13.91	49.50	7.66	1045.95	1049.79	2122.69	70.65	40.56	33.03	0.99	17.13	1.67	1.07	1066.18
12.39	98.70	7.65	1056.40	1060.36	2137.96	65.97	42.97	31.29	0.84	17.55	1.55	0.99	1075.33
11.60	150.20	7.61	1168.72	1173.14	2153.91	58.23	48.76	27.95	0.70	18.04	1.35	0.86	1188.85
11.04	200.70	7.58	1230.25	1234.94	2164.41	54.34	52.25	26.30	0.63	18.24	1.25	0.80	1250.87
10.30	252.80	7.57	1243.75	1248.54	2171.74	52.13	54.13	25.45	0.58	18.39	1.19	0.76	1263.86
9.85	297.80	7.57	1240.76	1245.56	2174.03	51.16	54.81	25.14	0.55	18.45	1.16	0.74	1260.38
8.48	400.90	7.58	1191.50	1196.19	2178.06	49.79	55.14	24.89	0.49	18.63	1.10	0.70	1209.15
5.75	701.90	7.61	1077.40	1081.81	2196.76	48.41	54.84	25.05	0.40	18.98	1.01	0.64	1091.51

5.08	798.80	7.63	1007.92	1012.08	2201.39	50.07	52.55	26.11	0.39	19.03	1.02	0.65	1020.74
4.62	901.40	7.65	952.56	956.51	2208.59	51.91	50.49	27.21	0.40	19.04	1.04	0.66	964.43
4.25	998.60	7.67	903.23	906.99	2213.67	53.81	48.52	28.33	0.40	19.01	1.06	0.67	914.32
3.96	1102.10	7.68	866.07	869.69	2218.63	55.36	47.01	29.27	0.40	18.98	1.06	0.68	876.57
3.68	1203.60	7.69	837.22	840.74	2223.58	56.50	45.91	30.03	0.40	18.96	1.06	0.68	847.25
3.43	1300.90	7.71	796.23	799.59	2223.48	58.45	44.07	31.23	0.41	18.87	1.08	0.69	805.68
3.09	1449.70	7.72	763.11	766.34	2231.18	60.07	42.75	32.29	0.41	18.82	1.07	0.69	772.04
2.81	1597.60	7.73	731.09	734.20	2233.99	61.62	41.39	33.37	0.42	18.74	1.07	0.69	739.55
2.59	1747.60	7.75	685.08	688.00	2231.39	64.50	39.11	35.20	0.43	18.54	1.08	0.70	692.94
2.28	2000.20	7.76	640.92	643.66	2233.61	67.38	37.01	37.20	0.44	18.34	1.08	0.69	648.17
2.06	2247.90	7.78	601.14	603.73	2231.72	70.29	34.99	39.27	0.46	18.10	1.07	0.69	607.89
1.92	2500.20	7.80	559.82	562.23	2222.62	73.62	32.76	41.68	0.48	17.78	1.06	0.69	566.07
1.83	2739.70	7.79	548.18	550.54	2222.61	74.21	32.18	42.52	0.48	17.73	1.02	0.66	554.28
1.80	2997.50	7.79	542.04	544.37	2227.59	74.54	31.87	43.16	0.48	17.71	0.98	0.64	548.06
1.78	3251.20	7.78	532.27	534.57	2224.72	74.97	31.31	43.97	0.48	17.65	0.93	0.61	538.18
1.76	3506.60	7.78	519.82	522.06	2214.13	75.27	30.60	44.86	0.49	17.56	0.89	0.59	525.59
1.73	3753.80	7.78	497.32	499.47	2204.49	77.20	29.31	46.62	0.50	17.33	0.87	0.57	502.84
1.74	3992.90	7.78	489.26	491.37	2204.33	77.85	28.82	47.48	0.51	17.26	0.84	0.56	494.68
1.74	4247.80	7.77	491.57	493.69	2206.09	76.95	28.96	47.52	0.50	17.33	0.79	0.52	497.02
1.74	4492.70	7.76	489.94	492.06	2205.60	76.54	28.86	47.83	0.50	17.34	0.75	0.50	495.38
1.75	4743.10	7.75	484.96	487.05	2204.80	76.64	28.56	48.44	0.50	17.32	0.72	0.48	490.34
1.77	4989.20	7.75	470.73	472.76	2203.02	78.28	27.70	49.92	0.52	17.15	0.70	0.47	475.95
1.79	5260.90	7.72	490.00	492.11	2206.34	74.85	28.81	48.49	0.49	17.45	0.64	0.43	495.44
1.80	5302.00	7.72	489.90	492.01	2206.41	74.79	28.80	48.53	0.49	17.45	0.63	0.42	495.34

TABLE S2. Carbonate system (Output conditions, bottom table) calculated based on modern salinity, temperature (°C), pressure (dbars), total alkalinity (μmol/kgSW) and pH data (Input conditions, top table) using CO2Sys at IODP1238.

Family **CALCIOSOLENIACEAE** Kamptner, 1927

Calciosolenia Gran, 1912

Family **CALCIDISCACEAE** Young & Bown, 1997

Calcidiscus leptoporus subsp. leptoporus (Murray & Blackman 1898) Loeblich & Tappan, 1978
Calcidiscus leptoporus subsp. quadriperforatus (Kamptner 1937) Geisen et al., 2002
Calcidiscus leptoporus subsp. small Young et al., 2003
Umbilicosphaera foliosa (Kamptner 1963) Geisen in Sáez et al., 2003
Umbilicosphaera sibogae (Weber - van Bosse 1901) Gaarder, 1970

Family **CERATOLITHACEAE** Norris, 1965; emend. Young & Bown, 2014

Ceratolithus cristatus Kamptner, 1950
Ceratolithus cristatus Kamptner 1950 CER *telesmus* type, sensu Jordan & Young 1990

Family **COCCOLITHACEAE** Poche, 1913; emend. Young and Bown, 1997

Coccolithus pelagicus (Wallich 1877) Schiller, 1930
Coccolithus pelagicus subsp. braarudii (Gaarder 1962) Geisen et al., 2002

Family **HELICOSPHAERACEAE** Black, 1971

Helicosphaera carteri (Wallich 1877) Kamptner, 1954
Helicosphaera wallichii (Lohmann 1902) Okada & McIntyre, 1977

Family **NOELAERHABDACEAE** Jerkovic 1970; emend. Young and Bown 1997

Emiliania huxleyi (Lohmann 1902) Hay & Mohler, in Hay et al. 1967
Emiliania huxleyi type A Young & Westbroek, 1991
Emiliania huxleyi type A overcalcified Young et al., 2003
Emiliania huxleyi var. corona (Okada & McIntyre 1977) Jordan & Young, 1990
Emiliania huxleyi type B Young & Westbroek, 1991
Emiliania huxleyi type B/C Young et al., 2003
Gephyrocapsa oceanica Kamptner, 1943
Gephyrocapsa muellerae Bréhéret, 1978
Gephyrocapsa ericsonii (McIntyre & Bé, 1967)
Gephyrocapsa omega Bukry 1973
Reticulofenestra Hay, Mohler & Wade, 1966

Family **PONTOSPHAERACEAE** Lemmermann, 1908

Pontosphaera Lohmann, 1902

Family **RHABDOSPHAERACEAE** Haeckel, 1894
Discosphaera tubifera (Murray & Blackman 1898) Ostenfeld, 1900
Family **SYRACOSPHAERACEAE** (Lohmann, 1902) Lemmermann, 1903
Syracosphaera pulchra Lohmann, 1902
COCCOLITH GENERA *INCERTAE SEDIS*
Gladiolithus flabellatus (Halldal & Markali 1955) Jordan & Chamberlain, 1993
NANNOLITH GENERA *INCERTAE SEDIS*
Florisphaera profunda Okada & Honjo, 1973

TABLE S3. List of identified species.

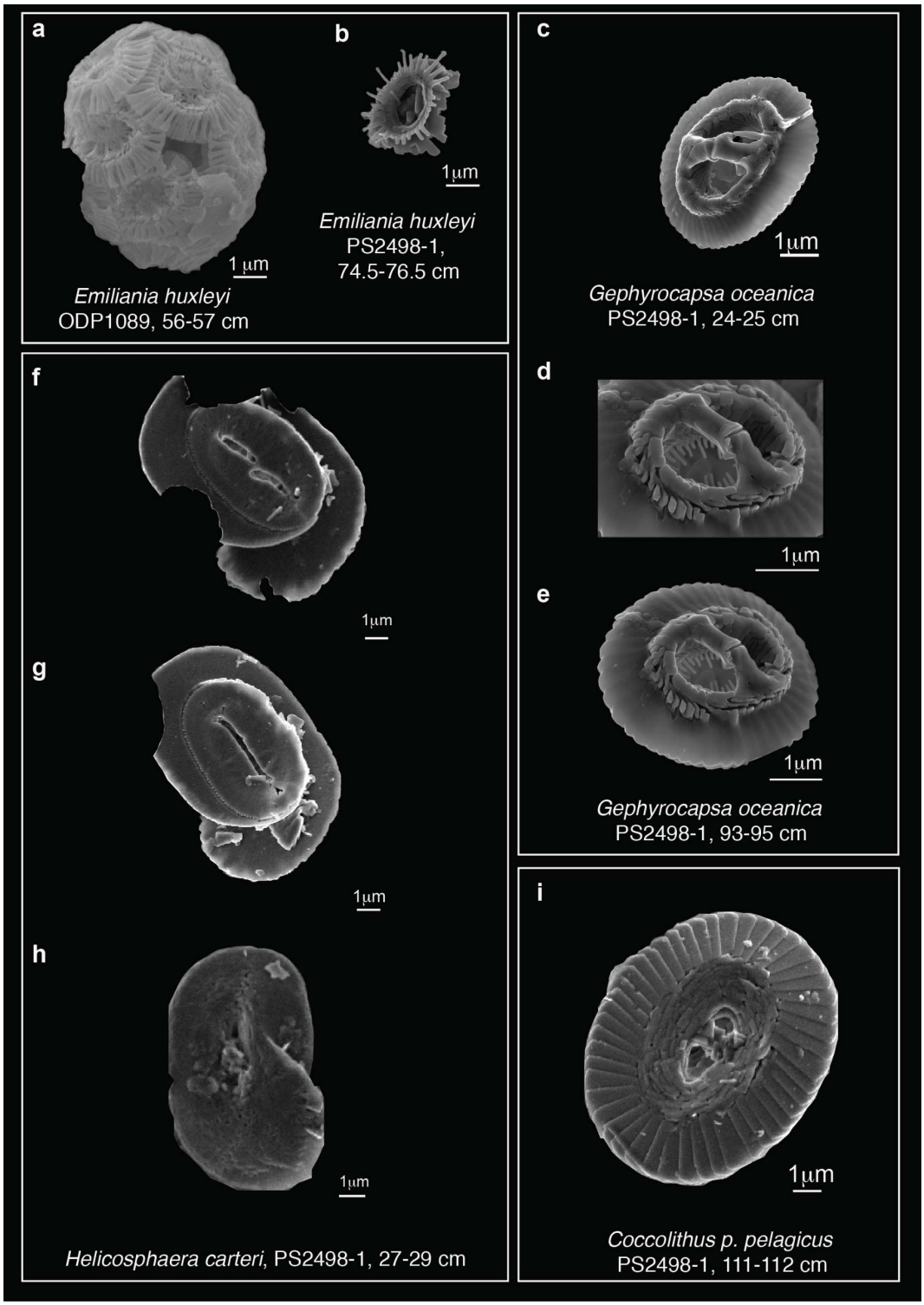

TABLE S4. SEM pictures of some coccolithophore species: a) *Emiliania huxleyi* complete coccosphere, ODP1089, 56-57 cm; b) *E. huxleyi* coccolith in distal view, PS2498-1; 74.5-76.5 cm; c) *Gephyrocapsa oceanica* coccolith in distal view, PS2498-1, 24-25 cm; d) *G. oceanica* details of a distal view central area and e) *G. oceanica* coccolith in oblique distal view, PS2498-1, 93-95 cm; f, g) *Helicosphaera carteri* coccoliths in distal view, and h) *H. carteri* in proximal view, PS2498-1, 27-29 cm; i) *Coccolithus p. pelagicus* coccolith in distal view, PS2498-1, 111- 112 cm.

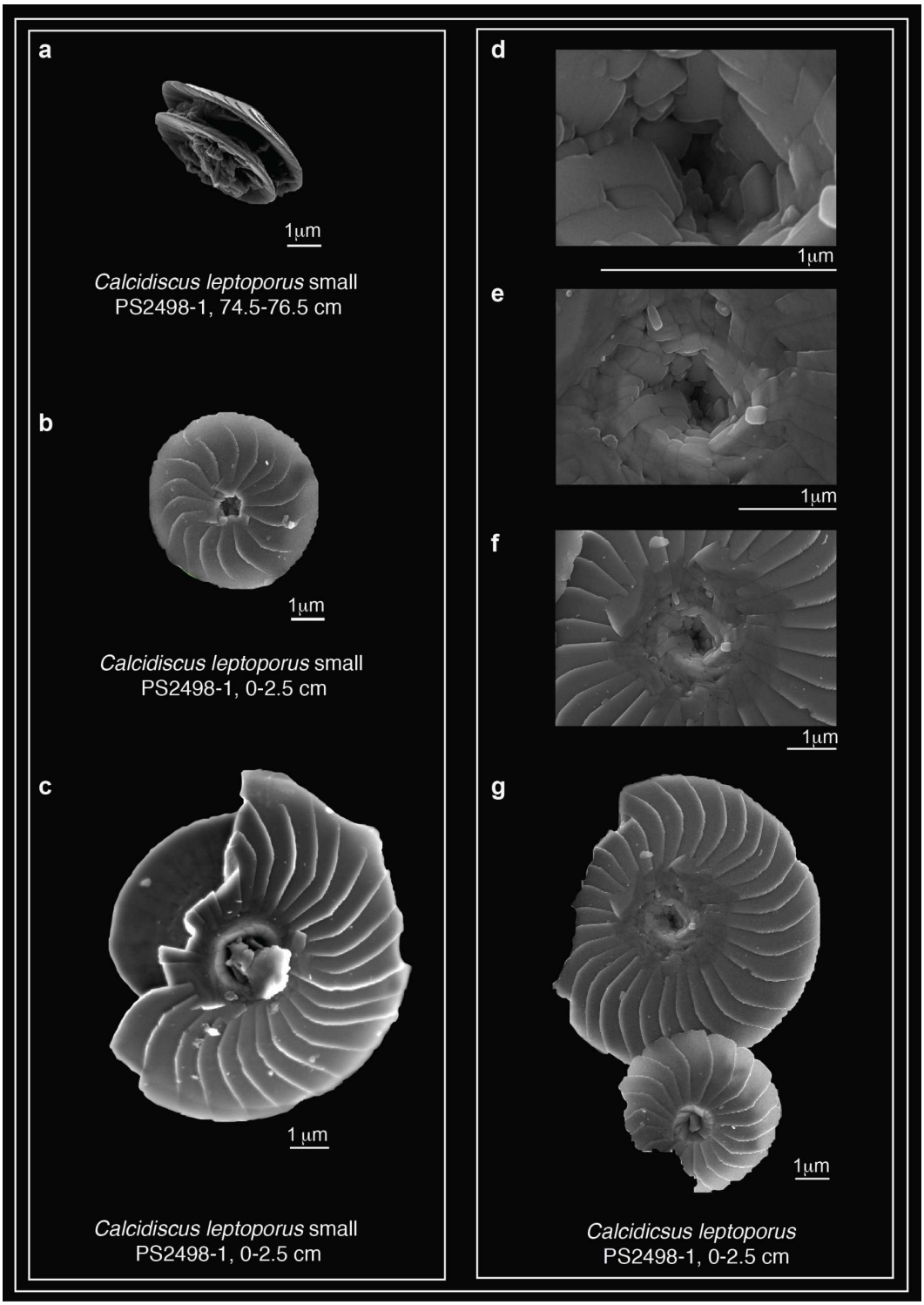

TABLE S5. SEM pictures of some coccolithophore species: a) *Calcidiscus leptoporus* small complete coccolith in oblique proximal view, PS2498-1, 74.5-76.5 cm; b) *C. leptoporus* small coccolith in distal view, PS2498-1, 0-2.5 cm; c) *C. leptoporus* small coccolith in oblique distal view, PS2498-1, 0-2.5 cm; d, e, f) *C. leptoporus* coccolith details of the inner part of the central opening (d, e) and central area (f) in distal view, g) *C. leptoporus* coccolith in distal view, PS2498-1, 0-2.5 cm.

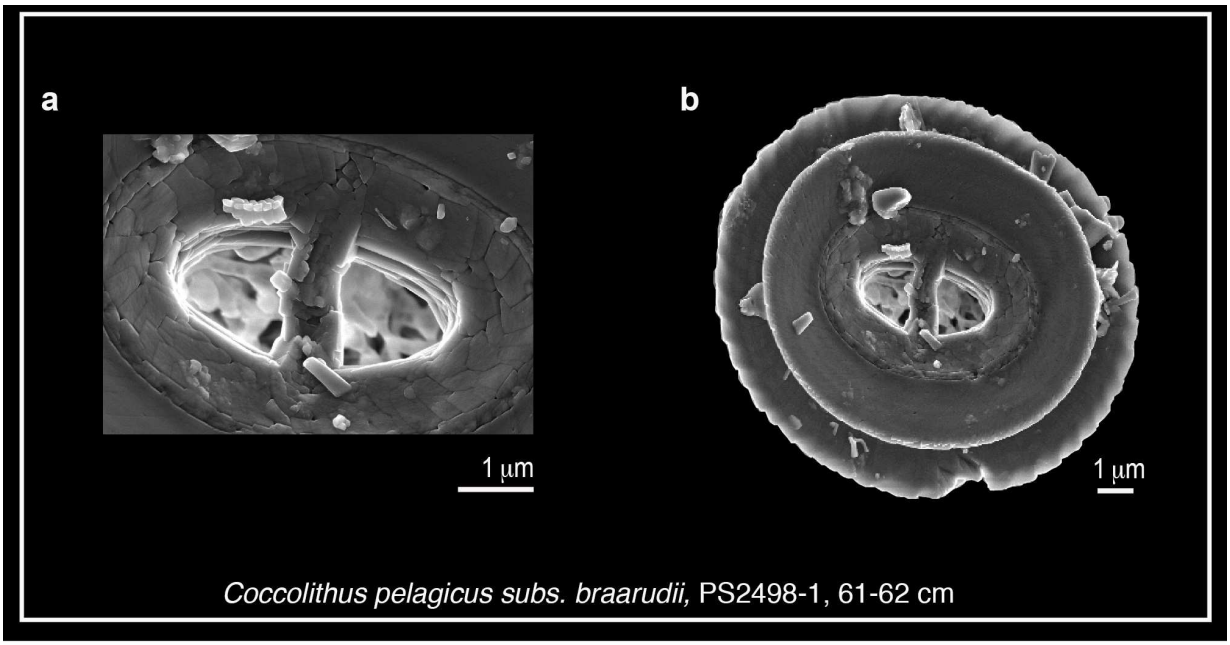

TABLE S5. SEM pictures of *Coccolithus pelagicus subs. braarudii*, a) a detail proximal view of the central area and b) a complete proximal view of the complete coccolith, PS2498-1, 61-62 cm.

Glossary of abbreviations

Agulhas Rings (ARs)
Agulhas Current (AC)
Antarctic Circumpolar Current (ACC)
Benguela Current (BC)
Bølling-Allerod (BA)
Brazil current (BC)
Calcite saturation horizon (CSH)
Carbonate compensation depth (CCD)
Circumpolar Deep Water (CDW)
Coccolith accumulation rate (ARc)
Coccolith dissolution index (CEX)
Costa Rica Coastal Current (CRCC)
Dissolved Inorganic Carbon (DIC)
Eastern Equatorial Pacific Ocean (EEP)
EPICA Dome C (EDC)
Heinrich stadials (HS1)
High-nitrate, low-chlorophyll (HNLC)
Last Glacial Maximum (LGM)
Last Glacial Period (LGP)
Length index (Li)
Light microscope (LM)
Low Circumpolar Deep Water (LCDW)
Lower photic zone (LPZ)
Marine Isotope Stage 1-2 (MIS1-2)
Meridional Overturning Circulation (MOC)
Northern Hemisphere (NH)
North Atlantic Deep water (NADW)
North Equatorial Countercurrent (NECC)
North Equatorial Current (NEC)
Ocean acidification (OA)
Pacific Deep Water (PDW)
Particulate Inorganic Carbon (PIC)
Particulate Organic Carbon (POC)
Peru-Chile Countercurrent (PCCC)
Peru Current (PC)
Photosynthesis versus calcification activity (P:C)
Polar Front (PF)
South Equatorial Current (SEC)
Southern Ocean (SO)
Subantarctic Mode Water (SAMW)
Total carbon content (TCO_2 (μmol/kg))
Slit length (SL)
South Atlantic current (SAC)

Système de Reconnaissance Automatique de Coccolithes (SYRACO)
Subantarctic Front (SAF)
Subtropical Front (STF)
Subsurface Equatorial Undercurrent (EUC)
Tube width (TW)
Upper Circumpolar Deep Water (UCDW)
Weddell Sea waters (WS)
Younger Dryas (YD)

ACKNOWLEDGEMENTS

Having a joint PhD between an Italian and a Spanish institution has given me the opportunity to meet many exciting people and form fruitful collaborations.

I would like to thank Prof. Claudia Agnini (Università degli Studi di Padova) for her commitment to this project, her feedback, and her ability to face the challenges that this project presented to all of us. I would like to thank Prof. Patrizia Ziveri (Institut de Ciència i Tecnologia Ambiental, ICTA, UAB) for always giving me her best science advice, her trust and support during these years. They both gave me the freedom to explore my scientific interests, and I appreciated their professional and personal guidance as women advancing in science. To my co- supervisor Prof. Graham Mortyn (ICTA, UAB) for always being very supportive, for his great humanity, linguistic checks and amusing conversations. I am grateful also to the Postdoc Michaël Grelaud (ICTA, UAB) for running efficient labs to support my research and also for discussions about coccolithophores, always a great source of ideas, coffee and fun. Thanks to Prof. Dick Norris (SCRIPPS Institution of Oceanography) for hosting me in his lab, at his wonderful brunches enriched with scientific and cultural discussions, for making me go kayaking in the Pacific Ocean and for showing me kindness, humanity and love for science.

Thanks to the technicians of the Servei de Microscòpia of the Universitat Autònoma de Barcelona and of the Università degli Studi di Padova, for introducing me to the SEM and FE-SEM respectively and helping during the work sessions.

A warm thought goes to all the wonderful colleagues/ friends that during this long path have helped me go through hard personal and professional times, providing the balance which I truly believe makes me love what I do. To Giulia, Arianna, Alice, Carlotta, Livio, Nicola, Olmo, Luca, Marianna, Barbara, Anna, Chiara, Elisa, Griselda, Laura, Miki, Emiliano, Francesco, Filippo, Alice, Shlomit, Cloè, Manu, Elisa, Ilaria, Annalisa and all the other wonderful students that I met in these three years.

Finally, to my Italian and US families, always in my heart.
This thesis is dedicated to all of you,
Chiara